Wind Farms Production: Control and Prediction

by

Tarek Hussein Mostafa EL-Fouly

A thesis
presented to the University of Waterloo
in fulfillment of the
thesis requirement for the degree of
Doctor of Philosophy
in
Electrical and Computer Engineering

Waterloo, Ontario, Canada, 2007

Author's Declaration

I hereby declare that I am the sole author of this thesis. This is a true copy of the thesis, including any required final revisions, as accepted by my examiners.

I understand that my thesis may be made electronically available to the public.

Abstract

Wind energy resources, unlike dispatchable central station generation, produce power dependable on external irregular source and that is the incident wind speed which does not always blow when electricity is needed. This results in the variability, unpredictability, and uncertainty of wind resources. Therefore, the integration of wind facilities to utility electrical grid presents a major challenge to power system operator. Such integration has significant impact on the optimum power flow, transmission congestion, power quality issues, system stability, load dispatch, and economic analysis.

Due to the irregular nature of wind power production, accurate prediction represents the major challenge to power system operators. Therefore, in this thesis two novel models are proposed for wind speed and wind power prediction. One proposed model is dedicated to short-term prediction (one-hour ahead) and the other involves medium term prediction (one-day ahead). The accuracy of the proposed models is revealed by comparing their results with the corresponding values of a reference prediction model referred to as the persistent model.

Utility grid operation is not only impacted by the uncertainty of the future production of wind farms, but also by the variability of their current production and how the active and reactive power exchange with the grid is controlled. To address this particular task, a control technique for wind turbines, driven by doubly-fed induction generators (DFIGs), is developed to regulate the terminal voltage by equally sharing the generated/absorbed reactive power between the rotor-side and the grid-side converters. To highlight the impact of the new developed technique in reducing the power loss in the generator set, an economic analysis is carried out. Moreover, a new aggregated model for wind farms is proposed that accounts for the irregularity of the incident wind distribution throughout the farm layout. Specifically, this model includes the wake effect and the time delay of the incident wind speed of the different turbines on the farm, and to simulate the fluctuation in the generated power more accurately and more closer to real-time operation.

Recently, wind farms with considerable output power ratings have been installed. Their integrating into the utility grid will substantially affect the electricity markets. This thesis investigates the possible impact of wind power variability, wind farm control strategy, wind energy penetration level, wind farm location, and wind power prediction accuracy on the total generation costs and close to real time electricity market prices. These issues are addressed by developing a single auction market model for determining the real-time electricity market prices.

Acknowledgements

I wish to express my deep gratitude to Prof. Magdy M.A. Salama and Prof. Ehab F. EL-Saadany for their supervision, guidance, continuous encouragement, helpful support, financial support, and valuable comments throughout the progress of my research and the writing of this thesis.

I am also grateful to Prof. Elham Makram, Prof. Fathy Ismail, Prof. Mehrdad Kezzareni, and Prof. Ramdan EL-Shatshat for joining my examining committee.

Special thanks to Dr. Tarek Abdel-Galil, Dr. Mostafa Marei, Dr. Hatem Zeineldin, and my colleagues for their support, interest, assistance and technical discussions during the course of this research.

I am also thankful to the OGSST for their financial support to this research.

Furthermore, I am very grateful to my wife Marwa for her patient and continuous encouragement that has enabled me to complete this work. Finally, I am very appreciative to my parents for their encouragement, guidance, and continuous support throughout my academic career.

To my parents, my wife, Marwa, and my children, Maya and Kareem

Table of Contents

List of Figures

List of Tables

Acronyms

ANFIS	Adaptive Network based Fuzzy Inference System
ANN	Artificial Neural Network
AR	Auto Regression
ARIMA	Auto Regression Integrated Moving Average
ARMA	Auto Regression Moving Average
CanWEA	Canadian Wind Energy Association
DFIG	Doubly Fed Induction Generator
DG	Distributed Generation
ERN	Elman Recurrent Network
EWEA	European Wind Energy Association
FES	Fuzzy Expert System
GAMS	General Algebraic Modelling System
GM	Grey Model
HCDG	High Cost Distributed Generation
HIRLIAM	High Resolution Limited Area Model
HOEP	Hourly Ontario Energy Price
LCDG	Low Cost Distributed Generation
LPF	Local Power Factor
MAE	Mean Absolute Error
MOS	Model Output Statistics
NLN	Neural Logic Networks
NLP	Nonlinear Programming Problem
NYISO	New York Independent System Operator
PF	Power Factor
RBF	Radial Basis Function network
RMSE	Root Mean Square Errors
SCADA	Supervisory Control And Data Acquisition
SCIG	Squirrel Cage Induction Generator
SP	Spot Market Price

UPF	Unity Power Factor
VR	Voltage Regulation
WA^SP	Wind Atlas Application and Analysis Program
WECS	Wind Energy Conversion Site
WF	Wind Farm
WRIG	Wound Rotor Induction Generator

Chapter 1
Introduction

1.1 Preface

Renewable energy technologies are clean sources of energy that have a much lower environmental impact than conventional energy technologies such as coal, oil, nuclear and natural gas. In addition, renewable energy resources will never run out while conventional sources of energy are finite and will some day be used up. Most renewable energy (solar, bio, wind, and wave) is derived from the sun, directly or indirectly, while other types of renewable energy resources (geothermal, hydrogen, and tidal) come from different sources other than the sun. For example, the geothermal energy comes from the Earth internal heat.

Wind energy resources are considered among the fastest growing energy resources all over the world, especially in the European Union, USA, and Canada. Wind energy offers numerous advantages including clean fuel sources that do not produce atmospheric emissions that cause acidic rain or greenhouse gases, can not be exhausted, is one of the lowest-priced renewable energy technologies at 6 to 8 ¢/ kWh, and finally, can be built on farms or ranches, benefiting the rural economy, where most of the best wind sites are found.

Multinational oil and gas companies report that renewable energy will provide as much as 10% of the world's energy supply by 2020, and increase as much as 50% by 2050 [1]. The European Union plans to produce 22% of its electricity from renewable resources by the year 2010, mostly from wind power [1, 2]. By the end of 2006, the total wind energy capacity, installed in the world, was 73.3 GW [3]. Moreover, the European Wind Energy Association (EWEA) estimates that 12% of the world's electricity will be generated from wind power by 2020 [4].

As for Canada, the total wind energy production, at the end of 2006, was 1460 MW with an average annual growth rate of 51 % (from 2000 to 2006). Currently, wind farms are installed in most Canadian provinces. Ontario is the province with the highest wind power generation with a total wind capacity of 413.71 MW. The largest Canadian wind farm is located in Ontario and it consists of 126 units, each generating 1.5 MW, with a total capacity of 189 MW [5].

The primary goal of the Canadian Wind Energy Association (CanWEA) is to generate more than 10,000 MW (10 GW) of electricity from wind energy by 2010 (10 X 10 Canada Wind Vision

Program). This will provide at least 5% of the Canadian electricity generation by 2010 [1]. Figure 1-1 presents the forecasted wind power capacity in Canada up to 2010 according to the Canada Wind Vision Program. It is noteworthy that the forecasted period started at 2000. It is noted from Figure 1-1 that it was expected that Canada would reach a total wind power capacity of 448 MW by the end of 2006. However, the total installation capacity at the end of 2006 was 1460 MW (almost three times the target) which indicates that CanWEA is moving fast to achieve its goal.

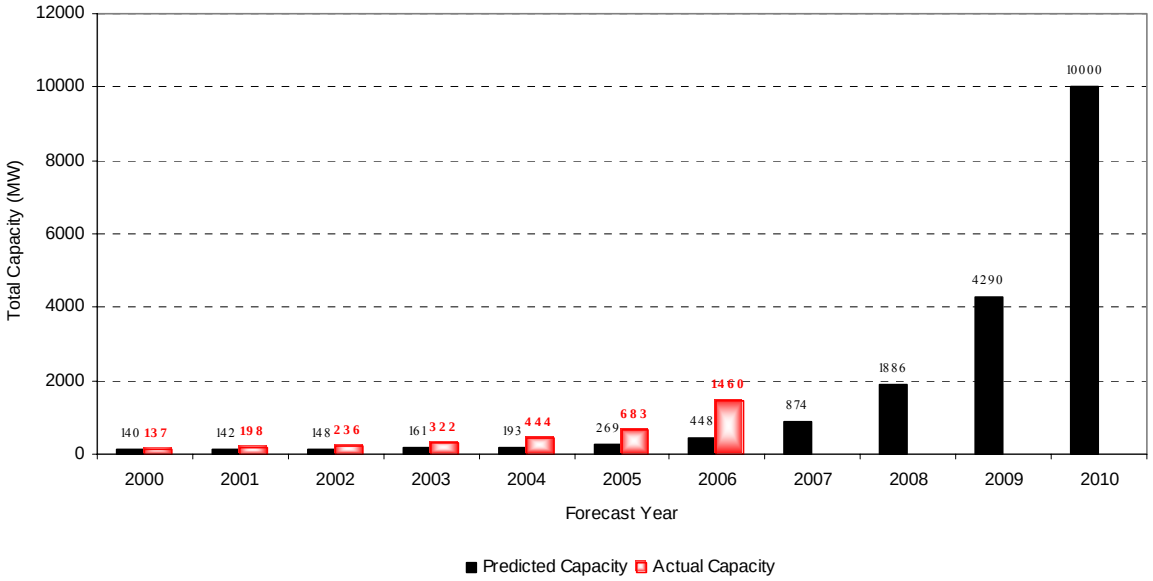

Figure 1-1: Canada's current and predicted wind power installation capacity.

It should also be noted that that over the last decade the cost of wind-generated electricity has dropped from 30 ¢/kwh to ranges from about 6 ¢/kwh - 8 ¢/kwh. Moreover, some studies by the British government and the US Department of Energy predict that the cost of wind energy will be 3.4 ¢/kwh to 5.5 ¢/kwh by 2020 [5, 6]. Despite this decrease in the cost of the wind power, the wind energy technology has a higher capital cost than fossil-fuelled generators. Roughly 75% of the cost is the turbine and tower cost, 20% is the foundation, transformation, grid connection, roads, engineering, construction finance, and insurance, and 5% is the sitting and land acquisition [7]. However, the running costs of wind energy are much more competitive than those of other energy technologies, because there is no fuel to purchase and the operating expenses are minimal.

This new revolution in electricity generation from wind energy has caught the attention of researchers and their interests are quite clear in numerous publications regarding wind turbines and wind farms. The rapid growth in the capacity of wind turbines and the number of the installed wind farms requires more intensive research in many fields. Researchers need to focus on the prediction of wind farms' output power, advanced reactive power control techniques for large wind farms, and developing more accurate models to simulate the dynamic performance of wind farms under various operating conditions. Moreover, the future plan for wind farms to operate as power plants and to become active controllable power elements in power systems [8] capable of replacing non-renewable energy resources power plants, necessitate more accurate methods for wind speed and energy prediction, as well as more accurate, reliable, and economical control techniques.

1.2 Thesis Objectives

Power systems economic analysis requires knowledge of the present and the expected future conditions of the power system. Current production and the hour-ahead and/or the day-ahead prediction of power production play a vital role in managing the power system to ensure secure and reliable operation. This affects the power system operation costs, day-ahead unit commitment process and hour-ahead and day-ahead electricity market clearing prices.

The main objective of this thesis is the development of new efficient techniques to control and predict the power production of wind farms equipped with variable-speed, inverter-based wind turbines. This objective can be broken down into the following:

Wind Characteristic Objectives

- Investigate the usage of previously developed Grey predictor rolling models for hourly (short term) wind speed forecasting and wind power prediction.
- Develop modified versions of the Grey predictor to enhance the prediction accuracy and eliminate overshoots in the predicted values of the traditional Grey models.
- Develop a new prediction model for medium term prediction (up to one day ahead) of wind speed and wind direction based on developing a linear model relating current observations to one year (or two years) old observations and project this linear model into the future for predictions.

- Test the accuracy of the proposed prediction models by comparing their outputs with those generated by the reference prediction model referred to as the persistent model.

Wind Farm Operation Objectives

- Develop a control technique for doubly-fed induction generators (DFIG) that is capable of regulating the terminal voltage and reducing the generation losses by equally sharing the generated/absorbed reactive power between the rotor-side and the grid-side converters.
- Develop a new aggregated model for wind farms while considering the irregular wind field distribution within the wind farm layout.
- Investigate the application of the developed control technique for large scale wind farms by using the developed aggregated model.

Economical Objectives

- Investigate the economic benefits due to the reduction in the generation losses for DFIGs.
- Simulate a single-auction electricity market model to investigate the possible impact of integrating wind farms to the utility grid on the total generation costs and the real-time electricity market prices.

1.3 Thesis Outline

Figure 1-2 provides a block diagram of the thesis skeleton. The thesis is organized as follows:

- **Chapter two** presents a literature survey of the available techniques for wind speed forecasting and wind farm output power prediction. Advantages and disadvantages of these techniques are presented. This chapter also surveys the previously developed models for wind farms. The proper fields of application of each model and their usage limitations are discussed. Previously developed control techniques and algorithms used for voltage regulation and reactive power control of wind farms are also reviewed. Finally, the developed studies to investigate possible economical impact of integrating wind farms to utility grids are surveyed.

The rest of this thesis is divided into two parts: The first part, presented in Chapter three, investigates the production prediction and control of a single variable speed wind turbine (VSWT) unit. This includes developing new models for the wind power prediction of a VSWT, and investigates a control technique to reduce its operational power losses. The second part, Chapters four, five, and six, investigates the operational aspects of wind farms. This includes, developing a new wind field model for wind farms dynamic operation studies, developing a new technique for the prediction of wind farm active power production and investigating the impact of wind farms integration to utility grids on electricity markets clearing prices. The contents of these parts (chapters) can be summarized as follows:

- **Chapter three** investigates the usage of previously developed Grey predictor rolling models for hourly wind speed forecasting and wind power prediction (short term prediction). The generated results revealed that these models sometimes cause overshoots in the predicted values that increase the prediction errors. Therefore, two new modified versions for the Grey rolling models are proposed to overcome the occurrence of these overshoots and reduce the generated errors. The accuracy of the models is tested by comparing their results with the corresponding results generated by the reference prediction model (the persistent model). Finally, a control technique for doubly-fed induction generators (DFIGs) wind turbines is developed. The aim for such technique is to regulate the terminal voltage by equally sharing the generated/absorbed reactive power between the rotor-side and the grid-side converters. The economic impacts on the generator losses is investigated and compared with that of the conventional control method where the rotor-side converters can generate/absorb reactive power while the grid-side converters are not allowed to do so.

- In **Chapter four**, a new aggregated model for wind farms that takes into consideration the wake effect and the time delay in modelling the wind field distribution of the different turbines within the farm is developed. The wind farm is modeled with DFIGs equipped with the control technique proposed in chapter three. This model is then used to simulate the dynamic response of large scale wind farm under various operating conditions.

- The Grey models presented in Chapter three are only efficient for one-step ahead prediction. These models exhibit a high prediction error for medium and long term prediction horizons such as day ahead prediction. However, these horizons are essential for several related power system operations such as day ahead electricity market bidding and reserve schedules.

Therefore, a new forecasting model for one day ahead wind speed, wind direction and consequently, wind power prediction is presented in **Chapter five.** The proposed prediction models are based on linearly relating the forecasted values to their corresponding historical values in previous years within the same time period and then projects this linear model into the future. The results are compared with those of the persistent model for accuracy checking.

- **Chapter six** simulates a single auction electricity market model for power networks with embedded wind generation. The presented market model was formulated as a Nonlinear Programming Problem (NLP) and solved using the MINOS solver in the General Algebraic Modelling System (GAMS) environment. This model was used to investigate the impact of wind power variability, wind farm control strategy, wind energy penetration level, wind farm location, and wind power prediction accuracy on the total generation costs and real-time electricity market prices.
- **Chapter seven** presents the thesis summary, conclusions and recommendations for future research areas.

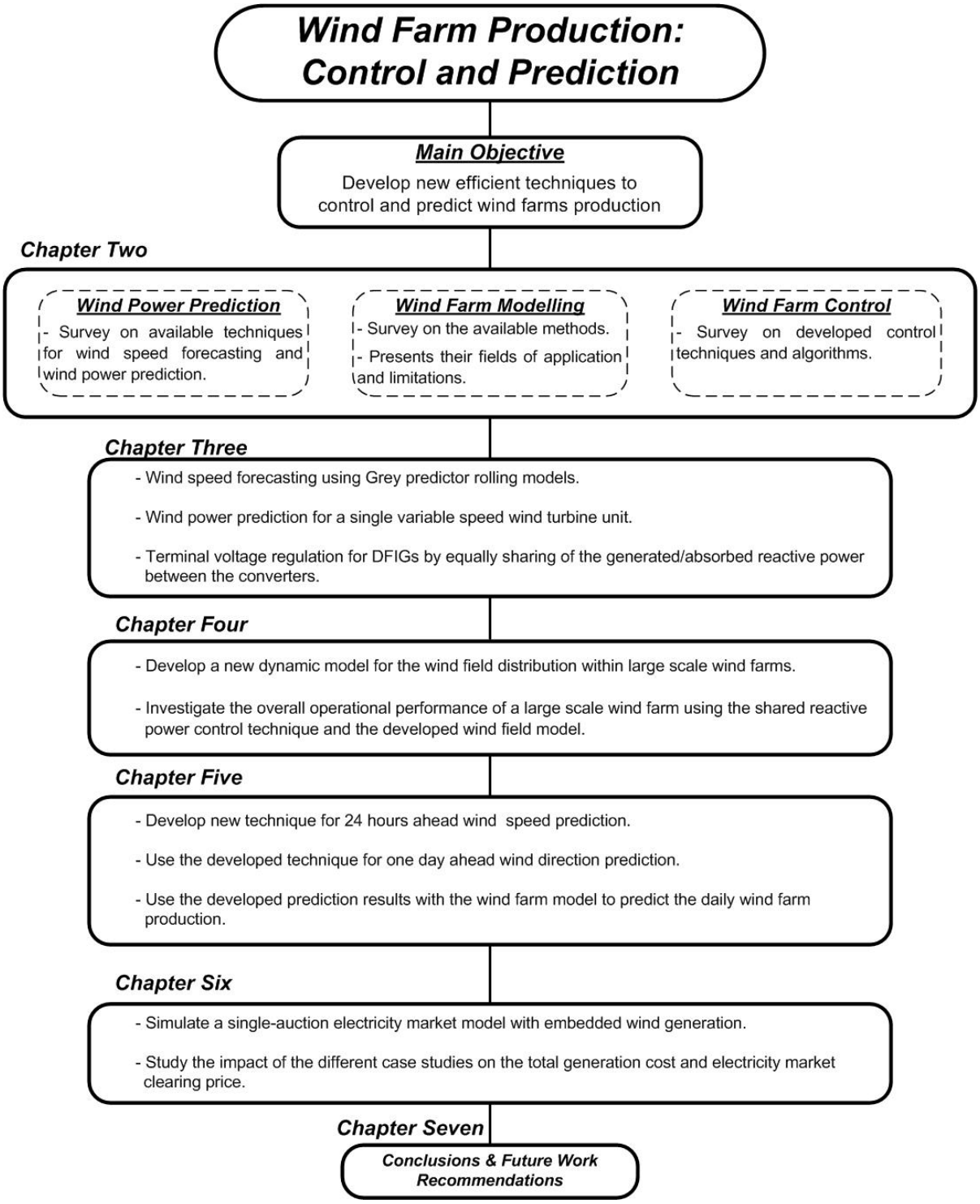

Figure 1-2: Block diagram of the thesis skeleton.

Chapter 2
Literature Survey

Wind is a form of solar energy, since it is caused by the differences in the heating levels of the atmosphere by the sun. Wind energy is captured by wind turbines that convert the kinetic energy of the wind into mechanical power. This mechanical power is converted into electricity by a generator inside the wind turbine [9]. This chapter introduces the basic anatomy of wind farms in terms of the concepts of operation of their wind turbines. This is followed by a literature survey for the main issues addressed within this thesis and they are; wind power prediction, wind farm modelling and control, and the impact of wind farm integration on the electricity market.

2.1 Wind Farm Anatomy

Wind turbines vary in their ratings from a fraction of kW to 2 MW. Turbines can operate as a single unit or few connected units to form what is known as a distributed wind system with capacities from a few kW up to 5 MW. Wind facilities work either as stand alone systems serving individual customers or as a grid connected to the power distribution network. Large arrays of wind turbines that are connected together to form what is known as wind farms with capacities that vary from 5 MW to several hundred megawatts. Usually, they are connected to the transmission system and sometimes to the distribution network [10]. The numbers of wind turbines that constitute a wind farm vary from a few turbines to several thousands of connected wind turbines. Figure 2-1 presents a block diagram for the main components of a general configuration of wind farms.

2.1.1 Wind Turbines

Wind turbines are the main components of wind farms. They are usually mounted on towers to capture the most kinetic energy. Turbines catch the wind's energy with their propeller-like blades shown in Figure 2-2. Two or three blades are usually used. These blades are mounted on a shaft to form a rotor. The main types of generators for wind turbines are; synchronous, squirrel cage induction, and doubly fed induction generators [11-16]. Permanent magnetic and switched reluctance generators are sometimes used [17-18]. Wind turbines can be used as stand-alone systems [19], or they can be connected to a utility power grid [20]. Sometimes turbines are hybrid with other resources

such as photovoltaic systems [21-22]. Brief explanations of the different types of wind turbines and their components are given in Appendix A.

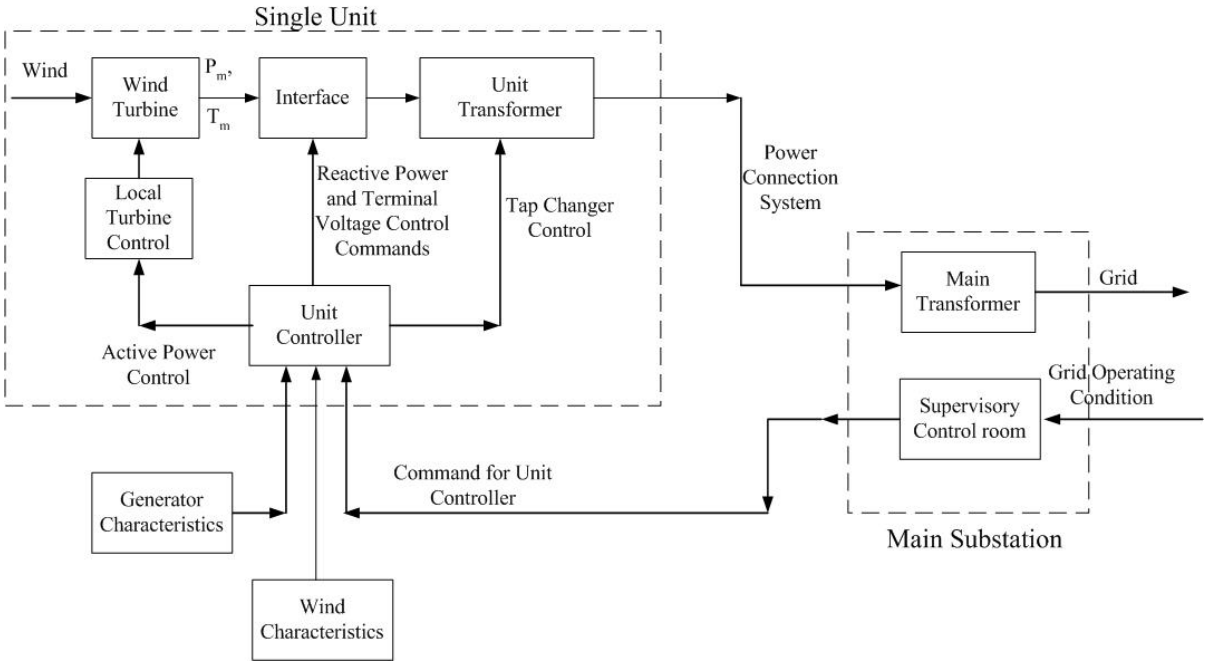

Figure 2-1: Main components of a wind farm.

2.1.2 Power Collection and Transmission System

A power collection and transmission system is required in wind farms to connect the wind turbines arrays with the other components of wind farms and to transmit the generated power to either distribution or transmission networks depending on the farm capacity and voltage level [10]. The most common configuration is that each turbine unit has a transformer connected to it. However, in some configurations, two or three turbine units are connected together to one transformer. The output power of the transforms is carried by medium voltage underground cables to an overhead or underground collection lines that transmit the power to the wind farm substation. Here, the primary transformer steps up the voltage to the required voltage level of the grid.

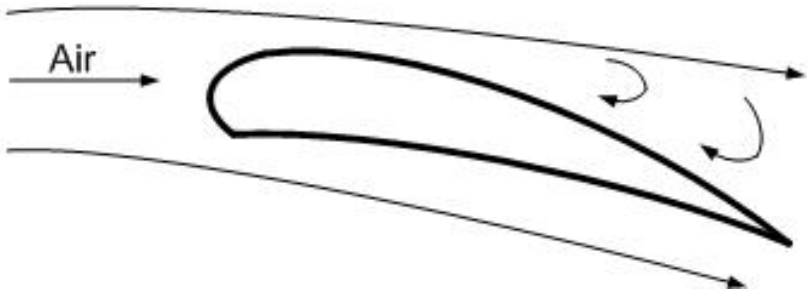

Figure 2-2: Cross-sectional area of a turbine blade.

2.1.3 Anemometers

Anemometers are either mounted on each wind turbine or on towers as high as 107 m at different locations on a wind farm. Often, each anemometer, the tower type, controls the input data for two or three turbines in order to reduce the cost of the required anemometers [23].

2.1.4 Control, Monitoring, and Communication Systems

Wind farms must be controlled in order to generate electricity when the wind speeds are sufficient and disconnected for low wind speed or very high wind speed conditions. In addition, the reactive power demand of the wind farm and the voltage at the point of common coupling must also be controlled under all operating conditions: normal, fault conditions, over-loading operation, and islanding. Generally, wind farms are equipped with two types of control systems: wind turbine control systems and a central automatic control system.

A wind turbine control system, consisting of the unit control and the local control in Figure 2-1, receives information about the wind (speed and direction), turbine temperature, vibration level, generator voltage, current and rotational speed, and the utility interconnection status. According to the received information, the turbine control system performs several control operations such as; turbine operation start or stop control, brake control for emergencies, pitch angle control for variable pitch turbines, yaw derive control for upwind turbines, generator synchronizing control for synchronous generators (where there is no interface), voltage regulation, reactive power control, and turbine transformer on-load tap changer control [23]. In some cases, to reduce the cost of the control system one control unit for two or more turbines can be used. This is known as the central control technique for multiple units. It receives data from the wind stations and the central control system of the farm to adjust several turbine units.

A central control and monitoring system is required for wind farms especially large farms with large arrays of wind turbines. Usually, this is achieved by using a Supervisory Control And Data Acquisition (SCADA) system. It allows a central computer system to monitor and control each turbine operation, as well as the entire wind farm operation. The SCADA is located in the central room, the substation of the wind farm, or even at a remote off site point. SCADA systems are capable of the following [24, 25].

1. modifying the output power or voltage of the individual units and/or the whole wind farm.
2. forcing the individual units to operate at specific modes.
3. optimizing the start up settings of the timers.

SCADA systems convey the following information.

1. wind speed.
2. number of starts, stops, and trips.
3. energy produced by each individual unit.
4. total energy produced by the farm.
5. generation time.
6. operation conditions at the trip instants.
7. trip type.
8. number of subsystem operations such as yaw drive, and breakers.
9. plot for power versus wind speed.

As for the communication system, two-ways communication signals are possible, between different wind turbines and the central control site. These systems consist of metallic conductors, microwave emitters and receivers, fibre optic cables, or carrier wave signals on the electrical power lines, depending on the system and the environmental requirements. Furthermore, a communication system with the interconnecting utility must be provided to interchange information between the wind farm and the utility operators about fault causes, durations, and wind turbine schedule outages.

2.2 Concepts of the Operation of Wind Turbines

The four concepts of operation of the currently used grid connected wind turbines are: constant speed wind turbines, limited variable speed wind turbines, variable speed wind turbines with partial scale frequency converter, and variable speed wind turbines with full-scale frequency converter [26, 27].

2.2.1 Type A: Constant Speed Wind Turbines

Usually, such turbines are equipped with squirrel cage induction generators, as shown in Figure 2-3. In this configuration concept, a gear box is used to couple the turbine shaft to the generator shaft. Such wind turbines have no pitch angle control and their rotors are designed so that their efficiency decrease at high wind speeds thus reducing the amount of mechanical power that can be extracted from the wind power. Also, compensation capacitors are used to provide sufficient reactive power for the induction machines. Sometimes synchronous generators are used, but in these cases, no compensation capacitors (and in some cases, no gear box) are required. These types lack the presence of active and reactive power control resulting in large fluctuation in the output power.

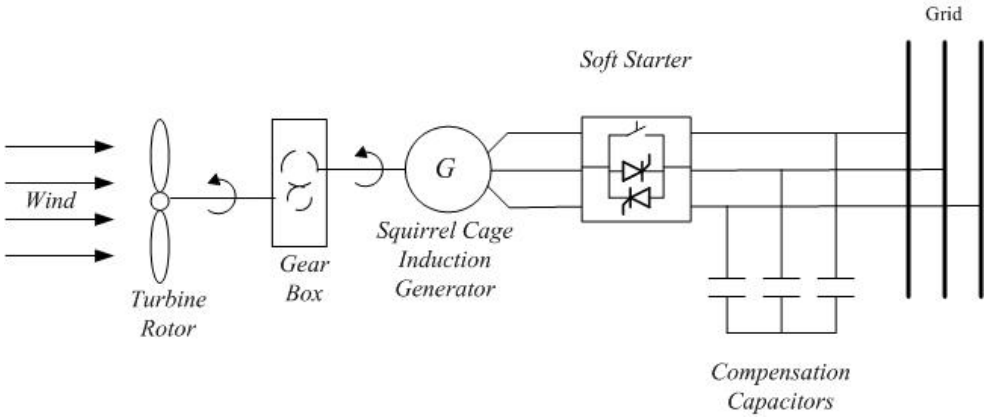

Figure 2-3: Type A: constant speed wind turbines.

2.2.2 Type B: Limited Variable Speed Wind Turbines

These types are equipped with Wound Rotor Induction Generators (WRIG) as shown in Figure 2-4**.** They are characterized by having variable additional rotor resistances that are controlled by an optical controlled converter that is mounted on the rotor shaft. By controlling the additional resistance, the generator slip is controlled. These types are referred to as OptiSlip turbines. The main drawback of these types is the power that is lost in the additional resistance.

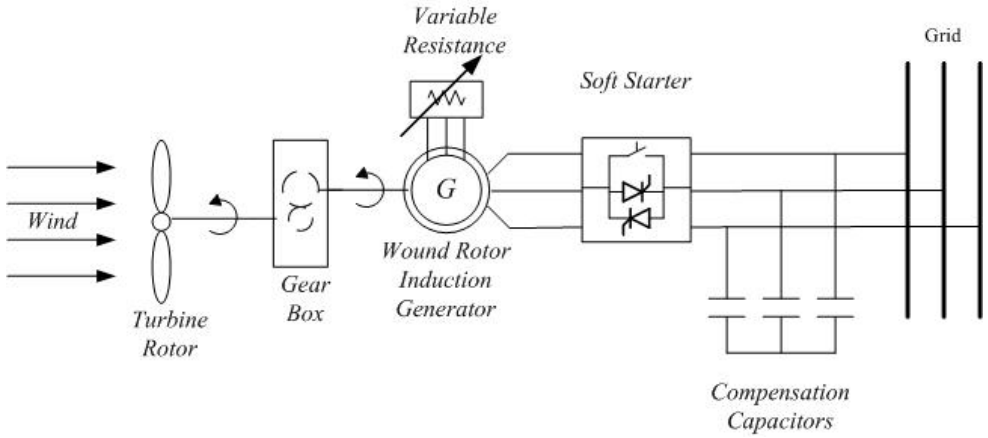

Figure 2-4: Type B: limited variable speed wind turbines.

2.2.3 Type C: Variable Speed Wind Turbines with Partial Scale Frequency Converters

These types are equipped with doubly fed induction generators as seen in Figure 2-5. In this concept, a gear box is also used. These types of wind turbines have back-to-back voltage source converters for feeding the rotor windings. These turbines have a pitch angle control to limit the power extracted at high wind speeds conditions. No compensation capacitors are used.

2.2.4 Type D: Variable Speed Wind Turbines with Full-Scale Frequency Converters

These types are equipped with direct drive synchronous generators as shown in Figure 2-6. In this concept, no gear box is used, since the synchronous generators are low speed multi-pole generators. Such types are equipped with back-to-back voltage source converters or diode rectifiers and voltage source converters to couple the generators with the grids. The pitch angle control provides a limit to the extracted power at high wind speeds conditions. In addition, squirrel cage induction generators are used with these types but gear boxes must be used and compensation capacitors may also be used.

Table 2-1 presents the development of installing the previously discussed concepts worldwide for the period from 1998 to 2002. Type A (constant speed) was the most dominant concept till 2000 when Type C (variable speed with partial scale converter) became the most dominant. Currently, in the European Union, Type C represents 45 % of the total installed capacity, compared to 30 % for Type A [27]. Consequently, this thesis is focused on studying the currently dominant type, variable speed wind turbines with partial scale frequency converters, referred to as DFIG.

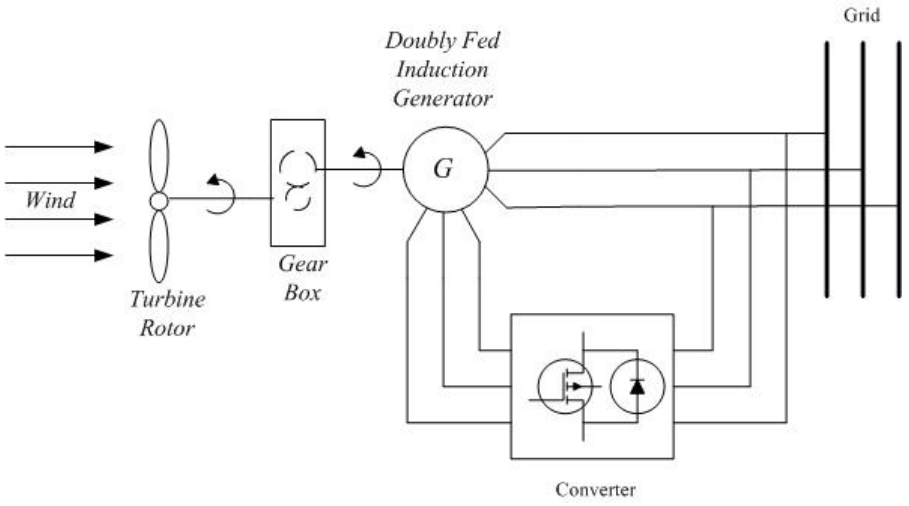

Figure 2-5: Type C: variable speed wind turbines with partial scale frequency converters.

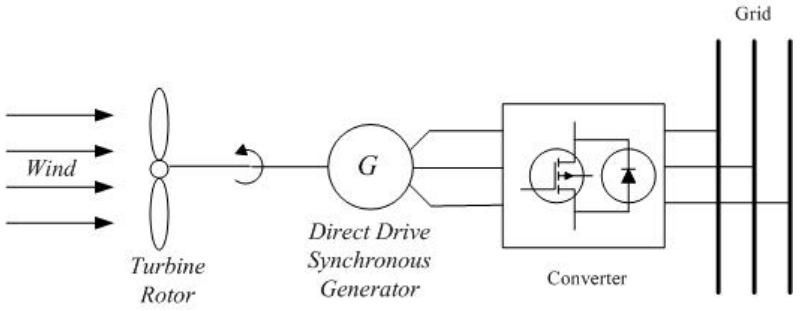

Figure 2-6: Type D: variable speed wind turbines with full-scale frequency converters.

Table 2-1: Percentage sharing of the different wind turbine concepts.

Concept	***% Share***				
	1998	***1999***	***2000***	***2001***	***2002***
Type A	39.6	40.8	39	31.1	27.8
Type B	17.8	17.1	17.2	15.4	5.1
Type C	26.5	28.1	28.2	36.3	46.8
Type D	16.1	14	15.6	17.2	20.3
Total Installed Capacity (MW)	*2349*	*3788*	*4381*	*7058*	*7248*

2.3 Wind Speed and Wind Power Prediction Techniques

Wind speed depends on temperature, pressure differences, and the terrain. Wind forecasting is essential for the power utility to schedule the connection and disconnection periods of wind farms or the conventional generators with the utility network for an optimal operational cost and a low environmental impact. Also, wind speed forecasting is crucial to simulate the output power from wind farms and to solve the load flow problems of electrical power systems with embedded wind generation [28]. This section provides a survey of the various methods for forecasting the wind speed and the wind power of wind farms.

2.3.1 Spatial Correlation-Based Methods

These techniques are based on using wind speed and data sets from neighbouring sites to the site under investigation for wind speed and wind power prediction. One of the methods is based on using a Fuzzy Expert System (FES) to forecast the wind speed and the electrical power at a wind energy conversion system site (WECS) [29]. For this method, the wind speed and direction measurements from several wind stations, installed around and in the WECS site via wireless modems to a central computer, are involved. This central computer runs the FES, which exploits any spatial correlation among the measuring stations' wind series. In this method, two genetic algorithm implementations are used and compared for training the FES. Figure 2-7presents the wind forecasting technique, based on the FES.

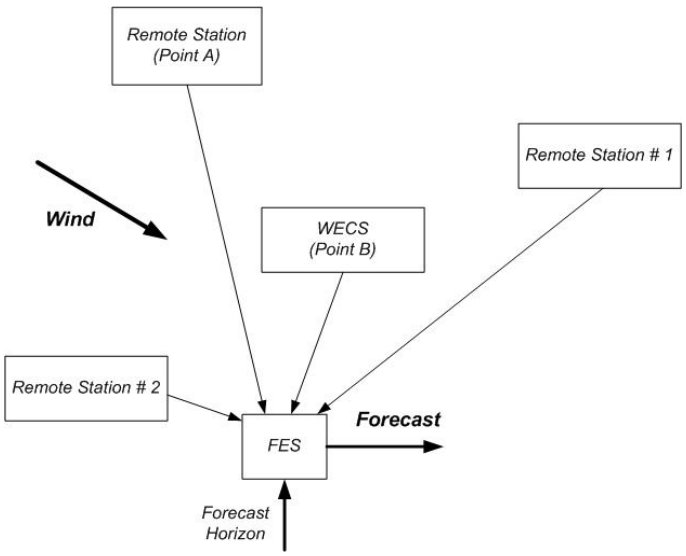

Figure 2-7: Wind forecasting system.

Another method has been developed for forecasting both the wind speed and the output electric power at a wind energy conversion system site (WECS) for a few hours ahead. The method depends on Artificial Neural Network (ANN) for forecasting [30]. This method is based on using the data of several sites to train the ANN model. The measurements are collected from sites 0.8 km to 40 km apart. Two cases were studied. The first case was a long distant one where the separation between the upwind and the downwind sites ranges from 10 km to 40 km, as displayed in Figure 2-8. Three cup anemometers are installed at the sites at a height of approximately 10 m. These anemometers are used to collect the required historical data and the ANN is trained by using two hours of previous data from all the sites with a window of 5 min; i.e. 24 data samples from each site. The outputs of the ANN are 8 forecasted values ahead with a window of 15 min.

The second case is a short distant one where the separation between the upwind and the downwind sites ranges from 0.5 km to 3 km, as shown in Figure 2-9. Pairs of anemometers are installed for two weeks to collect data with time delays shorter than 20 minutes.

Recently, advanced spatial correlation-based technique using local recurrent neural networks and advanced fuzzy models have also been developed for forecasting wind speed and wind power up to 36 hours ahead [31] - [33].

These models require sets of data from more than one site in order to achieve reasonable prediction accuracy. Moreover, these techniques are direction dependent. Consequently, wind direction data is also necessary for the accurate application of such techniques in wind speed forecasting.

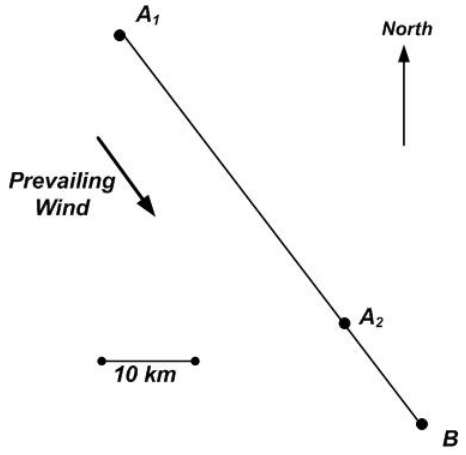

Figure 2-8: Long distant sites.

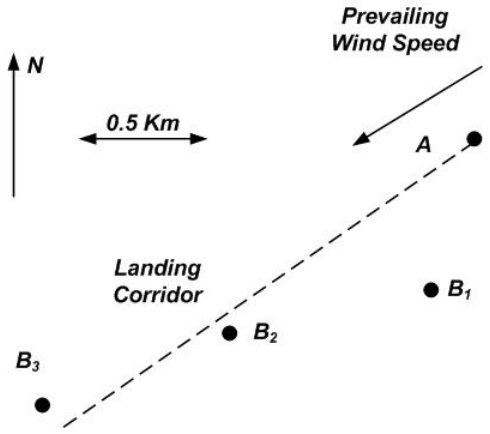

Figure 2-9: Short distant sites.

2.3.2 Time Series-Based Methods

Several time-series models have been developed for wind speed forecasting, including Auto Regressive (AR) models, Auto Regressive Moving Average (ARMA) models, and Auto Regression Integrated Moving Average (ARIMA) models. In addition, time series models based on ANN have been used for wind speed forecasting. Among these ANN-based methods, an Elman Recurrent Network (ERN), an Adaptive Network-based Fuzzy Inference System (ANFIS), a Radial Basis Function network (RBF), and a Neural Logic Networks (NLN) [34 - 39] are implemented.

These models require large sets of historical data for their parameter estimation and model training (up to weeks of recorded data). Moreover, the models have proven to be effective only for very short term predictions (a few hours ahead), especially, one step ahead prediction. Furthermore, it has been reported that ANN-based methods have some disadvantages such as; the absence of reliable theory to build the ANN structure and that the training process may be trapped in partial minimum and thus will not be able to reach the global optimization.

2.3.3 Statistical-Based Methods

Several statistical-based techniques have been reported for wind atlas preparations, the prediction of wind farms out-of-service and rated production periods, wind sites monthly and annual production, wind turbines optimum sites, predicting the performance of hybrid wind systems along with their annual production, consumption of fuel, and costs [40 - 42]. These techniques depend on analyzing historical wind speeds and wind direction data, recorded at the sites under investigation. Such

techniques are effective for economic-based studies and are not capable of hourly wind parameters forecasting.

Other types of Statistical-based techniques have been developed for hourly wind parameter prediction [43 - 44]. These techniques use online measurements and illustrative variables. Usually, they use the output of NWP especially for long term predictions which are often inaccurate.

2.3.4 Monte Carlo- Based Methods

There are two methods based on the Monte Carlo simulation for simulating the wind speed of wind farms. The first method consists of applying a series of steps to available sets of wind speeds with given Rayleih distributions and correlation matrices that are summarized as follows [45].

1. Use Monte Carlo simulation to generate wind speeds according to the Rayleigh distribution for each wind farm.
2. Subtract the mean wind speed of each wind farm from the obtained wind speed.
3. Divide the result by the standard deviation. This results in sets of uncorrelated standardized variables.
4. Use the correlation matrices formula to obtain the new values with the covariance matrix and the mean values.

The problem with this method is that if it is applied to a non-normal distribution, negative values of wind speeds are obtained which can be ignored, according to the researchers. These negative values represent 5% of the generated results for the simulation of wind speeds at seven wind farms that increases with the increased number of wind farms. Also, this method results in a different shape of the frequency distribution than that of the Rayleih distribution.

The second method depends on simulating the wind speed series by taking into account the previously obtained conditional probability in the first method. The procedure of this method as follows [45]:

1. Assume that we have n_1 numbers to represent the wind speed set for a given wind farm (farm 1).
2. Generate a random number r_1 to simulate the wind speed for a given wind farm 1 for a given hour such that $0 \leq r_1 \leq n_1$.

3. Determine the wind speed value Ur_1 to represent the wind speed for wind farm 1.
4. Count the number of times that Ur_1 appears in the set of data for wind farm 1.
5. Generate a random number r_2 to simulate the wind speed for wind farm 2 for a given hour such that $0 \leq r_2 \leq Ur_1$.
6. Determine the wind speed value Ur_2 that represents the wind speed for wind farm 2.
7. Count the number of times that Ur_2 appears in the set of data for wind farm 2 corresponding to the wind speed Ur_1 for wind farm 1.
8. Repeat for the remaining wind farms.

Similar to the first method, this method results in a different shape of the frequency distribution than that of the Rayleih distribution. Moreover, for both methods, the wind speed is assumed to be the same for all the turbine units in each farm. The first method is applied to the power network shown in Figure 2-10 to simulate the wind speed in each wind farm, and to predict the probability of occurrence of all possible active and reactive power.

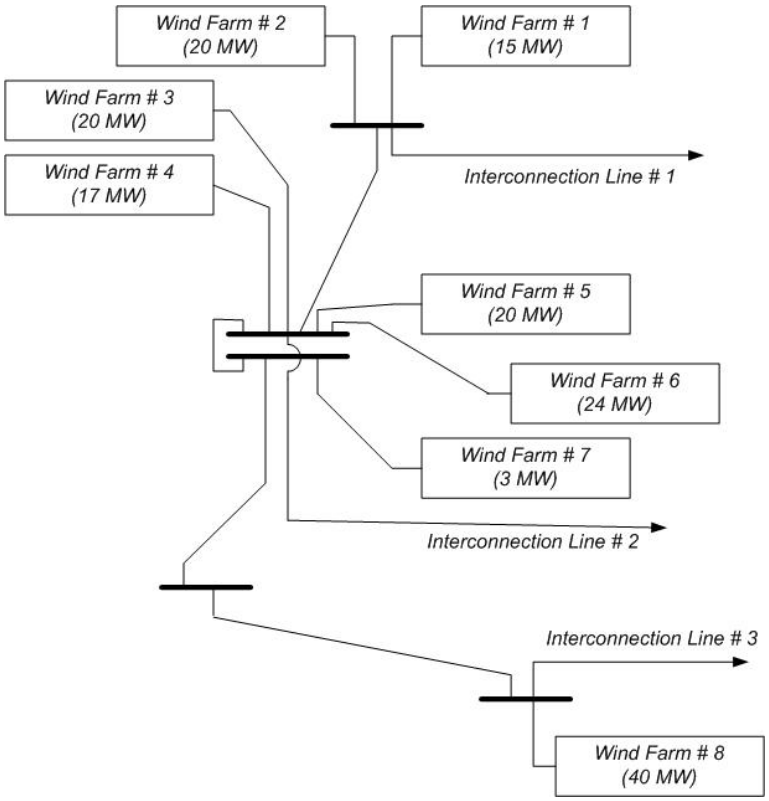

Figure 2-10: Power network under investigation.

2.3.5 Physical Power Prediction Model

Finally, several physical models have been developed that predict wind power production up to 48 hours ahead [46] – [48]. These models are based on using Numerical Weather Prediction (NWP) models, and take into consideration several factors including local surface roughness and its changes, the effects of obstacles and orography, speed up or down, local wind speed scaling within wind farms, wind farm layout, and wind turbines power curves [46, 47].

One of the developed physical models requires the use of the predictions of the wind speed from the High Resolution Limited Area Model (HIRLIAM) of the Danish Meteorological Institute, and is modified specifically for individual areas (sites of the wind farms) by using the geostrophic drag law to transform such predictions to the surface. Then the resulting surface wind speed is applied to a matrix, generated by sub-models of the WA^{S}P (Wind Atlas Application and Analysis Program) for considering some local effects such as shelter from obstacles, local surface roughness and its changes, and the effects of orography, speed up or down. The output of the WA^{S}P (found to have a root mean squared error RMSE of about 1.5 m/s in the wind speed prediction) passes through a Model Output Statistics (MOS 1) that scales the local wind speed. Then, the PARK model is used to introduce the effect of the wind farm layout (wake effect) and the power curves of the wind turbines. The output of the PARK model is corrected by the MOS 2 model. Figure 2-11 is a flow chart of the model. This approach is used to predict the wind farm power production from 0 to 36 hours ahead. The same approach has been modified and enhanced by using spatial smoothing effects to predict power production for as many as 48 hours [48].

These models have been involved in wind farms output power prediction, but are characterized by the following drawbacks [27].

- very complicated and very expensive.
- not reliable when weather service forecasts are delayed.
- generate large errors when there is a time shift between the forecast and the real data. This has been recorded to be very often the case.
- not effective for very short term prediction (few hours ahead).
- dependent on NWPs which are often inaccurate.

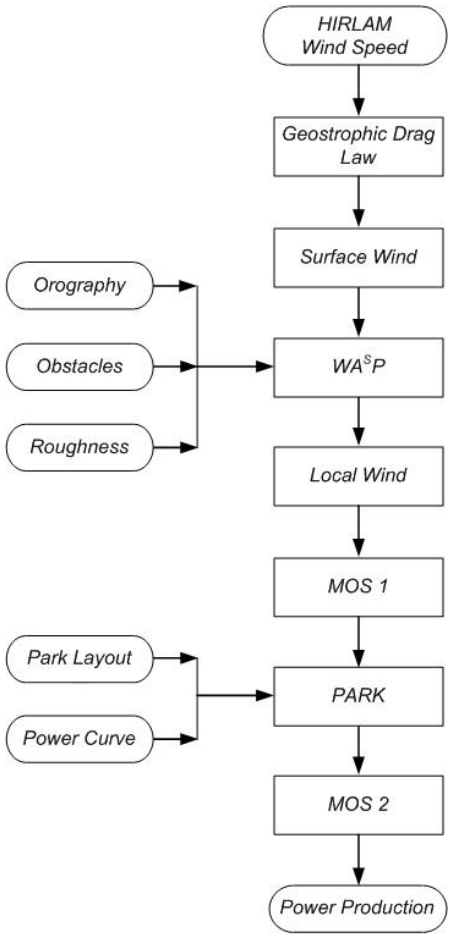

Figure 2-11: Flow chart of the physical prediction model.

2.4 Wind Farm Modelling Approaches

Wind farm modelling is necessary to investigate the performance of the farm either with a grid connection or as a stand alone system. The modelling helps in the study of the farm performance during normal modes of operation, as well as up-normal conditions such as fault conditions, islanding, voltage fluctuations and changes in the aerodynamic torque. Also, the accurate modelling of an electric grid with embedded wind farms is essential to study the impact of the farm on the grid and the dynamic interaction between the utility grid and the wind farm. During the last decade, several models have been introduced for wind farms depending on the purpose of the study. The developed models are briefly described in the following subsections.

2.4.1 Simple Third Order Model

One of the simplest models is the third order model shown in Figure 2-12. The state variables in this model are the induced rotor voltage, the angle of the rotor flux with respect to the chosen reference frame, and the rotor speed [49]. Mathematical expressions have been derived for each induction generator in the farm by using the synchronous rotating frame of reference. This model differs from the conventional model for the induction generators, proposed by Krause [50] in the fact that the Krause model is based on nine state variables, but this model ignores the stator transients. Moreover, in this developed model, the stator currents and voltages are derived directly from the flux linkages and the rotor variables.

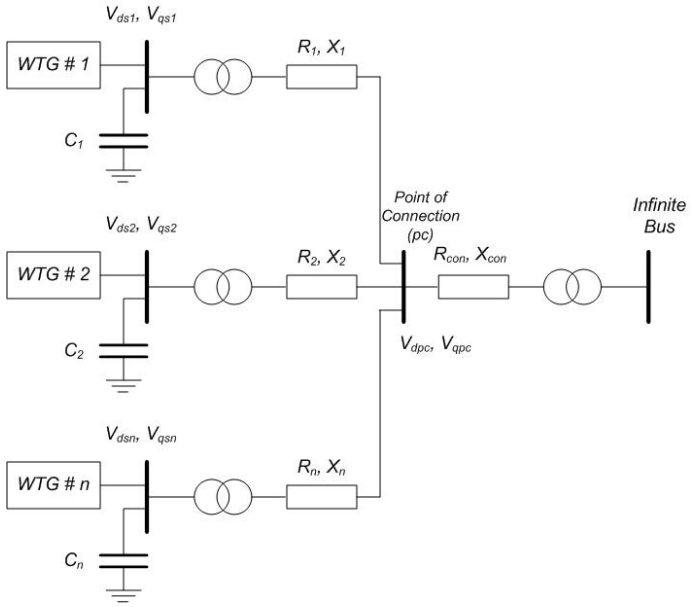

Figure 2-12: Simple wind farm third order model.

The connection of the circuit representing the wind farm is radial. Thus d- and q- axis transformations are chosen for the correction capacitors, connecting circuits, and the generators. The fourth-order Runge-Kutta method with a 1 ms time step is applied to solve this model. This model is used to investigate the dynamic performance of 500 kW and 1 MW wind turbines under various conditions such as sinusoidal oscillation in the driving torque, voltage disturbance at the network source, and frequency response. The results of the reduced model are compared and they are found to be in good agreement with the results of the traditional model proposed by [50]. However, the simulation results demonstrate only the performance of a wind turbine and not the entire farm which

indicates that it is assumed that the turbines are identical in operation which significantly simplifies the model. Moreover, the model does not include anything about the aerodynamic behaviour of the wind turbine and the model used for the turbines is the generators model only.

2.4.2 PQ and RX Models

Another approach in modelling wind farms includes the consideration of different wind speeds that cause different amounts of active power to be produced by each generator [51]. In this model, the farm is assumed to consist of *n* parallel connected doubly fed induction machines. Firstly after the model is developed for the doubly fed induction machine, the dynamic performance of this model was tested. Then, the output active and reactive power of each generator unit is calculated by the model under different wind conditions. From these power calculations, the total active and reactive powers of the farm are calculated, as illustrated in Figure 2-13.

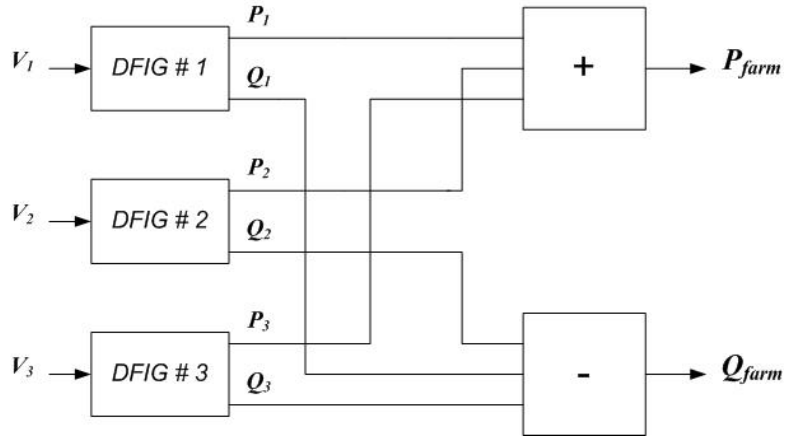

Figure 2-13: P and Q model for a wind farm.

The variation of the wind speed of each generator is simulated in two different ways,

1. a constant wind speed with different magnitudes that varies with time is assumed to be applied to each generator.
2. a sinusoidal type wind speed with different magnitudes and frequency is assumed to be applied to each generator.

In another study, the conventional PQ bus model for the wind farm is modified, where the generators' active power and the power factors are assumed and the reactive power is calculated by considering the steady state model of generators (in this study, the generators are the induction type

and assumed identical) [52-55]. The electric network is shown in Figure 2-14, and the model for the induction machines is illustrated in Figure 2-15. Here, the real power is calculated from the wind speed by using the power curves in the first iteration; then, it is assumed to be constant during the iterative simulation. As a result, the simulation is easier since the reactive power is dependent only on the buses voltages. The reactive power is calculated by one of two ways,

1. If the buses voltages are assumed constant, then the reactive power is constant and calculated from the first iteration.
2. if the buses voltages are not constant, then use the expressions relating the reactive power to the buses voltage and an iterative method (Newton Raphson).

The same study proposed another model of a wind farm, based on using the RX bus model instead of the PQ bus model. The algorithm in this model is summarized as follows [52-55].

1. Assume an initial value for the machines' slip (let it be the rated value).
2. Calculated the impedance Z.
3. Model the wind farm as an RX bus, including the admittance of the machines in the admittance matrix.
4. Calculate the voltages in the buses from the first power flow analysis.
5. Calculate the mechanical power of the turbines by computing $P_m = -I_R^2 \ R_R\left((1-s)/s\right)$.
6. Calculate the tip speed ratio and the power coefficient of the turbine, and then calculate the power extracted from the wind.
7. Compare both powers; if they are equal, then the simulation is finished; if not, modify the assumed value of the slip by solving $s_k = s_{k-1} + j^{-1}\Delta P_m$, where J is a factor depending on the machine parameters.

In this study the following assumptions are made.

1. The wind farm consists of two rows of turbines, separated by long distance to ignore the interaction between them.
2. The turbines in each row are close enough to each other to include their interactions.
3. In the case where the wind is perpendicular to the rows the wind speed is assumed the same for all machines. If the wind is parallel, then the given wind speed is considered to be the wind speed at the first machine in the row facing the wind, and the wind speed for

the rest of the machines in the row is approximated by $U_i = \{0.5/\ln(h/z_o)\}^{i}$. U_1, where U_1 is the given wind speed (wind speed at the site of the first machine), h is the hub height, and z_o is the roughness length and assumed to be equal to 0.002.

The Newton-Raphson method is adopted for the load flow analysis of the network with the wind farm, consisting of 50 identically stalled regulated WTG systems. These models are appropriate for load flow analysis. However, they are insufficient for dynamic analysis of wind farms performance under various disturbances. Moreover, the considered wake effect model is very simple and not accurate enough.

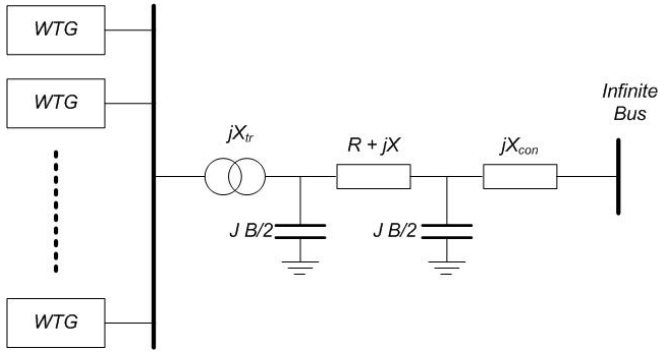

Figure 2-14: Electric network under study.

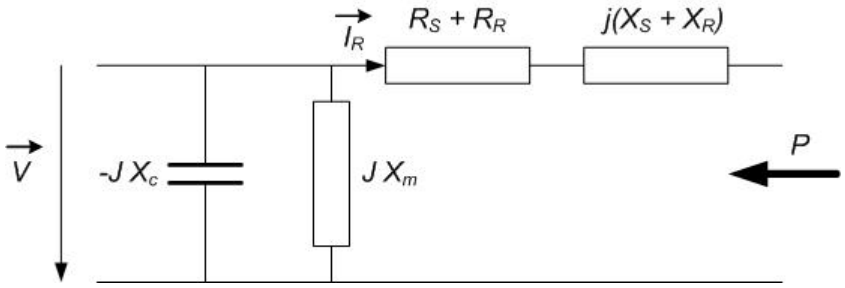

Figure 2-15: Induction machine steady-state model.

2.4.3 State Variable Matrix Model

Another model has been developed to investigate the load flow and transient stability analysis of the Cyprus power system with a small wind farm connection [56]. The Cyprus grid system is simplified to a 690 MW synchronous machine which is represented by using the synchronous rotating model. This machine represents node 1, as shown in Figure 2-16. The loads are represented by W_i and fed

through transmission line with impedance Z_{i+2}. The wind farm consists of 300 kW HAWTs, equipped with induction generators and represented by W_{n-2}. The farm is connected to the grid through impedance Z_n. A linearized model is used to model the wind farm turbines, as shown in Figure 2-17 (the wind farm aggregation effect is ignored in this model). A linearized model for the induction generator is developed by selecting the synchronous rotating frame of reference, and the overall system model is described as $\dot{x} = A_1 x + A_2 MX + BU$, where x is the state variable matrix, $MX = \Delta Im$ is the branch current matrix, $A1$, $A2$ are the matrices containing state equation parameters, and U is the control input.

These linearized models are efficient for specific operating points. Moreover, identical operating conditions for the involved wind turbines are assumed which in not realistic condition for large scale wind farms.

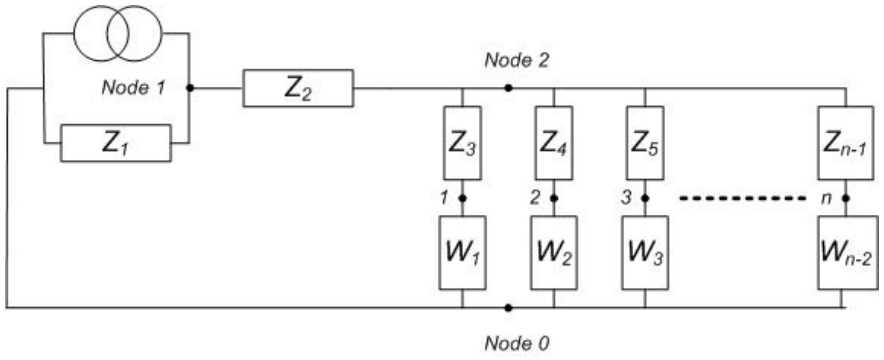

Figure 2-16: Power system with a grid connected wind farm.

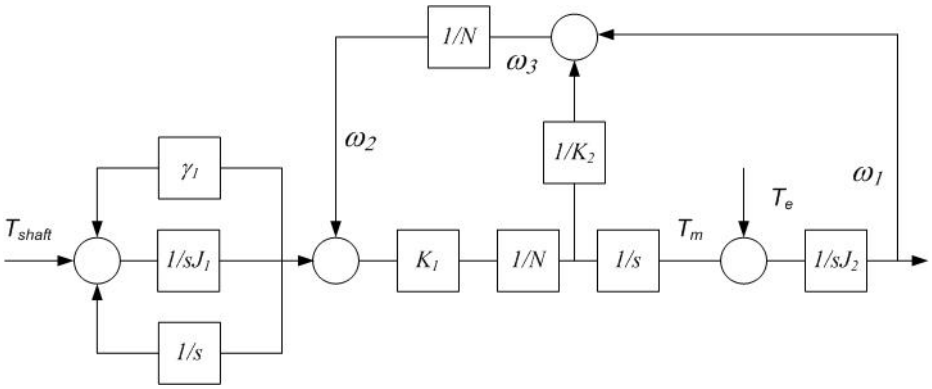

Figure 2-17: Dynamics of a wind turbine.

2.4.4 Aggregated Models

For the aggregation of wind turbines, the models of several identical wind turbines (even in the incoming wind) are combined in a single turbine model with a higher rating. The parameters are obtained by preserving the electrical and the mechanical parameters per unit, and increasing the nominal power to the equivalent of the involved turbines in the aggregation process [57 – 59].

This aggregated model reduces the computation and simulation times in comparison with the detailed model with different representations of tens or hundreds of turbines and their interconnections. However, the aggregated model requires specific care in choosing what to aggregate in order to be as close to reality as possible. In addition, this type of modelling is very difficult for wind turbines without a parallel distribution (i.e. in the form of an array which is the most common distribution for offshore wind farm, but not common for onshore wind farms).

In 2002, a structure of an aggregated model for wind farms was presented [26], and consists of the following.

1. an aggregated model for the wind speed.
2. an aggregated model for wind turbine.
3. a layout specification of the wind farm, specified by giving the x and y coordinates of each individual unit.

The main requirement for developing such a model is that it must adequately represent the behaviour of the wind farm during normal operation, as well as disturbances such as voltage drops and frequency changes. The assumptions proposed on using such model follow.

1. Neglect the impedance of the cables within the farm, since these impedances are small compared to those of the grid connections. However, the impedances of the transformers must be considered.
2. Assume the wind speed consists of a fully stochastic part that is different for each wind turbine, and a fully deterministic part which is the same for each wind turbine; however, it should be time shifted, depending on the layout of the park, the wind speed, and the angle of attack.

Figure 2-18 and Figure 2-19 represent the basic structures of the aggregated model for wind farms for constant speed or variable speed wind turbines [26]. The parameters for an aggregated model, representing a wind farm with constant speed wind turbines, are given in Table 2-2.

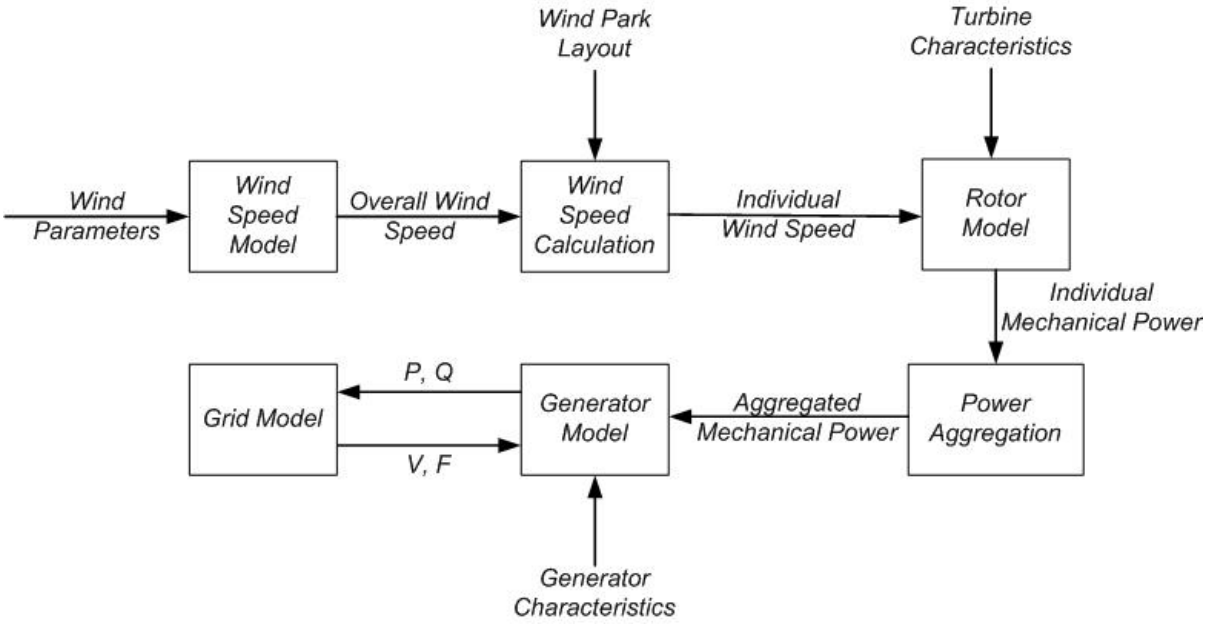

Figure 2-18: Aggregated model structure for a wind farm with constant speed wind turbines.

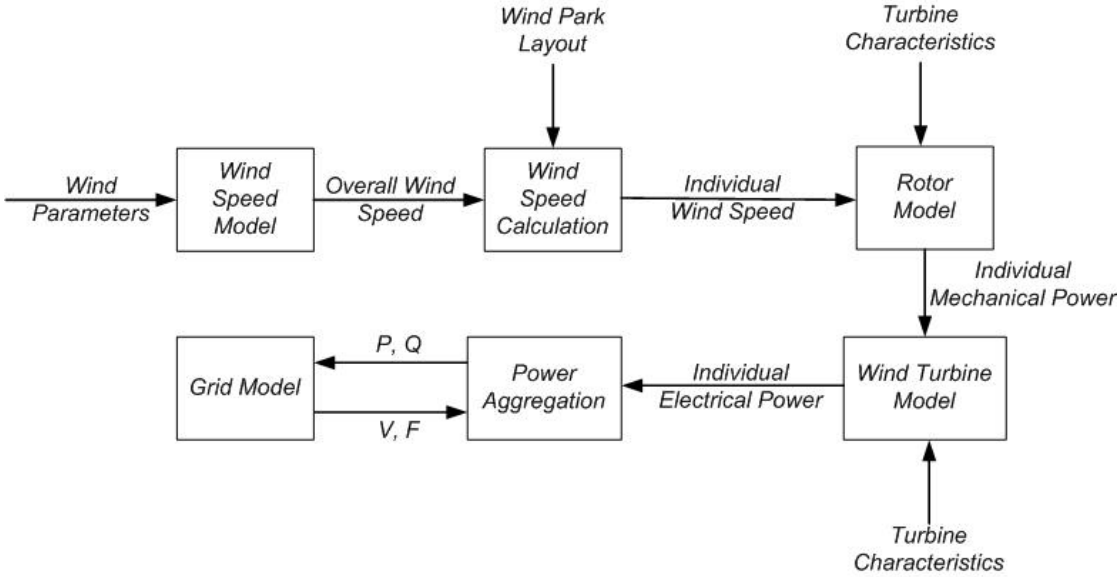

Figure 2-19: Aggregated model structure for a wind farm with variable speed wind turbine.

The parameters for the wind farm aggregated model with variable speed wind turbines are similar to those listed in Table 2-2, except that no model is required for the generator. For the individual turbine model, the parameters of the wind turbine such as minimum and maximum rotor speed, nominal power, and total inertia are required.

Table 2-2: Parameters for the wind farm aggregated model with constant speed wind turbines.

Subsystem	Parameters Required
Wind Speed Model	Measured wind speed sequence (or average wind speed value, gust, and ramp) and the direction of the wind
Individual Turbine Model	Air density, performance coefficients, and rotor diameter
Equivalent Generator Model	MVA base of the whole wind farm, generator time constants, generator inductances, rotor and generator inertia constant, and shaft parameters
Farm Layout	X and y coordination of each wind turbine

One of the approaches for the aggregated model is to consider a fixed speed stall-controlled wind farm consisting of 10 turbines. Each turbine is rated at 500 kW. The model represents a farm with one turbine model, equipped with an induction machine, and this is sometimes referred to as the single machine model. However, for this approach, it is assumed that the final turbine model has the same rating 500 kW [57]. The different parts of the wind turbine model have been developed in the form of separate modules. The wind speed is expressed in a time series, provided by the user of the wind farm. The aerodynamic torque expression becomes a function of the wind speed in the case of a fixed speed stall-controlled wind turbine since C_p is a function of the wind speed only; there is no change in the pitch angle or the rotational speed. The model for the mechanical drive train is the two mass model with a gear box assumed to be ideal. The model for the induction generator is a third order model. This aggregated model is used to investigate the impact of the wind farm on the voltage quality and the power system stability.

The last approach is modified in another study to investigate the transient stability of a fixed speed stall-controlled wind farm, composed of 36 wind turbines arranged in 3 rows, each with 12 turbines [58]. The incoming wind speed is assumed to be constant during the simulation and perpendicular to the rows. The value of the wind speed of the incoming wind represents the wind speed of the first row, and the values decrease by 10 % from one row to the next in the direction of

the wind. Thus, the aggregated model of the wind farm consists of 3 turbines; each turbine representing the aggregated model for the turbines in a given row. The resulting model configuration is given in Figure 2-20. The model of each equivalent wind turbine comprises an aerodynamic torque, drive train, and induction generator model that are modeled as explained in the last approach.

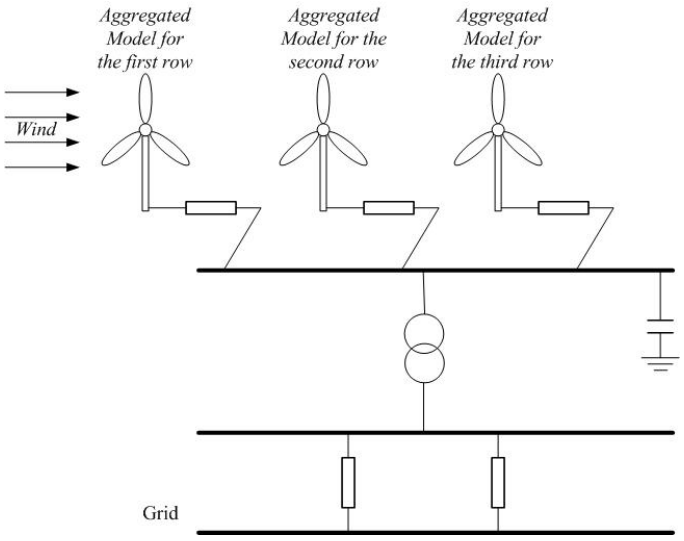

Figure 2-20: 3 turbines aggregated model.

2.4.5 Detailed Model

One of the detailed models was developed for a Danish wind farm of 6 identical wind turbines, identical in parameters and operating conditions, with a 2 MW capacity, connected to the grid as shown in Figure 2-21. The purpose of this model is to study the power quality impact, such as reactive power, power variation, and flickers, of the wind farm on the Danish power system under normal operating conditions [60]. The model was devised by the dedicated power system analysis tool, DIgSILENT. This model consists of models for the grid to which the turbines are connected, models for the electrical and mechanical components of wind turbines, including the aerodynamic aspects, and the wind speed model. The generators are induction generators. Figure 2-22 offers the block diagram of the simplified electrical model of the wind turbine, including the control block, starter, capacitor bank, and transformer. The model for the mechanical parts of the wind turbine is presented in Figure 2-23. The aerodynamic model is represented by the aerodynamic power equation. The wind speed model consists of two parts: a hub wind model that is used for modelling the fixed wind speed at the hub height and a rotor wind model, where the averaging of the hub wind speed over

the whole rotor, the rotational turbulence, and the tower shadow effect are considered. Similar operating conditions for all the turbines are assumed. Thus, the simulation results are carried out for only one turbine and compared with the measured values from the Danish wind farm and found to be in good agreement. However, this assumption is not valid for large scale wind farms.

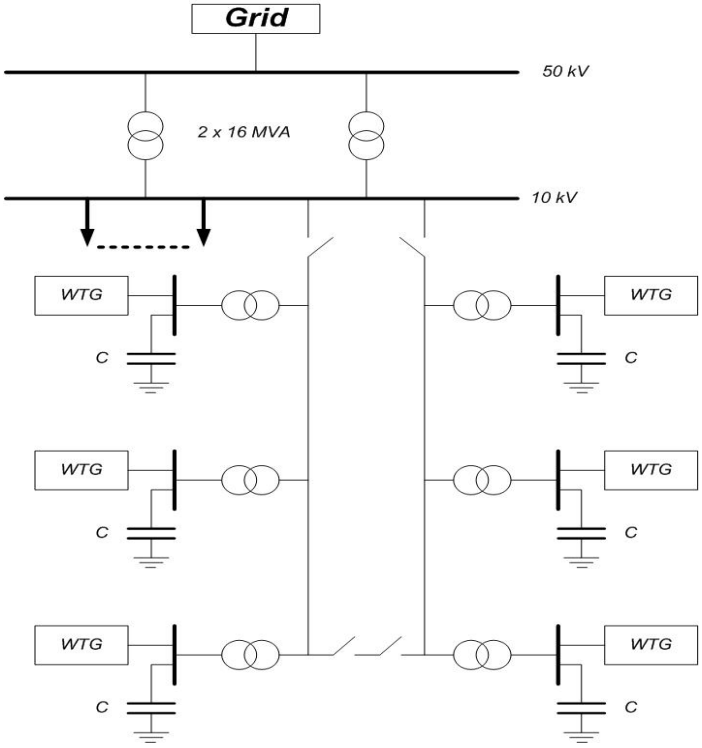

Figure 2-21: Network under investigation.

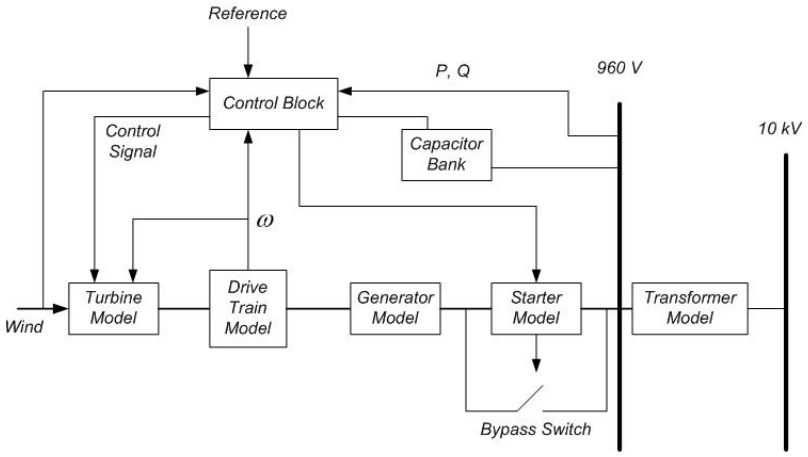

Figure 2-22: Wind turbine model.

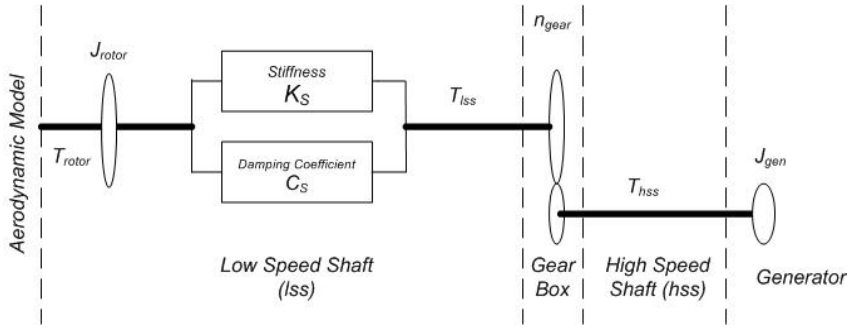

Figure 2-23: Mechanical components model.

Another approach has been used to investigate the importance of the wind turbines' mechanical system on the power system. The off-shore wind farm under investigation consists of 72 identical 2 MW wind turbines, arranged in 6 rows and each row consists of 12 turbines [61, 62]. The model for representing each wind turbine is given in Figure 2-24. A fifth order model is used for the involved no-load compensated induction generators, and the model of the wind turbine shafts is also included. Two assumptions for the wind speed are separately investigated. The first assumption is that a regular wind distribution exists within the wind farm, and that the wind turbines have the same operating point with a subjected wind speed of 12 m/s. The second assumption is based on the irregular wind distribution within the wind farm with an incident wind speed of 14 m/s at the sites of the wind turbine group facing the wind, and reduced by 0.5 m/s from one group to another in the direction of the wind. In the second assumption, two directions of the wind are investigated: perpendicular to and parallel to the wind turbines rows. The goal of this study is to compare the performance of the wind farm and the effect of the wind turbine shaft stiffness by using different wind farm models: detailed, aggregated (multi-machine), and single machine models. The PSS/E dynamic simulation tool is used to develop this model.

It is worth mentioning that, for large scale wind farms, developing such models will very difficult.

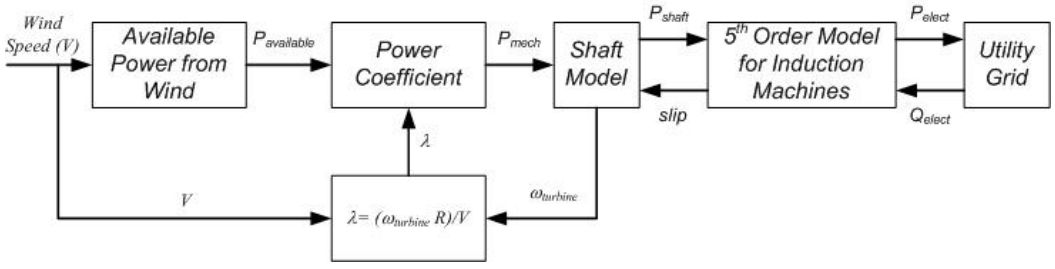

Figure 2-24: Wind turbine model used in the detailed wind farm model.

2.5 Wind Farm Control Techniques

Several schemes and techniques have been developed to control the active and reactive power flow to and from a wind farm via the interface between the wind farm and the utility grid. This section is a literature survey of the various control techniques, algorithms, and the regulators and compensators for the voltage regulation and the reactive power control of wind farms.

Among the proposed schemes, those dealing with the generator controllers such as the scheme that proposes the utilization of the rotary frequency converter for the interconnection between the doubly fed induction generators and the power system grid [63, 64].

2.5.1 Remote Voltage Control Techniques

Researchers have proposed a voltage control system to reduce and improve the impact of the dispersed generation such as wind farms on the distribution network [65]. In this study, the standard voltage level for the French network, 230 V +6 % -10 % for low voltage and 230 V +5 %, -5 % for medium voltage, is used. The impact of the generators on the voltage levels for medium voltage feeders depends on the generator power and the feeder loading (customer voltage levels). A new voltage control function has been developed to manage the voltage regulators of the substations transformers and the reactive power of the generators. This function checks the calculated voltage levels on the network periodically such that they do not exceed the limits (over voltage and/or voltage drops limits). Then, the function searches for an optimal combination of the on-load tap changer voltage level at the substation and the generator reactive power level. This function allows remote voltage regulation. However, to determine the voltage constraints, load flow calculations are required. Thus, this voltage regulation function depends on the results of the FACE (Advanced Function of Electrical Calculation) that depends on a back-forward sweep algorithm to analyze the load flow.

In this study, it was concluded that it is necessary to adapt the electric network by allowing the dispersed generators (wind farms) to communicate with the distribution control system. As a result, the FACE and the voltage regulation functions are provided with the required measurements for the voltage, and active and reactive power. Also, the remote terminal points (farm generators and substation transformer) should be adapted to receive set point values. The layout for the process is illustrated in Figure 2-25.

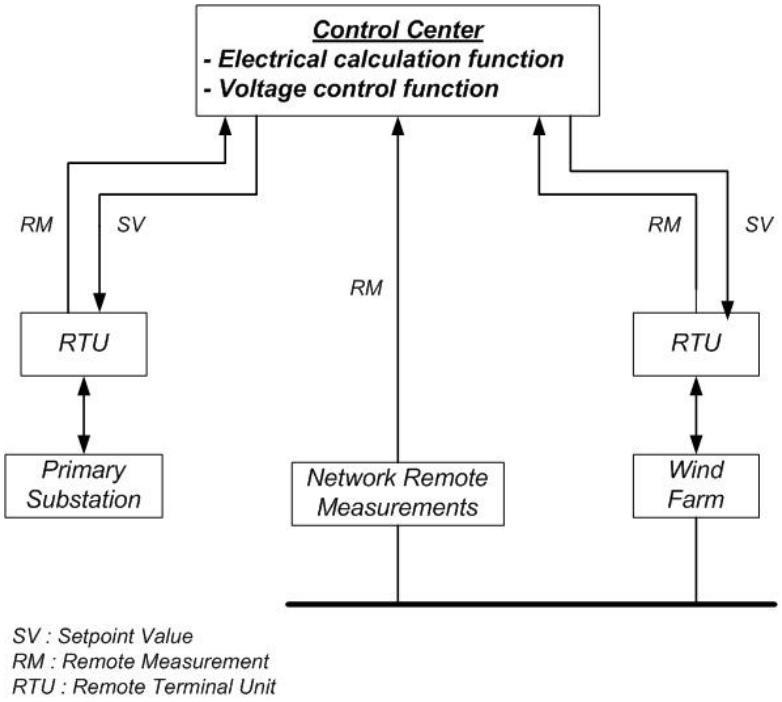

Figure 2-25: Process layout.

2.5.2 Supervisory Control of DFIGs based Wind Farms

Controlling the active and reactive power of the total wind farm is achieved by regulating the active and the reactive power of each machine separately [66-69]. A control technique that is derived from two cascaded control loops has been proposed. It is based on stator flux oriented vector control of Doubly Fed Induction Machines (DFIMs). In this case, the set point of the active power depends on the wind speed and that for the reactive power is fixed and determined by the network. The analysis and fixation of the limits of active/reactive power generation is pivotal for avoiding the thermal disconnection of the DFIM. These limits are established by including the machine and the converter limits in the form of limit curves. Once the references of the active and reactive generation are determined, the control law is designed by a control algorithm, implemented in a microprocessor that has the capability to follow the rapid changes in the references. The development of the algorithm is explained in the flow chart in Figure 2-26.

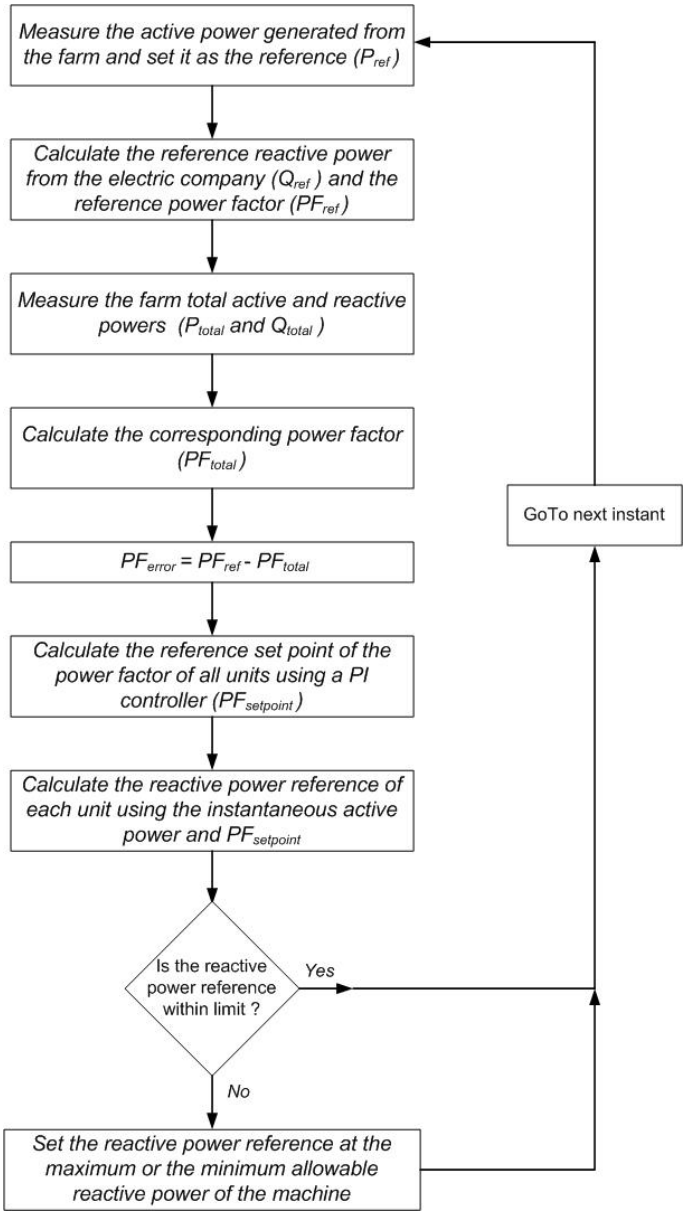

Figure 2-26: Flow chart for the reactive power algorithm.

The previously mentioned algorithm was modified in 2002, where the power factor angle is calculated instead of the magnitude of the power factor as in the previous algorithm [70].

This system has been studied once more by using a new algorithm, known as the stator flux oriented vector control algorithm, represented by the flow chart in Figure 2-27 [71-73]. The algorithm is designed according to the following rules.

1. The active power is calculated from the wind speed instantaneously.
2. The total reactive power is calculated from the active power and the desired power factor.
3. The reference currents for the rotor side (i_{rxref} and i_{ryref}) are obtained by activating a PI controller (for the active and reactive power).

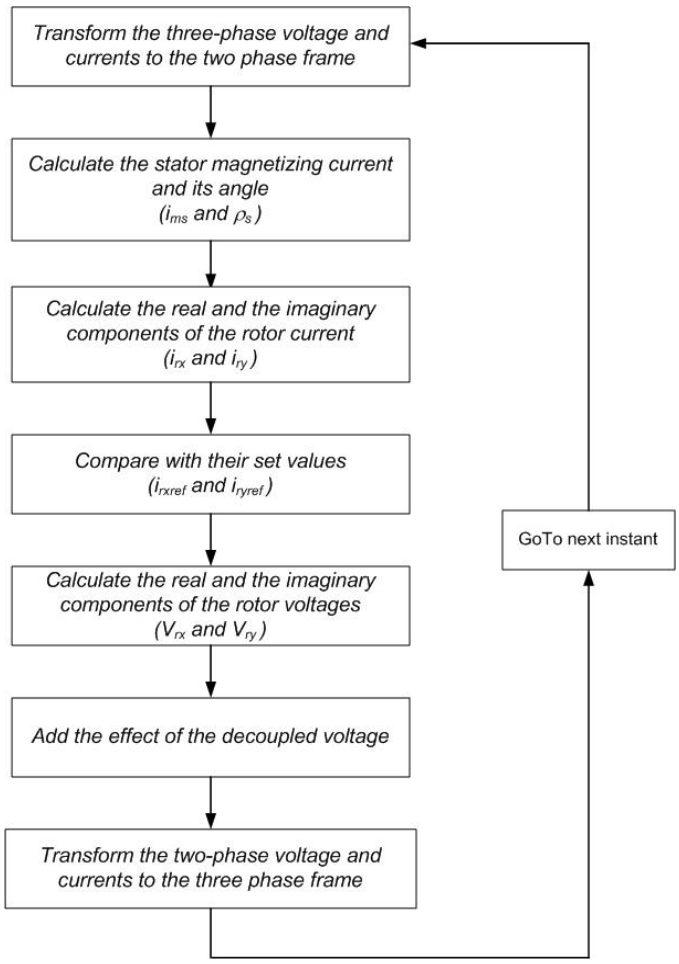

Figure 2-27: Flow chart for the stator flux oriented vector control algorithm.

Another integrated control system of wind farms has been developed [74]. The wind farm for investigating the validity of such control system was the Yerga wind farm in Spain. The farm layout consists of 37 variable speed pitched control wind turbines, equipped with doubly fed induction generator. The farm's total rated power is 24.42 MW. The local control system of each unit consists of two converters. The first converter is the rotor side converter (RSC) that controls the rotor current in

the stator flux frame reference to control the torque and the reactive power of the unit. The second is the supply side converter (SSC) which is a current-controlled PWM inverter to regulate the delivered/drawn rotor power to/from the grid. A block diagram of the control system is provided in Figure 2-28 and consists of the following blocks.

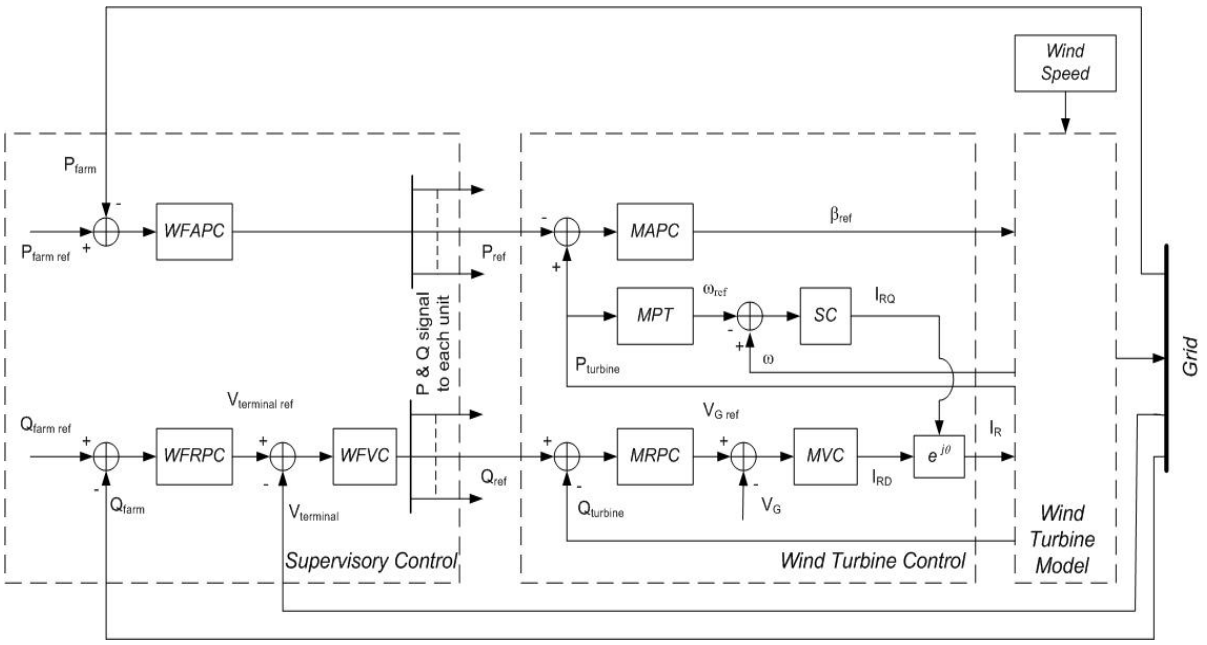

Figure 2-28: Control system block diagram.

- WFAPC: (Wind Farm Active Power Controller) To control the total active power of the wind farm and to generate the active power reference for the local units.
- WFRPC: (Wind Farm Reactive Power Controller) To control the total reactive power of the wind farm, to compute the reactive power error, and set up a voltage level reference at the wind farm substation.
- WFVC: (Wind Farm Voltage Controller) To compute the voltage error and set up a reactive power reference for each machine's reactive power controller.
- MVC: (Machine Voltage Controller) To compute the voltage error and set up an excitation current reference for the machine excitation current controller.
- MPT: (Maximum Power Tracking block) To ensure that the rotation speed maintains it optimum value.
- SC: (Speed Controller) To ensure that the rotation speed maintains its reference value.

- MRPC: (Machine Reactive Power Controller).
- MAPC: (Machine Active Power Controller).

2.5.3 Static VAR Compensators

The Advanced Static VAR Compensator (ASVC) has been introduced to control the reactive power of a wind farm [75]. The network with these types of compensators is shown in Figure 2-29. The ASVCs provide the reactive power requirements for the wind farm under different operating conditions. Also, ASVCs prevent over voltage under islanding conditions, unless the total reactive power in the network is less than that of the ASVCs capacities. In this study, three-level converters were used. These converters operate in a Selective Harmonic Elimination Modulation (SHEM) mode with a twelve pulse configuration.

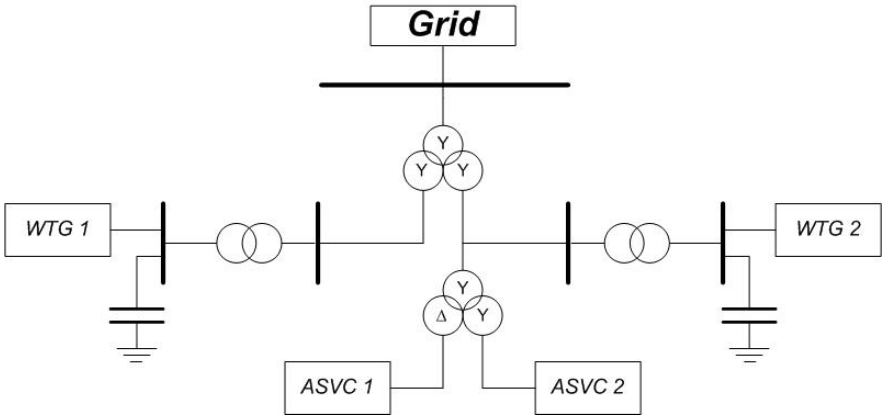

Figure 2-29: Network configuration.

2.5.4 STATCOMs

STATCOMs have been widely applied on wind farms. A technique strategy, based on a Unity Power Factor (UPF) strategy, is developed to control a STATCOM connected to a wind farm bus-bar, as shown in Figure 2-30 [76]. The UPF strategy depends on making the power factor at the connection between the wind farm and the distribution network equal to unity; thus, no reactive power flows between the farm and the network. This strategy is based on successive iterations between an AC load flow program and an algorithm for determining the STATCOM voltage setting, as exhibited in Figure 2-31. This strategy does not include the consideration of the power losses. To overcome this problem, another technique has been developed by using the Optimum Power Flow (OPF) analysis program to minimize the power losses by adjusting the STATCOM voltage level, as illustrated in Figure 2-32.

When the two techniques are compared, the results show that the increase in the power losses for the UPF strategy is not very significant (about 3 %) [72]. In this analysis, the STATCOM losses are ignored (< 10 % of the total network losses) [76].

Another case has been suggested to compare the two strategies, UPF and OPF. In this case, a critical condition, a high wind condition and light loading of the system, is examined. The UPF strategy amplifies the voltage rise unless the STATCOM is controlled to act as a reactive power sink. Also, the OPF strategy can regulate the voltage at the point of connection, accompanied by an increase in the network losses.

Another approach uses the STATCOM with a UPF technique [76]. In this technique, the STATCOM supplies the farm with the required VAR up to 4.5 MVAR beyond which the reactive power supplied to the farm remains constant, and a voltage control technique with a PI controller is used to maintain the voltage at the connection point. This approach is investigated under islanding conditions and normal operation with a mitigation technique for voltage fluctuation, resulting from passing the turbine blade of the turbine tower. Also, the last case has been simulated by applying a pulsating torque to the turbine with a magnitude variation of ± 20 %. However, in the results, the rotor speed increases continuously till the end time of the simulation which indicates that the system is unstable.

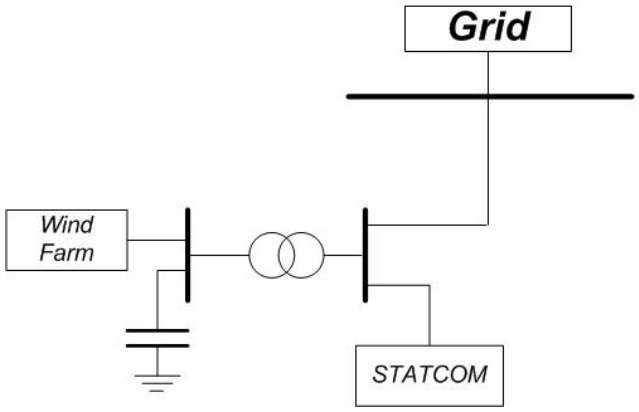

Figure 2-30: Network connection.

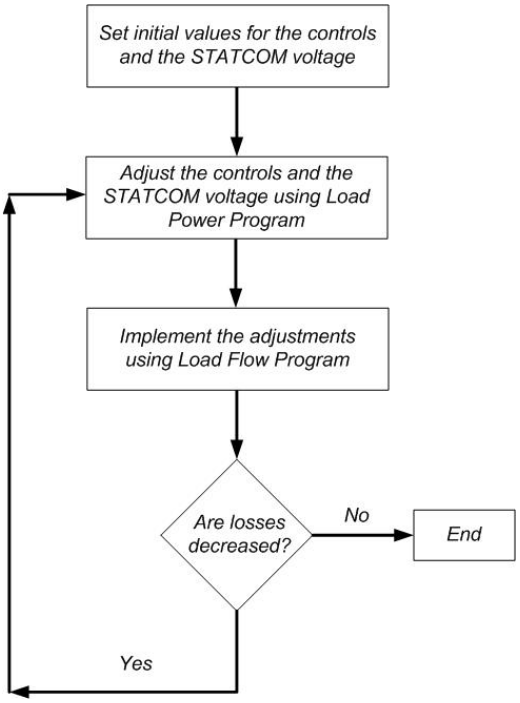

Figure 2-31: UPF algorithm.

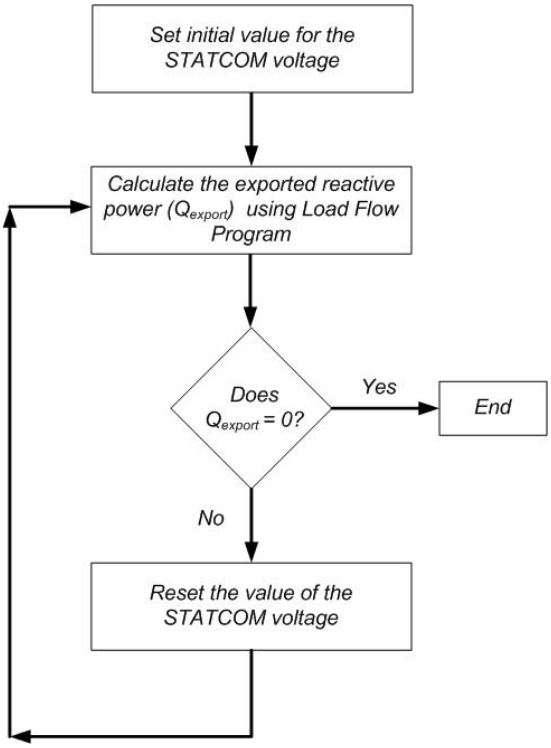

Figure 2-32: OPF algorithm.

Another application of the STATCOM for reactive power compensation is the wind farm installed in Western Denmark (Rejsby Hede wind farm) [77]. This farm consists of 40 wind turbines each with a 600 kW capacity, as illustrated in Figure 2-33. The control system is a multiprocessor configuration that has a sampling time of 1 ms. The control scheme, in Figure 2-34**,** consists of the following blocks.

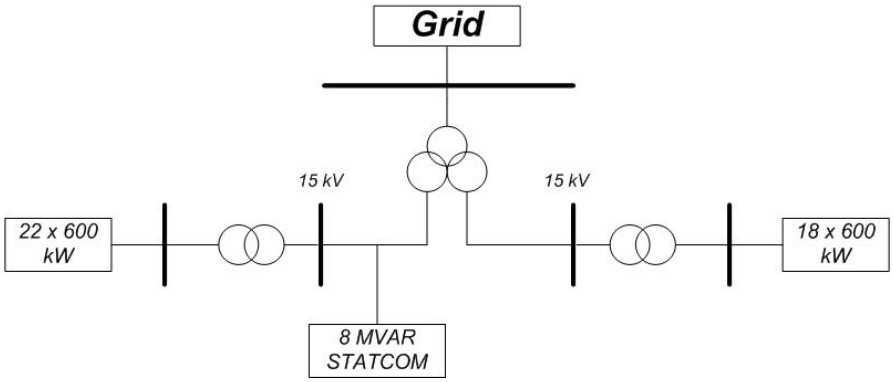

Figure 2-33: Network under investigation.

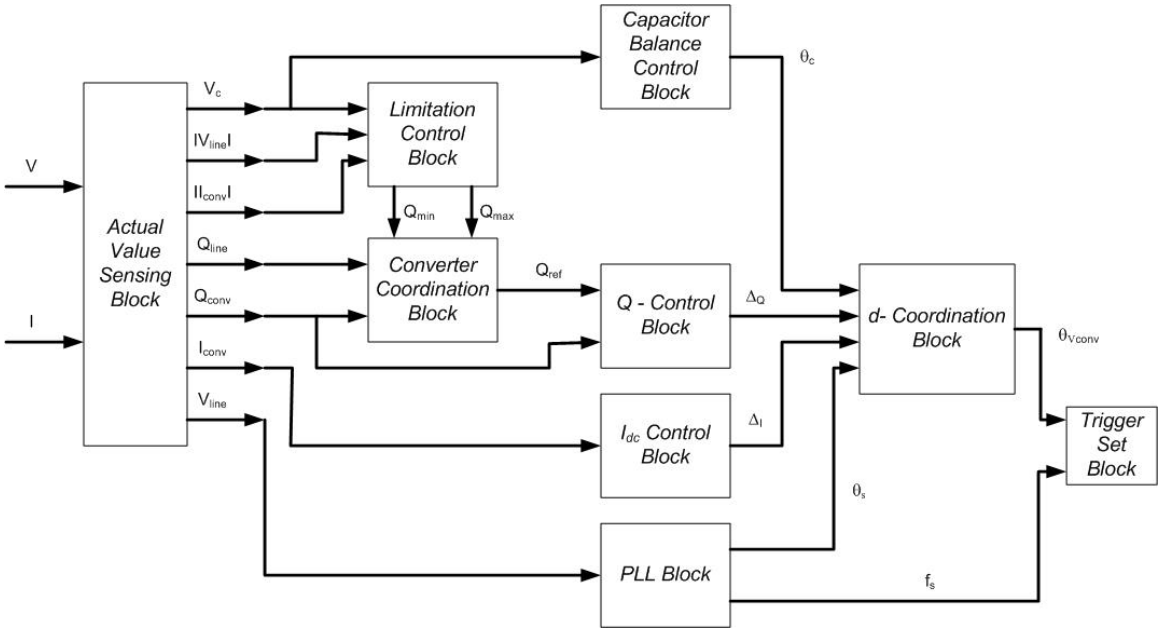

Figure 2-34: Control scheme.

- Q-Control: To determine the required reactive power output of the STATCOM by using the input reference value and the instantaneous value for the reactive power.

- PPL (Phase Locked Loop): To calculate the phase and frequency information of the bus bar fundamental voltage.
- D-Coordination: To produce the voltage phase angle of the required converter voltage space vector for the trigger set.
- Converter Coordination: To calculate the actual reactive power output of the wind farm and determine the reactive power reference.
- Trigger Set: To generate the switching signals for the GTO thyristors.
- Limitation Control: To determine the maximum and the minimum limits for the reactive power.
- Capacitor Balance Control: To take care of balancing the capacitor voltages.
- Actual Values Sensing: To process the input quantity of the STATCOM control.
- I_{dc} Control: To detect and control the DC component in the converter line voltage.

2.5.5 PWM-VSCs

The Pulse Width Modulated - Voltage Source Converter (PWM-VSC) is one of the devices to control wind farm outputs. Here, the feed-forward and feed-back control is employed to activate the four terminal PWM-VSC, as illustrated in Figure 2-35. Figure 2-36 displays the network connection under study. The control scheme consists of the following blocks [78-79].

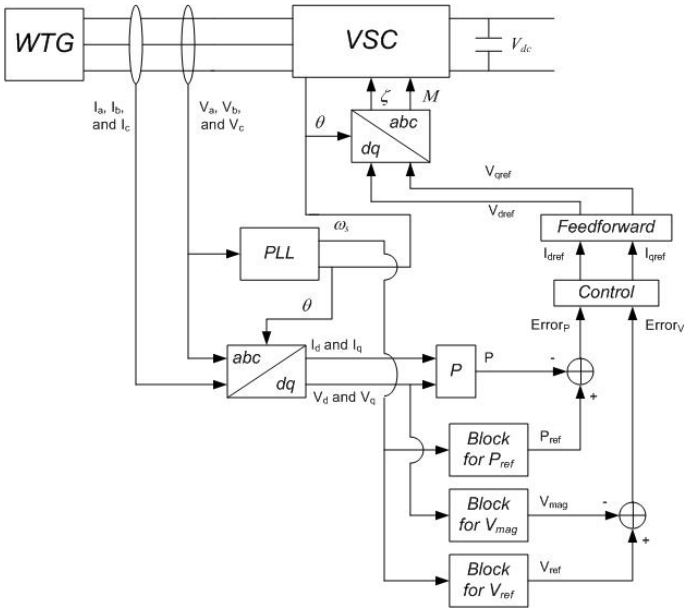

Figure 2-35: Feed-forward and feed-back control.

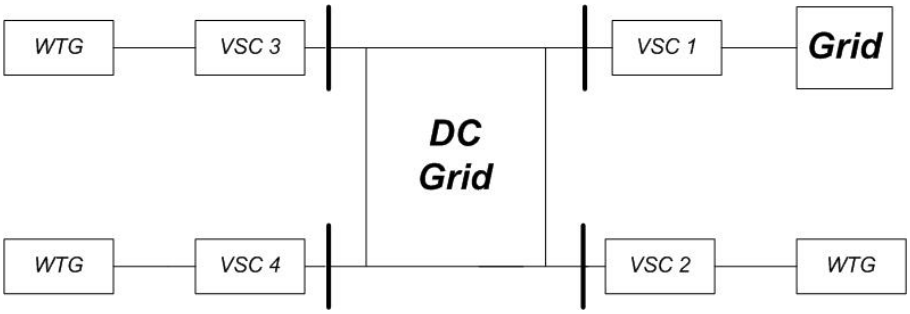

Figure 2-36: Network connection.

- Phase-Lock Loop: To measure the angular frequency of the turbine generator ω_s from the three phase voltages, and produce the time integral $\theta = \omega_s t$ (or the angle of the PLL).
- a-b-c to d-q Transformation: To transform the voltage and current measurements from the a–b –c frame to the d –q reference frame.
- Current Source Controller: To track the current references (i_{dref} ,an i_{qref}) so that during short-circuit faults the currents do not exceed the references.
- Feedback Control of AC Voltage Magnitude: To null the error between the measured value of the magnitude of the AC voltage and its reference value by i_{qref} in the negative feedback (PI).
- Feedback Control of Real AC Power: To null the error between the measured value of the the AC power and its reference value by i_{dref} in the negative feedback (PI).
- Inverse d-q to a-b-c Transformation: To transform the voltage and current measurements from the d-q frame to the a-b-c reference frame.

The function of each PWM-VSC is to control the wind turbine speed and to match the synchronous generator voltage magnitude to the DC bus voltage. To achieve such a target, the control scheme is designed so that at any wind speed, the electromechanical torque is equal to the mechanical torque, and both are equal to the optimal (maximum) torque corresponding to that speed. This is accomplished by using T_e, T_m, and $T_{opt.}$ versus the ω_m curves that must intersect at one point for any given wind speed.

An additional PWM-VSC (VSC 1) is used. This converter operates as an inverter and regulates the DC voltage level by balancing the drain DC current with the injected DC current by the wind turbines. Any unbalance results in the charging current of the DC bus capacitor. Also, this inverter

must automatically make the aggregated wind power available to the grid. In the feed-back control loop for the VSC 1, the measured value is the DC bus voltage and this is compared with its reference value to obtain the error signal which is applied to the power control of the VSC 1.

The same study has been repeated by using a wind farm, consisting of induction generators and the LVDC transmission instead of the HVDC transmission [80-81]. Figure 2-37 presents the control loop for the VSCs that are used to regulate the speed of rotation of the induction machines.

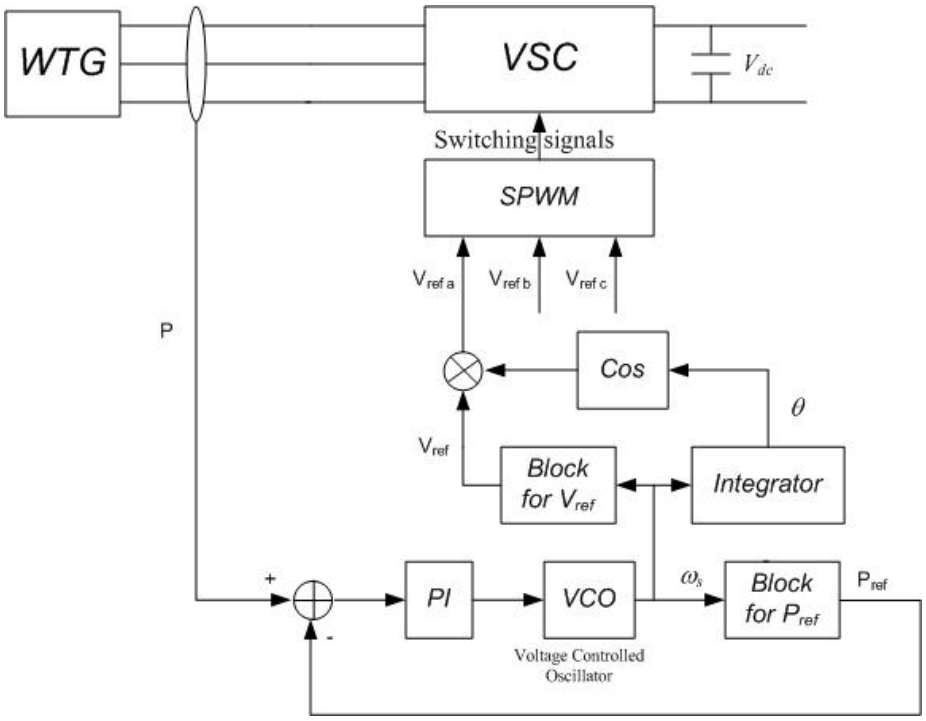

Figure 2-37: Feed-forward and feed-back control.

2.5.6 TCRs

Another approach proposes the use of a combined system of a capacitor, a thyristor controlled reactor (TCR) and a small-rated active filter (PWM-VSI) [82]. The configuration of the proposed system is presented in Figure 2-38. The goal of this approach is to regulate the wind farm reactive power. This configuration results in reducing the harmonic content of the currents and avoiding the possibility of resonance. However, the study is based only on a harmonic investigation without any further dynamic analysis for the wind farm behaviour.

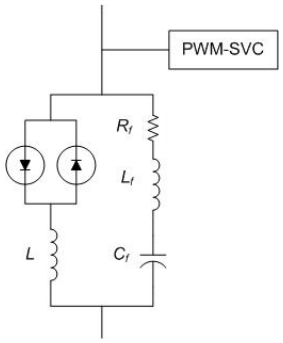

Figure 2-38: Configuration of the TCR system.

2.5.7 UPFCs

Other investigations introduce the usage of the Unified Power Flow Controllers (UPFC) for wind farm applications. One study uses a UPFC together with a dump load to investigate and test the transient and frequency response of a wind farm, consisting of 5, 300 kW, 3-blade HAWT [83]. The purpose is to ensure that the voltage, reactive power generation, and harmonic levels are within the limits during the farm operation. Also, the study includes the farm performance during islanding conditions. The simulation is carried out by using a behavioural programming tool called SABER with a programming language called MAST. The schematic diagram for the wind farm with the UPFC arrangement is given in Figure 2-39.

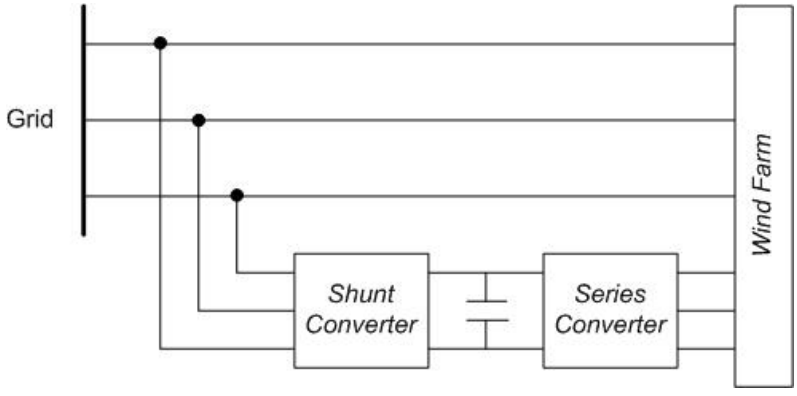

Figure 2-39: Wind farm and UPFC network.

The UPFC has also been investigated to provide wind farms with the required reactive power to maintain the voltage level [84]. In this research, the series branch of the UPFC is controlled via a

Fuzzy Logic Controller (FLC) and the shunt branch is controlled via a PI controller. The wind farm construction is similar to the one described in the previous paragraph, and the control scheme algorithm is summarized as follows:

1. The wind farm supply node voltage is subtracted from the required reference voltage to produce an error.
2. The FLC acts on the error to produce the required depth of modulation M.
3. A series voltage (V_{sr}) is inserted such that $V_{sr} = M\ V_{dc}$, where M is the modulation index and V_{dc} is the DC bus voltage.

In summary, active power control for wind farms, equipped with variable speed wind turbines, is usually carried out using maximum power tracking algorithm and the total generated active power is exported to the grid. On the other hand, the reactive power control can be achieved by installing additional units at the wind facility terminal such as TCRs, SVCs, UPECs, STATCOMs. Such techniques involve additional costs for installing these devices. Moreover, no reactive power control will be available in case of sudden operation failure of these devices. Techniques based on using a common PWM-VSC for a group of wind turbine is only applicable for wind farm with a DC connected grid. Such technique requires the installation of a high rating inverter at the AC grid terminal. Moreover, its reactive power control capability will be also limited, since both the total active and the total reactive power of the wind farm will flow through the inverter. Finally, the supervisor control techniques, that is based on using a local control system for each machine, and a supervisory control system to regulate the total active and reactive power of the wind farm, have been only applied for constant reactive power generation / absorbed or power factor regulation mode of operation. Such individual unit control-based techniques have not been applied for wind farm terminal voltage regulation.

2.6 Impact of Wind Farms on the Electricity Markets

Recently, some studies have been conducted to examine the expected impact of wind power integration on the operating costs of electric power system. In the case of advance contracting, it has been recorded that increased wind power prediction errors increase the risk of imbalance costs. Such imbalanced costs can be reduced by determining the optimum level of contract energy to be sold on the advance markets [85].

In 2004, a study was conducted to investigate the effect of wind power prediction inaccuracy on the cost of rescheduling generation units [86]. It is found that such costs increase with the increase in the prediction inaccuracy. A probabilistic approach has been also developed to determine the energy costs due to the associated errors with wind power prediction [87]. Consequently, a probability density function was used to model such errors. It was concluded that the prediction costs can be reduced by decreasing the prediction time horizon and by improving the accuracy of the forecast model.

An operation strategy for a grid connected wind power facility, with a connected storage device, has been developed for daily scheduling in power market. To follow the scheduling plan, the energy storage device has been used to smooth the variations in wind power production. An algorithm has been developed, to determine the optimal energy exchange with the market, for a specific period. The impact of the wind forecasting accuracy and the energy storage device sizing, on the system operation and economics, have been highlighted [88, 89].

2.7 Chapter Assessment

The continuously increasing penetration levels of wind facilities within utility grids increase the challenges for power system operators to successfully integrate such facilities with the grids. This chapter presents a literature survey that targets the integration challenges addressed within this thesis. Examining these previous efforts draw attention to the following.

- For one hour ahead wind power prediction, the proposed methods in the literature require large sets of historical data for model training or parameter estimation purposes.
- Previously developed techniques for medium-term wind power prediction (such as day-ahead prediction) do not consider the seasonal effect, depends on collecting data from several neighbouring sites, or depending on using very sophisticated and expensive techniques.
- Traditional voltage regulation-based techniques for DFIGs do not account for the relevant operational losses. Previously developed techniques to reduce such losses are suitable for the power factor regulation mode of operation.

- The existing wind field models for dynamic operational studies of wind farms are not sufficient. Moreover, in such models, the impact of the time delay between the incident wind speed profiles to each unit within the farm is ignored.
- To the best of the author's knowledge, no study addresses the expected impact of wind farm integration and the operating conditions (production variability, applied control strategies, and production prediction accuracy) on determining electricity market prices.

These technical and economic observations are the main motivations for this work. As previously mentioned in Chapter 1, the main objectives of this thesis are the development of new efficient techniques to control and predict the power production of wind farms, equipped with DFIG wind turbines, and to study their integration impact on electricity markets. These objectives can be summarized as follows:

- ♦ Develop a short-term prediction technique (one hour ahead) for wind speed and wind power using the Grey predictor models.
- ♦ Develop a new prediction model, for medium-term (up to one day ahead) wind speed, wind direction, and wind power prediction, based on relating current observations to one year (or two years) old observations.
- ♦ Develop a control technique, for doubly-fed induction generators (DFIGs), capable of regulating the terminal voltage and reducing the generation losses by equally sharing the generated/absorbed reactive power between the rotor-side and the grid-side converters.
- ♦ Develop a new aggregated model for wind farms while considering the irregular wind field distribution within the farm.
- ♦ Investigate the possible impact, of integrating wind farms to the utility grids, on the total generation costs and the real-time electricity market prices.

Chapter 3
Variable Speed Wind Turbine Output Power Prediction and Control

3.1 Introduction

As mentioned in Section1.3, the thesis is divided into two parts. This chapter elaborates on the first part which is related to the prediction and the control of the generated power of a single variable speed wind turbine. Such a study is useful to the owners of small wind facilities. To forecast the generated power from a single wind turbine, only forecasting the incident wind speed is necessary. The use of these forecasted values and the turbine's manufacture power curve for wind power prediction is discussed in the Sections 3.2 and 3.3. This is followed by presenting a new control technique for DFIG units, to reduce the operational power losses and increase the generated active power, in Section 3.4. Lastly, Section 3.5 provides the summary of the chapter.

3.2 Grey Predictor Rolling Models for Hourly Wind Speed Forecasting

Wind generation is highly dependent on the variable incident wind speed at the wind turbine sites resulting in high variability and uncertainty of the generated wind power. This has motivated researches to develop wind power prediction tools that are accurate and reliable. Therefore, developing a new technique for forecasting one step ahead average hourly wind speed and wind turbines' output power, based on using the Grey predictor rolling models, is necessary. The results from the proposed models are compared with the corresponding results from the traditional reference model; the persistent model where it is assumed that the next hour predicted value is equal to the current observation.

The mathematical formulation for developing the Grey predictor models is presented, and the traditional Grey model GM(1,1) is first investigated. This model achieved a good improvement over the persistent model. However, the generated results demonstrate the presence of intervals with overshoots in the predicted values. To reduce such overshoots, this section investigates the application of a modified version of the Grey predictor, referred to as the adaptive alpha GM(1,1) model. In this section, two newly modified versions, hereafter referred to as the improved Grey model

and the averaged Grey model are proposed. The samples that are studied demonstrate the effectiveness, accuracy, and superiority of the proposed improved and averaged Grey models for wind speed and wind turbines power prediction.

3.2.1 Data Preparation and Analysis

Four wind speed data sets, recorded at the Madison weather station [90], are used in the analysis, as presented in Figure 3-1. Sample 1 and Sample 2 are chosen to represent the most common pattern for the incident wind speed (consequently most common wind power generation pattern) [91], where the peak power (wind speed) intervals occur over night. Moreover, Sample 1 has a higher average wind speed than Sample 2. Sample 3 represents a different pattern (almost an opposite wind speed trend to that observed in Sample 1 and Sample 2), where the wind speed time series has an increasing trend at the beginning of the day and then a decreasing trend. These three mentioned samples have approximately smoothed wind speed variations with time; however, the last tested sample, Sample 4, represents a wind speed time series with higher wind speed randomness. Sample 2 and Sample 3 are also characterized by time intervals with wind speed values below the cut in wind speed of the wind turbine power curve used in this analysis. Each wind speed sample consists of 24 hour data set, recorded over 15 minutes' periods. The average of the hourly wind speed time series is obtained by applying an averaging process, before the prediction analysis, as follows.

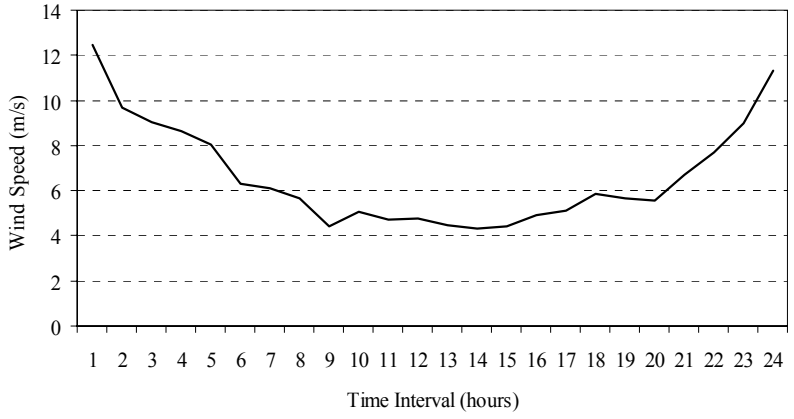

a) Sample 1

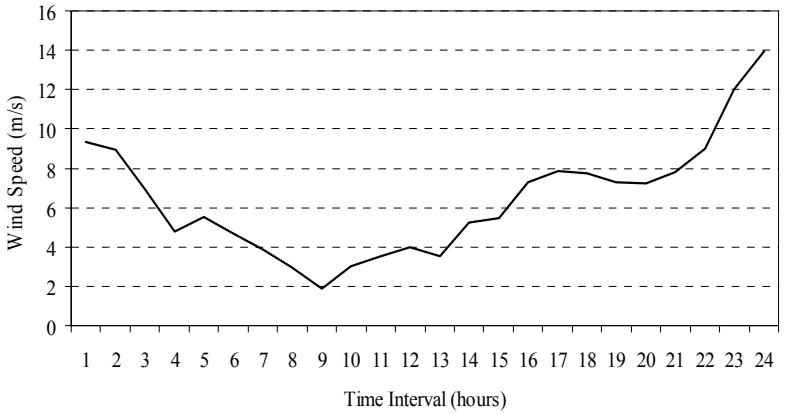

b) Sample 2

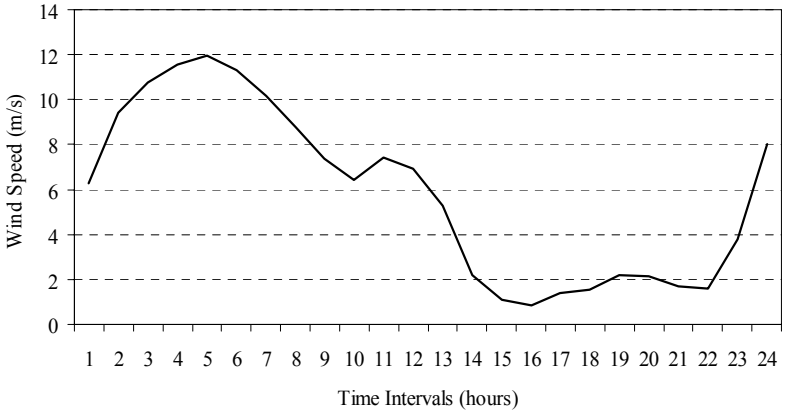

c) Sample 3

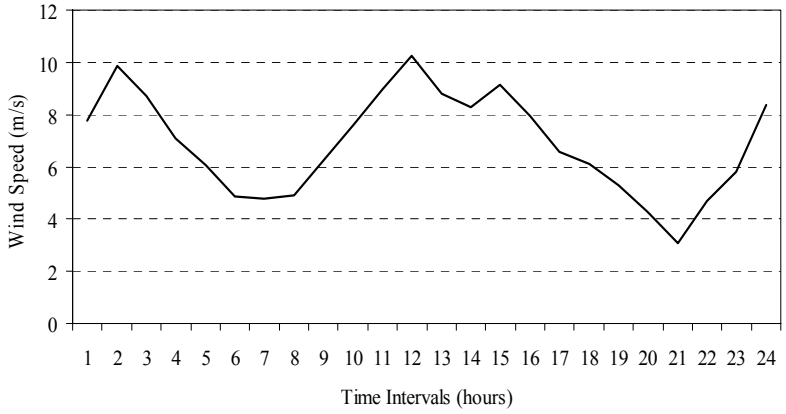

d) Sample 4

Figure 3-1: Wind speed time series samples under investigation.

$$X_{average}(j) = \frac{1}{4}\sum_{i=1}^{4} X_{recorded}(i) \quad \forall\ j = 1, 2, ..., 24\ , \tag{3-1}$$

where $X_{average}\ (j)$ is the hourly averaged data point during hour j, and $X_{recorded}\ (i)$ is the 15 minute recorded data points during hour j.

After the wind speed is predicted, the predicted wind speed time series is used as an input for the manufacturer power curve of the VESTAS V66-1.65 MW wind turbine, given in Figure 3-2, to predict the output wind power production. The power curve under investigation is characterized by a cut in wind speed of 4 m/s, rated wind speed of 16 m/s, and a cut out wind speed of 25 m/s.

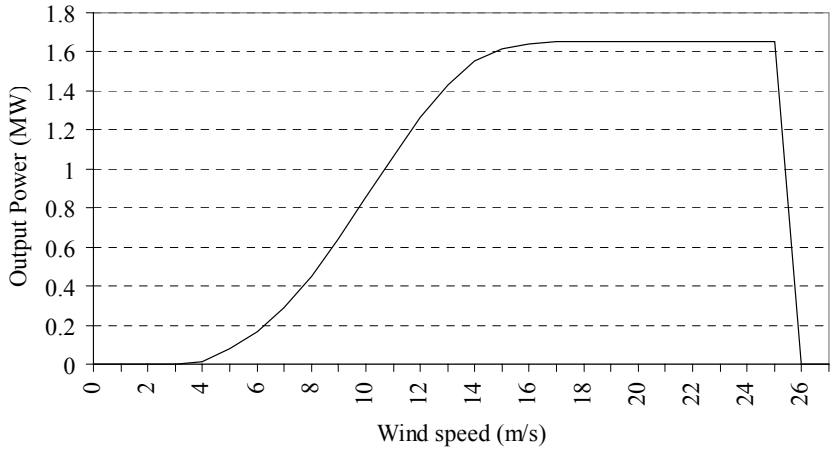

Figure 3-2: Power curve for the VESTAS V66-1.65 MW wind turbine.

3.2.2 Traditional Grey Rolling Model GM(1,1)

In 1982, Professor Julong Deng was the first to introduce the Grey systems [92 - 94]. They include any system with partially unknown information about its parameters, structure, and / or characteristics. Grey predictor models are characterized by the following [95].

- They need fewer historical data to develop the prediction model (as few as four historical data points).
- They are highly adaptive to the dynamic behaviour of the data.
- They need little computation effort and processing time.

Grey Predictor models have been involved in many prediction applications as follows

- Forecasting non-periodic time series such as stock prices indices [96]
- Predicting objects position and targets tracking in which the grey system predicts the future trend of an object or target, based on few historical measurements [97].
- Power system yearly peak load forecasting [95].
- Predicting the changes in the inertia and damping coefficients of the mechanical parts of induction servo motors and its control, according to indirect field orientation [98].

There are several models for the Grey predictor that are currently in use. This section investigates the usage of the most commonly used model and that is the traditional GM(1,1) model [99, 100]. The procedure to develop this model and the related prediction process are illustrated in Figure 3-4. The mathematical formulations describing each stage are summarized as follows.

1. Generate the first order Accumulated Generating Operation (AGO) series. This results in generating a new accumulated data series ($X^{(1)}$) that is characterized by a more smoothed regular pattern (less randomness) than the original data series ($X^{(0)}$) under analysis, as shown in Figure 3-3. This operation is expressed mathematically as

$$X^{(1)}(k) = \sum_{i=1}^{k} X^{(0)}(i) \qquad \forall\, k = 1,...n\,; \qquad , \tag{3-2}$$

   where $X^{(1)}$ represents the first order AGO data series, $X^{(0)}$ represents the original data series, n represents the sample data, and k and i represent the step for the AGO and the original data series, respectively.

2. Formulate the model's differential equation that relates its dependent variables with the independent ones. This differential equation is known as the Grey dynamic model. For the traditional GM(1,1) model, this differential equation is represented by one dependent variable and no independent variables and is written as follows:

$$\frac{dX^{(1)}}{dt} + aX^{(1)} = b \quad , \tag{3-3}$$

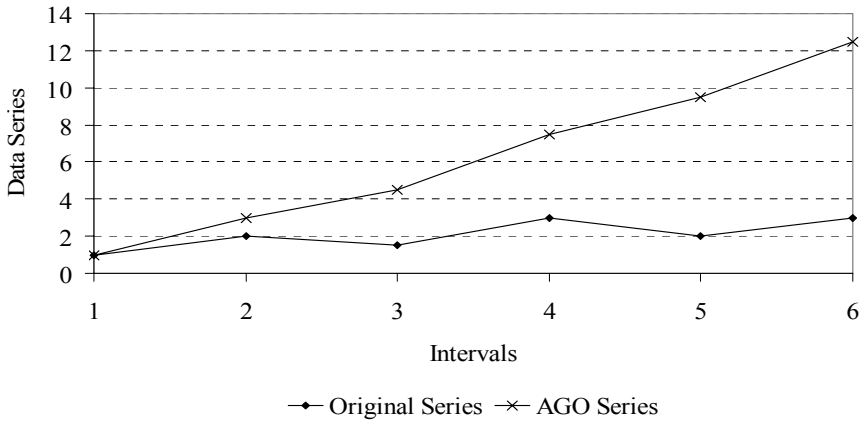

Figure 3-3: Original and AGO data series.

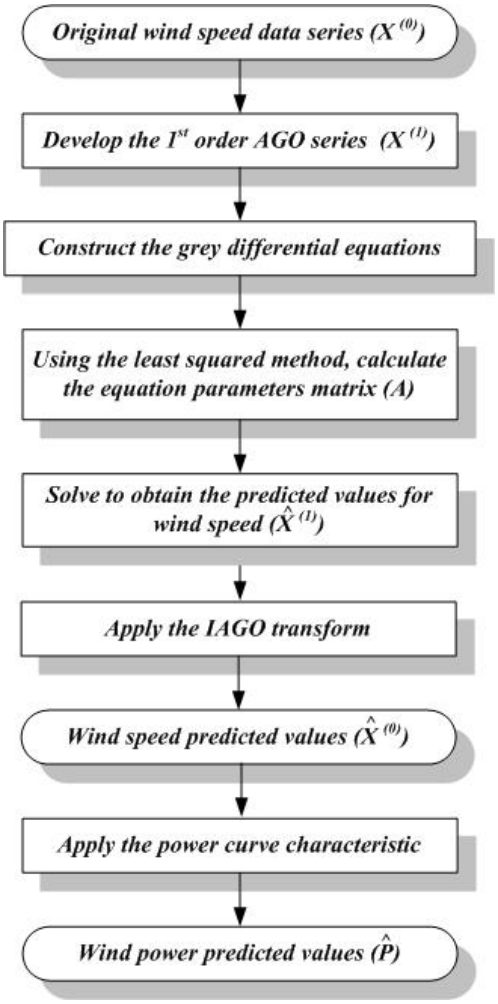

Figure 3-4: Prediction process using traditional GM(1,1) rolling model.

where X represents the dependent variable for the traditional GM(1,1), and a and b are the model coefficients (parameters) determined by the least square method.

3. The a and b parameters of the GM(1,1) are determined by the least squared method as follows;

$$A = \begin{bmatrix} a \\ b \end{bmatrix} = \left[\beta^T . \beta\right]^{-1} . \beta^T Y \quad , \tag{3-4}$$

where

$$\beta = \begin{bmatrix} -Z^{(1)}(2) & 1 \\ -Z^{(1)}(3) & 1 \\ \vdots & \vdots \\ -Z^{(1)}(n) & 1 \end{bmatrix} \quad , \tag{3-5}$$

$$Y = \begin{bmatrix} X^{(0)}(2) \\ X^{(0)}(3) \\ \vdots \\ X^{(0)}(n) \end{bmatrix} \quad , \tag{3-6}$$

and

$$Z^{(1)}(i) = \frac{X^{(1)}(i-1) + X^{(1)}(i)}{2} . \tag{3-7}$$

4. Calculate the forecasted or predicted values for the AGO series ($\hat{X}^{(1)}$) by applying

$$\hat{X}^{(1)}(i+1) = \left(X^{(0)}(1) - \frac{b}{a} \right) e^{-ai} + \frac{b}{a} \quad , \tag{3-8}$$

where i represents the step, and $X^{(0)}$ represents the first data in the original time series.

5. Transform the forecasted AGO series of data back to its original form (series) by the Inverse Accumulated Generating Operation (IAGO). This operation is considered to be the inverse of the AGO and is represented mathematically as

$$\hat{X}^{(0)}(1) = \hat{X}^{(1)}(1) \tag{3-9}$$

and

$$\hat{X}^{(0)}(i+1) = \hat{X}^{(1)}(i+1) - \hat{X}^{(1)}(i) \qquad \forall i = 1,2,3,.. \quad . \tag{3-10}$$

6. Use the provided manufacture power curves to calculate the predicted power generation of the turbine.
7. After the predicted interval becomes an observation, update the used input data by using the rolling modelling mechanism [101]. Here, the oldest historical data is eliminated and the recent observation is added to predict the next future interval.

The actual and predicted wind speed time series for the four tested samples are presented in Figure 3-5. This figure displays the results of the traditional GM(1,1) rolling and the persistent models. The figure demonstrates the effectiveness of the traditional GM(1,1) rolling model in tracking the actual time series better than that of the persistent model. The use of the traditional GM(1,1) rolling model results in the Mean Absolute Error (MAE) values of 0.76, 0.94, 1.12, and 1.1 m/s for Samples 1 to 4, respectively, that corresponds to 0.79, 0.97, 1.19, and 1.13 m/s, respectively, for the persistent model. Moreover, for the studied samples, the traditional GM(1,1) rolling model forecasts wind speed time series with an improvement, in the MAE, over the persistent model of 3.08, 3.09, 5.88, and 2.65 %.

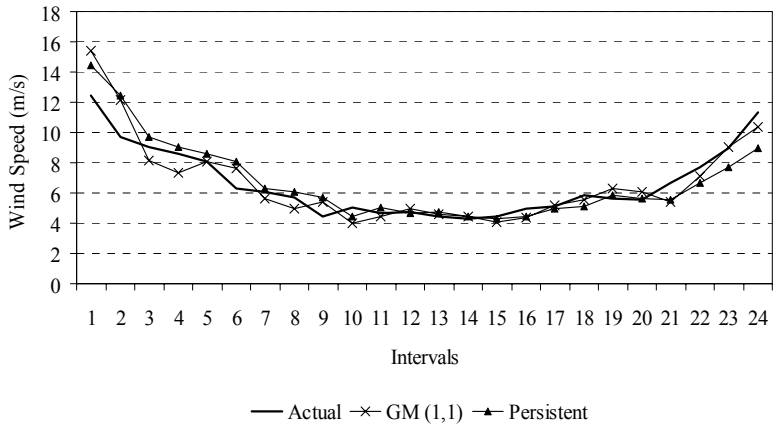

a) Sample 1

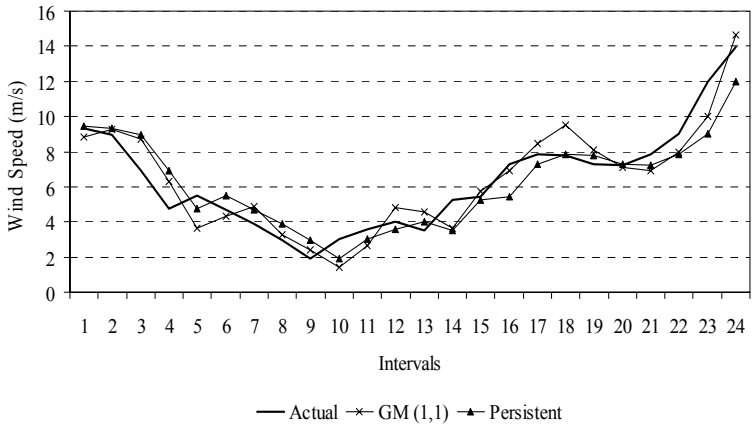

b) Sample 2

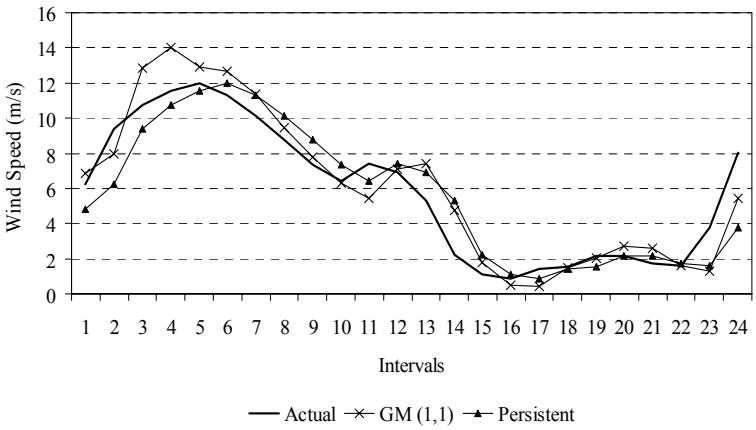

c) Sample 3

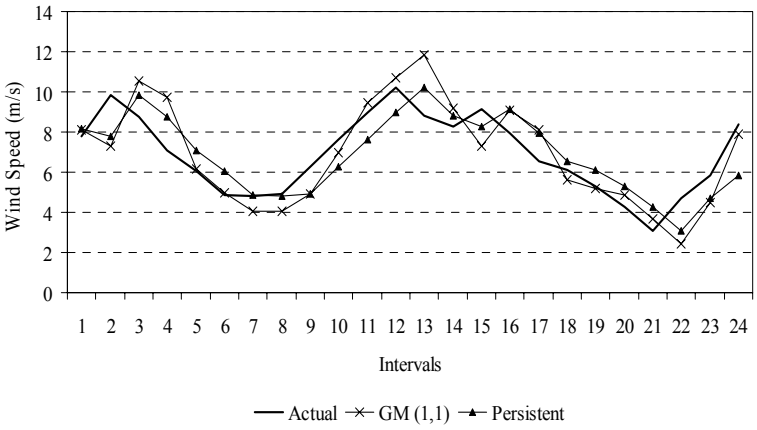

d) Sample 4

Figure 3-5: Wind speed prediction using traditional GM(1,1) rolling model and persistent model.

In [95] a model diagnostic checking process has been developed to evaluate and test the traditional Grey model's grade. This is carried out by calculating the residual (error) series $\varepsilon^{(0)}$ for the historical data, used in developing the model, as follows:

$$\varepsilon^{(0)}(i) = X^{(1)}(i) - \hat{X}^{(1)}(i) \quad . \tag{3-11}$$

The mean ($\bar{\varepsilon}$) and the standard deviation (S_1) of this series are calculated as follows:

$$\bar{\varepsilon} = \frac{1}{n}\sum_{i=1}^{n} \varepsilon^{(0)}(i) \tag{3-12}$$

and

$$S_1 = \sqrt{\frac{1}{n}\sum_{i=1}^{n}\left(\varepsilon^{(0)}(i) - \bar{\varepsilon}\right)^2} \quad . \tag{3-13}$$

The mean ($\bar{X}$) and the standard deviation (S_2) of the AGO series are calculated as follows:

$$\bar{X} = \frac{1}{n}\sum_{i=1}^{n} X^{(1)}(i) \tag{3-14}$$

and

$$S_2 = \sqrt{\frac{1}{n}\sum_{i=1}^{n}\left(X^{(1)}(i) - \bar{X}\right)^2} \quad . \tag{3-15}$$

Two evaluation indices, C (the relative performance of a model with a scattering degree S_2 and a fitness degree S_1) and P (smaller errors probability index), are then calculated by

$$C = \frac{S_1}{S_2} \tag{3-16}$$

and

$$P = prob\left(\left|\varepsilon^{(0)}(i) - \bar{\varepsilon}\right| \le 0.6745\, S_2\right) \quad . \tag{3-17}$$

The model is then graded according to Table 3-1. Figure 3-6 gives the C Indices for the developed

models by using the traditional GM(1,1). These figures reveal that the developed models grades are good. This has been also confirmed by the P evaluation index that is consistently equal to unity over the studied 24 hour data samples.

Table 3-1: Grey model grades.

Grade	Evaluation Indices	
	P	**C**
Good	> 0.95	< 0.35
Qualified	> 0.8	< 0.5
Just	> 0.7	< 0.45
Unqualified	<= 0.7	>= 0.65

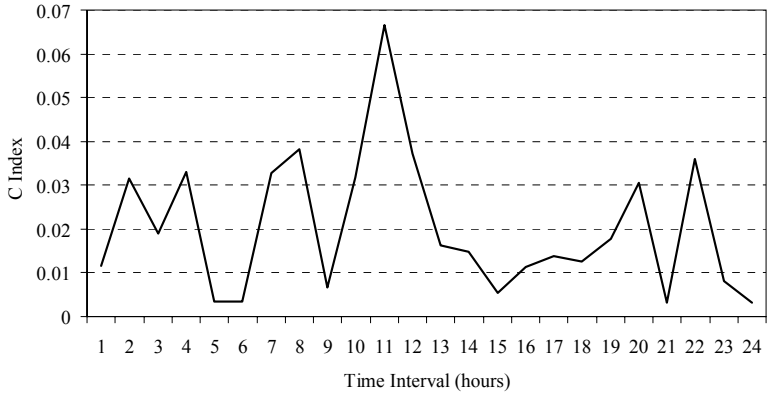

a) Sample 1

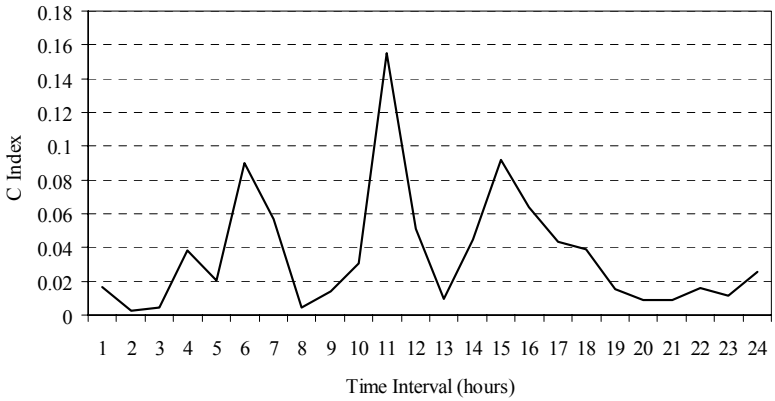

b) Sample 2

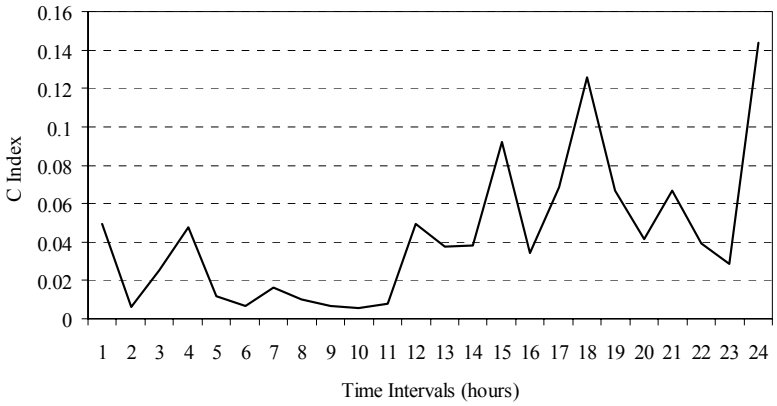

c) Sample 3

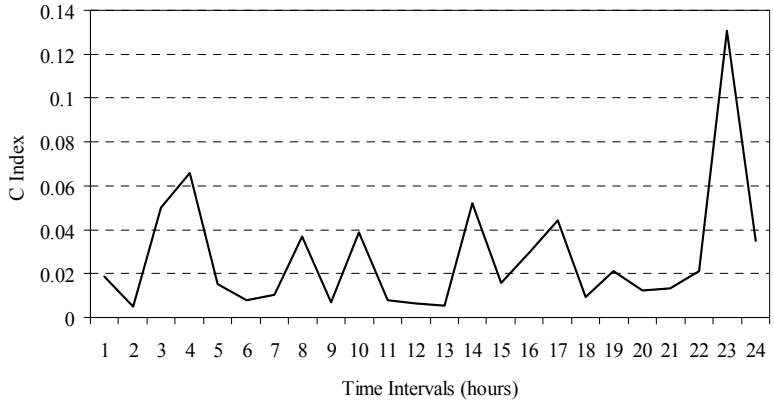

d) Sample 4

Figure 3-6: C Indices for the developed models using the traditional GM(1,1).

Despite the superiority of the newly developed model, the use of the traditional GM(1,1) in predicting continuously variable time series usually results in the occurrence of overshoots [101] that reduce the prediction accuracy. The following subsections investigates the previously developed technique to reduce these overshoots, hereafter, referred to as the adaptive alpha based GM(1,1) model, as well as introducing two new proposed models, hereafter, referred to as the improved and the averaged Grey models [102]. Reducing or eliminating such overshoots from the predicted results increases the overall prediction accuracy of the Grey model.

3.2.3 Adaptive Alpha-Based GM(1,1) Model

The adaptive alpha-based GM(1,1) model is developed by following the same procedure (stages) described in Section 3.2.2 for the traditional GM(1,1) model except for the formula used for calculating the $Z^{(1)}(i)$ terms, as demonstrated in Figure 3-7. In 1999, Chang et. al. proposed an adaptive $\alpha(i)$ for the $Z^{(1)}(i)$ terms [103] so that the formula for calculating these terms is expressed as

$$Z^{(1)}(i) = [1-\alpha(i)]\, X^{(1)}(i-1) + \alpha(i)\, X^{(1)}(i) \quad , \tag{3-18}$$

where $\alpha(i)$ is a weighting factor within the range $0 \le \alpha(i) \le 1$. For the traditional GM(1,1) model, this factor is set to 0.5.

In this model, the weighting factor $\alpha(i)$ is determined by what is known as the "average system slope" technique [101] that is summarized as follows.

1. Calculate the average slope coefficient (σ_{avg}) as follows:

$$\sigma_{avg} = \sqrt[n-1]{\frac{X^{(0)}(n)}{X^{(0)}(1)}} \quad , \tag{3-19}$$

   where $X^{(0)}(n)$ and $X^{(0)}(1)$ represent the last and the first data points in the original data series, respectively, and n represents the total number of data points used in developing the GM(1,1) model.

2. Determine the relative positions (k_j) for the remaining data points (excluding the first and the last points that are forced to match the data values of the real system end points) to force the data of the theoretical system model to equate the data of the real system model. This is mathematically formulated as follows (for 4-data points model):

$$X^{(0)}(1)\,\sigma_{avg}^{k_2} = X^{(0)}(2) \quad \Rightarrow \quad k_2 = \log\left(X^{(0)}(2) / X^{(0)}(1)\right) / \log\left(\sigma_{avg}\right) \quad , \tag{3-20}$$

$$X^{(0)}(1)\,\sigma_{avg}^{k_3} = X^{(0)}(3) \quad \Rightarrow \quad k_3 = \log\left(X^{(0)}(3) / X^{(0)}(1)\right) / \log\left(\sigma_{avg}\right) \quad , \tag{3-21}$$

and

$$X^{(0)}(1)\,\sigma_{avg}^{3} = X^{(0)}(4) \quad . \tag{3-22}$$

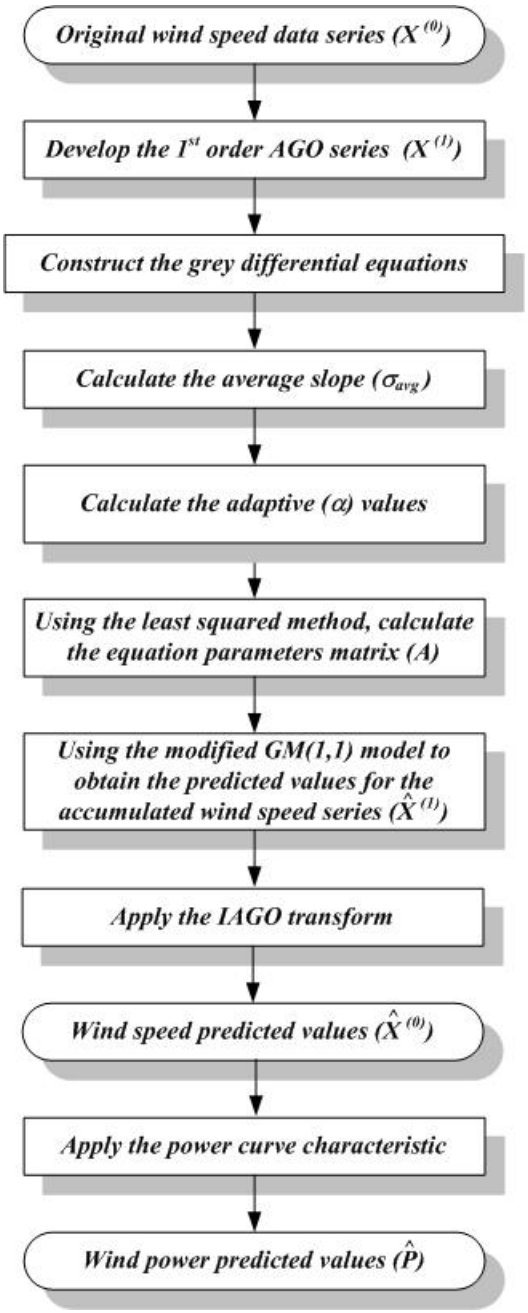

Figure 3-7: Prediction process using adaptive alpha based GM(1,1) rolling model.

3. Calculate the adaptive alpha set $\alpha(i)$ by the following if rules:

   a. $IF \quad k_2 \le 0 \quad Then \quad \alpha(2) = 0$ else $IF \quad k_2 \in (0,1) \quad Then \quad \alpha(2) = k_2$

   else $IF \quad k_2 \ge 0 \quad Then \quad \alpha(2) = 1$, (3-23)

   b. $IF \quad k_3 \le 1 \quad Then \quad \alpha(3) = 0$ else $IF \quad k3 \in (1,2) \quad Then \quad \alpha(3) = k_3 - 1$

   else $IF \quad k_3 \ge 2 \quad Then \quad \alpha(3) = 1$, (3-24)

   and

   c. $\alpha(4) = 1$. (3-25)

4. Proceed with step 3 as illustrated in the traditional GM(1,1)model while using the adaptive $Z^{(1)}(i)$ expression in (3.18).

The corresponding actual and predicted wind speed time series, for the four tested samples, and using the adaptive alpha based model, are presented in Figure 3-8. This model results in MAE values of 0.75, 0.87, 1.09, and 1.1 m/s for Samples 1 to 4, respectively, that correspond to an improvement, in the MAE, over the persistent model of 5.06, 10.31, 8.4, and 2.65 %. This reveals that more improvements in the MAE, over those of the persistent model, are achieved than those produced by the traditional model for all samples except the Sample 4 that reveals the same improvement level.

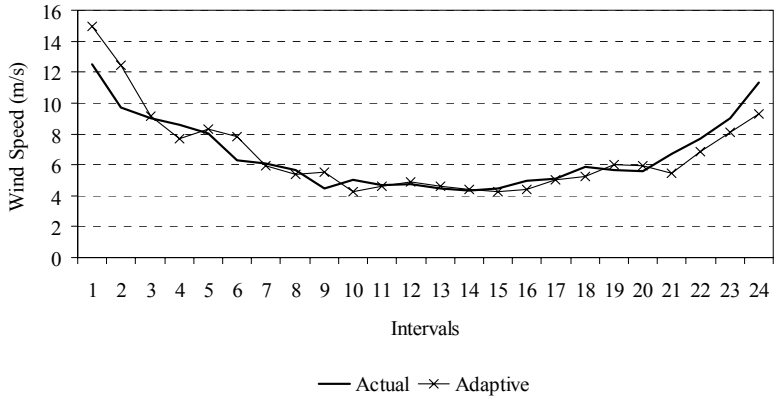

a) Sample 1

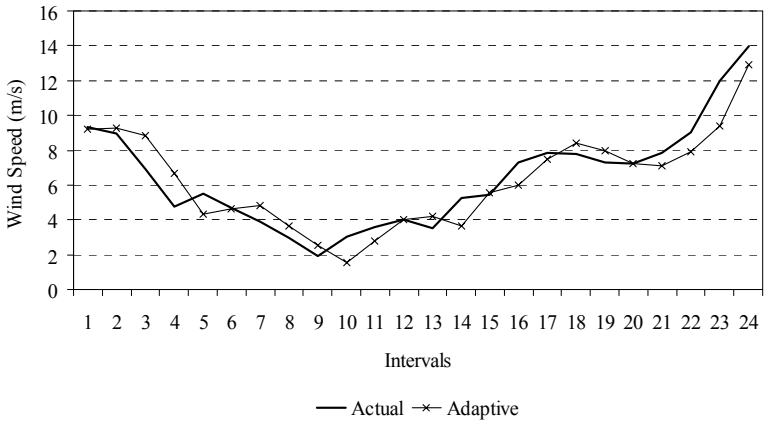

b) Sample 2

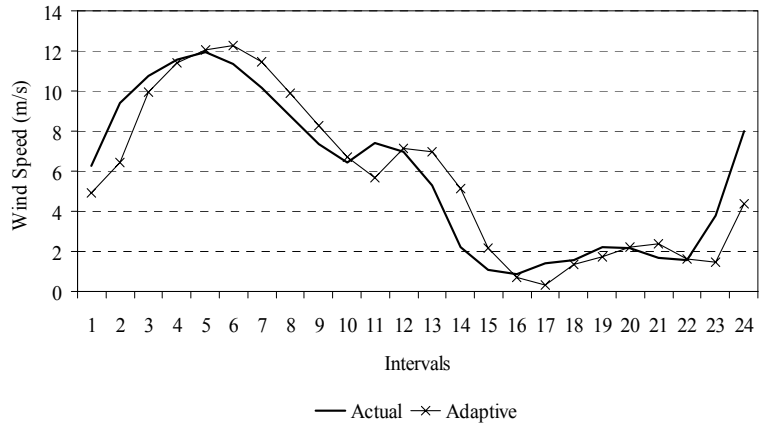

c) Sample 3

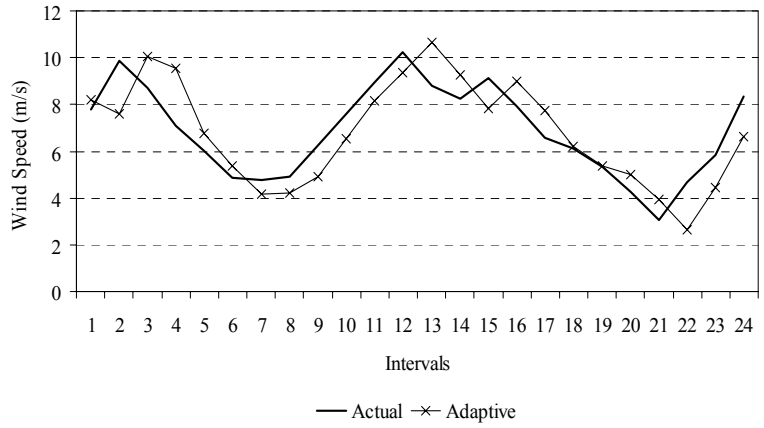

d) Sample 4

Figure 3-8: Wind speed prediction using the adaptive alpha based GM(1,1) rolling model.

A comparison of the results in Figure 3-8, with their corresponding results in Figure 3-5 reveals that the adaptive alpha-based model can reduce the overshoots in the predicted time series; however, for the intervals with no overshoots, the traditional model tracks the actual time series better. This motivates the author to investigate and develop more Grey-based models, as discussed in the following subsections.

3.2.4 Improved Shifted Grey Model

In an attempt to increase the prediction accuracy, an improved Grey model is proposed for wind speed and wind power prediction. This model is based on generating two shifted prediction models from the traditional GM(1,1) model, discussed in Section 3.2.2. Then, a hybrid of these new models is developed as the final prediction model. Figure 3-9 is a flow chart, representing the different stages for developing the proposed improved shifted Grey model. The mathematical formulations, describing each stage, are summarized as follows.

1. Follow Steps 1 to 4 in Section 3.2.2 for developing the traditional GM(1,1) model. Step 4 ends by developing the traditional GM(1,1) prediction model, to predicted the values for the AGO series ($\hat{X}^{(1)}_{GM}$), which is represented mathematically as

$$\hat{X}^{(1)}_{GM}(i+1) = \left(X^{(0)}(1) - \frac{b}{a} \right) e^{-ai} + \frac{b}{a} \quad . \tag{3-26}$$

2. Generate two shifted prediction models ($\hat{X}^{(1)}_{1}$ and $\hat{X}^{(1)}_{2}$). The goal of this stage is to generate an envelope like time series that contain the actual AGO series. This is formulated as follows:

$$\hat{X}^{(1)}_{1}(i+1) = \hat{X}^{(1)}_{GM}(i+1) + shift \tag{3-27}$$

and

$$\hat{X}^{(1)}_{2}(i+1) = \hat{X}^{(1)}_{GM}(i+1) - shift \, , \tag{3-28}$$

where *shift* represents the value by which the traditional GM(1,1) model is shifted and is chosen to be equal to the last data point in the first AGO series; i.e. $X^{(1)}(n)$, where $n = 4$ (4 data points are used to build the GM models) to ensure that the generated envelope contains

the actual AGO series.

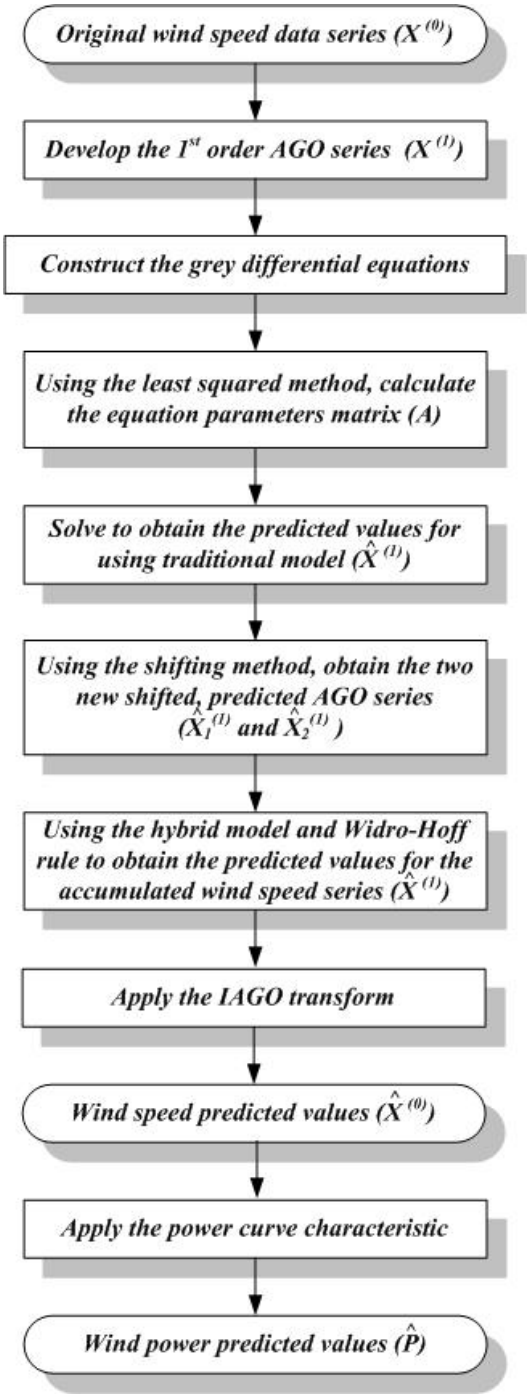

Figure 3-9: Prediction process using improved shifted GM(1,1) rolling model.

3. Take the new prediction models and create a hybrid to generate the final improved Grey model ($\hat{X}^{(1)}_{imp}$)as follows:

$$\hat{X}^{(1)}_{imp}(i+1) = w_1 \cdot \hat{X}^{(1)}_1 (i+1) + w_2 \cdot \hat{X}^{(1)}_2 (i+1) \tag{3-29}$$

and

$$w_1 + w_2 = 1, \tag{3-30}$$

where w_1 and w_2 represent the weights for the shifted models. These weights are updated by using the Least Mean Square (LMS) technique, known as the Widro-Hoff delta rule [104], [105], which is

$$W(i+1) = W(i) + \delta \cdot \frac{X^{(1)}(i) \cdot e(i)}{\left[X^{(1)}(i)\right]^T \cdot X^{(1)}(i)} \quad , \tag{3-31}$$

where $W(i)$ and $W(i+1)$ represent the current and the updated weights vector, δ is the learning parameter, $X^{(1)}(i)$ and $\left[X^{(1)}(i)\right]^T$ represent the shifted AGO series vector and its transposed vector, and $e(i)$ is the error vector given by

$$e(i) = X^{(1)}(i) - \hat{X}^{(1)}_{imp}(i) \quad . \tag{3-32}$$

4. Proceed with step 5 as illustrated in the traditional GM(1,1)model (Section 3.2.2).

Figure 3-10 displays the corresponding actual and predicted wind speed time series, when the improved shifted Grey model is employed. This model achieves levels of the MAE of 0.71, 0.95, 1, and 1.03 m/s for Samples 1 to 4, respectively. This corresponds to an improvement over the persistent model of 10.13, 2.06, 15.97, and 8.85 %, respectively. More improvements in the MAE are achieved for Samples 1, 3, and 4. However, for Sample 2 a drop in the percentage improvement of the MAE occurs, compared with that of the adaptive alpha-based model. Compared with the traditional model, Figure 3-10 reveals that the improved model manages to reduce the overshoots; however, the tracking feature for the actual time series is still worse than that of the traditional Grey model.

3.2.5 Averaged Grey Model

This model attempts to combine, to some extent, the good features of both the traditional GM(1,1) model (represented by good tracking and lower prediction error for the intervals without prediction overshoots) and the improved Grey model (represented by reducing the overshoots, and hence, reducing the prediction errors at the intervals where overshoots occur). This is carried out by averaging the results of both models as follows:

$$\hat{X}^{(1)}_{avg}(i+1) = \frac{\hat{X}^{(1)}_{GM}(i+1) + \hat{X}^{(1)}_{imp}(i+1)}{2} \quad , \tag{3-33}$$

where $\hat{X}^{(1)}_{avg}(i+1)$ represents the predicted future point by using the proposed averaged Grey model.

The corresponding actual and predicted wind speed time series, for the four tested samples with the averaged Grey model, are recorded in Figure 3-11. This model results in MAE values of 0.69, 0.85, 0.87, and 0.99 m/s for Samples 1 to 4, respectively, that correspond to an improvement over the persistent model of 12.66, 12.37, 26.89, and 12.39 %, respectively. This demonstrates the superiority of the proposed averaged model in wind speed forecasting over all the models presented in this section. Moreover, Figure 3-11 reveals that the tracking feature is enhanced when the proposed averaged model is used and is overall superior, when compared with the persistent model and the other presented Grey models.

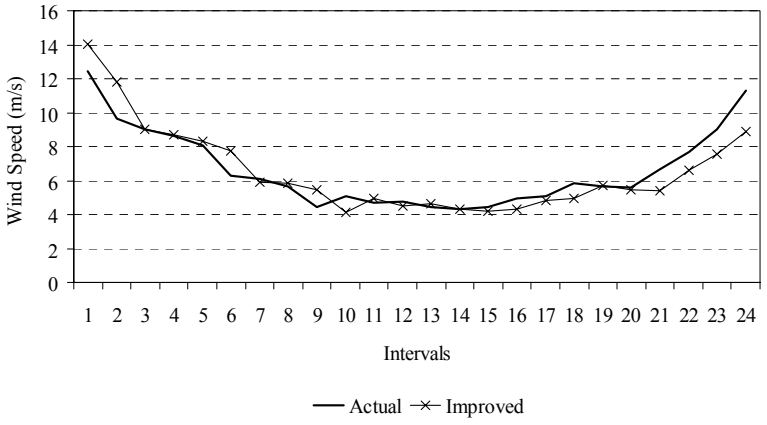

a) Sample 1

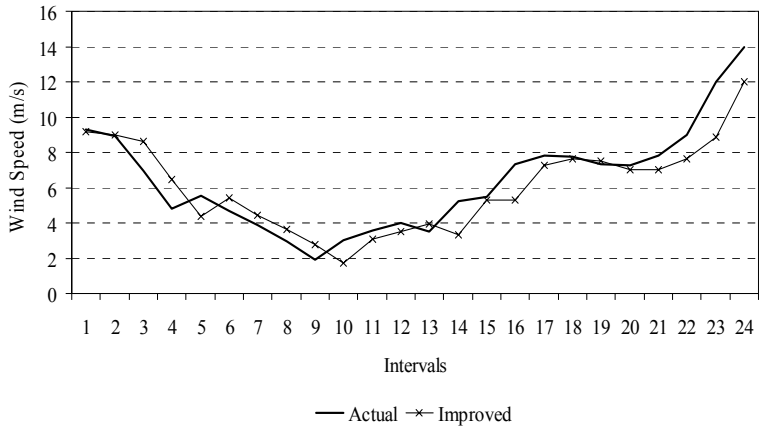

b) Sample 2

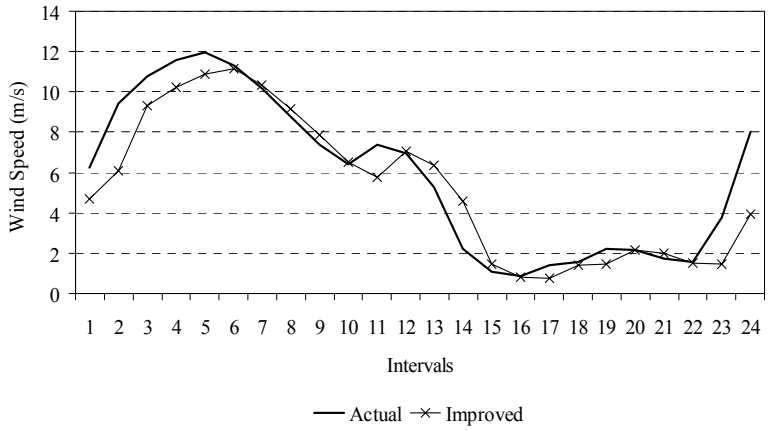

c) Sample 3

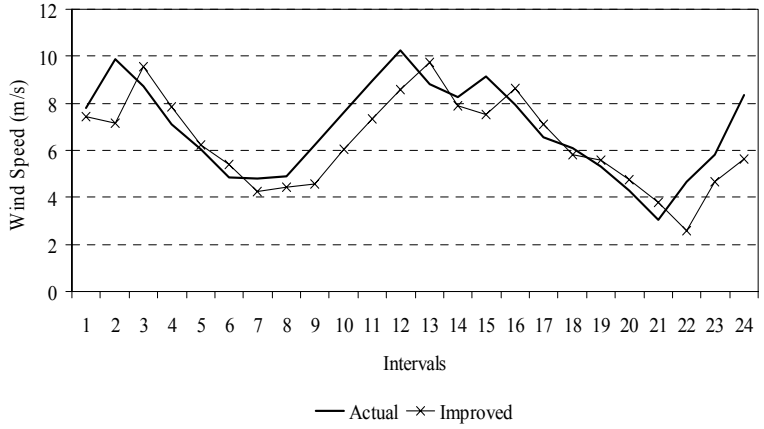

d) Sample 4

Figure 3-10: Wind speed prediction using the improved shifted GM(1,1) rolling model.

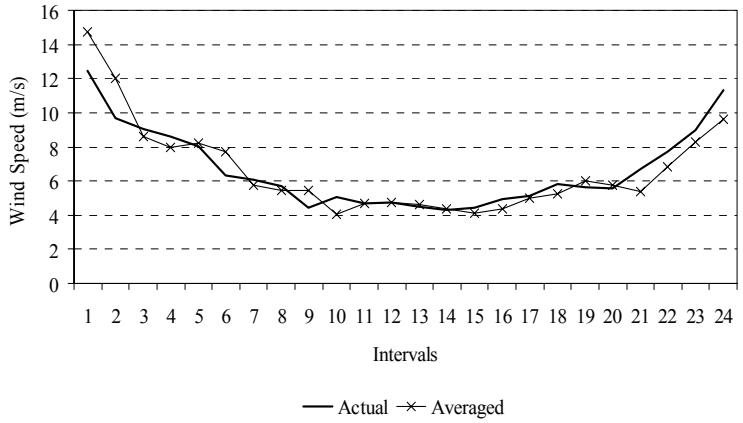

a) Sample 1

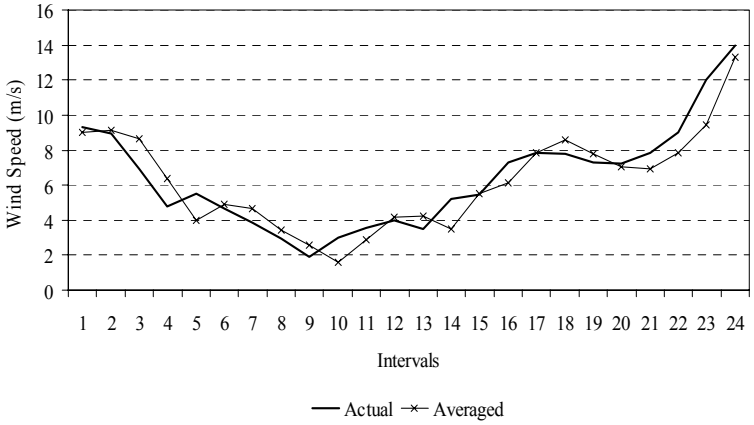

b) Sample 2

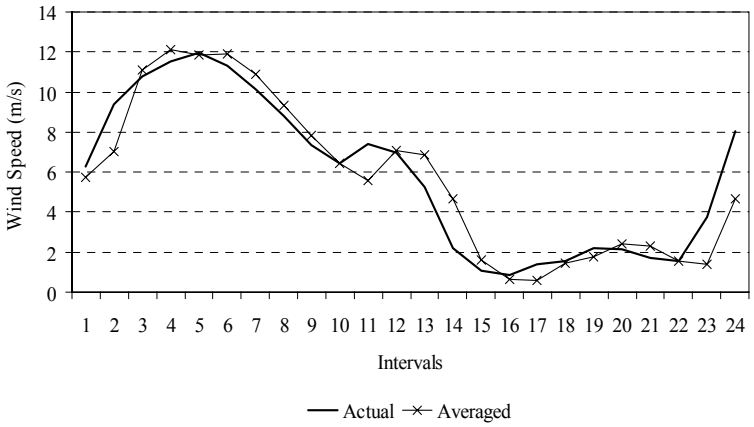

c) Sample 3

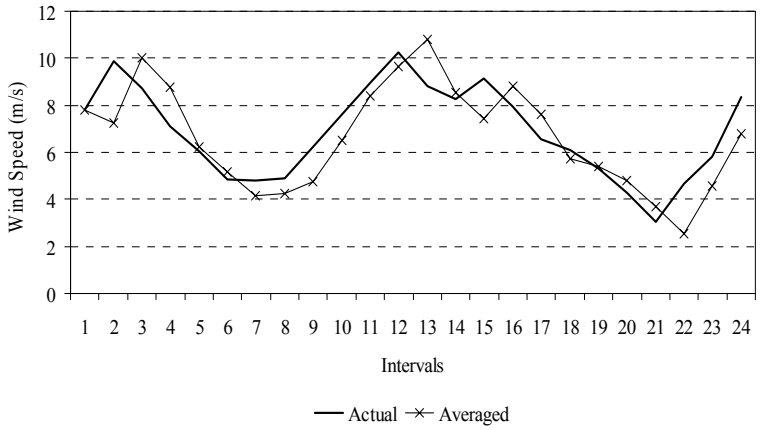

d) Sample 4

Figure 3-11: Wind speed prediction using the averaged GM(1,1) rolling model.

Table **3-2** provides a comparison of all the Grey models introduced in this section and the persistent model in terms of; the samples' MAE; and the samples' RMSE. Moreover, this table demonstrates the improvements of the newly developed models, compared with the persistent model. The table reveals that, for the four tested samples, the highest percentage of improvement is achieved when the proposed averaged GM(1,1) model is employed. Moreover, the table also reveals that the overshoot occurrence for the traditional GM(1,1) model can result in a negative percentage improvement on the RMSE scale, especially for samples with a high random wind speed variations such as in Sample 4.

Figure 3-12 represents the scattering and the linear relationships between the predicted and the actual values for the wind speed of the four data sets, predicted by the averaged GM(1,1) model. This linear relationship is expressed as

$$\hat{y}_i = m\, x_i + c \quad , \tag{3-34}$$

where, $\hat{y}_i$ and x_i are the predicted and the actual wind speed or power values at time interval, i, m, and c are the linear relationship coefficients obtained by using the least square method, where m is the scaling factor (slope of the linear relationship), and c is the y-axis (prediction-axis) intercept of the linear relation. The best linear relationship between the actual and the predicted values is achieved when $c = 0$ and $m = 1$.

Table 3-2: MAE (m/s), RMSE (m/s), and improvements for wind speed prediction.

	Parameter		Persistent	GM(1,1)	Adaptive	Improved	Averaged
Sample 1	***MAE***	Value	0.79	0.76	0.75	0.71	0.69
		% Improvement	-	*3.80*	*5.06*	*10.13*	*12.66*
	RMSE	Value	1.09	1.04	1.06	0.99	0.95
		% Improvement	-	*4.59*	*2.75*	*9.17*	*12.84*
Sample 2	***MAE***	Value	0.97	0.94	0.87	0.95	0.85
		% Improvement	-	*3.09*	*10.31*	*2.06*	*12.37*
	RMSE	Value	1.22	1.10	1.09	1.22	1.06
		% Improvement	-	*9.84*	*10.66*	*0.00*	*13.11*
Sample 3	***MAE***	Value	1.19	1.12	1.09	1.00	0.87
		% Improvement	-	*5.88*	*8.40*	*15.97*	*26.89*
	RMSE	Value	1.58	1.42	1.48	1.47	1.26
		% Improvement	-	*10.13*	*6.33*	*6.96*	*20.25*
Sample 4	***MAE***	Value	1.13	1.10	1.10	1.03	0.99
		% Improvement	-	2.65	2.65	*8.85*	*12.39*
	RMSE	Value	1.26	1.38	1.26	1.27	1.21
		% Improvement	-	-9.52	0.00	*-0.79*	*3.97*

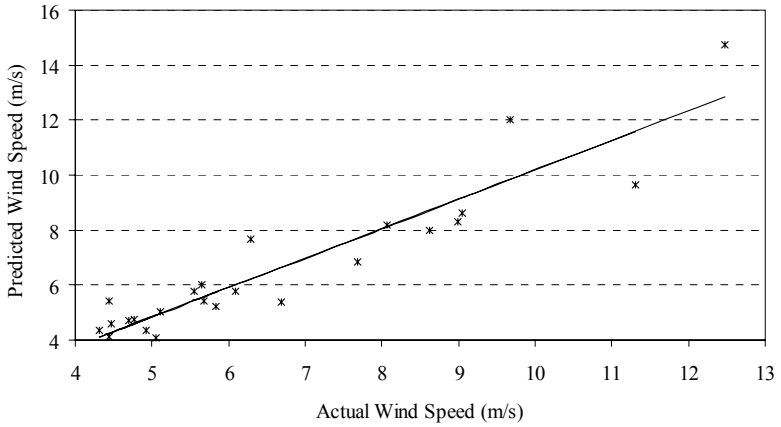

a) Sample 1

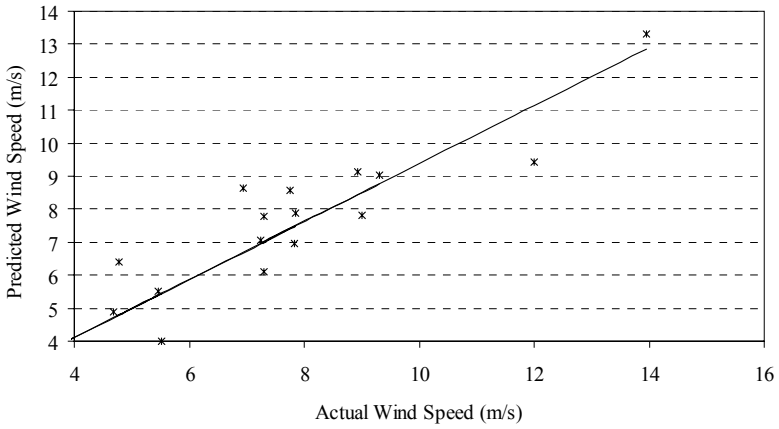

b) Sample 2

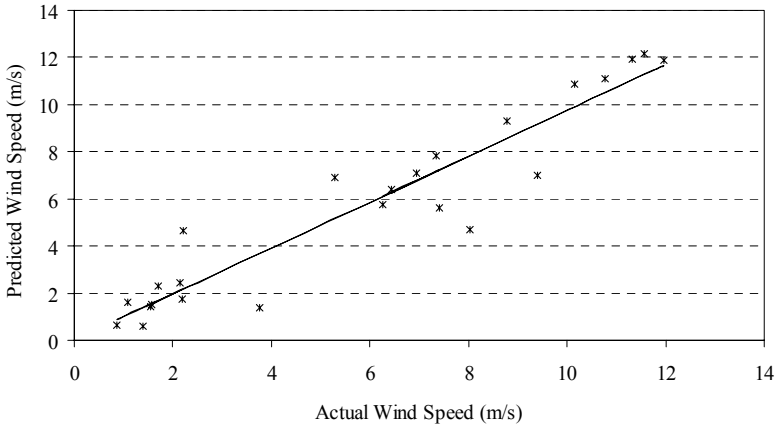

c) Sample 3

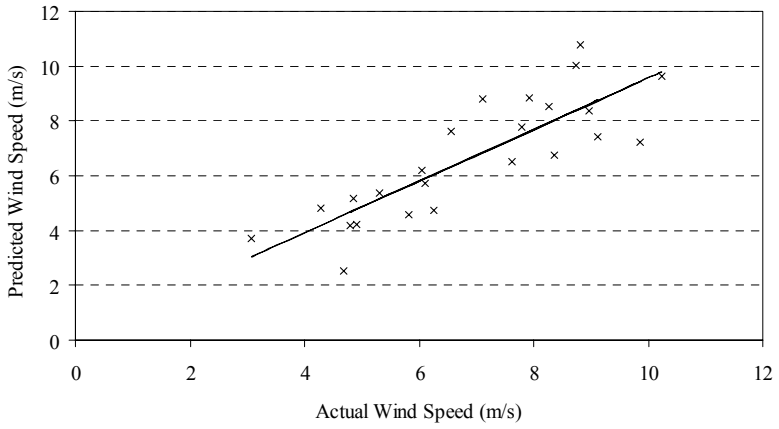

d) Sample 4

Figure 3-12: Actual and predicted wind speed using the averaged GM(1,1) rolling model relationships.

Figure 3-12 reveals a good scattering of the predicted values of wind speed. Table 3-3 indicates that the corresponding linear relationships between the predicted and the actual values. This table also reveals that the scaling factor is very close to unity, and that the y-axis intercept coefficient is very close to zero.

Table 3-3: Actual and predicted values linear relationship coefficients for the averaged GM(1,1) rolling model.

Samples	**Linear Relationship (MW)**
Sample 1	$-0.495 + 1.069\, x_i$
Sample 2	$0.618 + 0.876\, x_i$
Sample 3	$0.023 + 0.972\, x_i$
Sample 4	$0.157 + 0.942\, x_i$

3.3 Wind Power Prediction

This section investigates the usage of the proposed averaged model in wind power prediction. The generated results for the predicted wind speed time series by the proposed model is used as the input to the VESTAS V66-1.65 MW wind turbine power curve, as previously highlighted, to predict the wind power production. The generated actual and predicted wind power time series, when the averaged model is employed, for the four tested samples are presented in Figure 3-13. The figure demonstrates the effectiveness of the proposed averaged GM(1,1) rolling model for tracking the actual generated wind power time series.

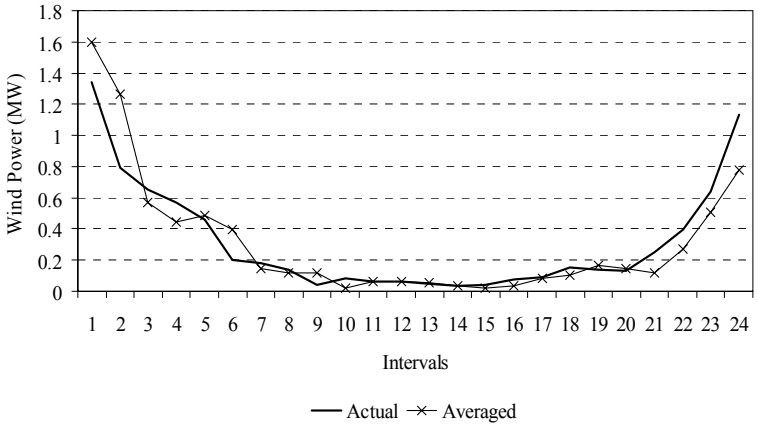

a) Sample 1

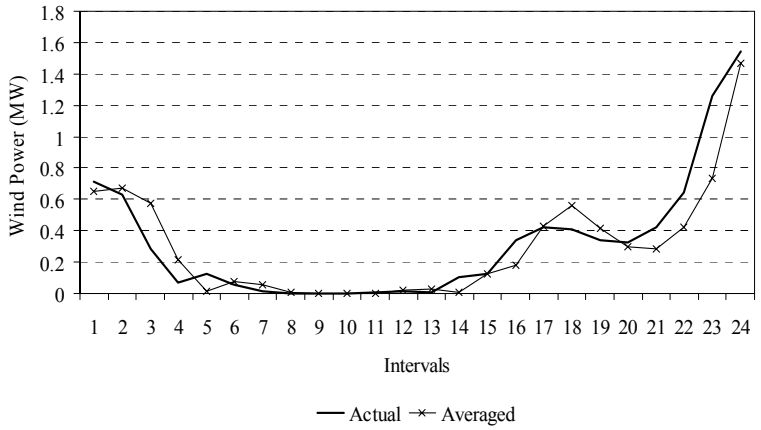

b) Sample 2

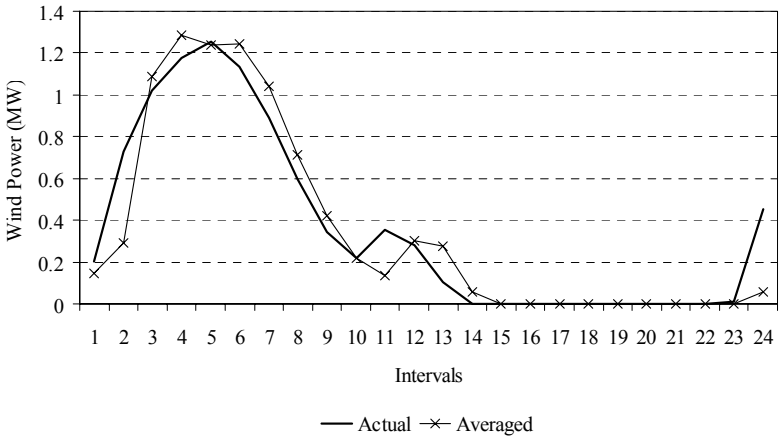

c) Sample 3

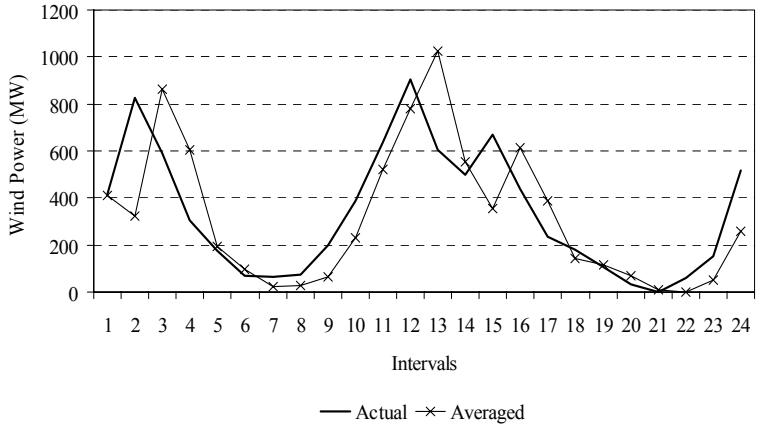

d) Sample 4

Figure 3-13: Wind power prediction using the averaged GM(1,1) rolling model.

Table 3-4 lists the MAE, RMSE, and average percentage error referred to the rated power (% error for the power prediction) for the generated results by the averaged GM(1,1) rolling model. This table also reveals a lower MAE, lower RMSE, and lower average percentage error values for the averaged GM(1,1) rolling model, compared with those of the persistent model. The table also reveals that the averaged model, for the studied samples, predicts the wind power more accurately than the persistent model; in fact, up to 36.31 % for the MAE, 25.83 % for the RMSE, and 36.34 % for the average percentage error. Also, it is demonstrated that for the wind sample with high level of randomness, such as sample 4, using the RMSE only in evaluating the accuracy of the prediction technique, deos not provide a suitable indication for evaluating the model accuracy.

Table 3-4: MAE (kW), RMSE (kW), average percentage error (% error), and improvements for wind power prediction.

	Parameter	**Persistent**	**Averaged**	***% Improvement***
Sample 1	***MAE***	116.01	95.50	*17.68*
	RMSE	184.81	150.97	*18.31*
	% error	7.03	5.79	*17.64*
Sample 2	***MAE***	109.84	93.80	*14.60*
	RMSE	179.70	150.96	*15.99*
	% error	6.62	5.69	*14.05*
Sample 3	***MAE***	131.60	83.81	*36.31*
	RMSE	194.90	144.55	*25.83*
	% error	7.98	5.08	*36.34*
Sample 4	***MAE***	159.89	139.84	*12.54*
	RMSE	194.74	194.16	*0.30*
	% error	9.69	8.48	*12.49*

Figure 3-14 presents the scattering and the linear relationships between the predicted and the actual values for the wind power prediction for the four data sets with the averaged GM(1,1) model. This figure exhibits a good scattering of the predicted values of the wind power.

Table 3-5 lists the corresponding linear relationships between the predicted and the actual values. This table reveals that the scaling factor and the y-axis intercept coefficients are very close to unity and zero, respectively.

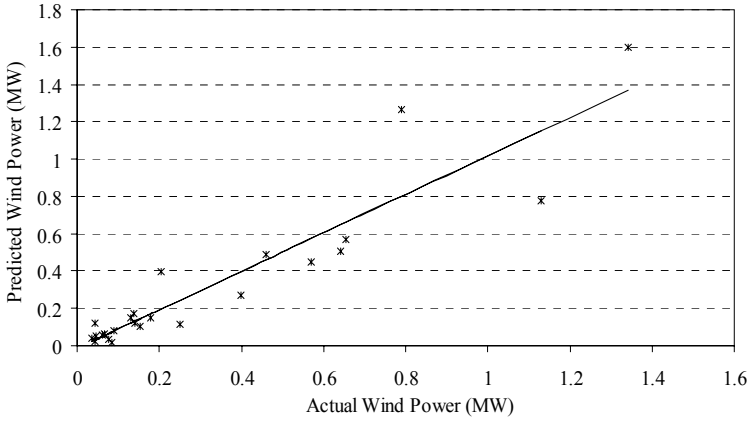

a) Sample 1

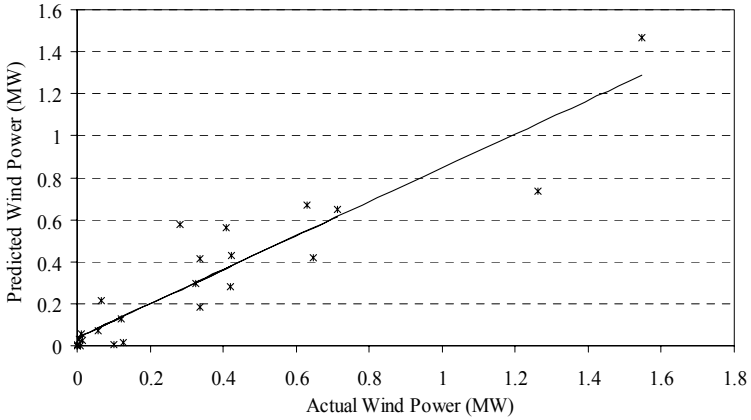

b) Sample 2

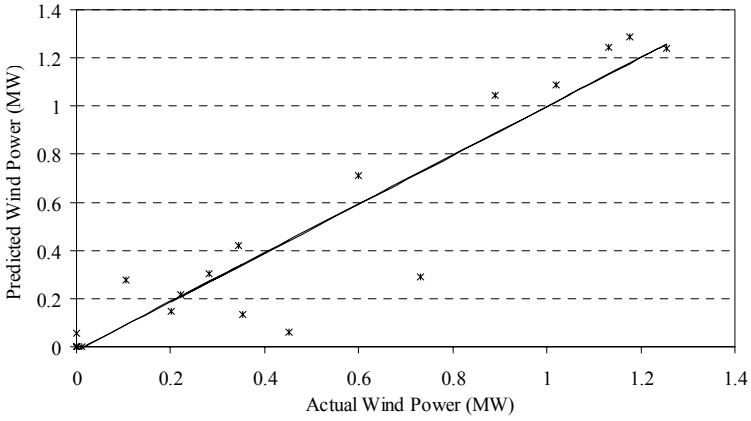

c) Sample 3

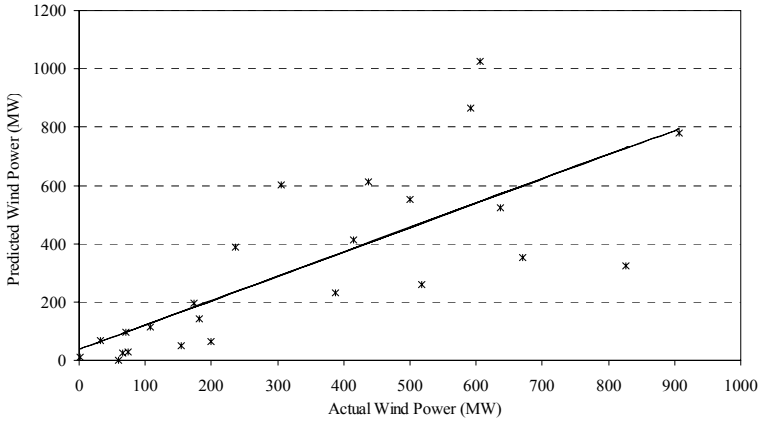

d) Sample 4

Figure 3-14: Actual and predicted wind power using the averaged GM(1,1) rolling model relationships.

Table 3-5: Actual and predicted values linear relationship coefficients for the averaged GM(1,1) rolling model.

Samples	Linear Relationship (MW)
Sample 1	$-0.015 + 1.032\, x_i$
Sample 2	$0.037 + 0.809\, x_i$
Sample 3	$-0.016 + 1.015\, x_i$
Sample 4	$0.037 + 0.836\, x_i$

3.4 Reactive Power Shared Voltage Regulation-Based Technique for DFIGs

The previous sections describe how the active power of a single variable speed wind turbine unit is predicted for one hour ahead operation. In this section, the development and investigation of a new technique for efficient active power generation from such units are described.

During the last decade, numerous variable speed wind turbines, equipped with DFIGs, have been installed all over the world, especially for wind turbines with capacities that exceed 1 MW. DFIGs have performed dynamically better than other types of wind turbines due to the following [27].

- the dynamic performance capability at subsynchronous and supersynchronous speed ranges
- the capability to generate constant frequency active power

- the decoupled control of the generated active and reactive power
- the reduction in the ratings for the used converters.

Table 3-6 provides a brief comparison between DFIGs (Type: C wind turbines) and Squirrel Cage Induction Generators (SCIGs) (Type: D wind turbines) [106].

Table 3-6: Comparison between DFIGs and SCIGs

DFIGs (Type: C)	***SCIGs (Type: D)***
Smaller (partial) rated converters (each converter is rated at 30 – 50 % of the machine rating)	Full rated converters (each converter is rated at 100 % of the machine rating)
Low frequency controlled rotor current	Power frequency controlled stator current
Wide range of speed operation	Limited range of speed operation
Complex construction	Simple construction
Required regular maintenance	Do not require regular maintenance
Complex gear box construction as its performance is affected by grid disturbances as the stator is directly connected to the grid	Simple gear box construction as its performance is decoupled from grid disturbances
Limited full torque control	Full torque control

The dramatic increase in the installation of wind driven DFIGs encourages researchers to develop various control techniques for DFIGs. This has been reflected in the numerous publications for the last decade [107 - 117]. Most of these techniques deal with the active and reactive power control of DFIG units [107 - 111]. In such techniques, the generated active power is controlled to track the maximum power characteristic curve of the unit, and the reactive power is controlled to regulate the

generated/absorbed reactive power, or to regulate the DFIG unit (farm) terminal power factor [107 - 109], including terminal unity power factor operation [110, 111]. However, this can result in a discontinued unit production, when the turbines' terminal is subjected to disturbances that result in a voltage limits violation, or when the system operators attempt to keep the terminal voltage within the pre-specified limits.

Recently, the research has been focused on developing control techniques that are capable of regulating the DFIGs terminal voltage [112 - 117]. Among these techniques is the implementation of a voltage security level, where the reactive power generated/absorbed is controlled to keep the terminal voltage within the pre-specified limits [112]. However, this technique does not provide a smooth voltage regulation. The most recent voltage regulation-based techniques involve controlling the rotor side converter in such a manner as to capture the maximum available active power and to regulate the stator terminal voltage [113 – 116]. In [117], another technique is established by controlling the rotor side converter for compensating the DFIG magnetizing reactive power, whereas the grid-side converter is controlled to regulate the terminal voltage. Current practices for voltage regulation mode involve deactivating the grid-side converter from exchanging any reactive power with the grid terminals, until the rotor-side converter reaches its rated value.

The controlling of DFIGs, for the power factor regulation mode of operation, and optimizing the generators power loss have been recently developed by optimizing the reactive current command ratio between the rotor-side and the grid-side converters [118]. This technique has been proven successful for such mode of operation. However, for the voltage regulation mode of operation, the final optimized formula is not feasible and provides inaccurate results. Moreover, this technique requires large sets of look-up tables for the voltage regulation mode. This section considers the loss reduction issue by proposing a control technique based on activating the two converters at all the operating points, and equally sharing the generated/absorbed reactive power between them. The connection diagram of the DFIG with a brief description for the converters' control actions and the required signals is presented in Figure 4-3. The following subsection introduces the proposed control technique and details of the control loops.

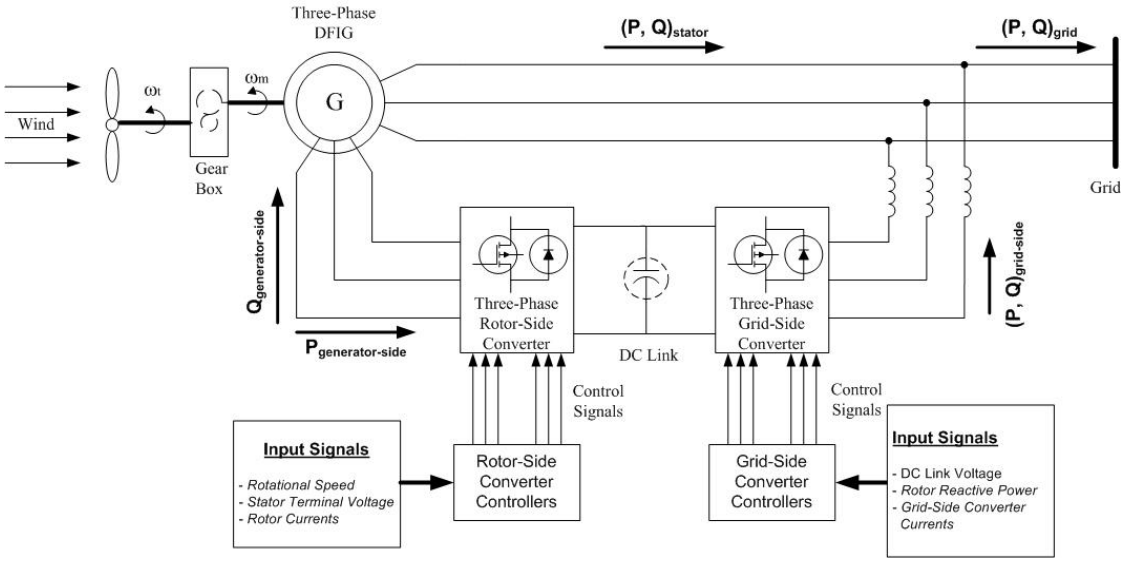

Figure 3-15: Connection diagram of the DFIG with the proposed control technique signals.

3.4.1 Control Loops

The proposed technique is based on regulating the wind farm terminal voltage and equally sharing the generated/absorbed reactive power between the rotor-side and the grid-side converters. In this way, the reactive current component that is flowing through the generator, as well as the total current and the power loss are reduced. This is carried out in parallel with other functions such as to regulate the DC bus voltage of the back-to back converter by controlling the active current component of the grid-side converter and tracking the maximum power carried out by the generator (rotor)-side converter. The following subsections provide a detailed description for the different control loops.

3.4.1.1 Rotor-Side Converter Control Loops

The functions of these loops are to track the maximum output power and to regulate the turbine terminal voltage. The q-axis component control loop is used to track the maximum output power by using the instant values of the incident wind speed and the generator rotational speed with a maximum power tracking characteristic for the turbine. The difference between the optimum power (P_{ref}) and the summation of the actual generated power and the power losses activates a PI control that generates the q-axis reference current (I^*_q). This reference current value is then compared with the actual q-axis rotor current to activate a PI controller which, in turn, generates the reference q-axis voltage reference signal (V^*_q) for the rotor-side converter.

The d-axis component control loop is employed to regulate the grid terminal voltage ($V_{Grid,\ actual}$) to a reference preset value ($V_{Grid,\ ref}$). The difference between the reference and the actual grid voltage values activates a PI controller to generate the d-axis reference current (I^*_d). This reference current value (I^*_d) is then compared with the actual d-axis rotor current to activate a PI controller which, in turn, generates the reference q-axis voltage reference signal (V^*_d) for the rotor-side converter. Figure 3-16 presents the rotor-side converter control loops.

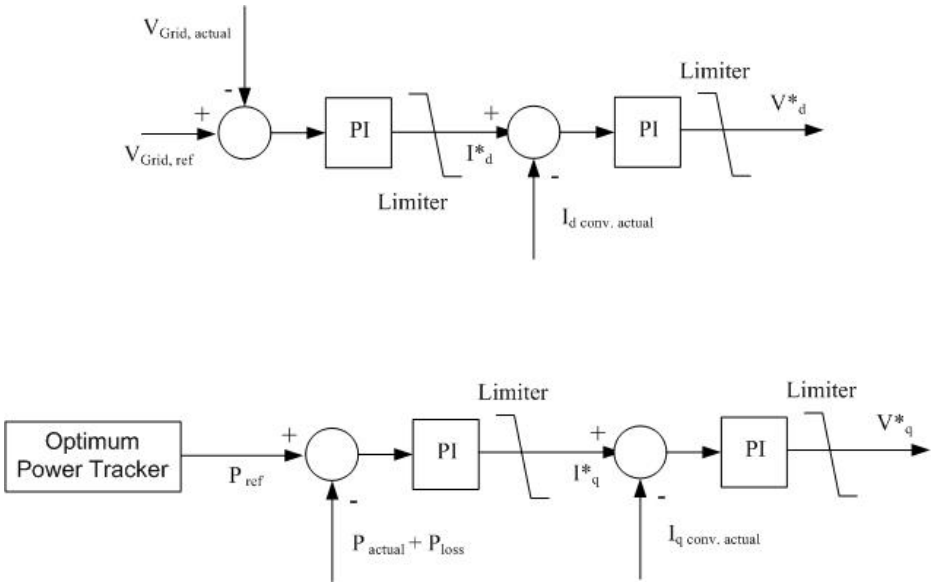

Figure 3-16: Control loops for the rotor-side converter.

3.4.1.2 Grid-Side Converter Control Loops

These loops are necessary to ensure that the reactive power is shared between the two converters and to regulate their DC bus voltage. The difference between the actual measured value ($V_{DC,\ actual}$) and the required reference value ($V_{DC,\ ref}$) activates a PI controller to produce the required d-axis current component control signal (I^*_d). This is then compared with the actual grid-side converter d-axis current, and the resultant error activates another PI controller to generate the d-axis voltage reference signal (V^*_d) for the grid-side converter.

Similarly, the q-axis voltage reference signal (V^*_q) is designated to equate the generated reactive power from the grid-side converter to the absolute reactive power generated by the rotor-side converter. The difference between the two reactive power activates a PI controller to generate the required q-axis current component control signal (I^*_q). This is then compared with the actual grid-side

converter q-axis current and the generated error activates another PI controller to produce the d-axis voltage reference signal (V^*_q) for the grid-side converter. Figure 3-17 presents the block diagrams for the grid-side converter control loops.

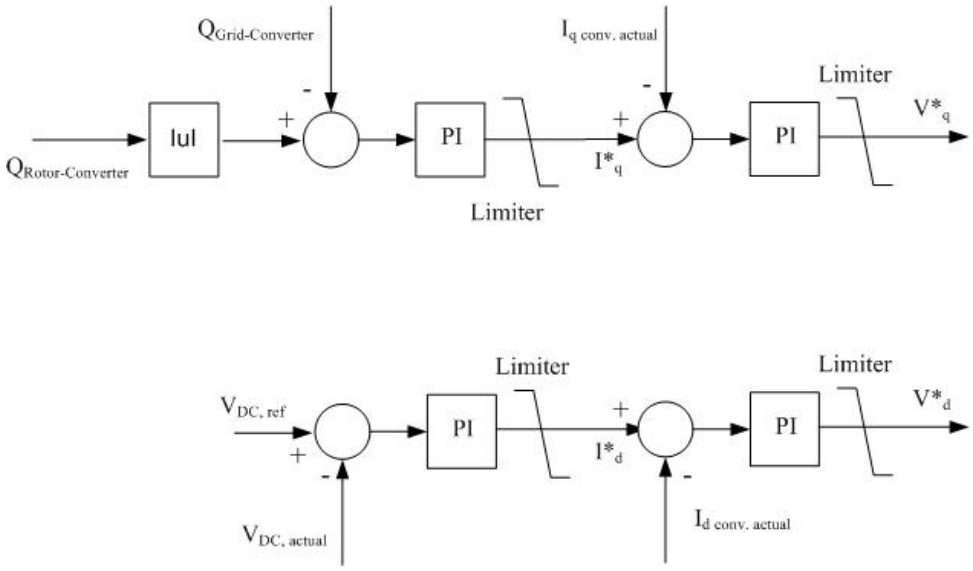

Figure 3-17: Grid-side converter control loops.

3.4.1.3 Pitch Angle Control Loop

Once the turbine rotational speed (ω) exceeds the reference value at which the output power of the turbine is 1 pu, the pitch angle actuator is activated to limit the turbine mechanical power to 1 pu. The corresponding block diagram for the pitch angle control loop is laid out in Figure 3-18. The maximum pitch angle is set to 45° and the pitch angle rate of change is limited to 2°/s.

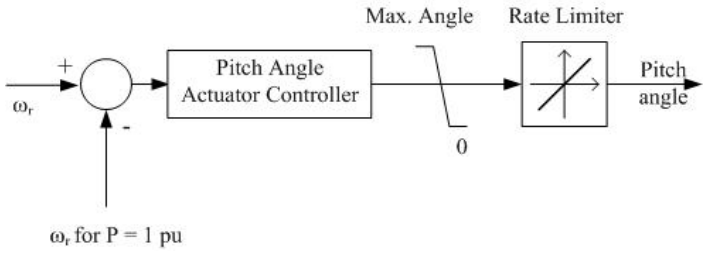

Figure 3-18: Pitch angle control loop.

3.4.2 System Description

The system under investigation and its components is shown in Figure 3-19. A 12 MW wind farm, equipped with 8 variable-speed DFIG wind turbines, is connected to a distribution network that is loaded with passive and active loads. Identical operation conditions are assumed for the wind turbines. Therefore, the wind farm aggregated model is used, and the farm is modeled by one 12 MW wind turbine unit. The system is simulated in the MATLAB/SIMULINK environment. Appendices B and C present the aerodynamic model used for the wind turbines and the system parameters [119].

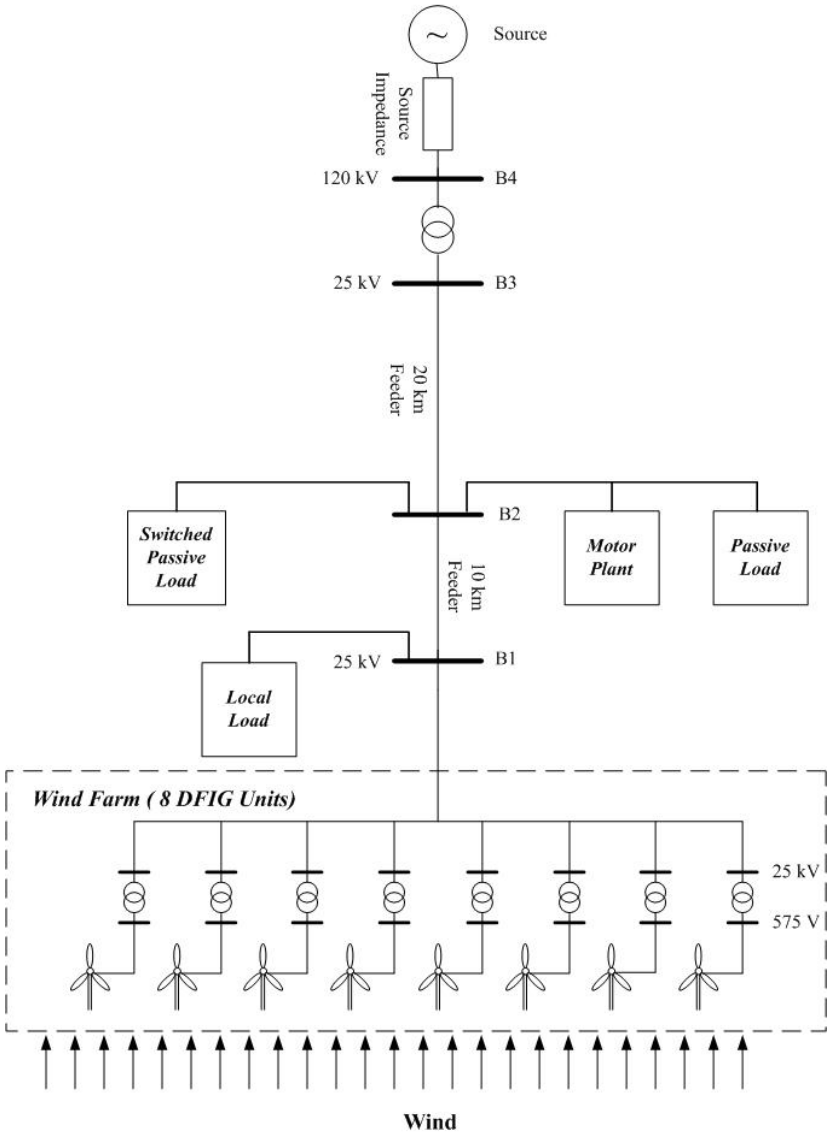

Figure 3-19: Grid-connected wind farm system under investigation.

3.4.3 Economic Evaluation

In this section, an evaluation of the economic benefits for this technique is conducted. The economic evolution is carried out by choosing the most common probability density function for wind speeds which is the Rayleigh probability density function that is expressed mathematically as [120]

$$f(v) = \frac{\pi\, v}{2\,\bar{v}^{2}} \exp\left[-\frac{\pi}{4}\left(\frac{v}{\bar{v}} \right)^{2} \right] , \qquad (3\text{-}35)$$

where *f(v)* represents the Rayleigh probability density function for a given wind speed *v*, and $\bar{v}$ represents the mean value for the wind speed.

The effect of changing the mean wind speed value on the shape of the Rayleigh probability density function is shown in Figure 3-20. The cumulative distribution function for the Rayleigh statistics *F(V)* is expressed as follows;

$$F(V) = prob(v \le V) = 1 - \exp\left[-\frac{\pi}{4}\left(\frac{V}{\bar{v}} \right)^{2} \right] . \qquad (3\text{-}36)$$

The area under the curve between any two points (with wind speeds V_1 and V_2) represents the probability for the incident wind speed to be within this range. This is computed by

$$\begin{aligned} prob(V_1 < v < V_2) &= F(V_1) - F(V_2) \\ &= \left\{ 1 - \exp\left[-\frac{\pi}{4}\left(\frac{V_1}{\bar{v}} \right)^{2} \right] \right\} - \left\{ 1 - \exp\left[-\frac{\pi}{4}\left(\frac{V_2}{\bar{v}} \right)^{2} \right] \right\} \\ &= \exp\left[-\frac{\pi}{4}\left(\frac{V_2}{\bar{v}} \right)^{2} \right] - \exp\left[-\frac{\pi}{4}\left(\frac{V_1}{\bar{v}} \right)^{2} \right] \end{aligned} \qquad (3\text{-}37)$$

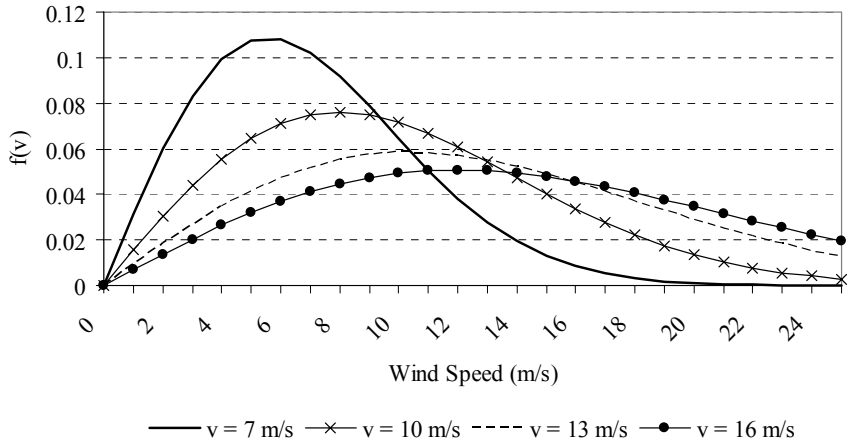

Figure 3-20: Rayleigh probability density function at different mean wind speeds.

The system in Figure 3-19 is studied under various incident wind speed values. At each value, the generated active power is recorded for the proposed technique and the traditional technique, where there is no reactive power exchange with the grid-side converter. The savings (increase) in the generated active power by using the proposed technique is recorded at each value for the wind speed, as illustrated in Figure 3-21. This figure reveals that at around 10 m/s, there is no savings in the generated power. This occurs because this wind speed value is corresponding to rotating the DFIG at the synchronous speed, and thus, no reactive power flows through the rotor circuit. Consequently, both the traditional and the proposed technique generate the same active power.

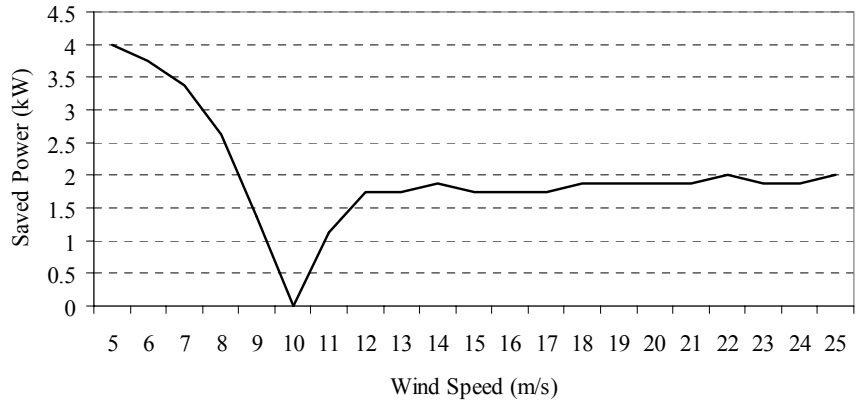

Figure 3-21: Power savings at different incident wind speeds.

This figure reveals that, at low wind speeds, saved power of 4, 3.75, and 3.38 kW (per wind turbine unit) is achieved for incident wind speed values of 5, 6, and 7 m/s, respectively. This is corresponding to 13.85 %, 3.45 %, and 1.67 %, respectively, of the corresponding generated power at these wind speed values. At high wind speeds, the percentage of the saved power is reduced to 0.13%.

The number of hours that the wind farm is subjected to a given wind speed range is calculated by using equation (3.37). To calculate the saved energy, these hours are multiplied by the corresponding power savings in Figure 3-21. An average annual energy cost of 71.87 $/MWh is used to calculate the annual savings that is recorded in Figure 3-22 for different mean wind speed values. This cost value represents the mean cost value for the Hourly Ontario Energy Price (HOEP) for 2005 [121]. This figure conveys that the proposed technique can increase the annual energy revenue by $1134 per wind turbine unit. Therefore, for a wind farm of 100 similar units, this control technique can result in an overall annual running costs savings of $113,400.

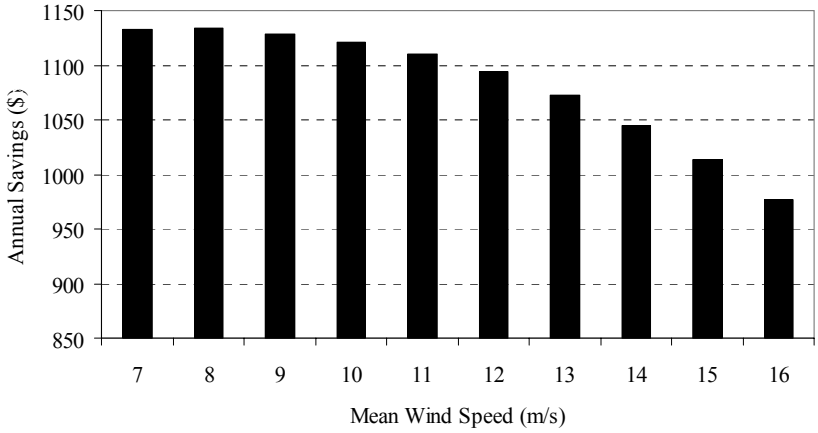

Figure 3-22: Annual savings per wind turbine unit.

3.4.4 Simulation Results

Three different simulation scenarios are carried out to validate the effectiveness and the accuracy of the proposed control technique. The first scenario is conducted to evaluate the system performance under changes in the wind speed. In the second scenario, the system is investigated, when the source bus is subjected to voltage sag. Finally, in the third scenario, the performance due to changes in the nearest bus loading conditions is examined.

3.4.4.1 Wind Speed Variation

This subsection investigates the performance of the control technique, when the system is subjected to variations in the incident wind, as shown in Figure 3-23. Here, the switched passive load is assumed connected throughout the simulation period. In Figure 3-24, the farm's terminal voltage is presented, that indicates that the voltage regulation control loop successfully regulates the farm's terminal voltage at the preset value (1 pu) despite of the variations in the incident wind speed. The reactive power produced by the farm, that is required to regulate the terminal voltage, is shown in Figure 3-25. This figure illustrates that at higher wind speed levels; less reactive power is required for the voltage regulation.

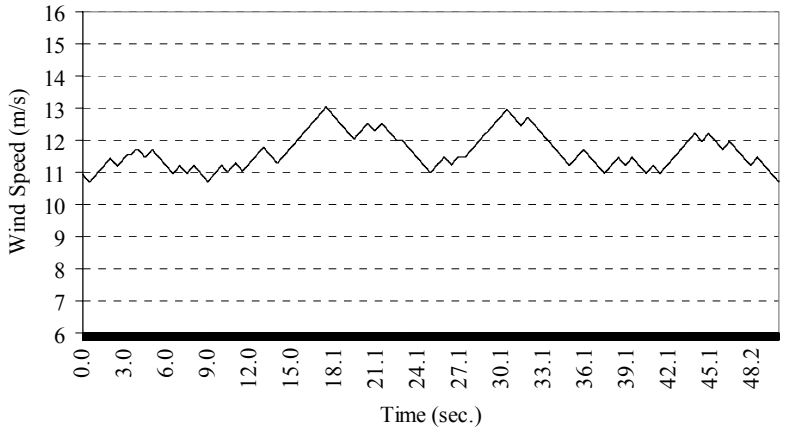

Figure 3-23: Wind speed variation with time.

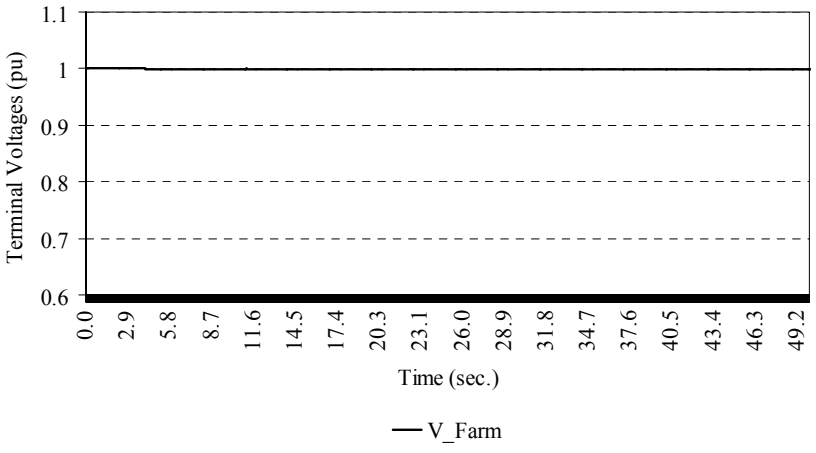

Figure 3-24: Wind farm terminal voltage variation with time.

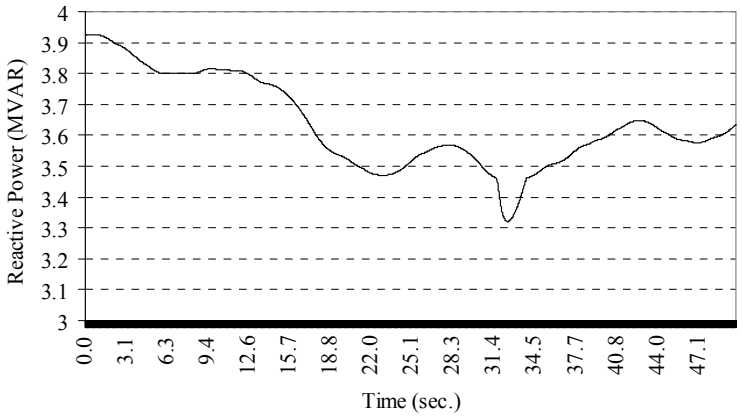

Figure 3-25: Wind farm generated reactive power variation with time.

The generated reactive power by each converter (for the aggregated 12 MW wind turbine model) is presented in Figure 3-26. This figure shows that the generated reactive power by the rotor-side converter is negative which means that the rotor circuits generate reactive power that flows to the rotor-side converter. This is the case when the DFIG rotates at speed levels above the synchronous speed (supersynchronous speed range), as illustrated in Figure 3-27 that presents the variation in the DFIG rotational speed with time. Figure 3-26 also reflects the effectiveness of the grid-side control loop in tracking the absolute value of the generated reactive power of the rotor-side converter. Figure 3-28 demonstrates the variation in the generated active power, which increases with the increase in the incident wind speed and vise versa.

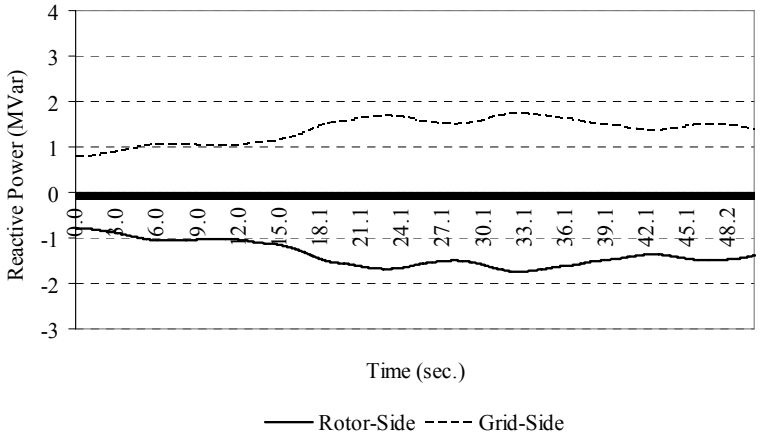

Figure 3-26: Rotor-side and grid-side converters reactive powers variation with time (for the aggregated 12 MW wind turbine model).

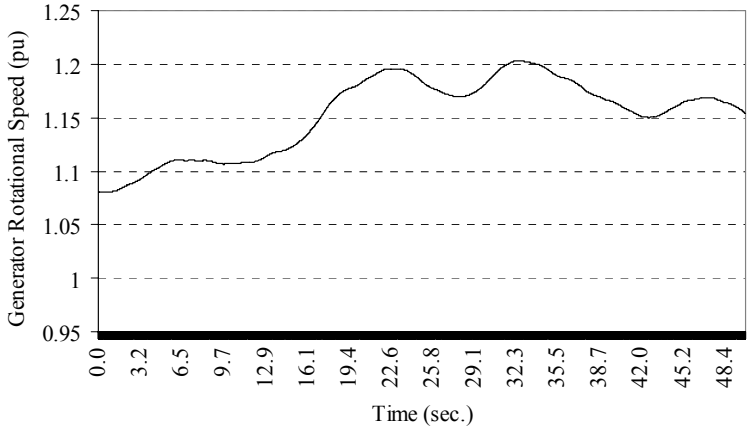

Figure 3-27: Wind turbine rotational speed variation with time (for the aggregated 12 MW wind turbine model).

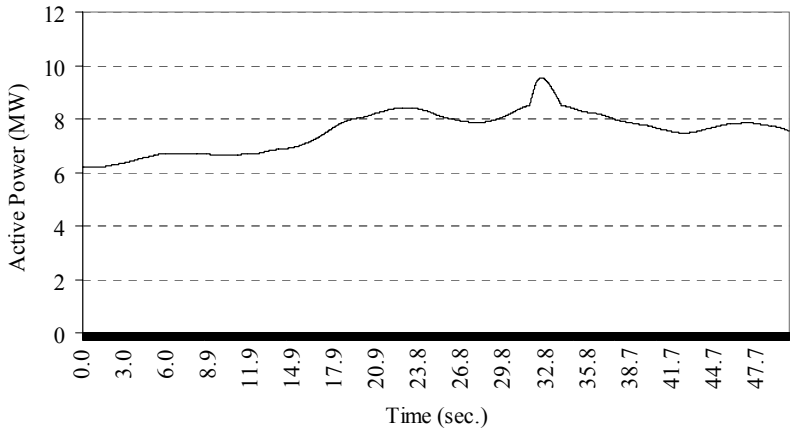

Figure 3-28: Wind farm output power variation with time.

3.4.4.2 Voltage Sag at the 120 kV Supply Bus (B4)

In this scenario, the 120 kV supply bus (B4) is subjected to a voltage sag of 0.15 pu at t = 2 s and lasts 1.5 second, where the incident wind speed is assumed constant at 13 m/s during the simulation period. Here, the switched passive load is also assumed to be connected. The buses voltages, recorded for this case, are shown in Figure 3-29. Obviously, the proposed control technique is effective in regulating the farm terminal voltage, while both the B2 bus and the supply bus (B4) experience voltage drops.

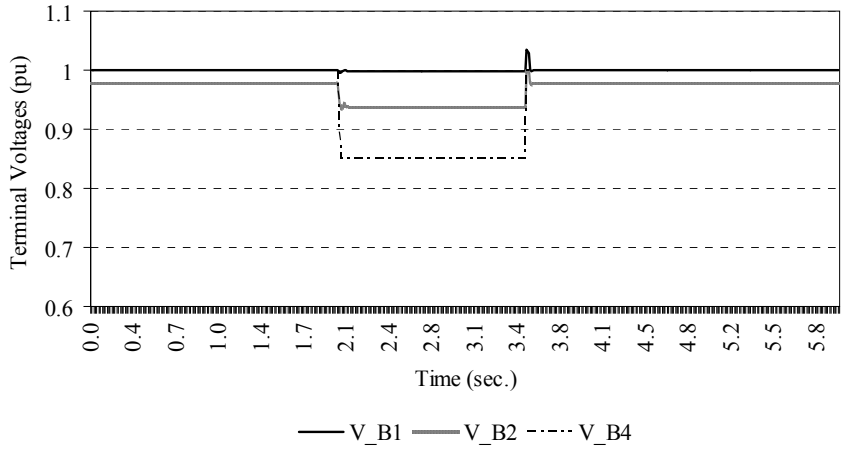

Figure 3-29: Terminals' voltage variation with time (proposed control scheme).

Figure 3-30 presents the generated reactive power from the farm (and the corresponding generated reactive power per wind turbine unit) that is required to regulate the terminal voltage to 1 pu. The reactive power generated by each converter (for the aggregated 12 MW wind turbine model) is presented in Figure 3-31. The effectiveness of the grid-side control loop in tracking the absolute value of the generated reactive power of the rotor-side converter during voltage sag disturbances is demonstrated. Figure 3-32 shows the generated active power from the farm terminals. Regarding the action of the DC link control loop in Figure 3-33, the DC voltage is effectively regulated at the preset value of 1.2 kV despite the changes in the operating conditions.

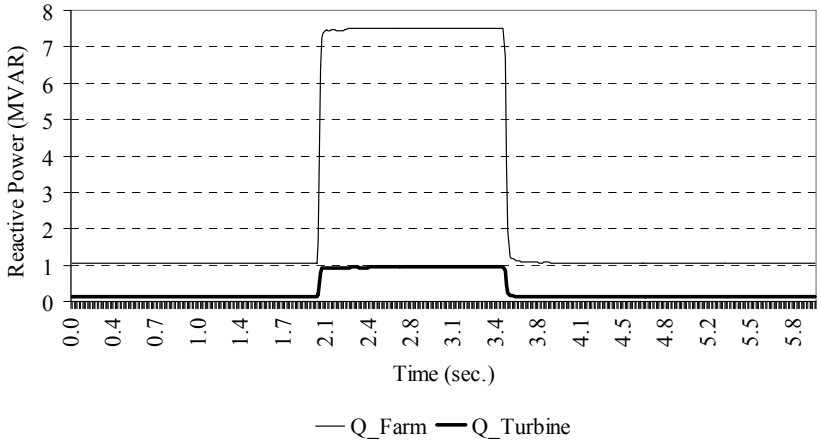

Figure 3-30: Wind farm generated reactive power variation with time.

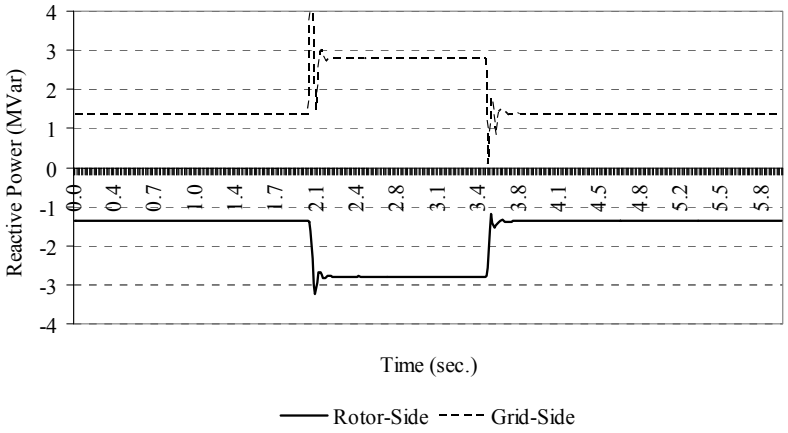

Figure 3-31: Rotor-side and grid-side converters reactive powers variation with time (for the aggregated 12 MW wind turbine model).

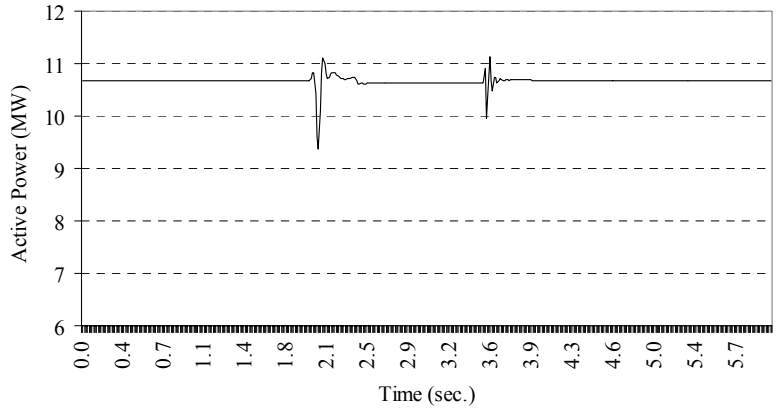

Figure 3-32: Wind farm output power variation with time.

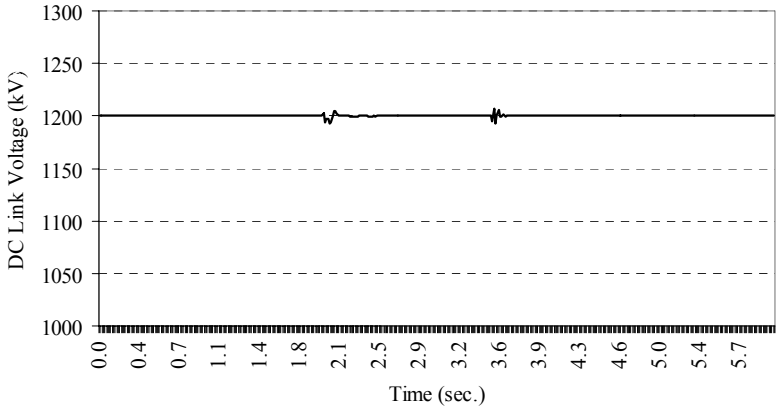

Figure 3-33: DC link voltage variation with time (for the aggregated 12 MW wind turbine model).

3.4.4.3 Load Switching

The effect of changing the network loading condition at the nearest bus (B2) to the wind farm terminals is examined in this scenario. The switched passive load is assumed to be disconnected for five seconds in the simulation period, and then connected for the next five seconds, as indicated by the current injected into this load as shown in Figure 3-34. This figure shows that the current is zero for the first five seconds and after t = 10 s, which indicates the disconnection of the load during these periods. The incident wind speed is assumed constant at 13 m/s during the assessment.

The corresponding wind farm terminal voltage and the different bus voltages, after the proposed control technique is used, are presented in Figure 3-35. The supply voltage remains constant at 1 pu during the simulation, whereas the B2 bus voltage drops to 0.964 pu during the load connection period. Moreover, it is evident that the proposed voltage regulation technique can be managed successfully to regulate the farm's terminal voltage to 1 pu during the disturbances.

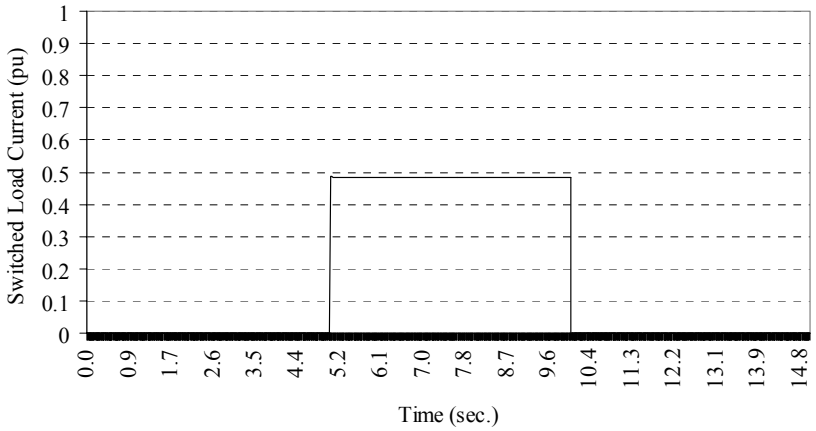

Figure 3-34: Switched load current variation with time.

The generated reactive and active powers from the farm and the generated reactive power from each converter (for the aggregated 12 MW wind turbine model) are recorded in Figure 3-36, Figure 3-37, and Figure 3-38, respectively. Figure 3-37 shows that the generated active power is the same during the steady state operations period, whether the load is connected or not. This is due to the fact that the generated active power is mainly determined by the incident wind speed which is assumed constant during this simulation. Finally, Figure 3-39 reveals the effectiveness of the DC bus control loop in regulating the DC bus voltage at 1200 V during the disturbances.

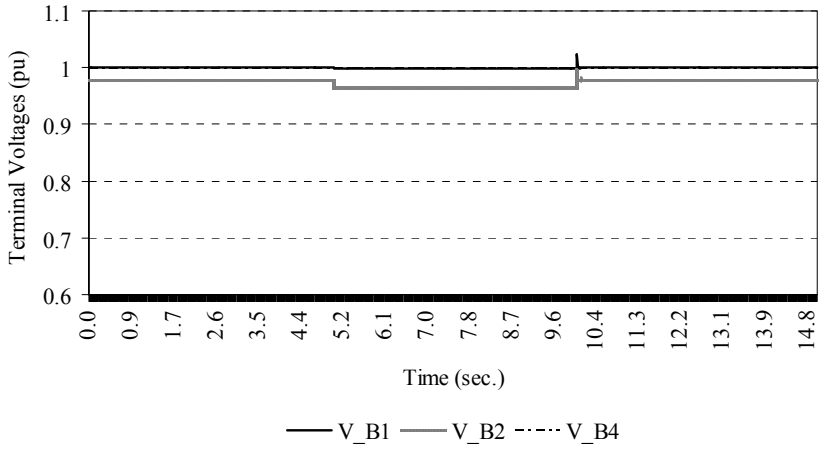

Figure 3-35: Terminals' voltage variation with time.

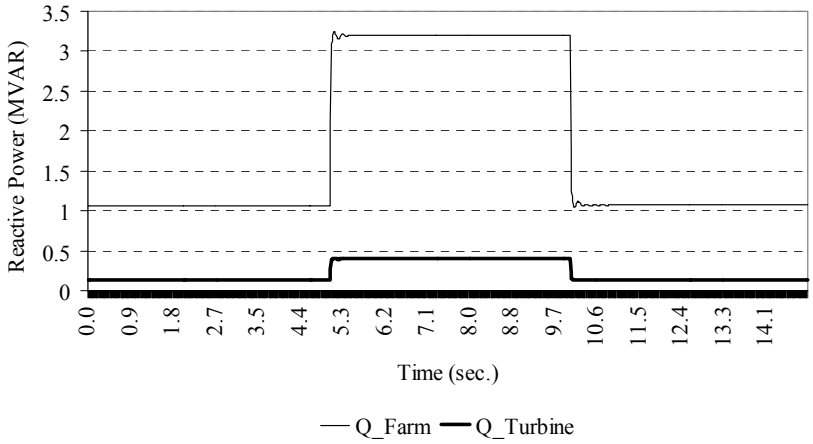

Figure 3-36: Wind farm generated reactive power variation with time.

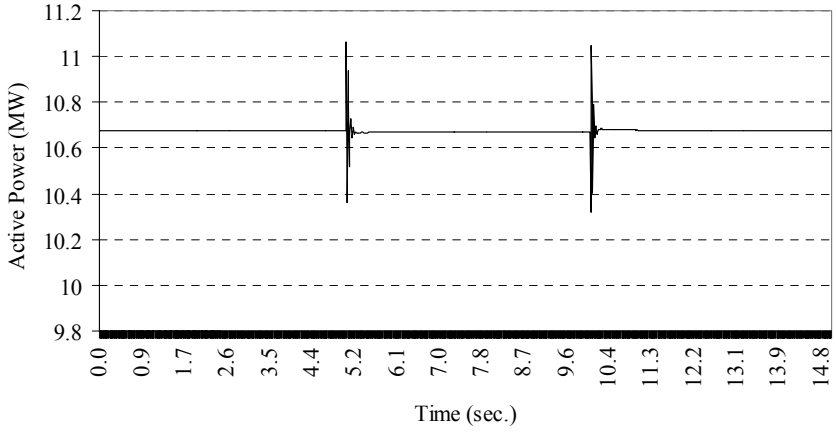

Figure 3-37: Wind farm output power variation with time.

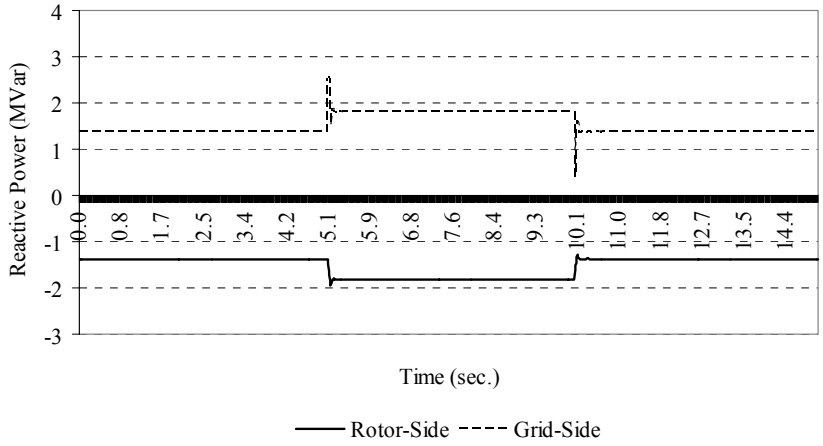

Figure 3-38: Rotor-side and grid-side converters' reactive powers variation with time (for the aggregated 12 MW wind turbine model).

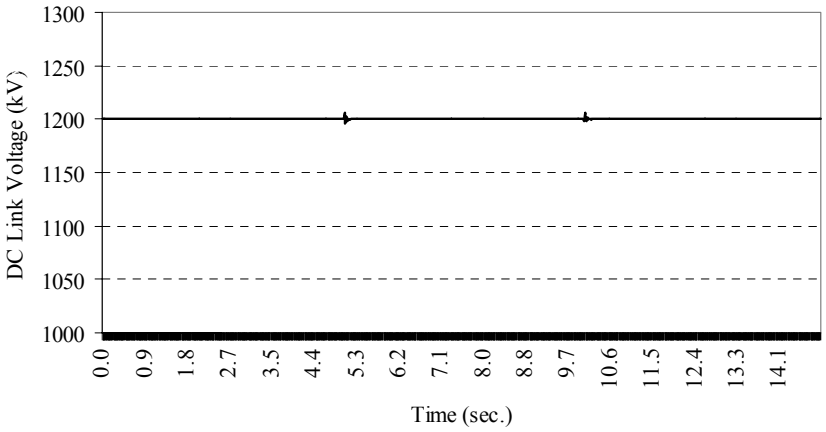

Figure 3-39: DC link voltage variation with time (for the aggregated 12 MW wind turbine model).

3.5 Chapter Assessment

This chapter deals with operational aspects of a single variable speed wind turbine unit. It focuses on how the generated power of these turbines is predicted and efficiently controlled. A new tool for predicting one-hour ahead average hourly wind speed and wind power, by using the Grey prediction technique {GM(1,1)}, is introduced. The generated results from the traditional GM(1,1) model reveal the effectiveness of the proposed model in tracking the actual wind speed time series with an improvement over the persistent model as much as 5.88 % for the MAE and 10.13 % for the RMSE. However, this model is characterized by the occurrence of some overshoots in the predicted time

series. Such overshoots can result in predicting the wind speed time series that is worse than the prediction of the persistent model.

To overcome the overshoot occurrence, the application of the adaptive alpha-based Grey model is examined. This model achieved higher MAE percentage improvement, than the persistent model. However, the results indicate that this model lacks the good tracking characteristic for the actual wind speed time series, achieved by the traditional model. Therefore, an improved Grey model is proposed to reduce the overshoots and the prediction errors. However, the improved model does not achieve higher improvement levels for all the tested wind speed data samples.

Furthermore, this chapter introduces the averaged Grey model that has a higher level of accuracy, for the studied samples, in the wind speed forecasting than the persistent model and the other Grey models. Moreover, it also exhibits a very good tracking feature and reduced overshoots. The results, when the averaged Grey rolling model is used, reveal an improvement in the prediction accuracy, compared with that of the persistent model, of the wind speed up to 26.89 % for the MAE, and 20.25 % for the RMSE and for wind power up to 36.31 % for the MAE, 25.83 % for the RMSE, and 36.34 % for the average percentage error. In addition, the results demonstrate that the predicted values of the proposed averaged model for wind power prediction have a very good linear relationship with their corresponding actual values.

Finally, a new technique for DFIGs voltage regulation is presented. This technique is based on activating both converters (rotor-side and grid-side) for reactive power generation in such a way that the reactive power generated/absorbed by the converters is equally shared at all the operating points. This technique manages to reduce the power losses within the DFIG units, and consequently, generates more active power. The economic evaluation for this technique reveals that the proposed technique results in an annual savings as high as $1134 per wind turbine unit. The performance of the proposed technique is examined under various operating conditions including incident wind speed variation, voltage sags disturbances, and changing the load levels at the nearest bus. The results reveal the effectiveness of the proposed technique in regulating the wind farm terminal voltage to a preset value despite the disturbances. The new technique is characterized by its simplicity and robustness, compared to the previously proposed techniques for optimum wind power loss reduction.

Chapter 4
Efficient Voltage Regulation-Based Technique for Large Scale DFIGs Wind Farms

4.1 Introduction

The previous chapter involved with the operation of a single turbine unit. The following chapters, including this chapter, are focused on same operational challenges, generated power control and prediction, but for large scale wind farms. In this chapter, a new model is presented for the wind field distribution within wind farms to investigate the possible impact of the integration of wind farms into power system grids. This model is also essential for the prediction of wind farms power production that will be explored in the next chapter.

A new aggregated model is proposed for wind farms that take into consideration the wake effect and the time delay in the incident wind speed for several wind turbines. Then, the farm model is combined with the control technique developed in Section 3.4 to simulate the dynamic response of a large scale wind farm under various operating conditions.

4.2 Impact of Proper Wake Effect and Time Delay Models on the Dynamic Performance of Wind Farms

This section investigates the impact of the proper modelling of the wake effects and wind speed delays of several rows of wind turbines on the dynamic performance accuracy of the wind farm models. A wake effect model, previously developed and successfully used in wind turbines micrositting applications [122], is adopted in the study to develop a more accurate wind field model of wind farms.

The results of three modelling scenarios are compared to highlight the impact of the novel model developed to represent the wake effects and wind speed time delay. In the first scenario, the wind wake effect and time delay are ignored. Consequently, all the wind turbines are assumed to be subjected to the same wind speed profile. In the second scenario, the wind wake effect is modelled by reducing the incident wind speed values by 0.5 m/s from one row to the next row, in the direction of the incident wind [14]. For the last scenario, the proposed model, based on the wind effect model,

developed for wind turbines micrositting applications, while considering the effect of the delay time between the wind speed profiles incident on the different wind turbines' rows, is considered.

4.2.1 System Description

The system under investigation is shown in Figure 4-1. A 45 MW wind farm, equipped with 30, 1.5 MW, variable-speed DFIG wind turbines, is connected to a distribution network loaded with passive and active loads. The wind turbines are assumed arranged in a 5 row x 6 column configuration, where the wind direction facing the rows, as shown in Figure 4-2. The operation conditions are assumed identical for the wind turbines sharing the same row. Therefore, the entire wind farm is aggregated to 5 turbines of 9 MW each, variable-speed DFIG wind turbines. Each 9 MW unit represent the aggregated model of each row (hereafter, referred to as Row1, Row2, ..etc.)

The connection diagram of the DFIG with a brief description for the converters' control actions and the required signals is presented in Figure 4-3. In this study, each DFIG is controlled to regulate its terminal voltage to unity by using the conventional voltage regulation technique, where the voltage regulation is carried out via the rotor-side converters, while the reactive power command for the grid-side converter is set to zero. The entire system is simulated in the MATLAB/SIMULINK environment. Appendix C presents the system parameters.

4.2.2 Wake Effect and Delay Time Model

The semi-empirical wake model, developed by katic et al. [21, 123] is used in this study. Figure 4-4 is a schematic diagram illustrating the wake effect. With the conservation of the momentum, the wind speed velocity at distance X behind a wind turbine is expressed by computing

$$U_x = U_o\left(1-\frac{\left(1-\sqrt{1-C_T}\right)}{\left(1+2\,k\,\frac{X}{D}\right)^2}\right), \tag{4-1}$$

where U_x is the wind speed at distance X, U_o is the initial free stream wind speed incident at the first wind turbines row, C_T is the thrust coefficient, k is the wake decay constant assumed equal to 0.11 [123], and D is the wind turbine diameter.

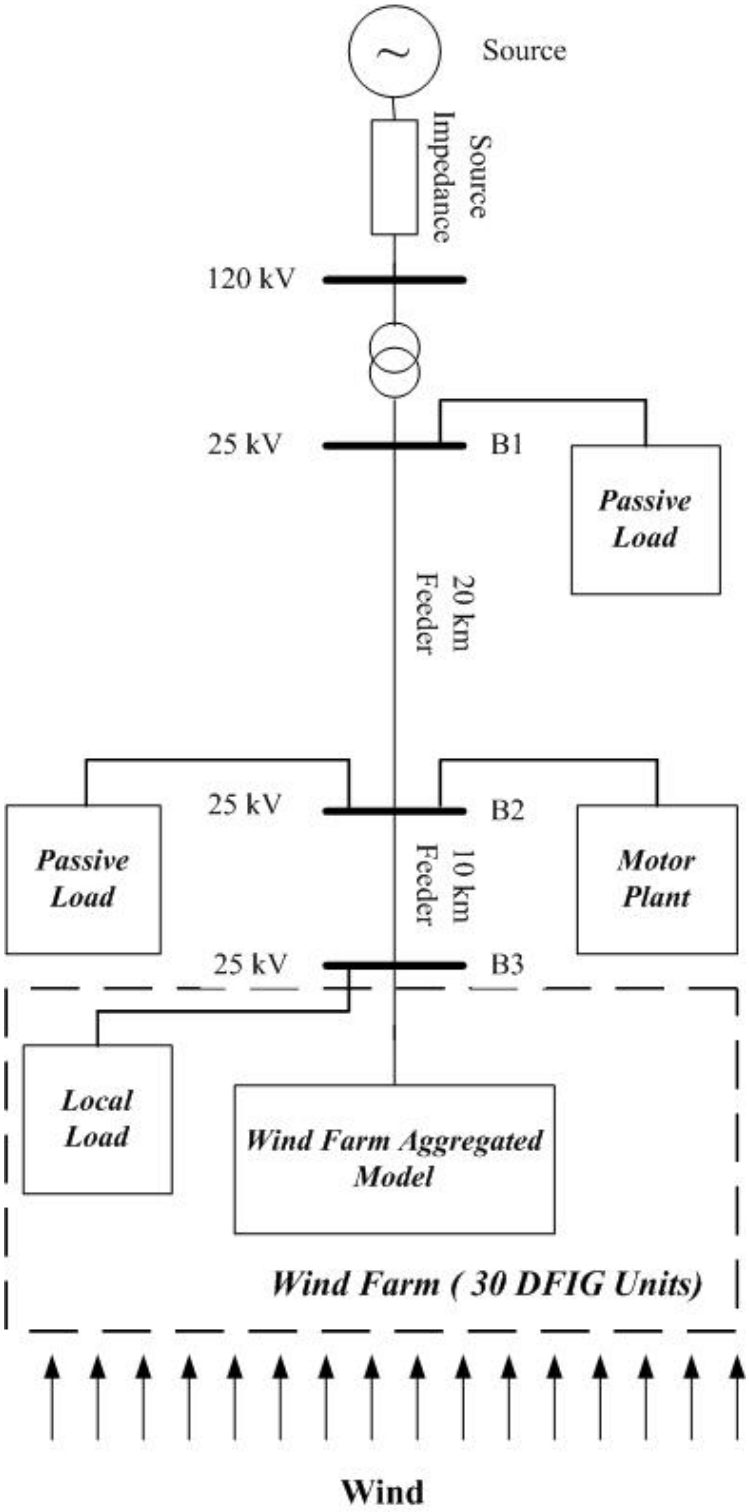

Figure 4-1: System under investigation.

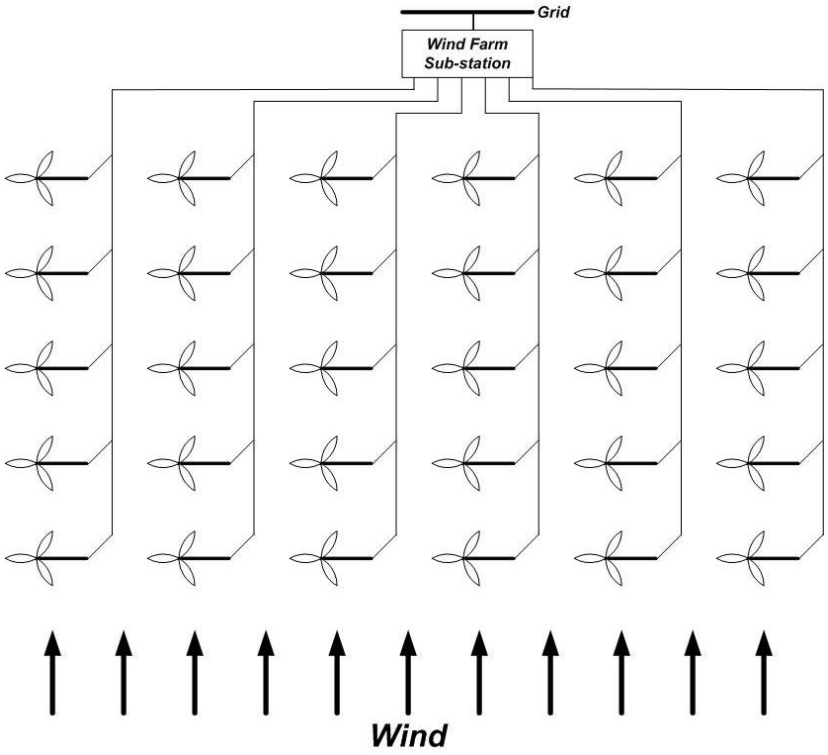

Figure 4-2: Wind turbine configuration within the wind farm.

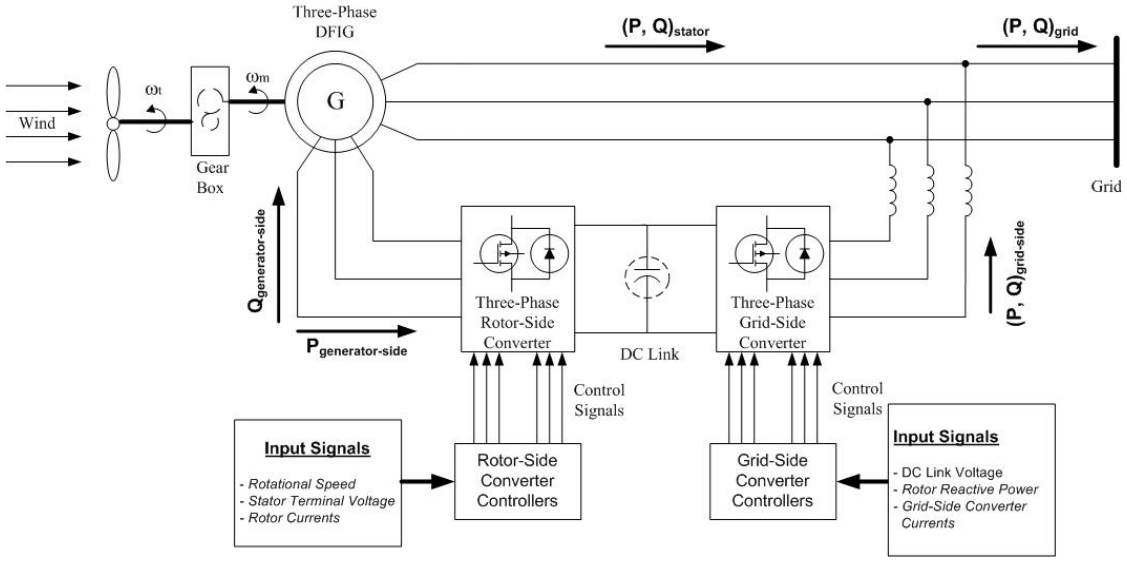

Figure 4-3: Connection diagram of the DFIG with the proposed control technique signals.

The wake diameter (D_x) at a distance X is related to the wind turbine diameter (D) as follows:

$$D_x = D + 2\,k\,X\,. \tag{4-2}$$

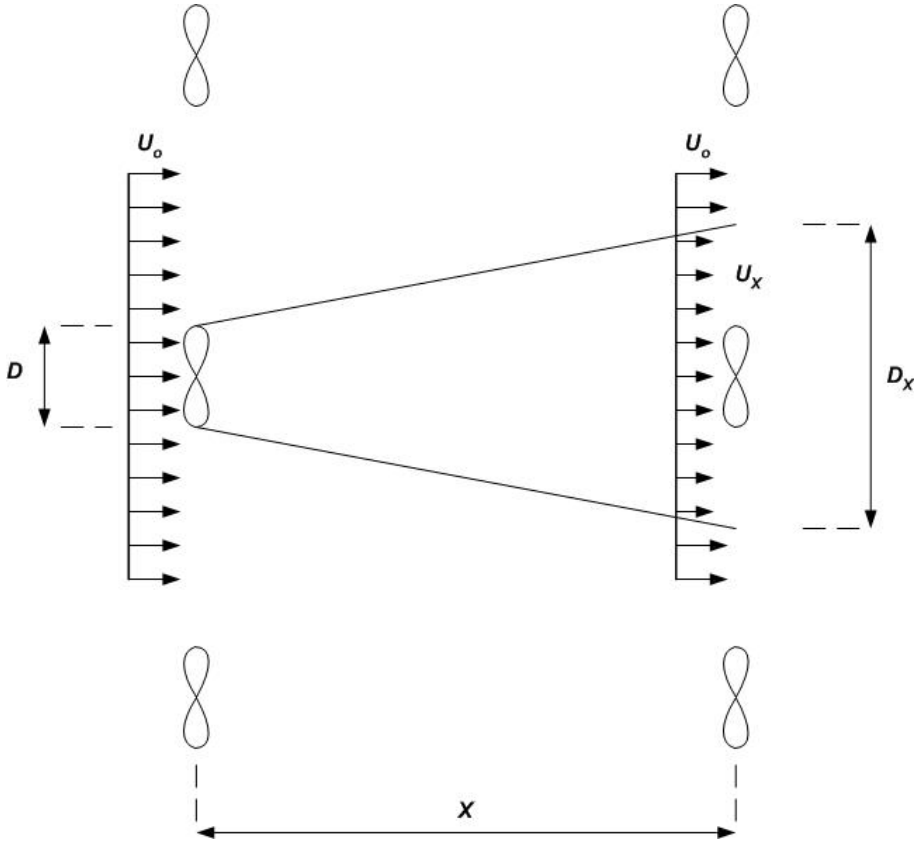

Figure 4-4: Schematic diagram for wake effect.

The wind speed delay time between two successive wind turbine rows, separated by a distance X is expressed as,

$$t_x = \frac{X}{\overline{u}}\,, \tag{4-3}$$

where t_x is the wind speed delay time, and $\overline{u}$ is the mean wind speed velocity at distance $X = 0$.

4.2.3 Simulation Results

For the identical operation scenario, all the wind turbine experience the same wind speed profile as the first raw (free stream wind speed) illustrated by Figure 4-5. When a constant wake effect is considered in the second scenario (hereafter referred to as the wake scenario), a constant wind speed reduction of 0.5 m/s is assumed for the successive rows. The resultant wind speed profiles for the different wind turbine rows are given in Figure 4-6. Finally, the wind speed profiles for the dynamic wake effect and time delay, hereafter referred to as the proposed scenario), are provided in Figure 4-6.

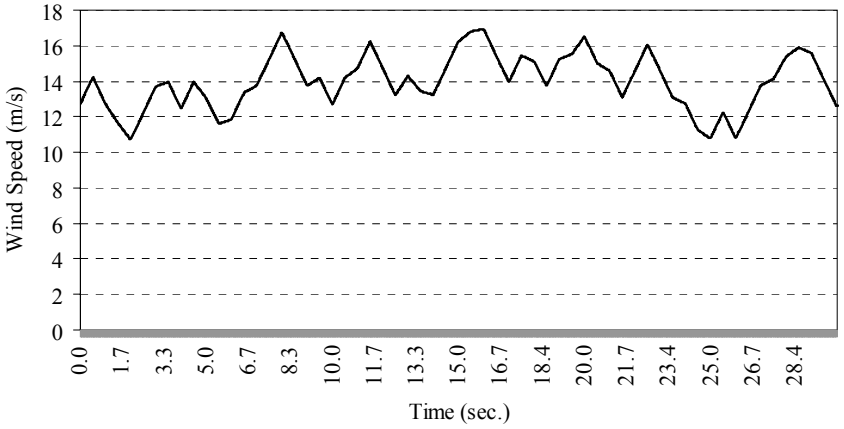

Figure 4-5: Wind speed profiles: Identical model.

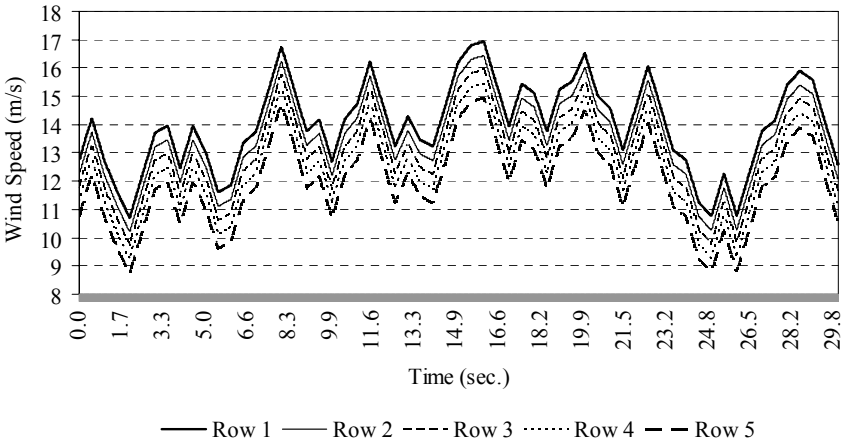

Figure 4-6: Wind speed profiles: Wake model.

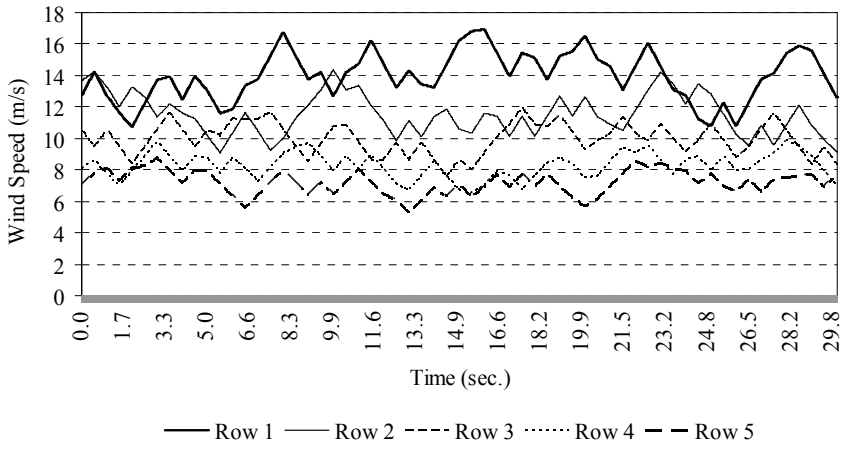

Figure 4-7: Wind speed profiles: Proposed model.

The total generation of the wind farm active power for the three modelling scenarios are presented in Figure 4-8. It is evident that the fluctuation levels in the generated power are higher for both the identical and the wake model, primarily due to ignoring the delay effect. These fluctuations are significantly reduced for the proposed model, whose performance is close to that of real applications. Moreover, this figure illustrates that the use of the dynamic wake model, the proposed model (the wake effect varies with the variations in the incident wind speed), reduces the simulated generated power, compared with the identical and wake model.

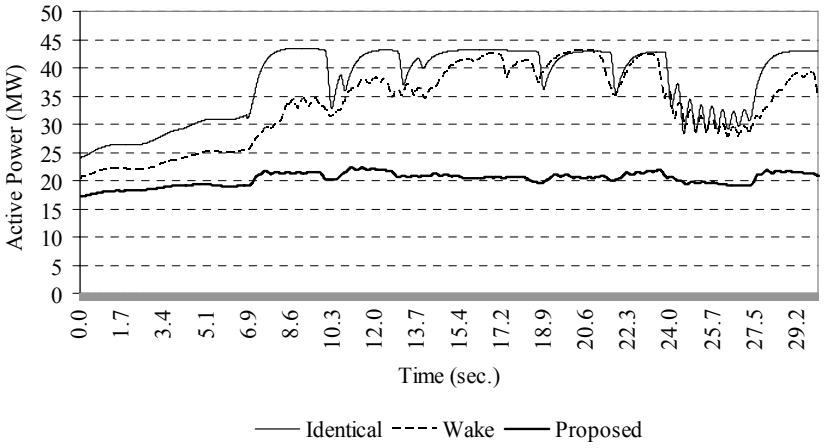

Figure 4-8: Wind farm total active power generation.

Figure 4-9 presents the voltage profile at bus B2 for the three scenarios. It is clear that when the simulated generated power, depicted in Figure 4-8, increases, the voltage drop across the 10 km feeder increases, and consequently the voltage level at the B2 bus decreases. This reduction in the voltage level affects the performance of the active loads (motor plant) connected to B2 as illustrated by the currents drawn by the motor plant, shown in Figure 4-10. This figure reveals that the plant currents suddenly drop to zero (at t =6.75s for the identical model and t = 8.4 s for the wake model), while there is always a supplied current to the plant for the proposed model. This sudden drop in the plant current is due to the activation of the plant protective system due to the under-voltage conditions at B2, as illustrated by Figure 4-9.

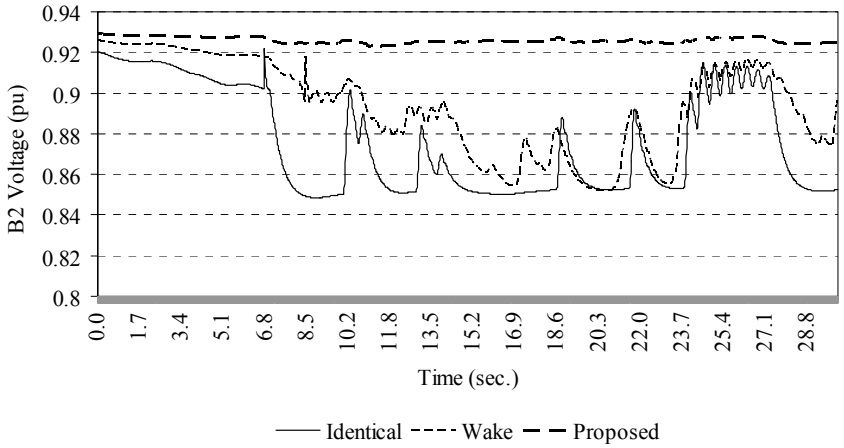

Figure 4-9: Voltage profile at Bus B2.

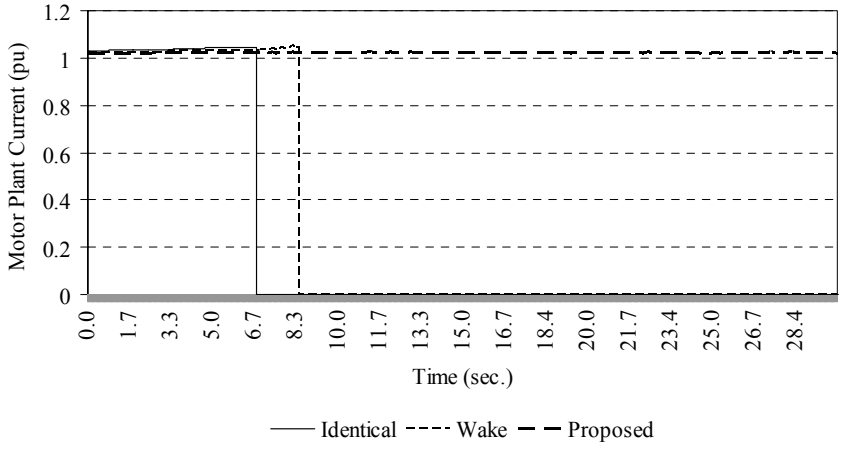

Figure 4-10: Motor plant current variation.

These figures also demonstrate that system analysts may conclude the requirements for installing a voltage regulator device at bus B2 to boost the bus voltages, and ensure the continuous operation of the motor plant when simulating the wind farm by using identical or constant wake models. However, with proper modelling of the wind field distribution within the farm, and thus the appropriate simulation for the wind power fluctuations, such regulating devices are not required.

In the identical operation, all the aggregated turbine models for each row generate the same power profile, as shown in Figure 4-11. For the wake model, the aggregated of each row has its own profile; the first row facing the wind generates the highest level of active power, followed by the second row, and so on. This is not the case when the time delay effect is considered, as shown in Figure 4-13 where Row 2 sometimes generates more real power than Row 1. This takes place for the time intervals when Row 2 experience higher wind speed values than those in Row 1, as observed in Figure 4-7.

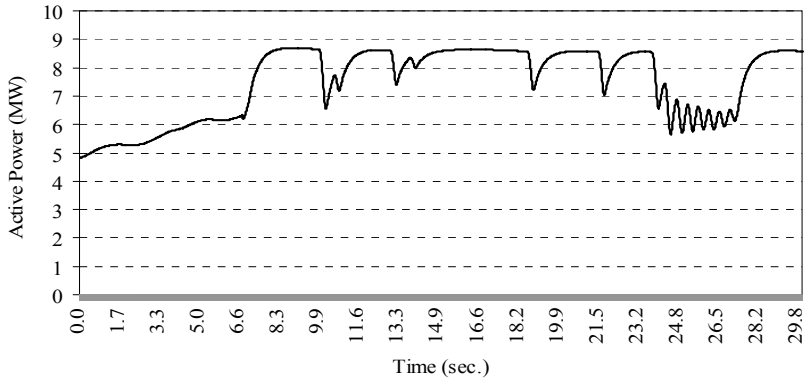

Figure 4-11: Real power generation profile: Identical model.

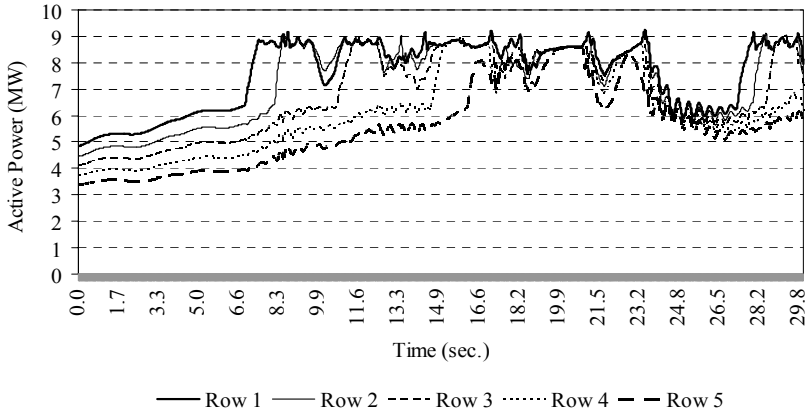

Figure 4-12: Real power generation profiles: Wake model.

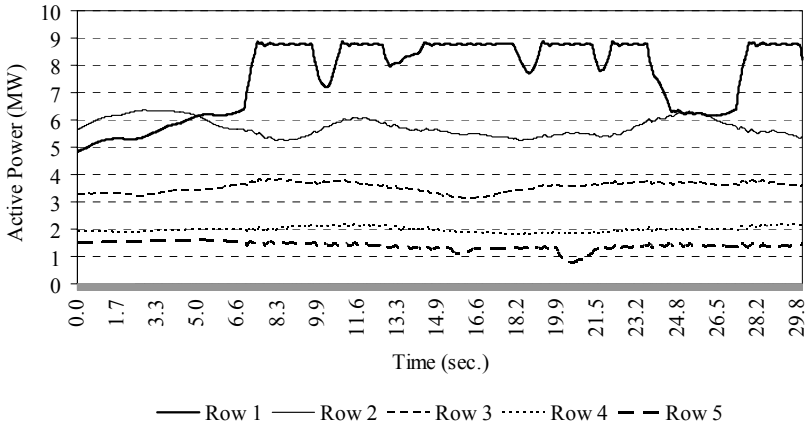

Figure 4-13: Real power generation profiles: Proposed model.

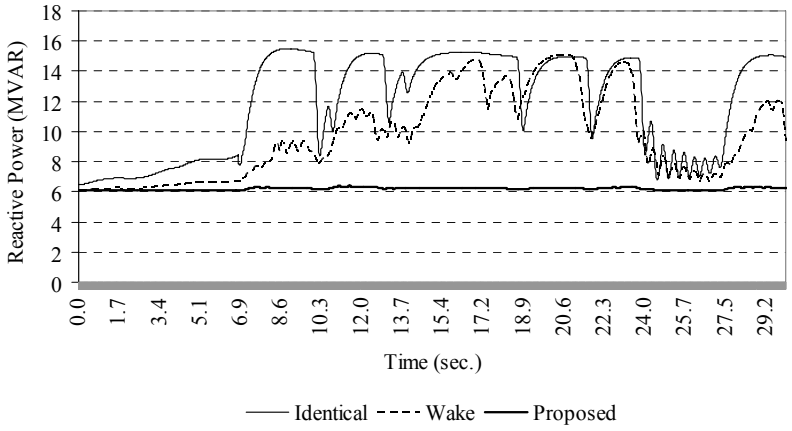

Figure 4-14: Wind farm total reactive power generation.

The total wind farm reactive power generation for the different modelling scenarios is presented in Figure 4-14. This figure reveals higher fluctuation levels in the generated reactive power for both the identical and the wake model than the generated reactive power level for the proposed model. Figure 4-15, Figure 4-16, and Figure 4-17 exhibit the reactive power generation variation for each wind turbine row for the three modelling scenarios.

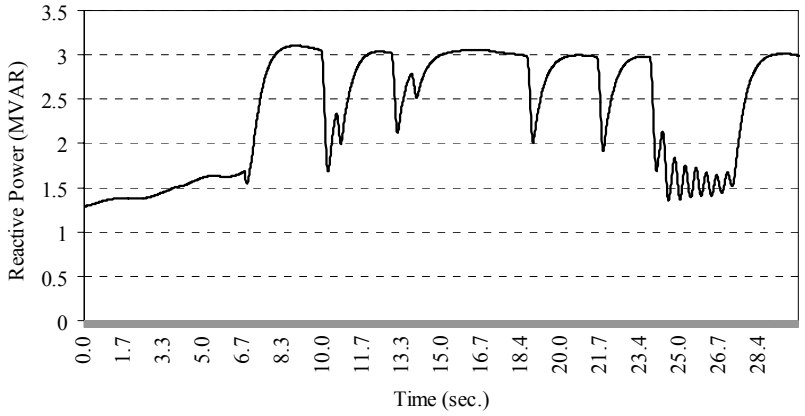

Figure 4-15: Reactive power generation profile: Identical model.

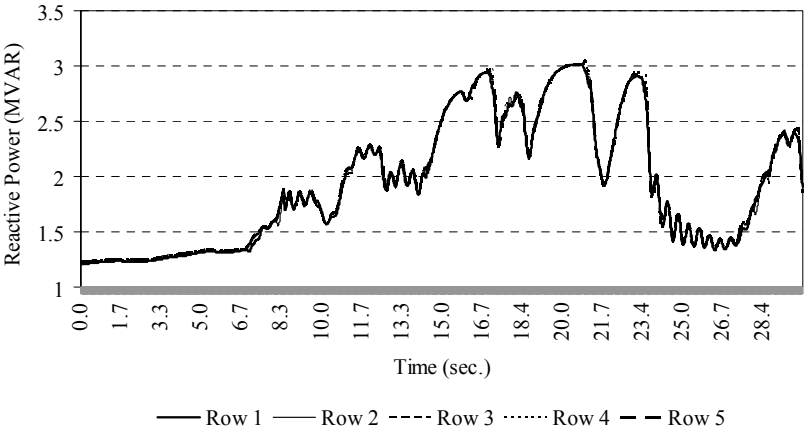

Figure 4-16: Reactive power generation profiles: Wake model.

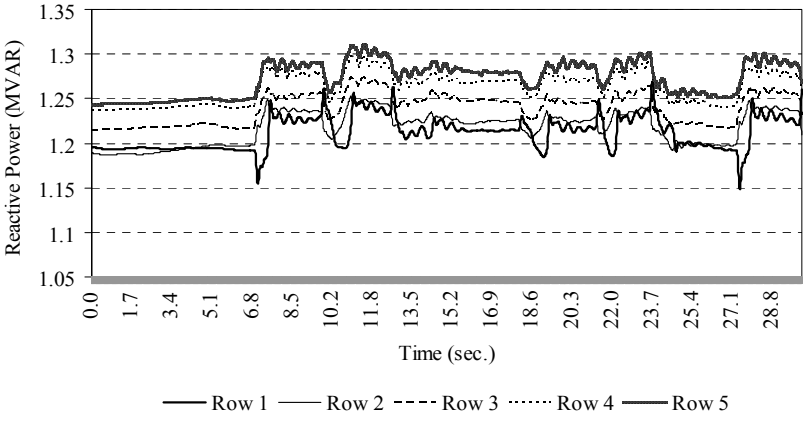

Figure 4-17: Reactive power generation profiles: Proposed model.

4.3 Wind Farm Voltage Regulation

In this section, the performance of a wind farm modeled as proposed in the previous section and equipped with the DFIG controlled with the voltage regulation technique, developed in Section 3.4, is investigated. The network under investigation is similar to that in Figure 4-1. The incident wind speed profiles for the aggregated model of each row are given in Figure 4-18. The total wind farm, real and reactive power generations, are recorded in Figure 4-19 and Figure 4-20, respectively. Figure 4-21 presents the regulated wind farm terminal voltage which indicates the effectiveness of the proposed control technique.

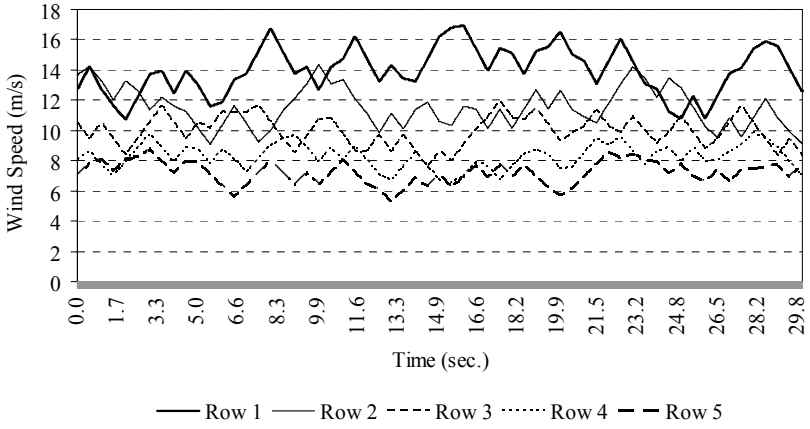

Figure 4-18: Wind speed profiles.

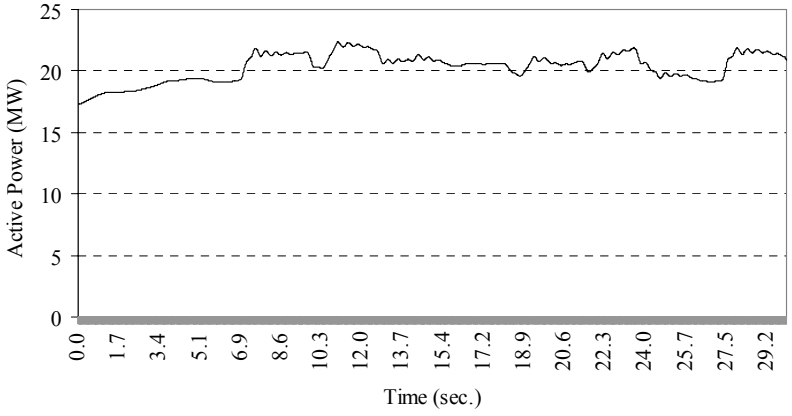

Figure 4-19: Wind farm real power generation.

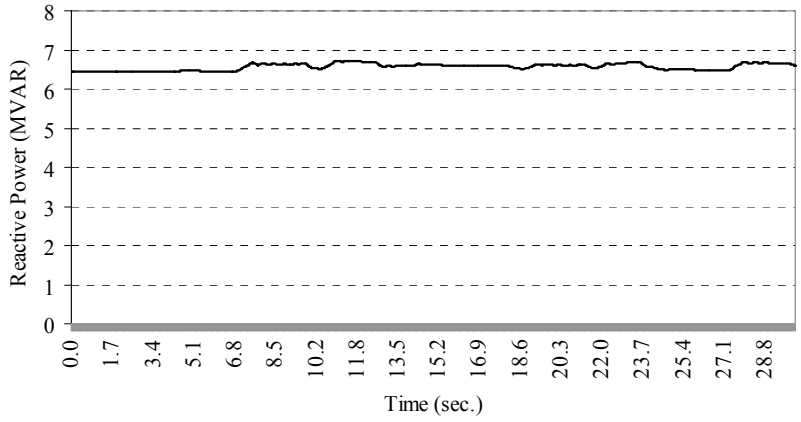

Figure 4-20: Wind farm reactive power generation.

The generated real power of each row of the proposed aggregated model is given in Figure 4-22. The corresponding profiles for the rotors' rotational speeds are presented in Figure 4-23. Figure 4-24 displays the variations in the pitch angle of the aggregated model for each row. It can be seen that the pitch angle control loop is activated for the aggregated model of Row 1 only. This agrees with the results in Figure 4-23 where the rotational speed of Row 1 is the only profile that exceeds the 1.2 pu limit for activating the pitch angle control. The generated reactive power from the aggregated model of each row is shown in Figure 4-25. Finally, the generated reactive power from the grid-side and rotor-side converters of the aggregated model of each row are displayed in Figure 4-26 – Figure 4-30. The effectiveness of the proposed control technique in sharing the generated / absorbed reactive power between the two converters is obvious.

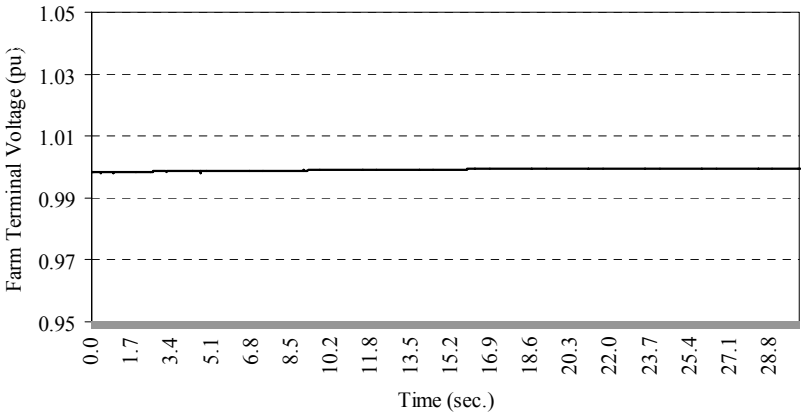

Figure 4-21: Wind farm terminal voltage.

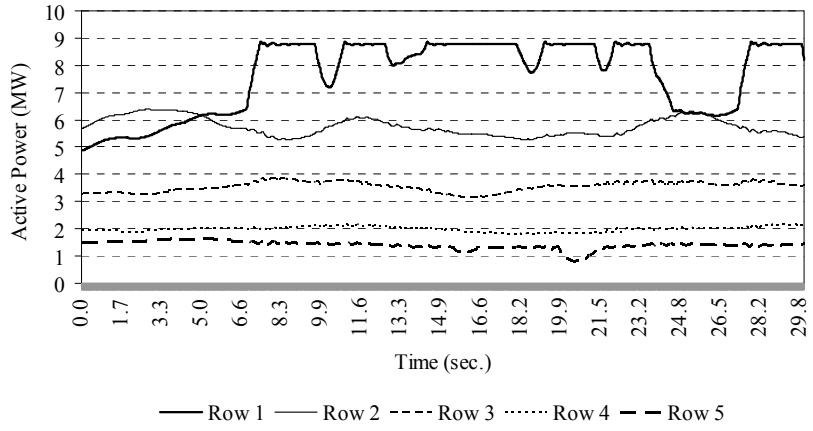

Figure 4-22: Aggregated turbine model active power generation for each row.

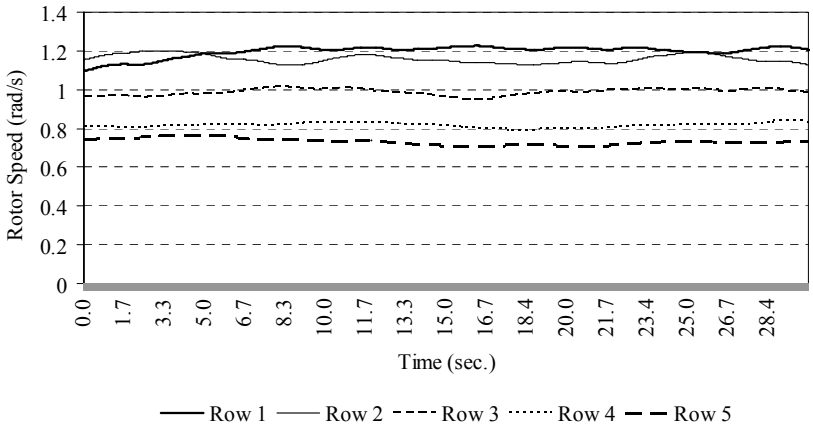

Figure 4-23: Aggregated turbine model rotational speed variation for each row.

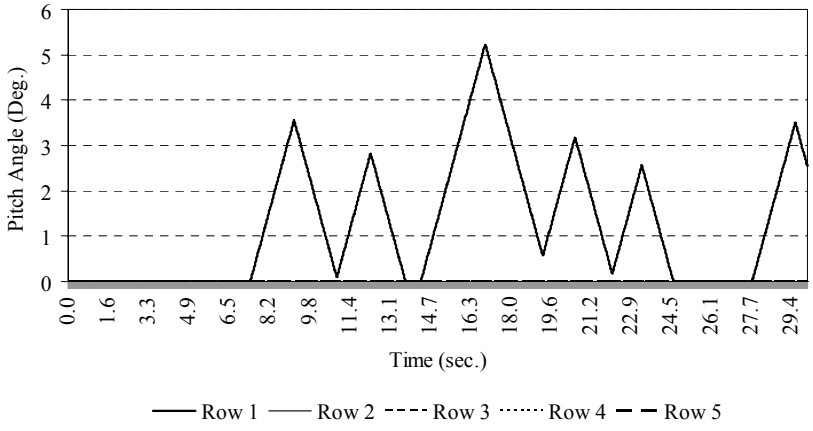

Figure 4-24: Aggregated turbine model pitch angle variations for each row.

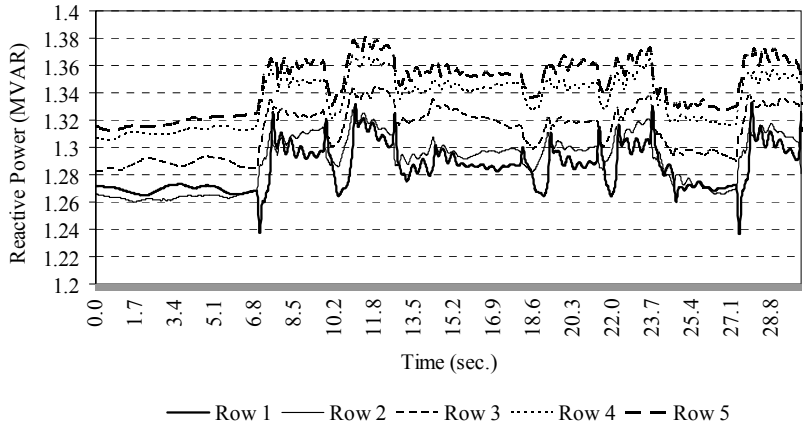

Figure 4-25: Aggregated turbine model reactive power generation for each row.

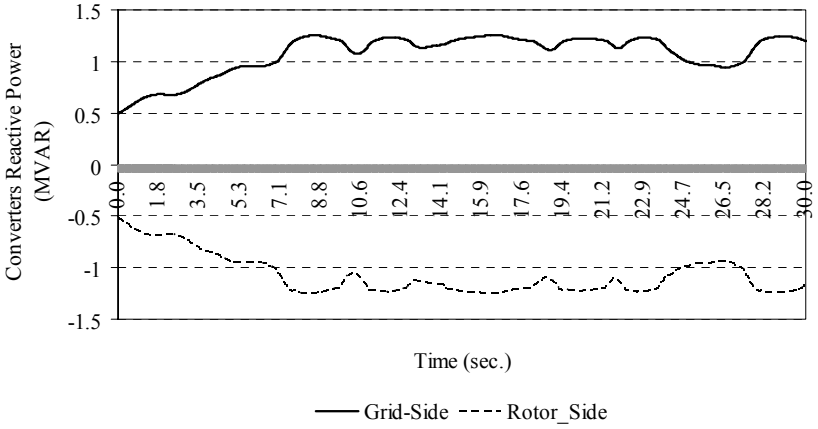

Figure 4-26: Grid-side and rotor-side converters reactive power generation for Row 1.

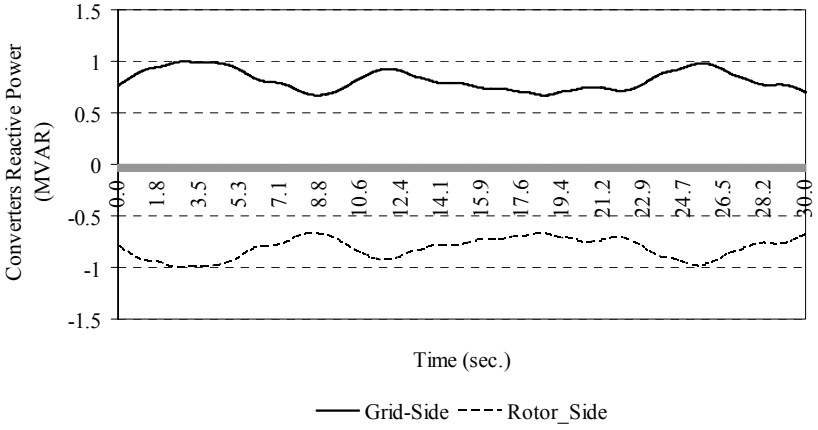

Figure 4-27: Grid-side and rotor-side converters reactive power generation for Row 2.

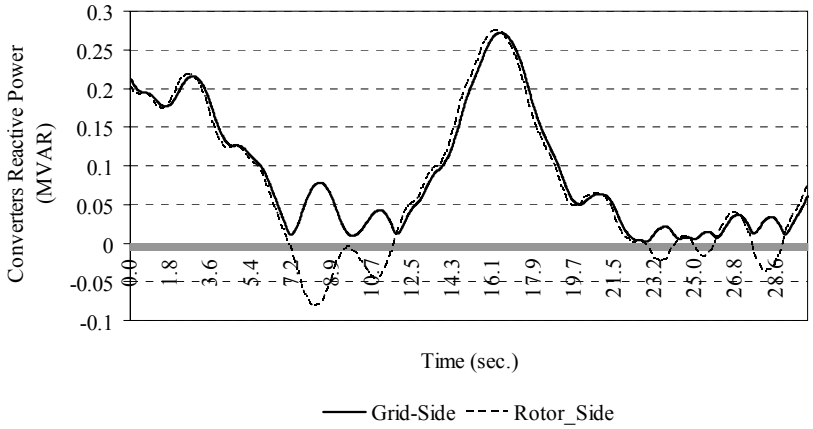

Figure 4-28: Grid-side and rotor-side converters reactive power generation for Row 3.

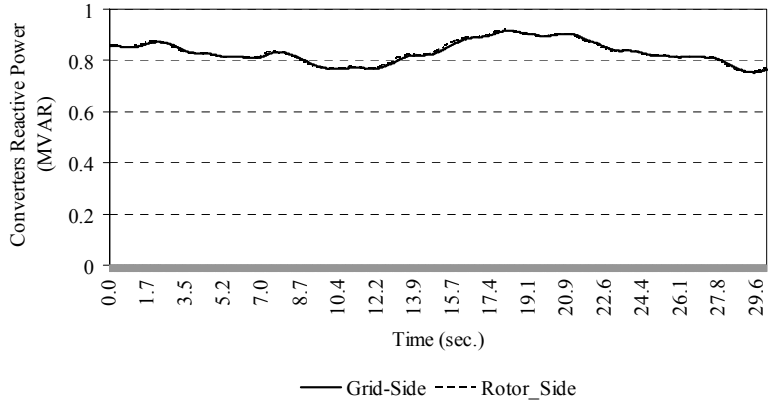

Figure 4-29: Grid-side and rotor-side converters reactive power generation for Row 4.

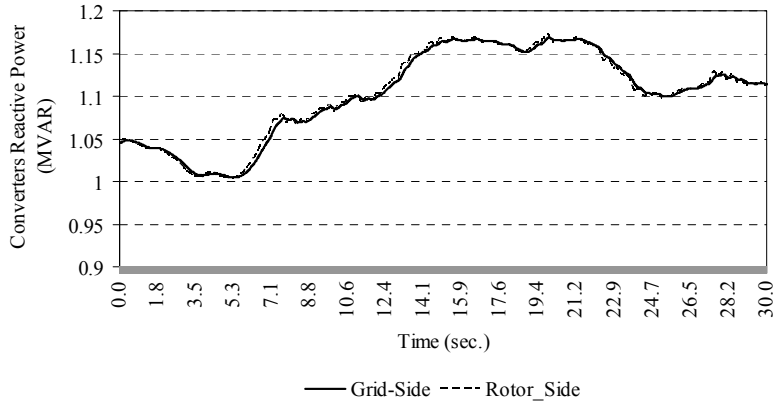

Figure 4-30: Grid-side and rotor-side converters reactive power generation for Row 5.

4.4 Chapter Assessment

This chapter investigates the impact of ignoring the proper modelling of the wind field profiles within the wind farm on the dynamic performance accuracy of the wind farm models. Previously developed wake model and a time delay model are used for developing a more accurate wind field model for wind farms. Three different modelling scenarios are compared to highlight the impact of ignoring the wake effect and wind speed time delay models. Finally, the performance of the developed wind farm model, combined with the proposed control technique is examined to determine the effectiveness of the proposed technique.

The new proposed wind field model is not only needed for dynamic performance studies but also for wind farm power prediction, that will be discussed in the next chapter.

Chapter 5
Half Day and One Day Ahead Prediction of Wind Power for Large Scale Wind Farms

5.1 Introduction

Due to the expected high penetration levels of wind energy generation, wind farms are required to operate as controllable power plants. This increases the necessity for more accurate and reliable techniques to predict the output power production of wind farms. Wind power prediction is also an essential process for the following.

1. Wind farms units' maintenance
2. Optimal power flow between conventional units and wind farms
3. Electricity marketing bidding
4. Power system generator scheduling
5. Energy reserve and storage planning and scheduling.

Many factors affect wind power prediction, including accurate forecasting models for wind speed and direction at the farm site, accurate techniques for wind speed simulation for the entire farm layout, and finally, sufficient information about the farm characteristics and layout. The forecasting horizon required for wind farms output power prediction depends on the required application, as illustrated in Table 5-1. This table also presents the developed techniques for each prediction horizon.

In this chapter, a new forecasting model for wind speed and direction is proposed. This model is based on relating the forecasted value to its corresponding historical value in previous years for the same time period [124, 125]. A linear prediction model is developed, where current data and previous data for the same time period but one (or two) years in the past are related. Then, the same model is applied to the data from the next historical period to predict the corresponding wind speed and direction for the next period in the current wind data series.

Table 5-1: Different horizons for wind power prediction.

Purpose	Horizon	Approaches
Unit Maintenance	0 (Nowcasting)	- Time Series / Statistical Approaches
Control	Few seconds or minutes	- Time Series / Statistical Approaches
Small Power Systems Operation	1 - 6 hours	- Time Series / Statistical Approaches
Interconnected Power Systems' Operation	1 – 72 hours	- Time Series / Statistical Approaches - Physical Models
Maintenance Planning	1 – 7 days	- Time Series / Statistical Approaches - Physical Models

5.2 Data Analysis

Two data sets for each wind speed and each wind direction time series are selected in this analysis. All the sets are recorded at the Madison weather station: one set is recorded during the winter season, and the other during the summer season. Each sample consists of data recorded for 3 days (72 hours) over 15 minute periods. These data pass through an averaging process to obtain the average hourly data series for wind speed and direction before the prediction analysis starts. The averaging process is straight forward for the wind speed series such that

$$X_{average}(j) = \frac{1}{4}\sum_{i=1}^{4} X_{recorded}(i) \qquad \forall\ j = 1, 2, ..., 72 \quad , \tag{5-1}$$

where $X_{average}\ (j)$ is the hourly averaged data point, and $X_{recorded}\ (i)$ is the recorded data points during hour j.

However, for the wind direction data series, some problems occur if the recorded data, which will be averaged during a certain hour, contains points that belong to Sector # 1 and Sector # 4, simultaneously. For example, numerical averaging for the wind directions of 350 °, 355 °, 5 °, and 10 ° results in an average wind direction of 180 ° which is not physically correct; it should be 0 ° (360 °). Figure 5-1 presents the sector's classification for the wind direction data. In such cases, 360 ° is added to the points that belong to Sector # 1 before the averaging process. If the resultant averaged value is greater than 360 °, 360 ° is subtracted from the result to produce the actual hourly averaged value. Similarly, if the data points, that will be averaged, belong to Sector # 1, Sector # 2, and Sector

4, simultaneously, 360° is added to the points that belong to Sector # 1 and Sector # 2 before the averaging process. Otherwise, the averaging process is performed directly by using equation (5.1).

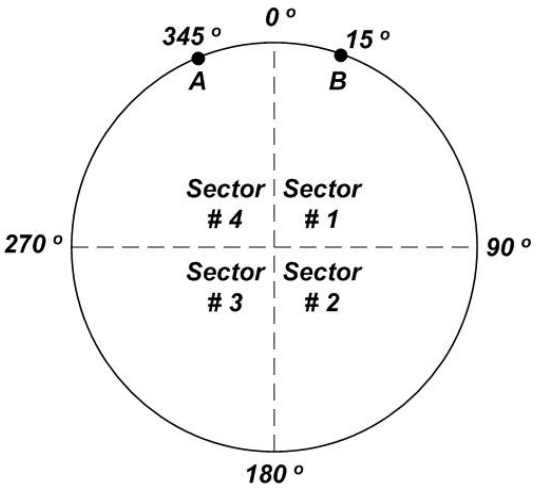

Figure 5-1: Wind direction data sector classification.

A similar situation occurs, when the absolute error is calculated for the wind direction prediction error. This can be easily illustrated by assuming that the actual wind direction value is represented by point *A* in Figure 5-1 and the predicted value is represented by point *B*. The numerical absolute error, in this case, will be 345° - 15° = 330°, whereas the actual absolute error is only 30°. This problem is solved by calculating two errors at each analyzed data point, and the actual error is the minimum of these two calculated errors as follows:

$$error1(j) = Actual(j) - Predicted(j) \qquad \forall\ j = 1, 2, ..., 72 \quad , \qquad (5\text{-}2)$$

$$error2(j) = 360° - error1(j) \qquad \forall\ j = 1, 2, ..., 72 \quad , \qquad (5\text{-}3)$$

and

$$error(j) = \min\left[error1(j), error2(j)\right] \qquad \forall\ j = 1, 2, ..., 72 \quad . \qquad (5\text{-}4)$$

5.3 Model Development

Two models are developed and examined during this investigation. The first model, hereafter referred to as the one-year model, is established by using the nearest historical data of *n* points from the current year (2005) and *n* data points from one previous year time series (2004), for the same time interval. This is done to develop a linear model relating both data series. These historical data are

used to obtain the model coefficients by using the least square method. The next *n* data points from the one year old series (2004) {the *n* data points following the *n* data points used in model building and parameters estimation} are used as an input to the built linear model to predict the next (future) *n* points for the current data series (2005). The one-year model is represented by the following formula:

$$\hat{Y}_{2005}(n+i) = a + b\, X_{2004}(n+i) \quad \forall \quad i = 1, 2, \ldots, n \quad , \tag{5-5}$$

where $\hat{Y}_{2005}(i)$ represents the predicted values for the 2005 wind data series, $X_{2004}(i)$ is the corresponding actual values for the 2004 wind data series, *i* represents the step, and *a* and *b* are the model parameters that can be estimated by using the least square method expressed as follows:

$$A = \begin{bmatrix} a \\ b \end{bmatrix} = \left[\beta^T . \beta\right]^{-1} . \beta^T Y \quad , \tag{5-6}$$

Where,

$$\beta = \begin{bmatrix} 1 & X_{2004}(1) \\ 1 & X_{2004}(2) \\ \vdots & \vdots \\ 1 & X_{2004}(n) \end{bmatrix} \quad , \tag{5-7}$$

$$Y = \begin{bmatrix} X_{2005}(1) \\ X_{2005}(2) \\ \vdots \\ X_{2005}(n) \end{bmatrix} \quad . \tag{5-8}$$

The second model, hereafter referred to as the two-years model, uses data of *n* points from the current year (2005) and two previous years' series (2003 and 2004), for the same time interval, to develop a linear model relating the data series and estimate the model's parameters. The next *n* data points from the two years old series (2003 and 2004) {the *n* data points following the *n* data points used in model building and parameters estimation} are used as an input to the built linear model to predict the next (future) *n* points for the current data series (2005), as illustrated in Figure 5-2. The two-year model is represented by

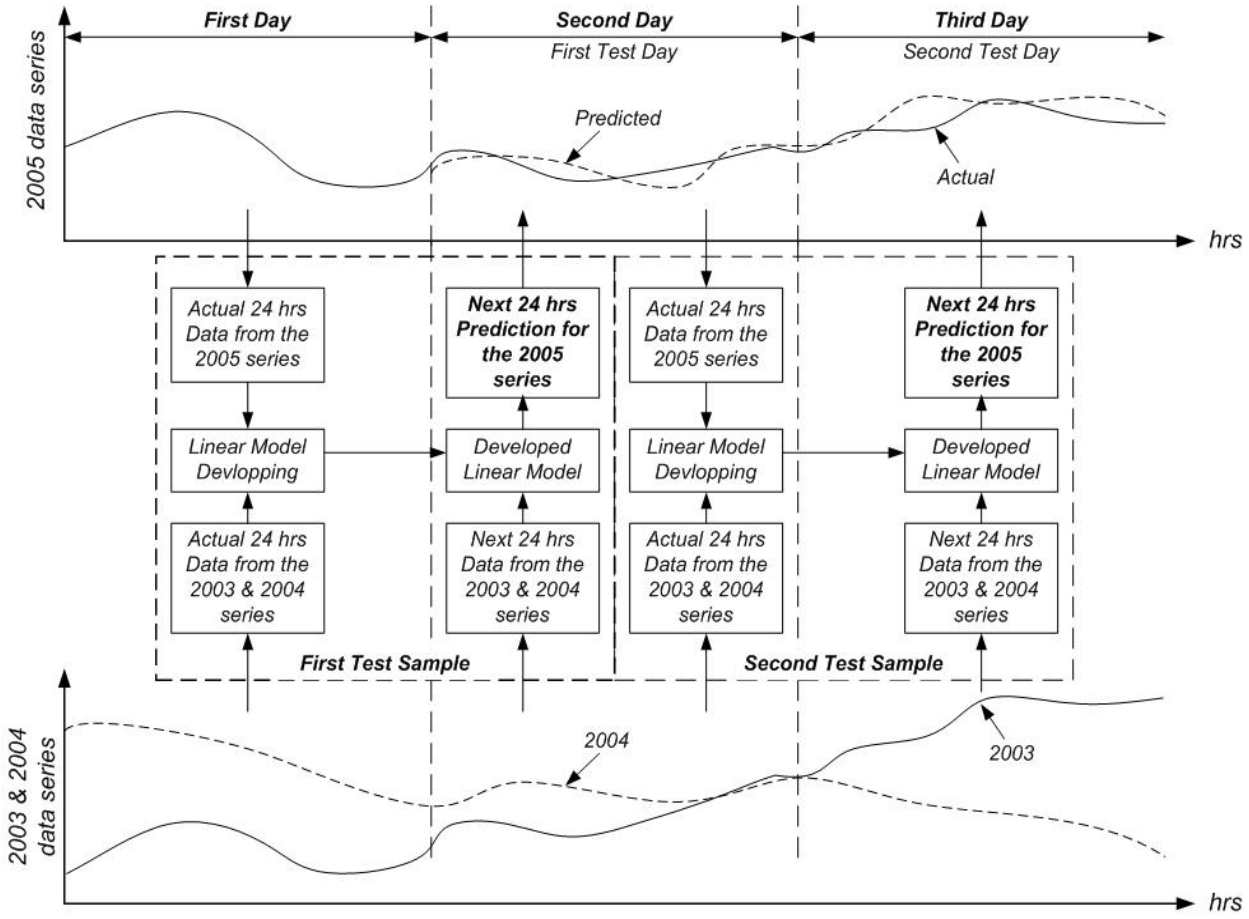

Figure 5-2: Two-year model for the one day ahead (n = 24) prediction of wind speed or wind direction.

$$\hat{Y}_{2005}(n+i) = a + b_1\ X_{2004}(n+i) + b_2\ X_{2003}(n+i) \qquad \forall \quad i = 1, 2, \ldots, n \quad , \qquad (5\text{-}9)$$

where $X_{2003}(i)$ is the corresponding actual values for the 2003 wind data series, and a, b_1 and b_2 are the model parameters that can be estimated by using the least square method expressed as follows:

$$A = \begin{bmatrix} a \\ b_1 \\ b_2 \end{bmatrix} = \left[\beta^T . \beta\right]^{-1} . \beta^T Y \qquad , \qquad (5\text{-}10)$$

where,

$$\beta = \begin{bmatrix} 1 & X_{2004}(1) & X_{2003}(1) \\ 1 & X_{2004}(2) & X_{2003}(2) \\ \vdots & \vdots & \vdots \\ 1 & X_{2004}(n) & X_{2003}(n) \end{bmatrix} \quad . \tag{5-11}$$

5.4 Wind Speed Prediction

To evaluate the proposed models for wind speed prediction, two data sets (summer and winter) are selected. Each set consists of three data time series for three successive years, consisting of 72 recorded wind speed values. The study is carried out for two prediction horizons: 12-hours ahead (half-day ahead), and 24-hours ahead (one-day ahead). The results from the proposed models are compared with those from the persistent model (assuming the forecast value of the next step in the future is the last measured value).

5.4.1 Wind Speed Prediction Results

The data set that is recorded during the winter season is given in Figure 5-3. The data for the first 24 recorded hourly averaged wind speed is dedicated totally or partially (for the 12-hour horizon) in developing the prediction models for the next time interval. This is followed by moving the evaluation window by a time interval of *n* data points, where *n* is set equal to the horizon within this study. Figure 5-4 and Figure 5-5 present the actual (2005 data series) and predicted wind speed time series by applying the proposed models for the different prediction horizons. These figures reveal the effectiveness of the proposed models in tracking the time series of the actual data, especially for the two-year model.

The MAE, the RMSE, and the coefficient of correlation "r", for the two proposed models and the persistent models, are recorded in Table 5-2, as well as the improvements in the MAE and the RMSE when compared to the persistent model. This table indicates the improved accuracy of the proposed models, compared to that of the persistent model as reflected by the lower MAE, lower RMSE, and higher coefficients of correlation. The results in this table demonstrate that this accuracy is improved by using the two-year (2-Year) model instead of the one-year (1-Year) model. Furthermore, this table shows that the 1-Year model predicts the wind speed series with an improvement in the MAE over the persistent of 44.5% for the 12-hour ahead prediction and 17.4% for the one-day ahead prediction.

These percentages are improved to 55.5% and 46%, respectively for the 2-Year model. Moreover, the 1-Year model predicts the wind speed series with an improvement in the RMSE over the persistent model of 43.8% for the 12-hour ahead prediction and 18.5% for one-day ahead prediction that are improved to 57.3% and 45%, respectively for the 2-Year model.

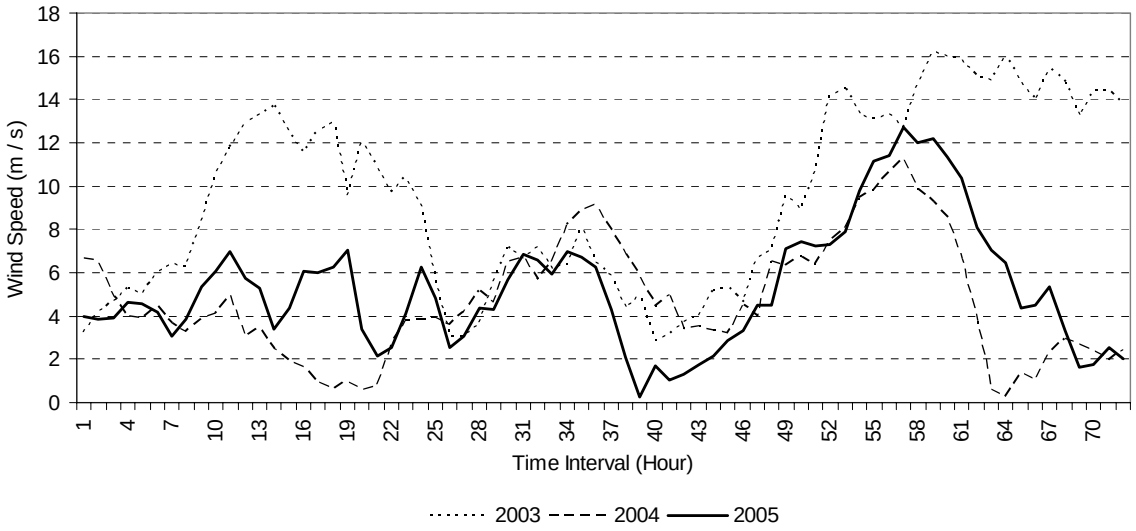

Figure 5-3: Wind speed data series for the investigated period as recorded during the winter seasons for three successive years.

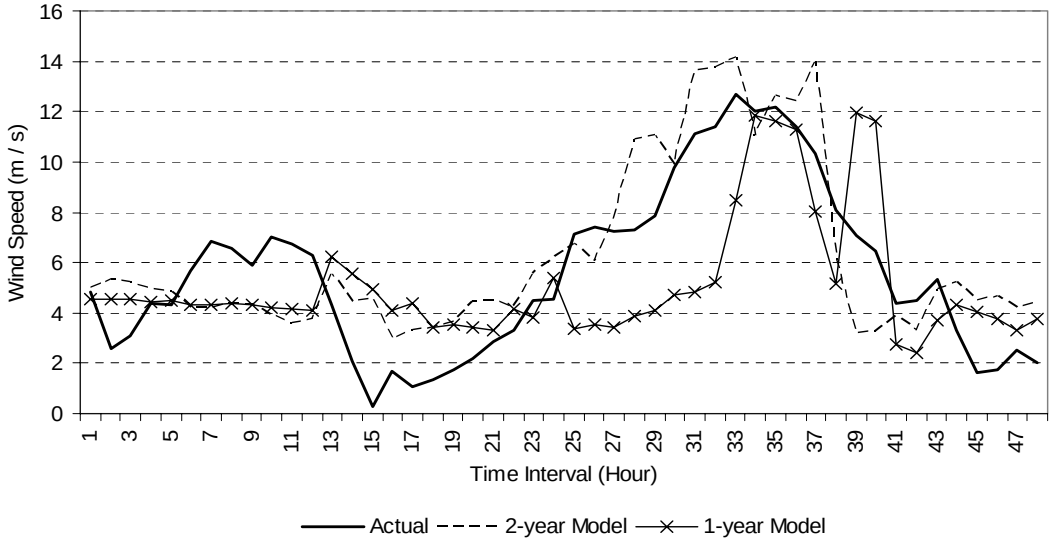

Figure 5-4: Half-day ahead predicted wind speed for the winter data sample.

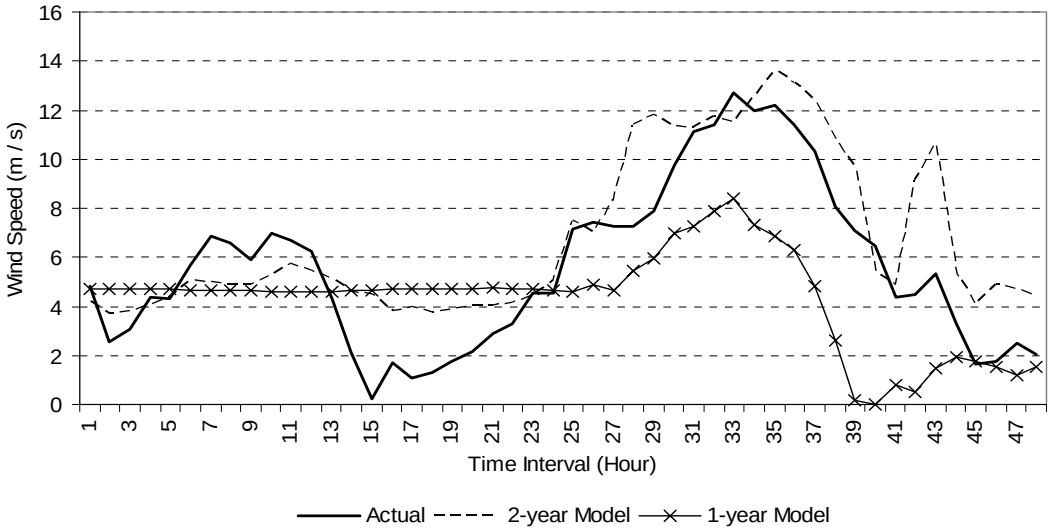

Figure 5-5: One-day ahead predicted wind speed for the winter data sample.

Table 5-2: MAE, RMSE, correlation coefficient, and improvements for the wind speed prediction (winter sample).

Model		***n = 12***	***n = 24***
Persistent	***MAE***	4.23	3.132
	RMSE	5.05	3.83
	r	-0.34	-0.51
1-Year Model	***MAE***	2.349	2.587
	RMSE	2.84	3.122
	r	0.56	0.51
% Improvement for 1-Year Model	***MAE***	44.468	17.401
	RMSE	43.761	18.501
2-Year Model	***MAE***	1.881	1.691
	RMSE	2.155	2.107
	r	0.81	0.86
% Improvement for 2-Year Model	***MAE***	55.532	46.009
	RMSE	57.326	44.992

In Table 5-2, the generated coefficients of correlation from the proposed models are more accurate than those from the persistent model. The novel models' coefficients of correlation range from 0.51 to 0.86.

A similar analysis is carried out for a data set recorded during the summer season as seen in Figure 5-6. Figure 5-7 and Figure 5-8 denote the actual and the predicted wind speed time series by the use of the proposed models for the different prediction horizons. The figures reflect the accuracy of the proposed models, in tracking the time series, compared with the actual data.

Figure 5-6: Wind speed data series for the investigated period as recorded during the summer seasons for three successive years.

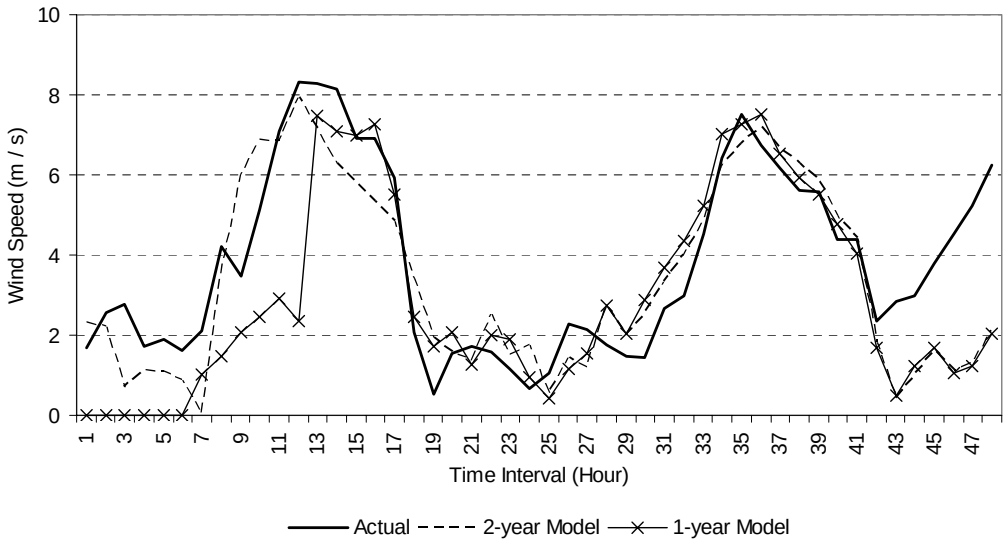

Figure 5-7: Half-day ahead predicted wind speed for the summer data sample.

Table 5-3 lists the evaluation parameters for this set of data. This table reveals lower value for the MAE, and RMSE, and higher coefficients of correlation for the newly developed models, compared to the corresponding values of the persistent model. For this set of data, the 1-Year model predicts the wind speed series with an improvement in the MAE over the persistent model of 51.1% for the 12-hour ahead prediction and 39.6% for the one-day ahead prediction. These percentages are improved to 60.6% and 54.4%, respectively, for the 2-Year model. Moreover, the 1-Year model predicts the wind speed series with an improvement in the RMSE over the persistent model of 49.7% for the 12-hour ahead prediction and 42.4% for the one-day ahead prediction that are improved to 61.1% and 55.3%, respectively, for the 2-Year model.

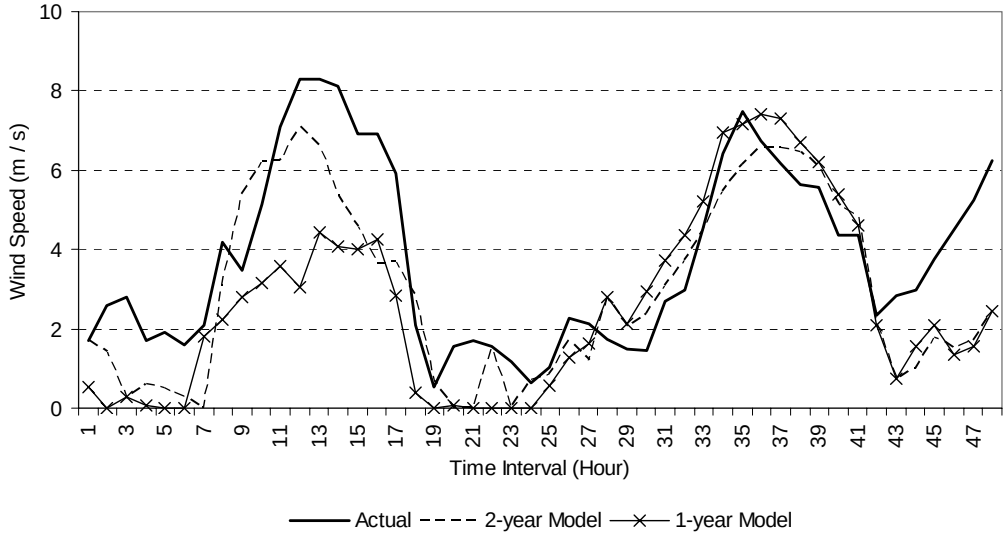

Figure 5-8: One-day ahead predicted wind speed for the summer data sample.

Also, Table 5-3 indicates better coefficients of correlation from the proposed models, compared to those from the persistent model. The proposed models coefficients of correlation range from 0.73 to 0.82.

5.4.2 Actual and Predicted Wind Speeds Relationship

The goal of this section is to determine the degree of scattering of the predicted values compared with that of the actual values and their linearized relationship. The results from the proposed models are compared with the corresponding values from the persistent model. Figure 5-9 – Figure 5-16 display the resultant relationships between the predicted and the actual values for different prediction

horizons for the proposed models and the persistent model for the winter and summer season data sets. This linear relationship is expressed by computing

$$\hat{y}_i = m\, x_i + c \quad , \tag{5-12}$$

where x_i is the actual wind speed value at time interval i, $\hat{y}_i$ is the predicted wind speed value at time interval i, and m and c are the scaling factor and the y-axis (prediction-axis) intercept of the linear relation, respectively.

Table 5-3: MAE, RMSE, correlation coefficient, and improvements for wind speed prediction (summer sample).

Model		***n = 12***	***n = 24***
Persistent	***MAE***	2.853	2.776
	RMSE	3.759	3.552
	r	0.13	-0.06
1-Year Model	***MAE***	1.395	1.676
	RMSE	1.891	2.046
	r	0.75	0.73
% Improvement for 1-Year Model	***MAE***	51.104	39.625
	RMSE	49.693	42.394
2-Year Model	***MAE***	1.123	1.267
	RMSE	1.463	1.589
	r	0.81	0.82
% Improvement for 2-Year Model	***MAE***	60.638	54.359
	RMSE	61.083	55.267

These figures reveal that the scattering is highly reduced with the proposed models, especially the 2-Year model, compared to that of the persistent model. The estimated values for the linear relationship coefficients are listed in Table 5-4 and Table 5-5 for the winter and the summer data sets, respectively. It is evident that the proposed models are capable of predicting the wind speed data series with linear relationship scaling factors ranging from 0.305 to 0.79 for the 1-Year model and from 0.816 to 0.838 for the 2-Year model. These results are much better than the results from the persistent model that are very low and sometimes reveal negative signs. The tables also show that the y-axis intercepts are greatly reduced, when the wind speed is predicted by applying the proposed models.

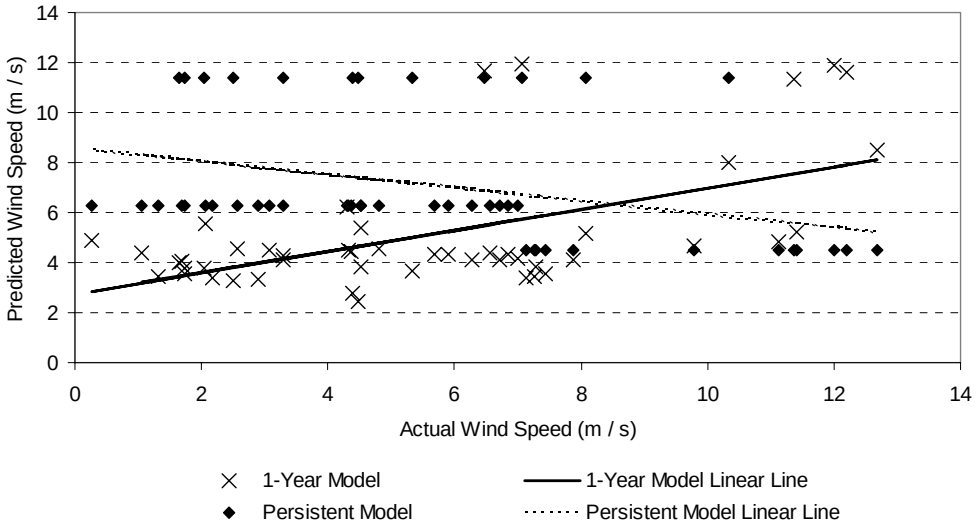

Figure 5-9: Relationship between actual and predicted wind speed for the half-day ahead prediction of the winter data sample using the 1-Year model and the persistent model.

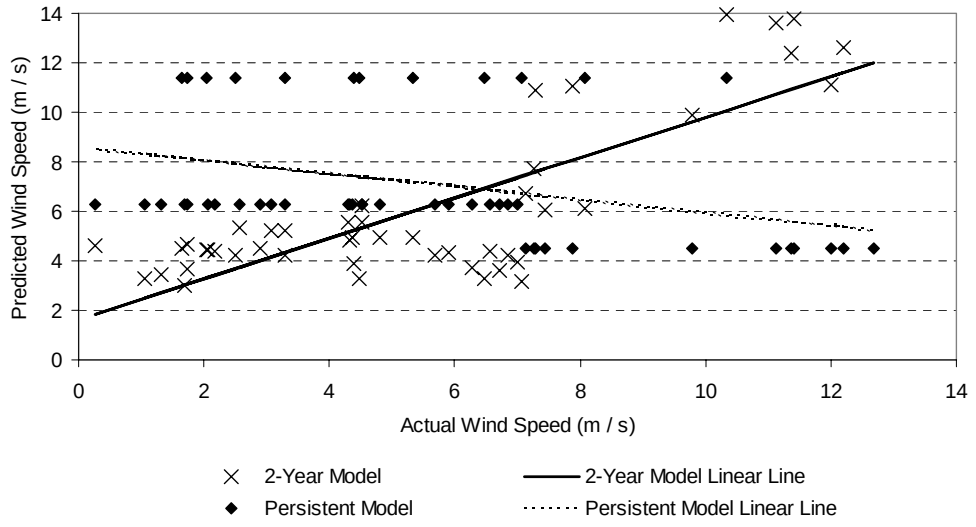

Figure 5-10: Relationship between actual and predicted wind speed for the half-day ahead prediction of the winter data sample using the 2-Year model and the persistent model.

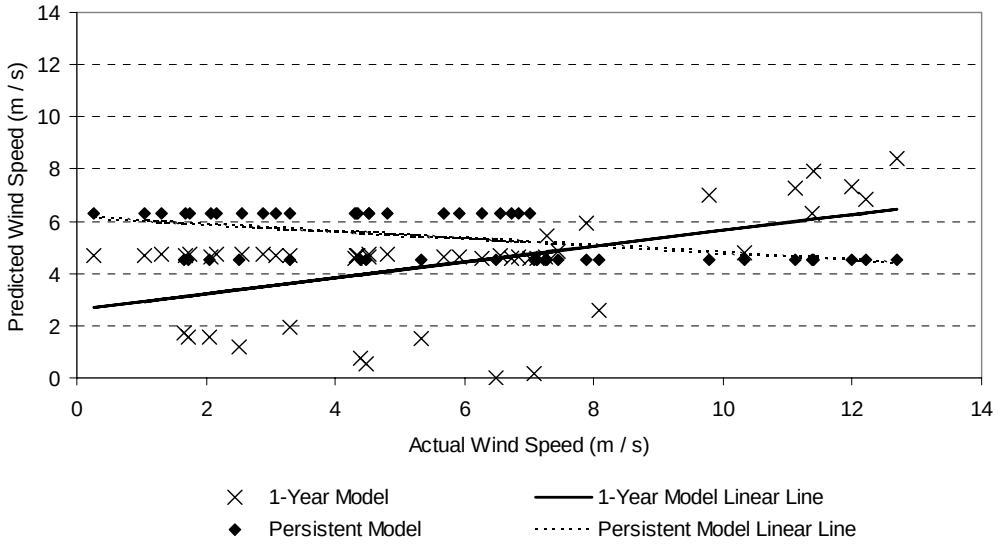

Figure 5-11: Relationship between actual and predicted wind speed for the one-day ahead prediction of the winter data sample using the 1-Year model and the persistent model.

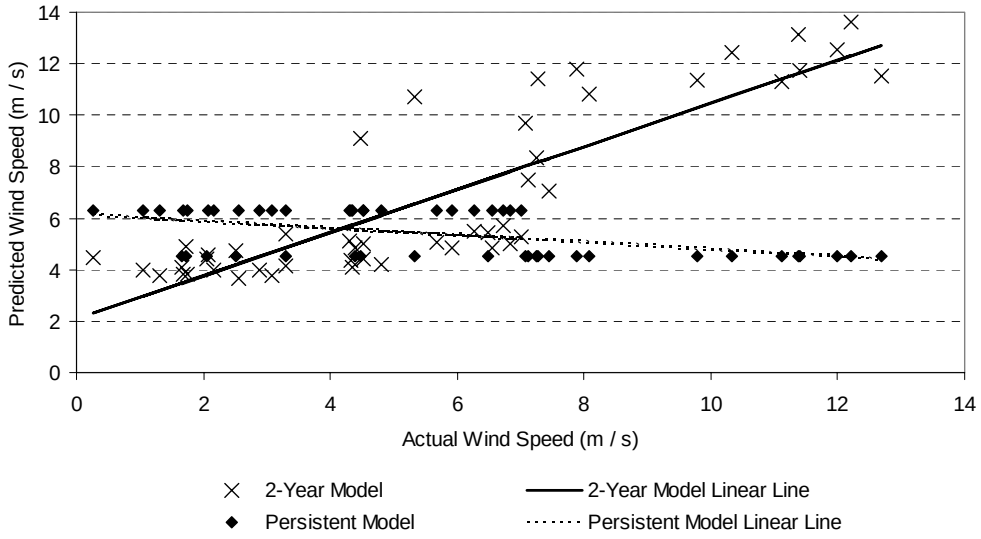

Figure 5-12: Relationship between actual and predicted wind speed for the one-day ahead prediction of the winter data sample using the 2-Year model and the persistent model.

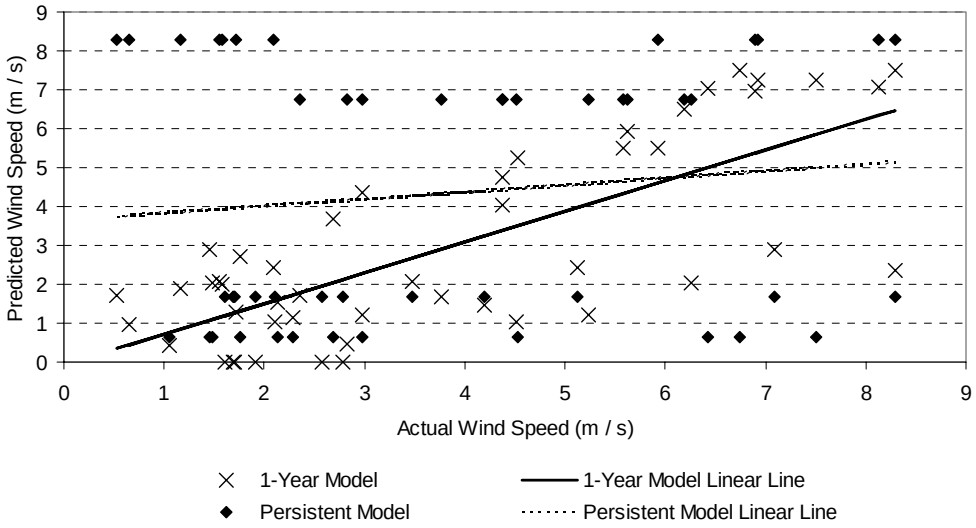

Figure 5-13: Relationship between actual and predicted wind speed for the half-day ahead prediction of the summer data sample using the 1-Year model and the persistent model.

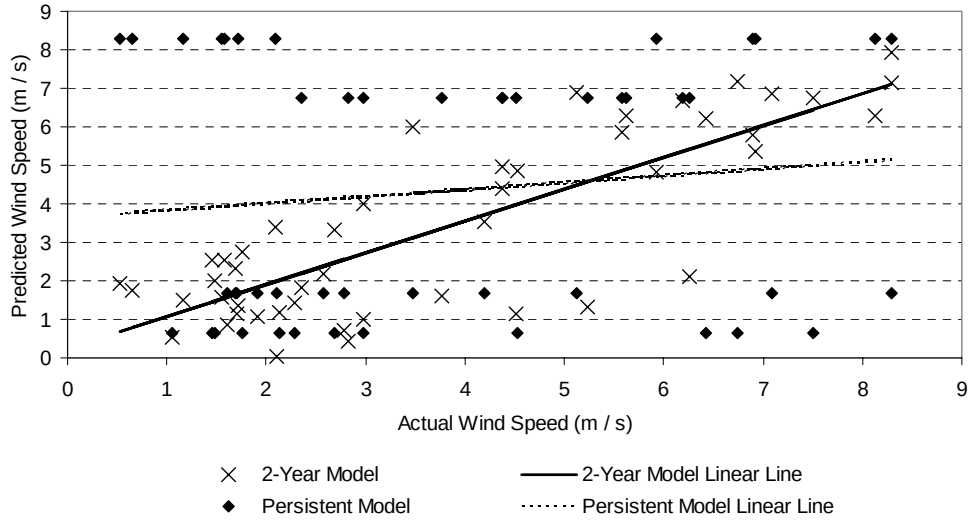

Figure 5-14: Relationship between actual and predicted wind speed for the half-day ahead prediction of the summer data sample using the 2-Year model and the persistent model.

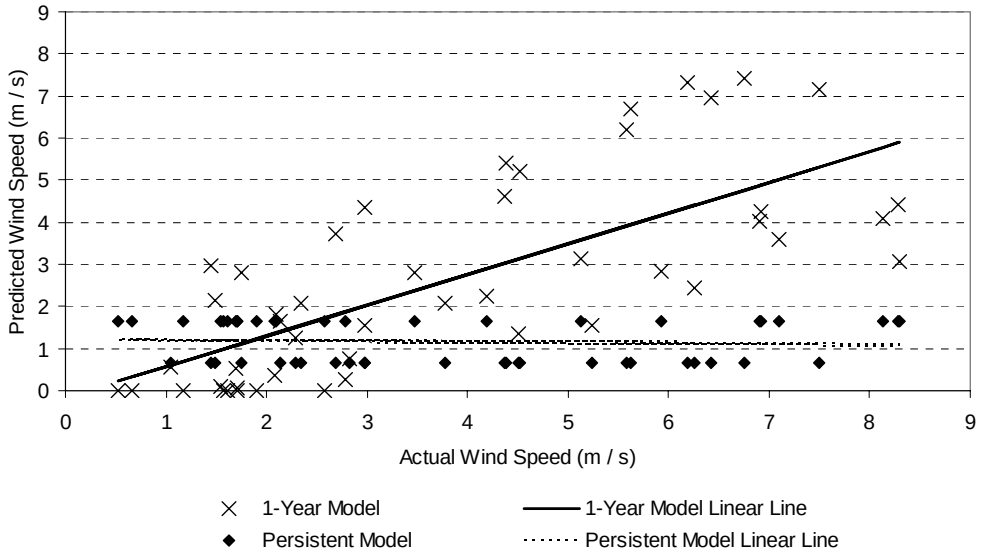

Figure 5-15: Relationship between actual and predicted wind speed for the one-day ahead prediction of the summer data sample using the 1-Year model and the persistent model.

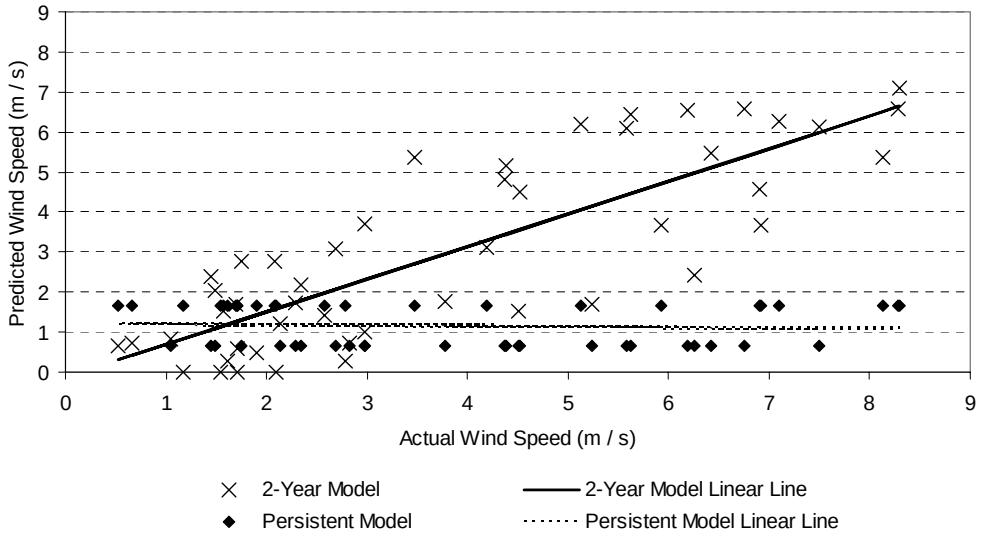

Figure 5-16: Relationship between actual and predicted wind speed for the one-day ahead prediction of the summer data sample using the 2-Year model and the persistent model.

Table 5-4: Scale factors and y-axis intercepts for wind speed prediction (winter sample).

Horizon (hours)	Model	Coefficients	
		c	m
12	***Persistent***	8.589	-0.264
24		6.162	-0.136
12	***1-Year Model***	2.753	0.422
24		2.606	0.305
12	***2-Year Model***	1.644	0.816
24		2.086	0.838

Table 5-5: Scale factors and y-axis intercepts for wind speed prediction (summer sample).

Horizon (Hours)	Model	Coefficients	
		c	m
12	***Persistent***	3.652	0.181
24		1.214	-0.014
12	***1-Year Model***	-0.077	0.790
24		-0.164	0.730
12	***2-Year Model***	0.253	0.826
24		-0.129	0.816

5.5 Wind Direction Prediction

The goal in this section is to evaluate the proposed models in the wind direction prediction. A similar analysis to the one in Section 5.4 is carried out for two wind direction time series data sets, recorded at the Madison weather station for three successive years during the winter and summer seasons.

5.5.1 Wind Direction Prediction Results

The recorded wind direction data series and the prediction results of the proposed models are presented in Figure 5-17 - Figure 5-19 for the winter season data set and Figure 5-20 – Figure 5-22 for the summer season data set. The figures reveal the effectiveness of the proposed models in tracking the time series of the actual data. These figures, sometimes, reveal sudden changes such as those that occur between the 65^{th} and the 66^{th} recorded data points in the 2005 data series in Figure 5-17. Such changes are due to the data shifting between the 360° and the 0°. Table 5-6 and Table 5-7 present the evaluation parameters for the winter and the summer sets of data, respectively.

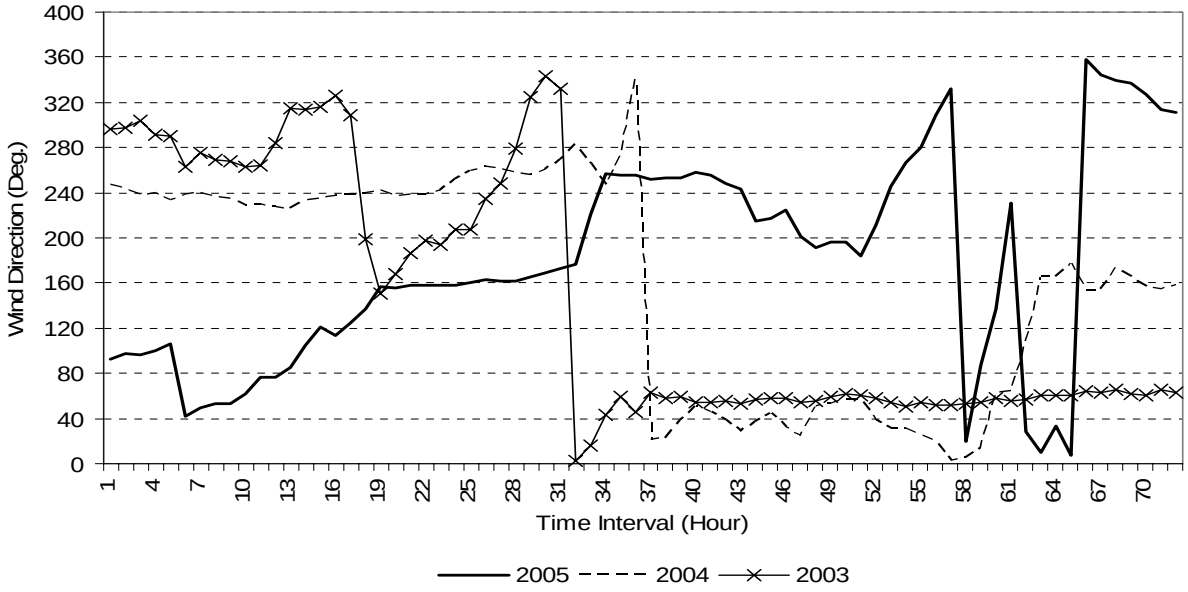

Figure 5-17: Wind direction data series for the investigated period as recorded during the winter seasons for three successive years.

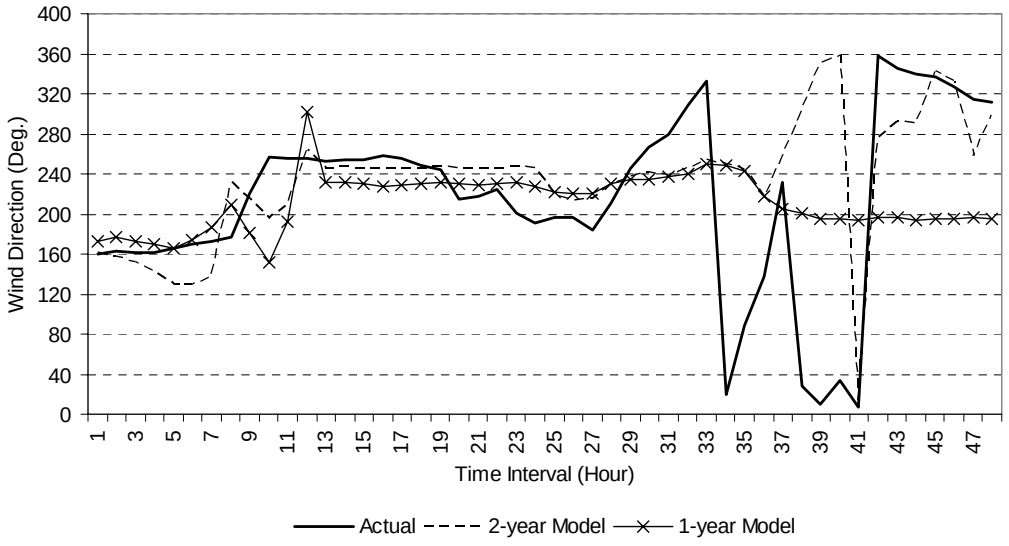

Figure 5-18: Half-day ahead predicted wind direction for the winter data sample.

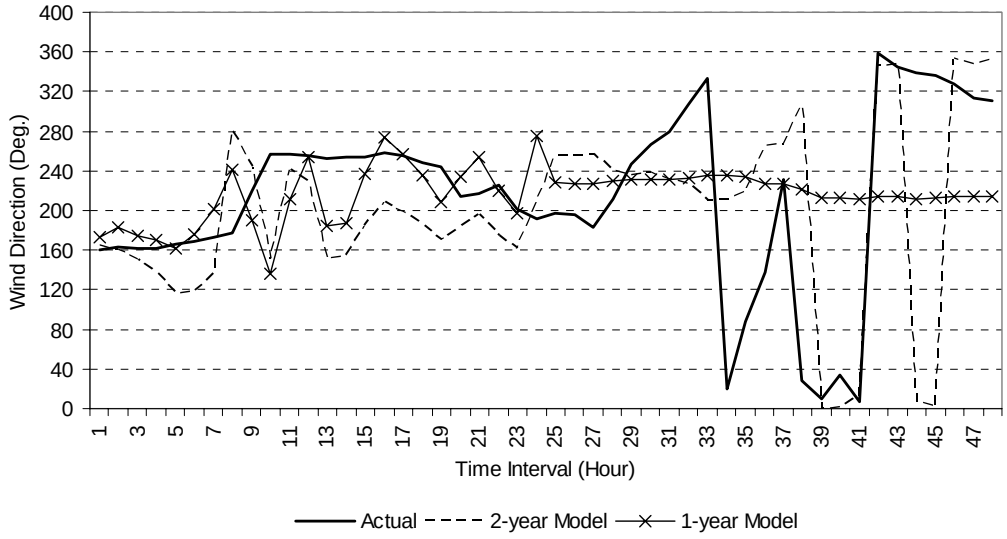

Figure 5-19: One-day ahead predicted wind direction for the winter data sample.

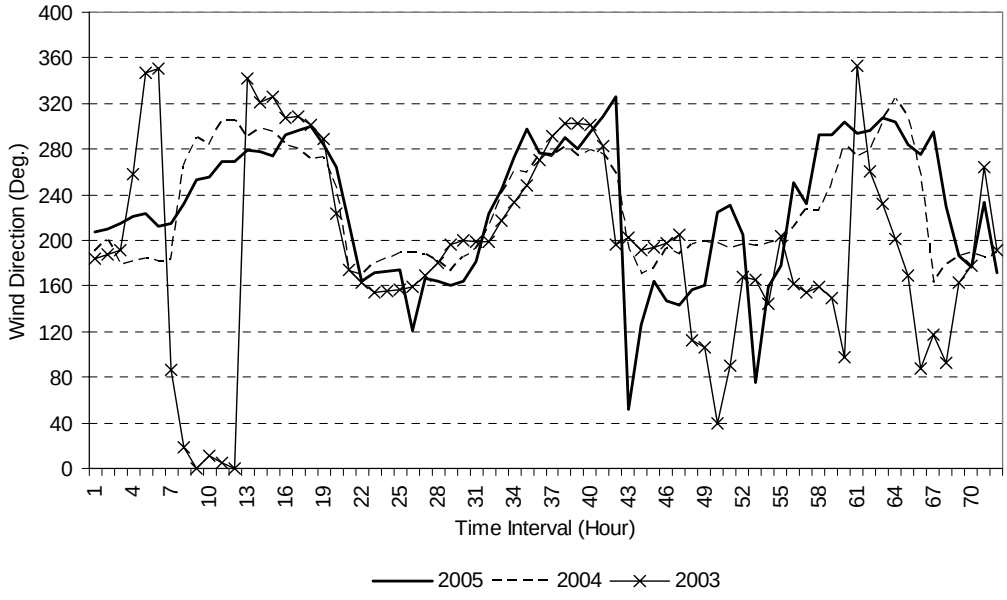

Figure 5-20: Wind direction data series for the investigated period as recorded during the summer seasons for three successive years.

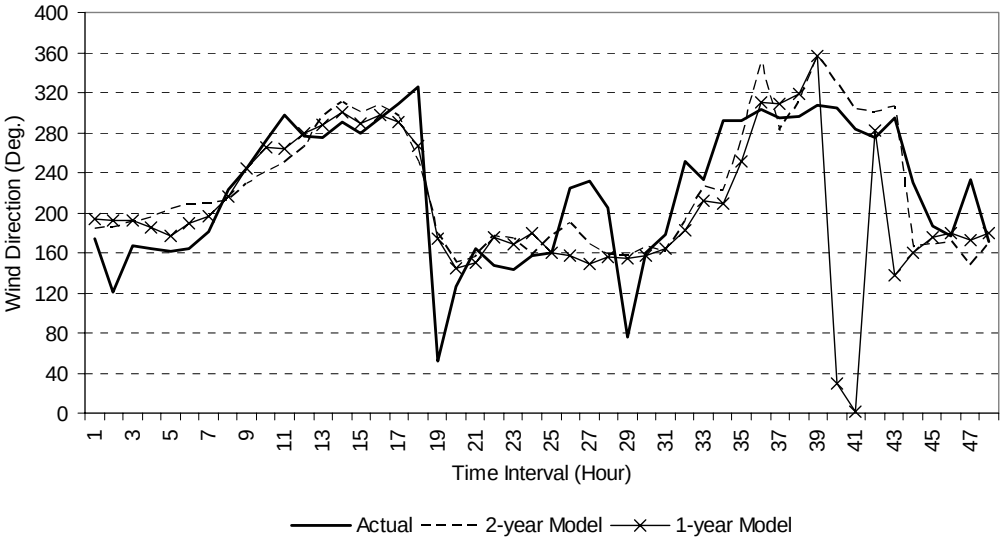

Figure 5-21: Half-day ahead predicted wind direction for the summer data sample.

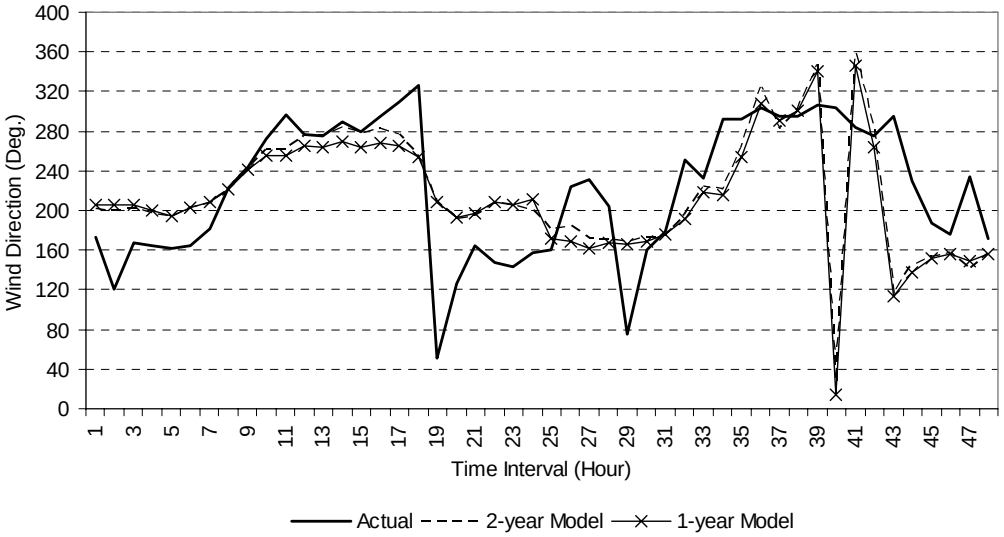

Figure 5-22: One-day ahead predicted wind direction for the summer data sample.

Table 5-6: MAE, RMSE, correlation coefficient, and improvements for wind direction prediction (winter sample).

Model		***n = 12***	***n = 24***
Persistent	*MAE*	67.1	81.253
	RMSE	8.191	9.014
	r	0.10	-0.01
1-Year Model	*MAE*	62.26	62.475
	RMSE	7.89	7.904
	r	0.13	0.09
% Improvement for 1-Year Model	*MAE*	7.213	23.111
	RMSE	3.675	12.314
2-Year Model	*MAE*	34.65	49.826
	RMSE	5.886	7.059
	r	0.29	0.37
% Improvement for 2-Year Model	*MAE*	48.361	38.678
	RMSE	28.145	21.689

Table 5-7: MAE, RMSE, correlation coefficient, and improvements for wind direction prediction (summer sample).

Model		***n = 12***	***n = 24***
Persistent	*MAE*	60.862	74.563
	RMSE	7.801	8.635
	r	0.20	-0.20
1-Year Model	*MAE*	34.845	43.074
	RMSE	5.903	6.563
	r	0.47	0.42
% Improvement for 1-Year Model	*MAE*	42.748	42.231
	RMSE	24.331	23.994
2-Year Model	*MAE*	32.031	40.82
	RMSE	5.66	6.389
	r	0.80	0.46
% Improvement for 2-Year Model	*MAE*	47.371	45.254
	RMSE	27.449	26.01

These tables indicate lower values of the MAE and RMSE, and higher coefficients of correlation for the proposed models than the corresponding values of the persistent model. The 1-Year and the 2-Year model predict the wind direction series with an improvement in the MAE over the persistent model up to 42.75% and 48.36%, respectively for the 12-hour ahead prediction, and 42.23% and

45.25%, respectively for the one-day ahead prediction. It is obvious that the proposed models produce better coefficients of correlation than those from the persistent model. The proposed models predict the wind direction with coefficients of correlation as high as 0.8.

5.5.2 Actual and Predicted Wind Direction Relationship

Figure 5-23 – Figure 5-30 present the relationships between the predicted and the actual values for different prediction horizons, for the proposed models and the persistent model, for the winter and summer season data sets. The scattering is highly reduced with the proposed models, especially the 2-Year model, compared to that of the persistent model.

The estimated values for the linear relationship coefficients are presented in Table 5-8 and

Table **5-9** for the winter and the summer data sets, respectively. These tables reveal that the proposed models predict the wind direction data series with linear relationship scaling factors ranging from 0.029 to 0.479 for the 1-Year model and from 0.199 to 0.72 for the 2-Year model. These results are substantially improved than the results from the persistent model that are very low and sometimes show negative signs. The tables also show that the y-axis intercepts have been greatly reduced when the wind speed is predicted by using the proposed models.

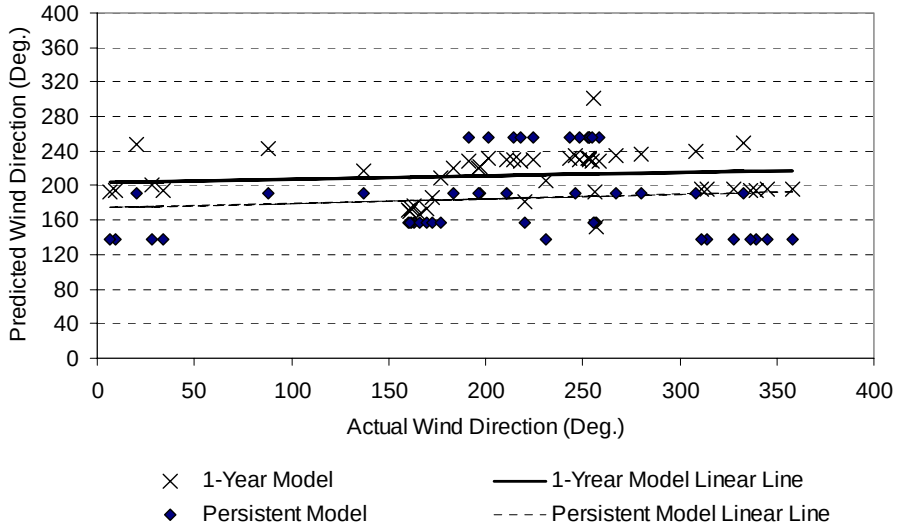

Figure 5-23: Relationship between actual and predicted wind direction for the half-day ahead prediction of the winter data sample using the 1-Year model and the persistent model.

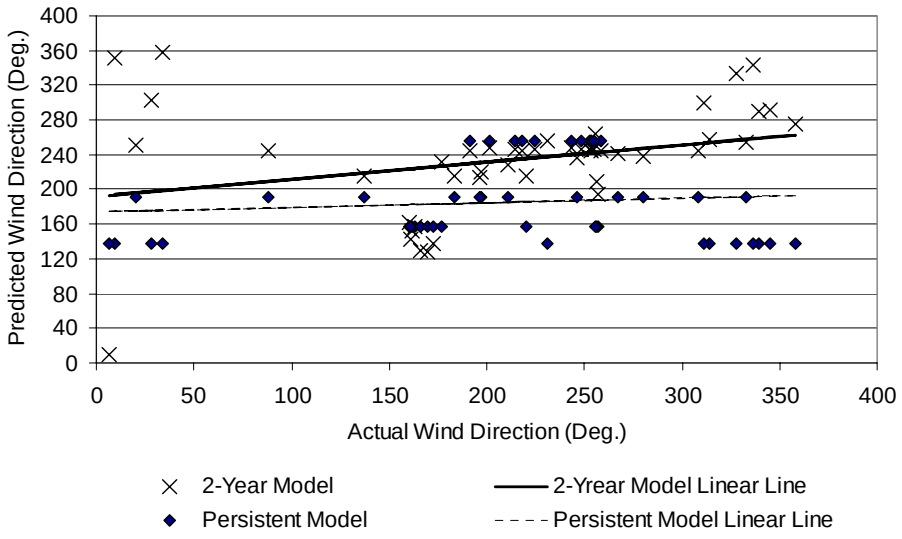

Figure 5-24: Relationship between actual and predicted wind direction for the half-day ahead prediction of the winter data sample using the 2-Year model and the persistent model.

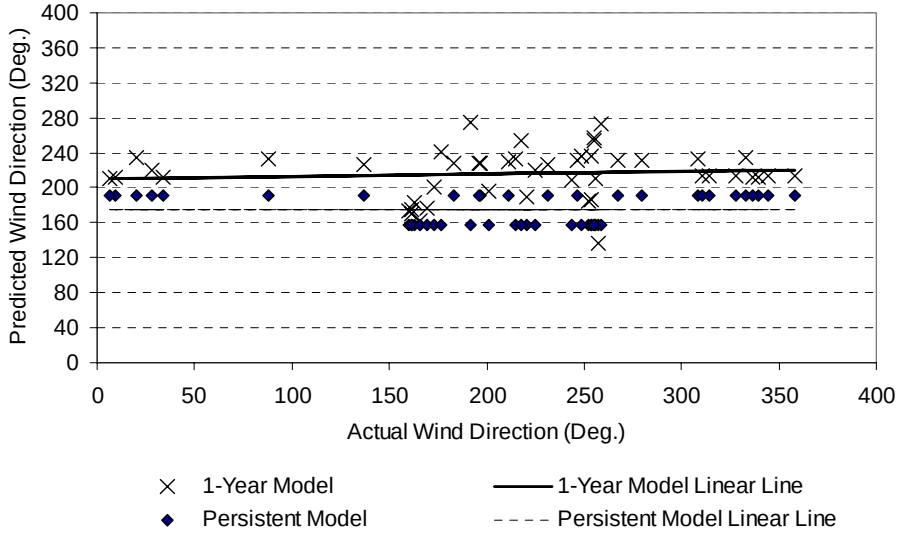

Figure 5-25: Relationship between actual and predicted wind direction for the one-day ahead prediction of the winter data sample using the 1-Year model and the persistent model.

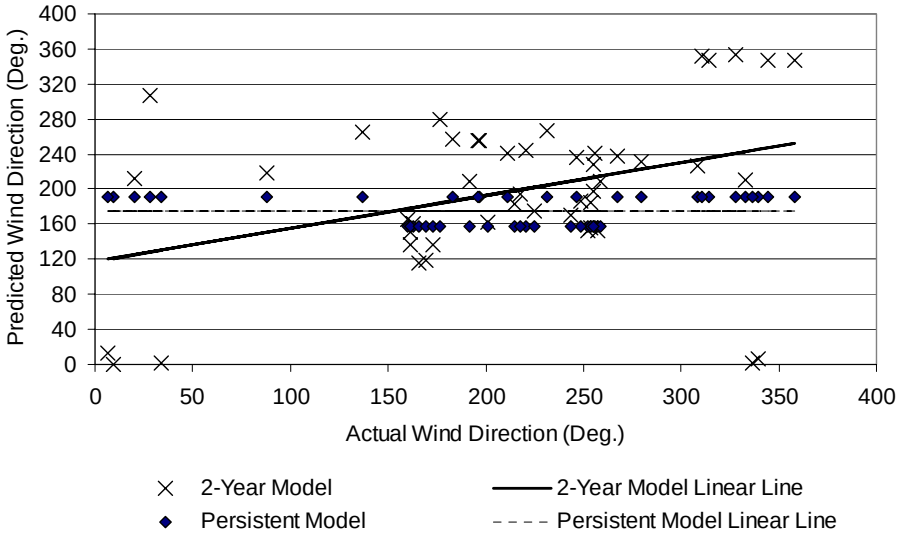

Figure 5-26: Relationship between actual and predicted wind direction for the one-day ahead prediction of the winter data sample using the 2-Year model and the persistent model.

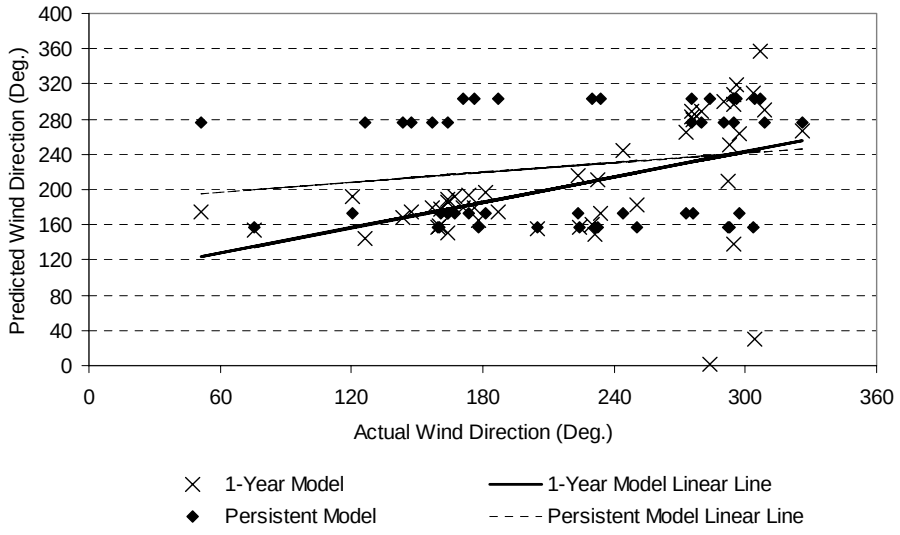

Figure 5-27: Relationship between actual and predicted wind direction for the half-day ahead prediction of the summer data sample using the 1-Year model and the persistent model.

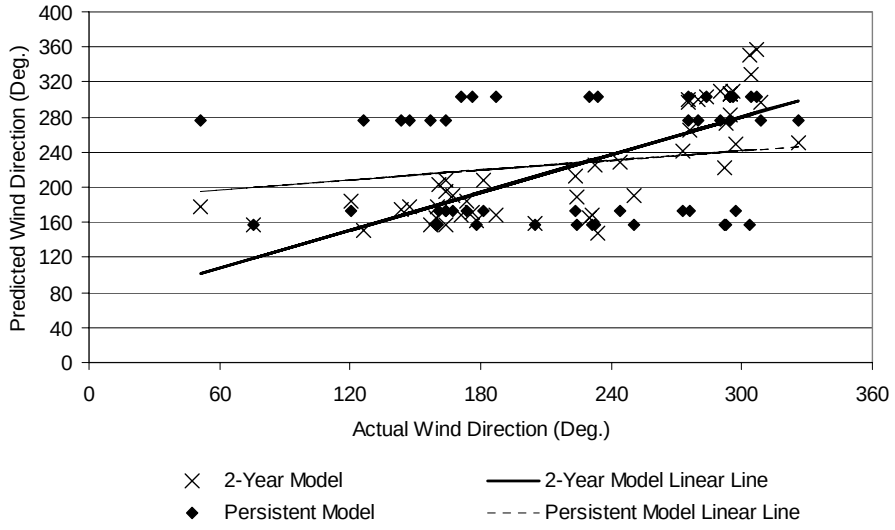

Figure 5-28: Relationship between actual and predicted wind direction for the half-day ahead prediction of the summer data sample using the 2-Year model and the persistent model.

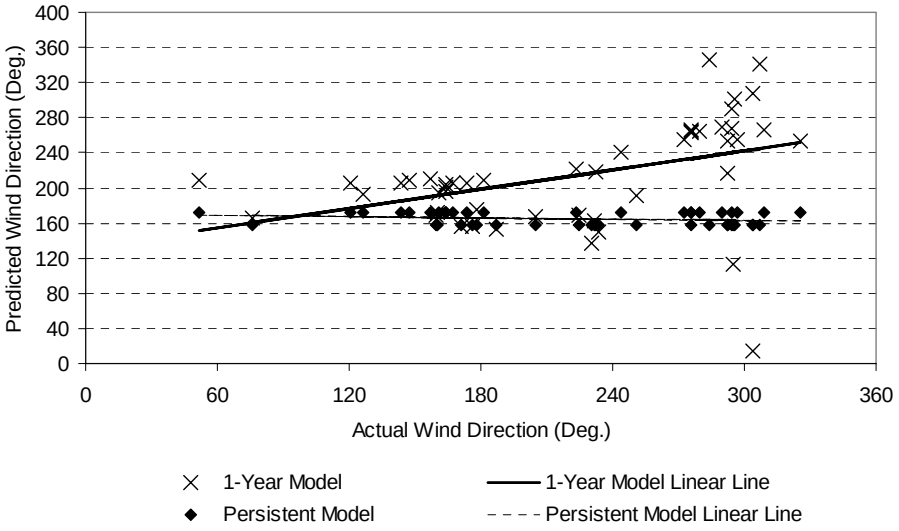

Figure 5-29: Relationship between actual and predicted wind direction for the one-day ahead prediction of the summer data sample using the 1-Year model and the persistent model.

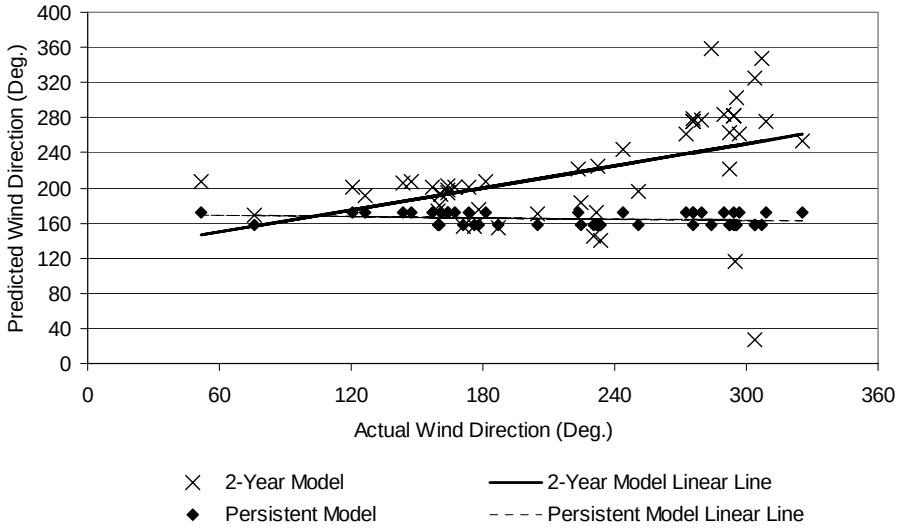

Figure 5-30: Relationship between actual and predicted wind direction for the one-day ahead prediction of the summer data sample using the 2-Year model and the persistent model.

Table 5-8: Scale factors and y-axis intercepts for wind direction prediction (winter sample).

Horizon (Hours)	Model	Coefficients	
		c	m
12	***Persistent***	174.153	0.053
24		174.819	-0.001
12	***1-Year Model***	203.324	0.040
24		210.172	0.029
12	***2-Year Model***	191.761	0.199
24		117.184	0.378

Table 5-9: Scale factors and y-axis intercepts for wind direction prediction (summer sample).

Horizon (Hours)	Model	Coefficients	
		c	m
12	***Persistent***	186.537	0.184
24		169.987	-0.023
12	***1-Year Model***	99.389	0.479
24		133.345	0.362
12	***2-Year Model***	64.343	0.720
24		124.449	0.419

5.6 Wind Power Prediction

In this section, the generated results for the wind speed and wind direction forecasting are used as an input data to the wind farm model, considering the dynamic wake effect, presented in Section 4.2.2, and the manufacture power curves for the VESTAS V66-1.65 MW to determine the predicted wind power production, as illustrated in Figure 5-31. Since the step variation for the forecasted results in this study is 1 hour, the effect of the time delay (a few seconds) is ignored. A look-up table is developed to model the impact of wind direction changing on the wind field distribution within the wind farm. For each range of wind direction, this look-up table determines the number of wind turbines that are subjected to free stream wind profiles and the number of wind turbines subjected to wind speed profiles reduced due to the wake effect as well as the strength of the wake effect.

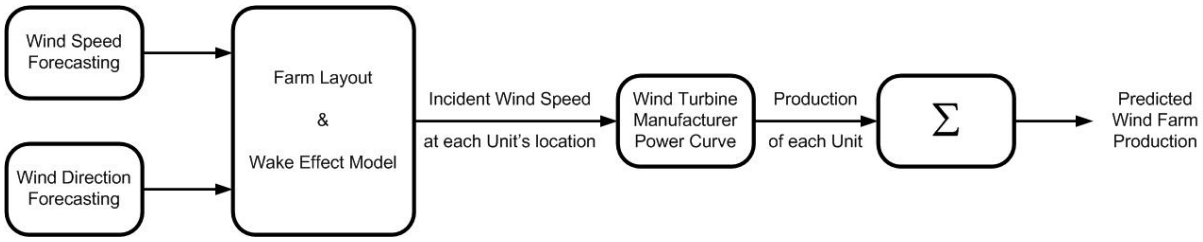

Figure 5-31: Wind farm power prediction.

Unfortunately, there are no real data available from operating wind farms to compare the predicted wind power values. Therefore, the results generated in this section are presented against simulated actual values (real power values simulated for actual recorded values of the wind speed and wind direction). Figure 5-32 - Figure 5-35 present the results for the 2-Year model.

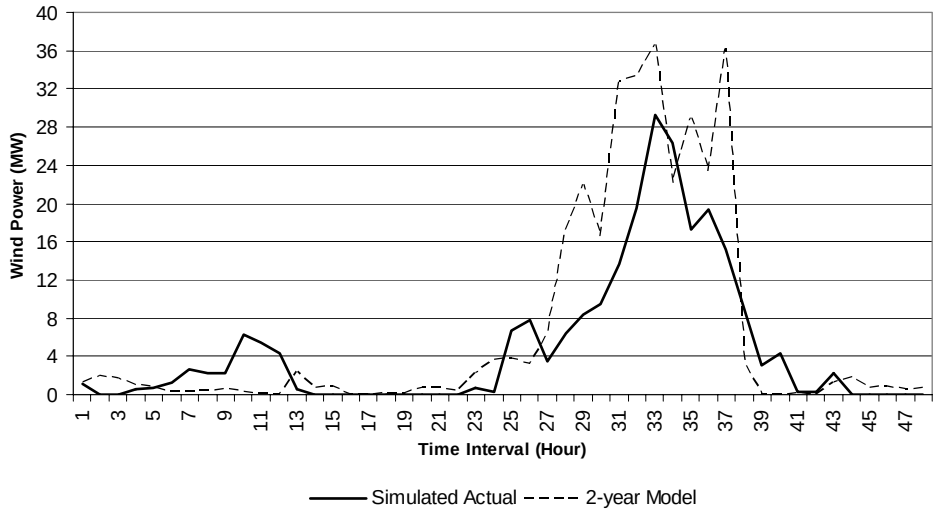

Figure 5-32: Half-day ahead predicted wind power for the winter data sample.

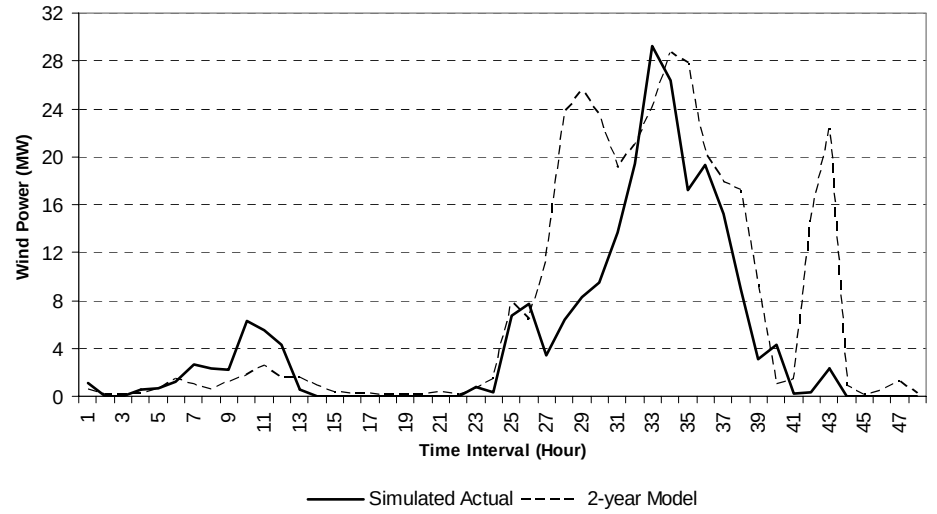

Figure 5-33: One-day ahead predicted wind power for the winter data sample.

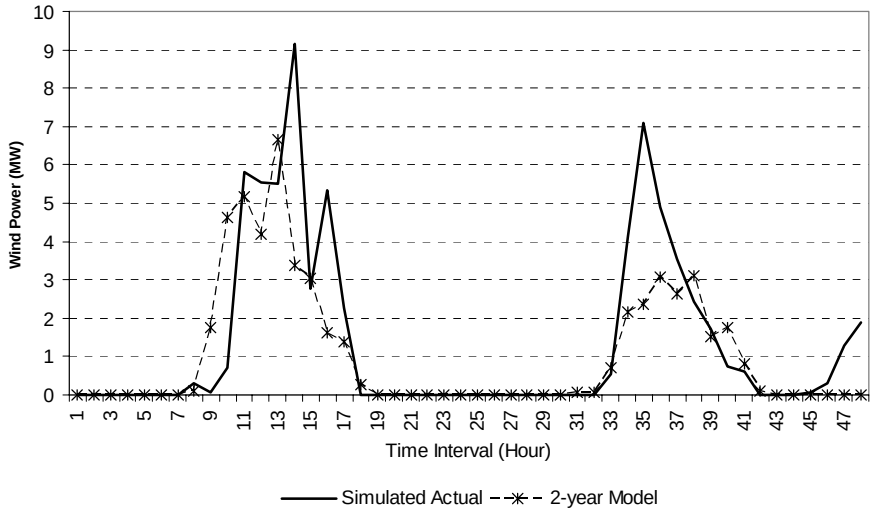

Figure 5-34: Half-day ahead predicted wind power for the summer data sample.

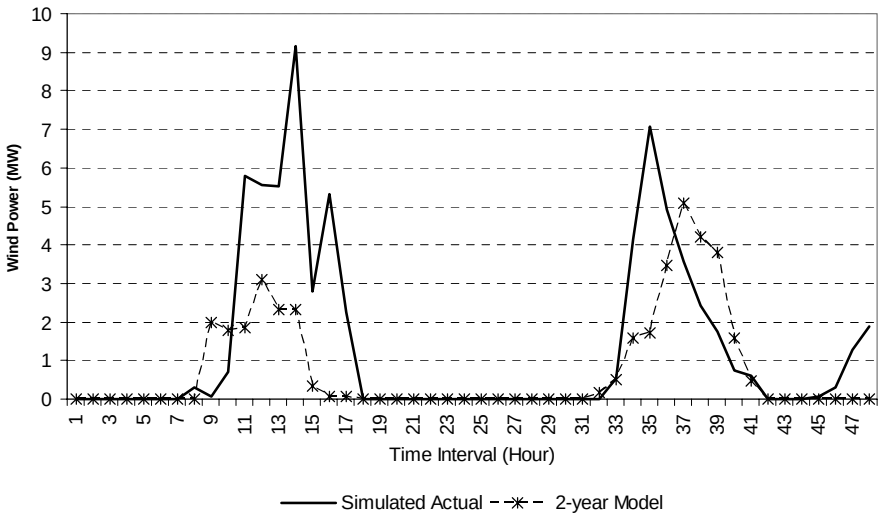

Figure 5-35: One-day ahead predicted wind power for the summer data sample.

5.7 Chapter Assessment

A new technique is proposed for wind speed and wind direction forecasting up to 24 hours ahead (one-day ahead prediction). The newly developed technique is based on assuming a linear relationship between the current set of data series and one (or two) years in the past data series. This linear relationship is then extended to the near future. The proposed models are characterized by the following:

- Very simple and cheap.
- Require reasonable amounts of data for model parameter estimation. However, these models require large data storage devices to record the yearly based data which are nowadays available due to the rapid revolution in the computing tools and electronic storage devices.
- Independent wind speed and direction forecasting.
- Effective for a few hours ahead and day ahead prediction.
- Independent of the data, collected from other sites.
- Independent of the NWP (Numerical Weather Prediction) models results.

The proposed models are so effective that they predict the wind speed for one-day ahead with a significant improvement, up to 54.4% for the MAE and up to 55.3% for the RMSE, over the persistent model. In addition, the novel models predict the wind direction for one-day ahead with an improvement as high as 45.3% for the MAE and as high as 26% for the RMSE, over the persistent model. Moreover, the newly developed models produce reduced scatter, higher coefficients of correlation, and higher scaling factors than those produced by the persistent model.

In addition, the results reveal that, at the Madison weather station, the proposed models generate better results during the summer season than those generated during the winter season. This occurs because the data recorded during the summer seasons are more related to each other than those recorded during the winter seasons.

Chapter 6
Wind Farm Integration Impact on Generation Costs and Electricity Market Prices

6.1 Introduction

As discussed in Section 2.6, some studies have been recently conducted to investigate the economic impact of the integration of wind farms into power systems. Such studies include examining the expected impact of wind power integration on electric power system operating costs [85], investigating the effect of wind power prediction inaccuracy on the cost associated with rescheduling generation units [86], and developing a probabilistic approach to determine the energy costs due to the associated errors with wind power prediction [87]. However, to the best of the author knowledge, no study has addressed the expected impact of wind farms integration and their operating conditions, such as production variability, applied control strategies, and production prediction accuracy, on determining electricity market prices.

This chapter investigates the impact of wind power variability, wind farm control strategy (including voltage regulation techniques such as the proposed technique in Section 4.3), wind energy penetration level, wind farm location, and hourly wind power prediction accuracy (such as the prediction accuracy when using the Grey predictor model developed in Section 3.2.5) on the total generation costs and close to real-time electricity market prices. These issues are addressed by developing a single auction market model for determining the close to real-time electricity market prices. To demonstrate and highlight the impact, different case studies are introduced.

6.2 Network Configuration

Figure 6-1 exhibits the 9-bus network configuration under study [126]. It consists of a 6-bus transmission system and a 3-bus distribution system linked via a 100 MVA transformer. The transmission system is supplied from two central generation stations that are connected to Bus 1 (G1) and Bus 3 (G2). The total generation capacities of these stations are 300 MVA and 600 MVA, respectively. A 130 MW wind farm is connected at bus 8, unless otherwise is stated. The network

parameters for both the transmission and the distribution systems are given in Table 6-1. In addition, the generation data, demand data, and generation cost function parameters at each bus are presented in

Table **6-2**.

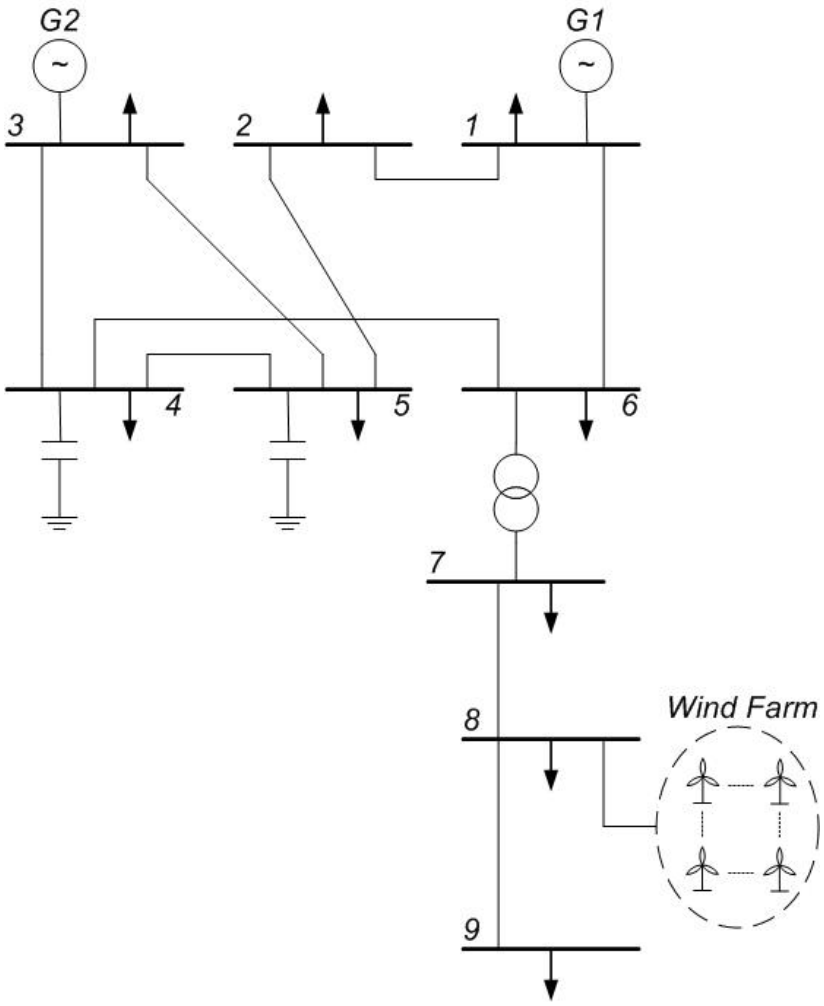

Figure 6-1: Network configuration under investigation.

At each bus, the connected load is assumed to be time varying. This is introduced into the system by using the scaling factor at each time interval as given in Figure 6-2. This scaling factor represents the percentage demand at each time interval, one hour, referred to the maximum daily demand. The scaling factor for this study, is derived from the daily load demand variation, recorded by the New

York Independent System Operator (NYISO) [127]. Finally, the net load at each bus, at a given time interval, is calculated by using the following formula:

$$P_{d,\,net}(i,t) = P_d(i)\ x\ Scaling\ Factor(t)\ , \qquad (6\text{-}1)$$

where $P_{d,\,net}\ (i,t)$ is the net demand at time interval t at bus i, $P_d\ (i)$ is the maximum daily demand at bus i given in
Table **6-2**, and *Scaling Factor (t)* represents the loading level at time interval t.

Table 6-1: Network parameters.

Buses	***Reactance (pu)***	***Resistance (pu)***	***Line Charging (pu)***
1 – 2	0.1097	0.021	0.004
1 – 6	0.2732	0.0824	0.004
2 – 5	0.3185	0.107	0.005
3 – 4	0.2987	0.0945	0.005
3 – 5	0.1804	0.0662	0.003
4 – 5	0.1792	0.0639	0.001
4 – 6	0.098	0.034	0.004
6 – 7	0.1	0	0
7 – 8	0.082	0.054	0
8 – 9	0.082	0.054	0

6.3 Problem formulation

Generally, there are two structures of electricity markets: the single auction market and the double auction market [128]. This study is focused on the single auction market structure [128], where the market price is settled according to the total demand and the bids submitted by the generators. The objective with such market structure is to maximize the social welfare and that is equivalent to the minimization of the total generation cost function. This study considers the minimization of the total generation cost as the objective in this market solution [129], [130]. Therefore, the optimization problem involves minimizing the total cost generation function J (represented by the fuel cost function) that is expressed as follows:

Table 6-2: Generation and load data.

Bus	***a*** ***($/MWh^2)***	***b*** ***($/MWh)***	***c*** ***($/h)***	P_{max} ***(pu)***	P_{min} ***(pu)***	Q_{max} ***(pu)***	Q_{min} ***(pu)***	P_d ***(pu)***	Q_d ***(pu)***
1	0.01	25.5	9	2.5	0.5	1.5	-0.2	0.92	0.29
2	0	0	0	0	0	0	0	0.78	0.39
3	0.05	8.5	5	5	1	3	-0.2	0.73	0.19
4	0	0	0	0	0	1	0	0.67	0.24
5	0	0	0	0	0	1	0	1.12	0.31
6	0	0	0	0	0	0	0	0.26	0.12
7	0	0	0	0	0	0	0	0.2	0.05
8	0	0	0	1.3	0	1.3	-1.3	0.4	0.2
9	0	0	0	0	0	0	0	0.3	0.13

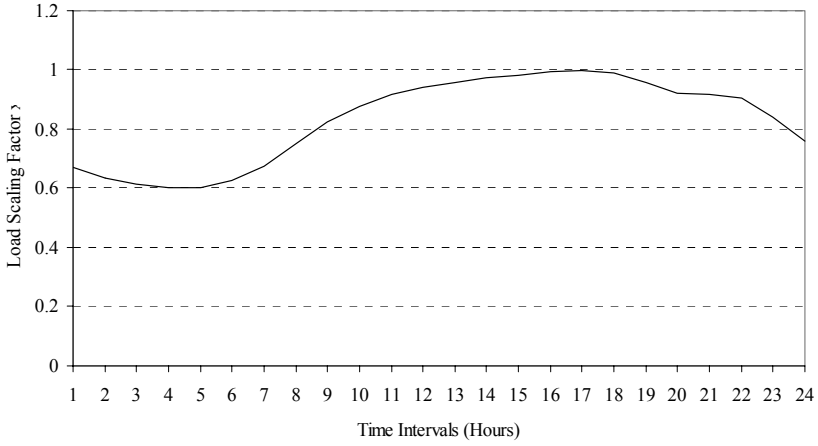

Figure 6-2: Load scaling factor variation curve with time.

$$J = \sum_{i=1}^{N} a_i P_i^2 + b_i P_i + c_i \quad , \tag{6-2}$$

where P_i is the generated power of generator i, a_i, b_i, and c_i are the generation cost function parameters for generator i, and N is the number of generators.

The total cost generation function is minimized subject to the following constraints:

- *Power Flow Equations:* The two basic equations that govern the flow of power in power systems' networks are written as follows:

$$P_i - PD_i = \sum_j |V_i||V_j|Y_{i,j}\cos(\theta_{i,j} + \delta_j - \delta_i) \tag{6-3}$$

and

$$Q_i - QD_i = -\sum_j |V_i||V_j|Y_{i,j}\sin(\theta_{i,j} + \delta_j - \delta_i) \quad , \tag{6-4}$$

where V_i and δ_i are the voltage and the power angle at bus i, respectively, $Y_{i,j}$ and $\theta_{i,j}$ are the bus admittance matrix element and its associated angle, respectively, P_i and PD_i are active power generation and demand at bus i, respectively, and Q_i and QD_i are the reactive power generation and demand at bus i, respectively.

- *Generator Limits:* These limits are used to ensure that the active and reactive power generation at the generator buses are within their acceptable boundaries. They are expressed mathematically as

$$P_i^{Min} \le P_i \le P_i^{Max} \tag{6-5}$$

and

$$Q_i^{Min} \le Q_i \le Q_i^{Max} \quad , \tag{6-6}$$

where P^{Min}, P^{Max}, Q^{Min} and Q^{Max} are the minimum and maximum limits for the active and reactive power to be generated by each generator, respectively.

- *Voltage Limits:* Such limits are introduced to the formulation to ensure that the voltages at the load buses are within acceptable levels. These limits are formulated as follows:

$$V_i^{Min} \le V_i \le V_i^{Max} \quad \forall\, i \in 1,.....N_L \quad . \tag{6-7}$$

For the generator buses, the voltage is fixed as follows:

$$|V_i| = \text{constant} \quad \forall\, i \in 1,.....N_G \quad , \tag{6-8}$$

where V_i^{Min} and V_i^{Max} are the minimum and the maximum voltage limits at the load bus *i*, and N_L and N_G are the number of load and generator buses, respectively.

- *Wind Farm Operation Constraints:* Wind generation is variable in nature due to the variability of the incident wind speed at the wind turbine site. Such variability is introduced to the formulation by using the variable, daily average, per unit, wind generation curve in Figure 6-3 (unless otherwise stated). This curve was recorded by the NYISO at one of their wind farm sites [127].

  As for the wind farm bus voltage limits (Bus 8 voltage limits, unless otherwise stated), the bus is treated as a generator bus, when the wind farm is operated at the voltage regulation mode. Otherwise, it is treated as a load bus.

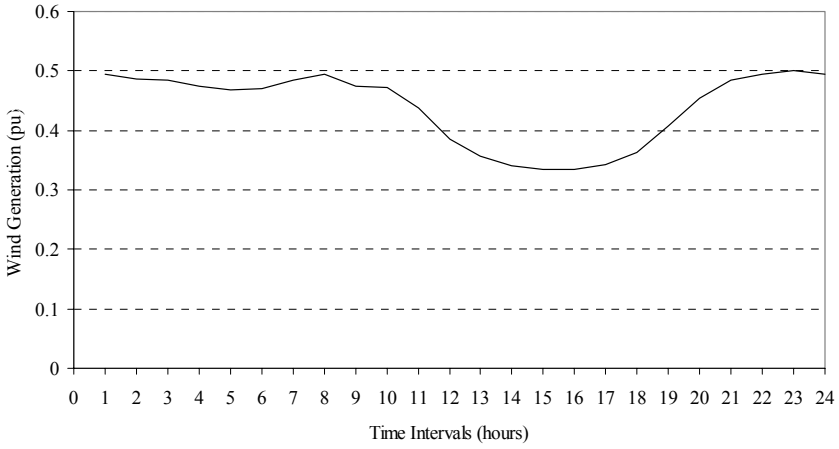

Figure 6-3: Average daily wind farm generation curve.

- *Market Pricing Mechanism:* There are various pricing mechanisms for determining the electricity market price: *the uniform*, where all the generators and loads in the network sell or buy electricity with the same uniform price; *the locational*, where each bus has its own electricity price and this is usually its marginal cost; and *the zonal*-based pricing, where the network is divided into zones that are created by using either sensitivity calculations or electrical distances, and then each zone will has its own uniform market price [131].

  This study focuses on using the uniform market price mechanism (since this is the market pricing mechanism used in Ontario [132]) in determining the network electricity market prices. This is adopted by solving the above market model to determine the highest value of the bus incremental cost that is set as the market price [126]. Thus,

$$\rho \geq \lambda_i \qquad \forall \quad i \in 1, ...N_t \quad , \tag{6-9}$$

where ρ represents the uniform electricity market price, and λ_i is the local marginal cost at a bus i that is calculated by using the Kuhn-Tucker's condition of optimality, and N_t is the total number of buses.

6.4 Simulation Results

The presented market model is formulated as a Nonlinear Programming Problem (NLP) and solved by using the MINOS solver in the General Algebraic Modelling System (GAMS) environment [131]. In this work, several case studies are designed to highlight the effect of production variability, wind generation control strategies, penetration levels, installation locations, and prediction accuracy. The simulation results of each individual case study will be investigated in the next subsections.

6.4.1 Case Study 1: Wind Power Variability

The objective of this case study is to analyze the impact of wind farm (WF) generation on the electricity market-clearing price. The market price for a system with existing wind generation (as an example of a non-dispatchable DG unit) is compared with that of the case where there is a diesel DG (as an example of a dispatchable DG unit that is capable of continuous active power generation). These aforementioned results are then compared with the market price in the absence of a diesel DG and wind farm on Bus 8. In all the cases, the Bus 8 voltage is assumed to be regulated to unity. In addition, two different actual wind power generation patterns (shown in Figure 6-3), hereafter referred to as Wind 1 and Wind 2, are considered. Each pattern represents the average wind generation pattern for three-month periods, as recorded by the NYISO during the winter season (Wind 1 or Sample 1) and summer season (Wind 2 or Sample 2) [127]. Moreover, two different cost functions, given in Table 6-3 for the diesel DG, are included in this case, and are referred to as Low Cost DG (LCDG) and High Cost DG (HCDG).

Figure 6-4 - Figure 6-7 show the active power generation at bus 8, the reactive power generation at bus 8, the market clearing price, total generation cost, and the voltage at Bus 8, respectively. Referring to Table 6-3 and Figure 6-4, it can be seen that as the diesel DG generation cost increases, the DG generated active power decreases within some intervals. The main system market price is affected by the presence of both the wind farm and diesel DG, as seen in Figure 6-6. In fact, the presence of any type of DGs decreases the electricity market price. By comparing the market price for

wind farm case with that of diesel DGs, it can be seen that the loads on the system might undergo market spikes, especially when there is a low wind power generation. The high fluctuation in market prices with a wind farm is due to the stochastic nature of the generated wind. However, the market price is still lower than the case where there is no existing generation at Bus 8. With respect to the generation costs (refer to Figure 6-7), the total generation costs decrease in the presence of either a wind farm or another DG type. It is observed that the generation cost can be reduced, when the wind power generation is increased. Figure 6-8 presents the corresponding impact on the active power generation at the two central stations.

Table 6-3: Generation cost function parameters and reactive power limits for Bus 8.

Connected DG to Bus 8	***a*** ***($/MWh^2)***	***b*** ***($/MWh)***	***c*** ***($/h)***	Q_{max} ***(pu)***	Q_{min} ***(pu)***
WF	0	0	0	0.6	-0.6
LCDG	0.004	12	5	0.6	-0.6
HCDG	0.008	24	10	0.6	-0.6

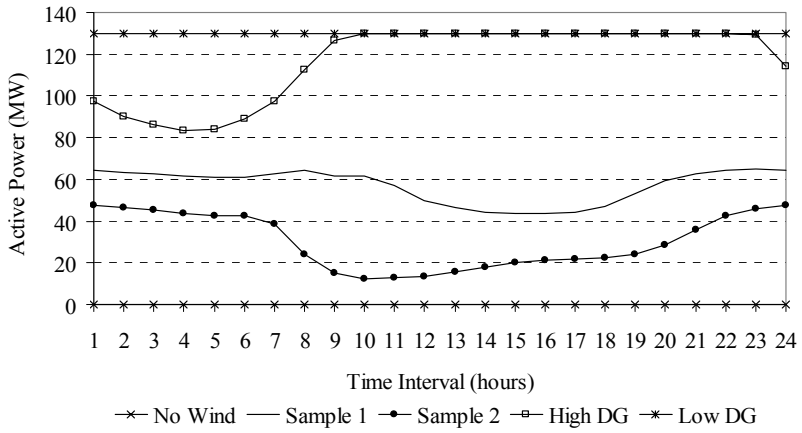

Figure 6-4: Active power generation at Bus 8.

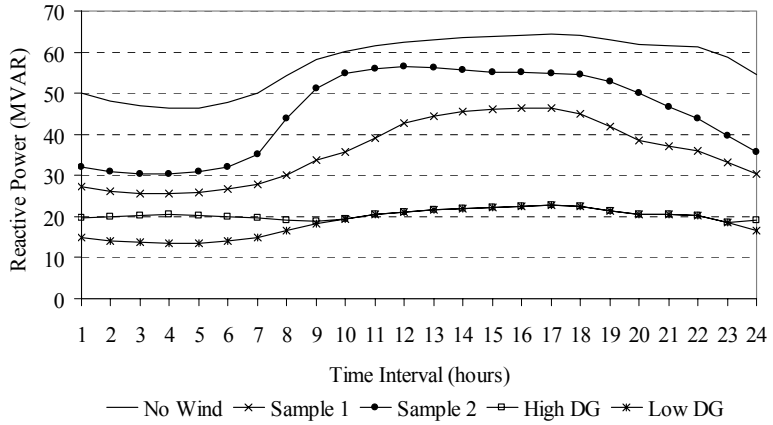

Figure 6-5: Reactive power generation at Bus 8.

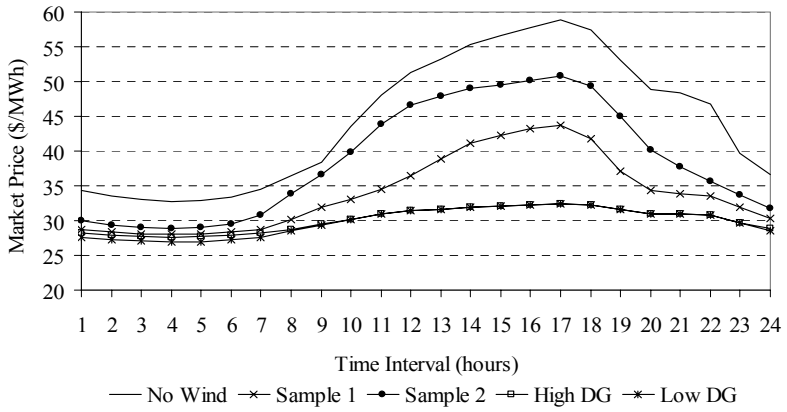

Figure 6-6: Market clearing price.

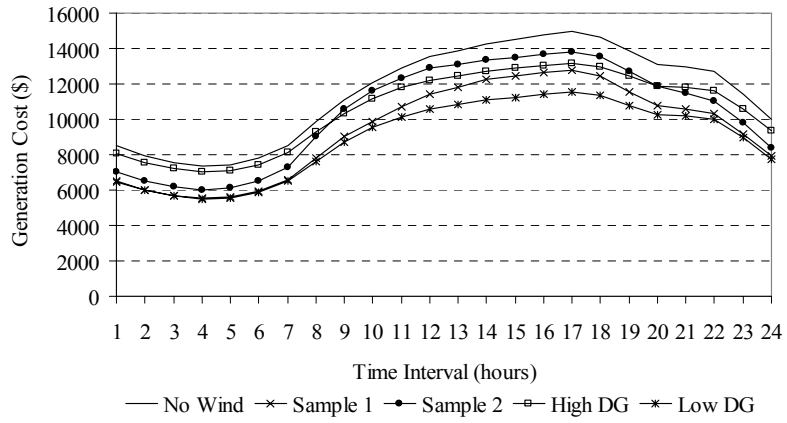

Figure 6-7: Total generation cost.

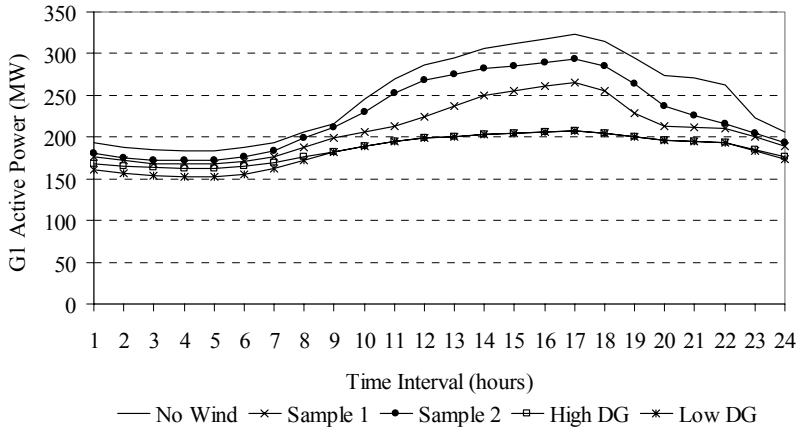

a) Central station G1

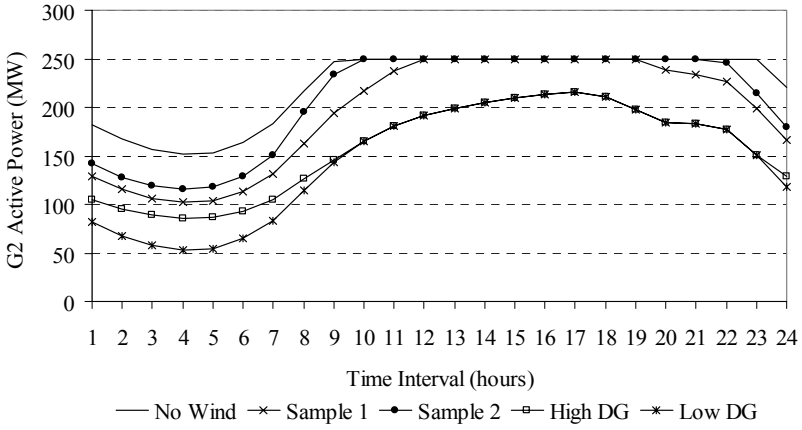

b) Central station G2

Figure 6-8: Central stations' active power generation.

6.4.2 Case Study 2: Wind Farm Control Strategy

In this case, different control strategies for wind farm production are considered to examine the effect of the reactive power injection of the wind farm on the electricity market prices. Wind farms are currently allowed to supply/absorb reactive power to/from the network. In this case, the following operational procedures are investigated:

- ***Unity power factor (UPF) operation***: The wind farm is not allowed to exchange reactive power with the network; i.e. $Q_{farm} = 0$.

- ***Voltage Regulation (VR)***: The wind farm terminal voltage (Bus # 8) voltage is regulated to unity. In this case, the reactive power generated or consumed by the farm varies according to the OPF operation constraints, provided that the farm apparent power is within pre-specified limits.
- ***Power Factor (PF) Regulation***: The consumed reactive power by the wind farm is controlled to regulate the farm's terminal power factor at 0.8 leading.
- ***Local Power Factor (LPF) Regulation***: The wind farm reactive power is regulated in such a way as to maintain the Bus 8 power factor at unity. This is achieved by generating reactive power from the wind farm that is set to equal the reactive power demand at Bus 8.

Figure 6-9 exhibits the voltage variation at Bus 8, associated with each of the considered control strategies. The lowest voltage level is attained when the UPF mode of operation is used. The corresponding market clearing prices for each control mode is presented in Figure 6-10. Figure 6-11 demonstrates the difference (savings, from the demand side point of view) in the market clearing prices, referred to the UPF control mode of operation. These figures reveal that there is almost no effect of the control strategies on the market price for low loading conditions (below 70% of the maximum daily demand). However, during high demand periods (especially during the peak demand intervals) a difference in market prices up to 7.5 $/MWh is observed. Moreover, these figures show that the UPF mode of operation has the highest electricity market prices, and the VR mode has the lowest values.

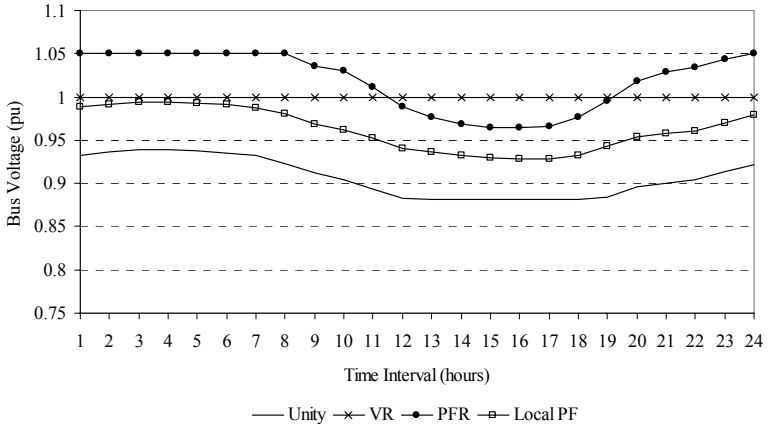

Figure 6-9: Terminal voltage at Bus 8.

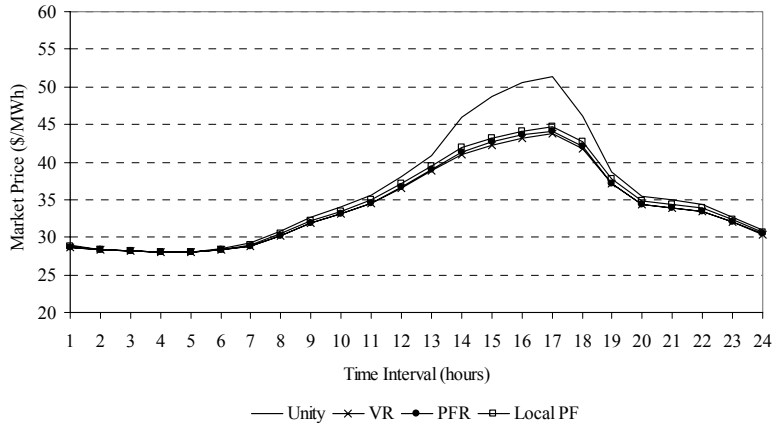

Figure 6-10: Market clearing price.

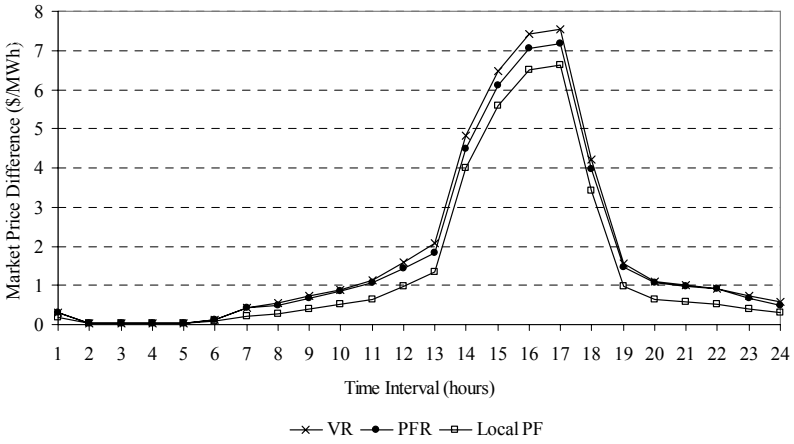

Figure 6-11: Difference in the market clearing price.

Figure 6-12 and Figure 6-13 provide the total generation cost and the difference in the total generation costs (referred to the UPF control mode of operation), respectively, for each control mode. These figures reveal that changing the control strategy slightly affects the total generation costs (about 0.8% for the time interval with the peak generation cost). In this study, the generation cost difference is calculated such that the positive values indicate a savings in the generation costs, compared with that of the UPF control mode. Figure 6-13 records that the highest savings is achieved, when the wind farm is controlled by using the VR mode of operation. Figure 6-14 conveys the impact of changing the control strategy on the active power generation at the two central stations. Also, this

figure shows that the G1 active power generation is slightly affected, especially during the periods with a peak load demand. Moreover, the figure reveals that the G2 active power generation is almost not affected, even during the periods with a peak load demand, as the generation hits the maximum limits.

The difference in electricity costs, due to market price difference, is determined by the following:

$$G(t) = \left[\lambda(t) - \lambda_{ref}(t)\right] \cdot \sum_{i=1}^{N_G+N_L} P_i(t) \quad , \tag{6-10}$$

where $G(t)$ is the gain in the electricity costs due to the market price difference at time interval t, $\lambda_{ref}(t)$ is the reference case study market price at time interval t, $\lambda(t)$ is the considered case study market price at time interval t, and $P_i(t)$ is the demand at bus i at time interval t.

The daily average electricity cost difference (gain) is determined and found to be equal to 950.4 \$/hr, 895.9 \$/hr, and 741.7 \$/hr for the VR, PF, and LPF cases, respectively, referred to the UPF case study. These positive daily averages indicate a gain in the customer savings in electricity bills or a loss in the generator revenue. The corresponding daily average generation cost difference (savings in generation costs) is found to be 58.7 \$/hr, 58.6 \$/hr, and 45.8 \$/hr, respectively.

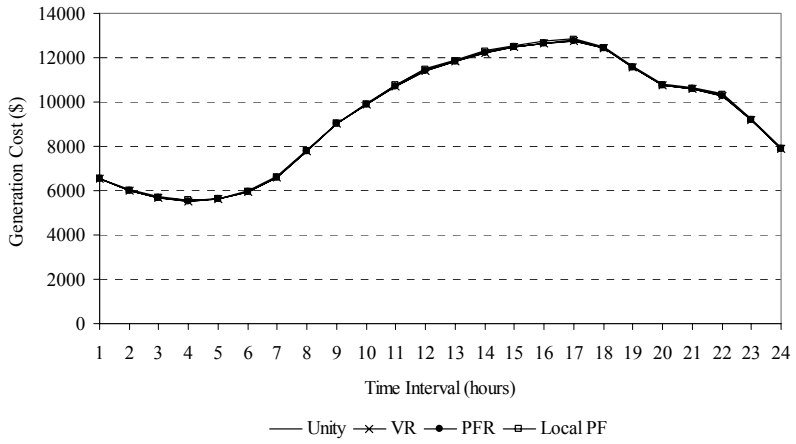

Figure 6-12: Total generation cost.

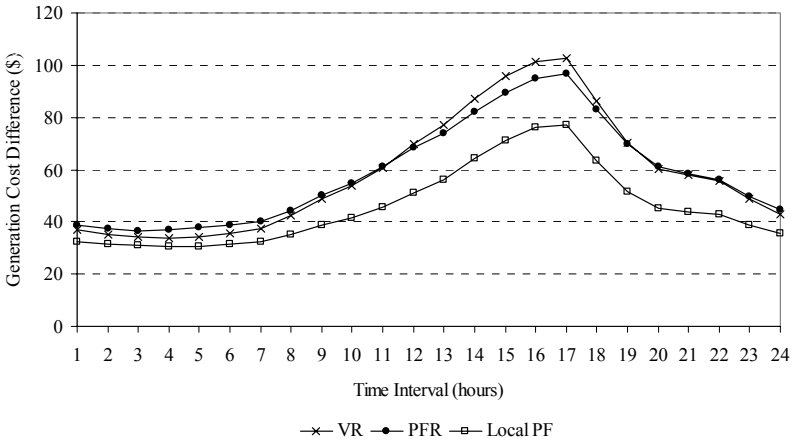

Figure 6-13: Difference in the total generation cost.

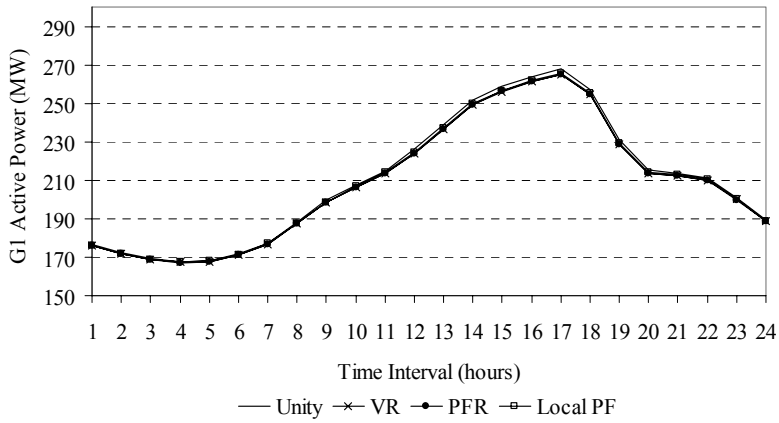

a) Central station G1

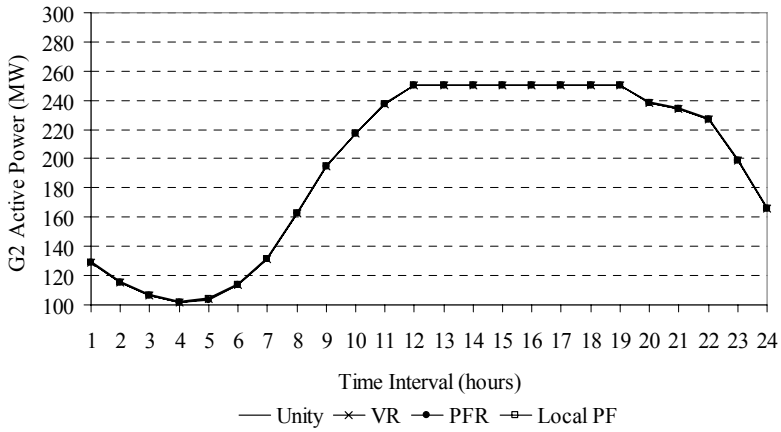

b) Central station G2

Figure 6-14: Central stations' active power generation.

6.4.3 Case Study 3: Wind Power Penetration Level

In this case study, the goal is to analyze the impact of the penetration level of the wind farm on the electricity market-clearing price. The wind farm is assumed to operate by using the voltage regulation mode. Three different ratings for the wind farm are examined: 130 MW, 195 MW, and 260 MW. Figure 6-15 displays the reactive power generation at Bus 8 for the different ratings. With the increase in the wind farm rating, and consequently, the generated active power, the required reactive power generation to regulate the bus voltage is reduced. The corresponding market clearing prices in Figure 6-16 reveal a decrease in the market prices with an increase in the penetration level, especially during the period of high demand and low wind generation. Moreover, it is demonstrated that such a reduction is very small for the periods with the lowest demands. This is clarified by plotting the savings in the market clearing prices, referred to the corresponding market prices when the wind farm rating is 130 MW, as signified in Figure 6-17. The corresponding daily average electricity cost difference (savings) is found to be equal to 1232.5 $/hr and 1859.1 $/hr for the 195 MW and 260 MW cases, respectively, referred to the 130 MW case.

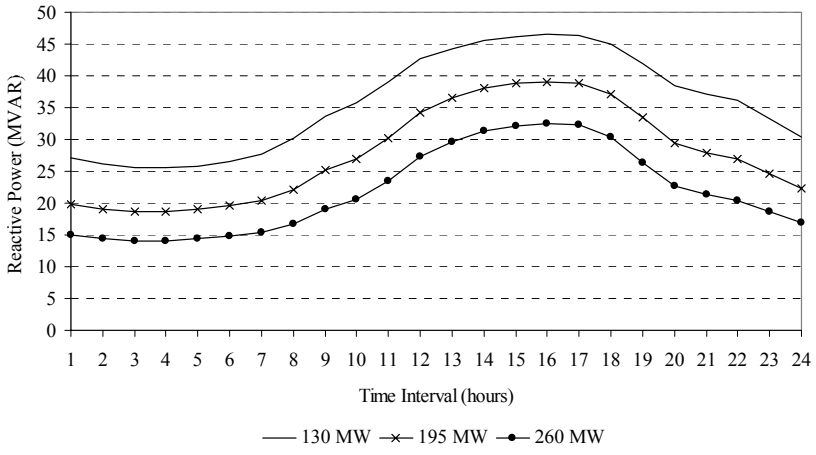

Figure 6-15: Wind farm reactive power generation at Bus 8.

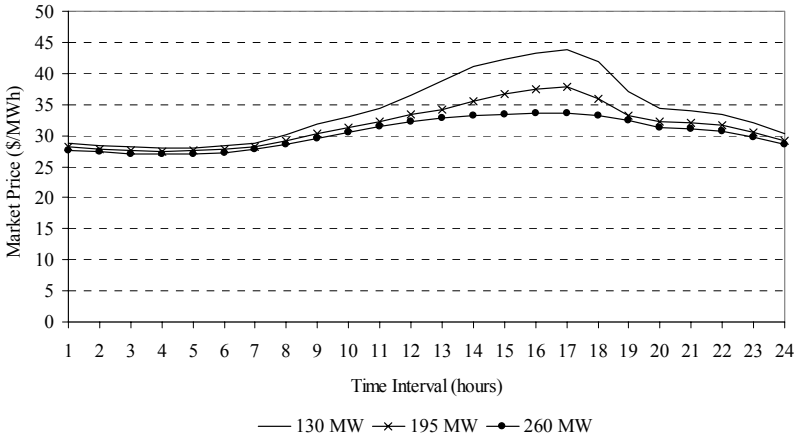

Figure 6-16: Market clearing price.

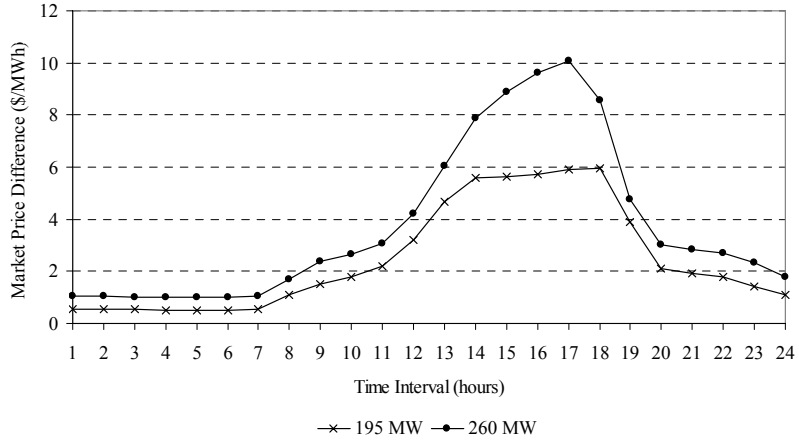

Figure 6-17: Difference in the market clearing price.

Figure 6-18 presents the corresponding impact on the active power generation at the two central stations. A reduction in the active power generation at the central stations occurs with the increase in the wind generation penetration level. Moreover, this increase in the penetration level is associated with a reduction in the wind farm reactive power generation to regulate the bus terminal voltage to unity, as illustrated earlier in Figure 6-15.

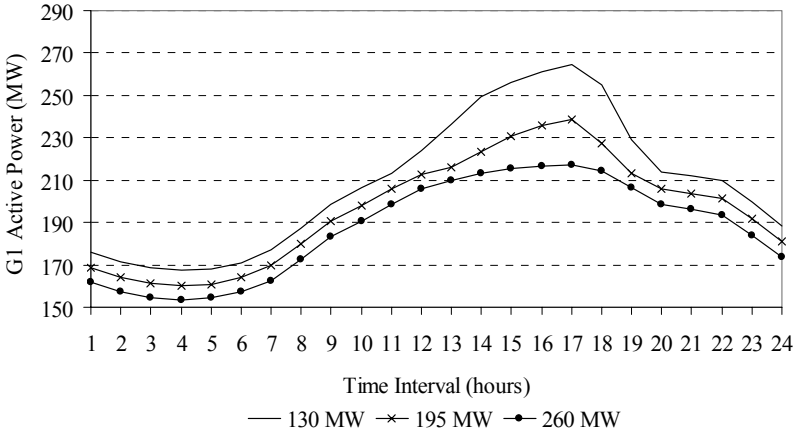

a) Central station G1

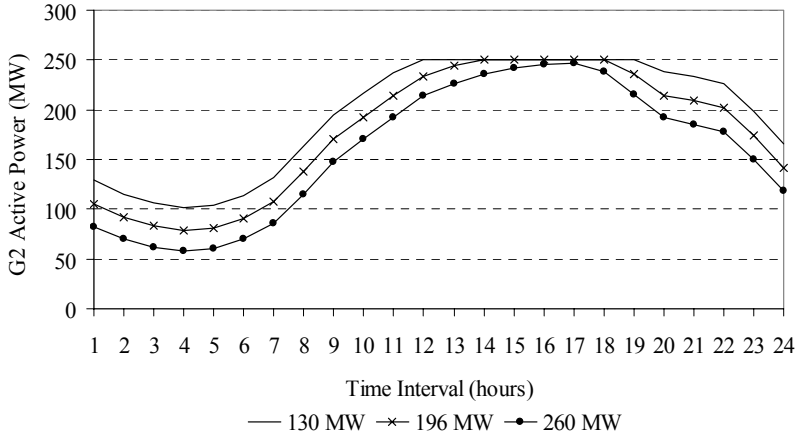

b) Central station G2

Figure 6-18: Central stations' active power generation.

With respect to the total generation cost in Figure 6-19, a reduction in the generation costs is observed with the increase in the penetration level. Figure 6-20 records the savings in the total generation costs, in relation to the 130 MW case. This figure demonstrates an increase in the net generation costs savings that is almost double, when the additional wind capacity is doubled (from 65 MW, in case of a total capacity of 195 MW, to 130 MW, in case of a total capacity of 260 MW). The corresponding daily average generation cost difference is found to be equal to 876.4 $/hr and 1674.1 $/hr for the 195 MW and 260 MW cases, respectively.

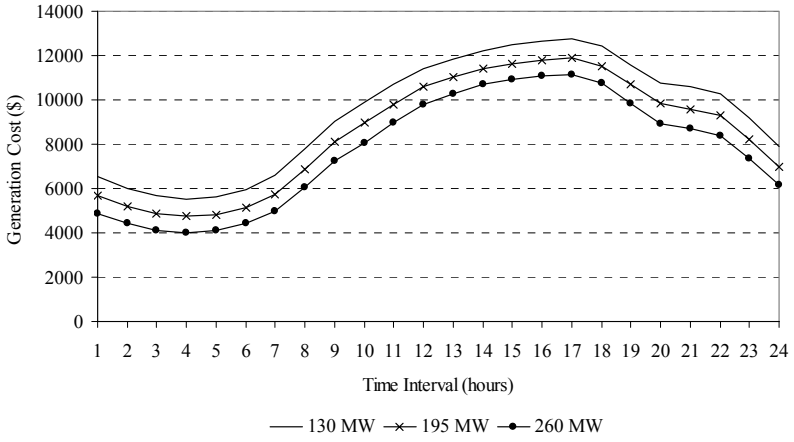

Figure 6-19: Total generation cost.

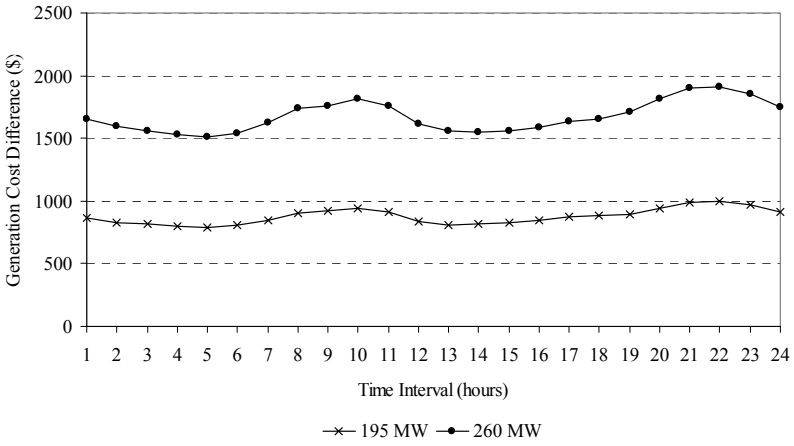

Figure 6-20: Difference in the total generation cost.

6.4.4 Case Study 4: Wind Farm Location

This case is dedicated to examine the impact of different installation locations for wind generation facilities. The three buses at the distribution system are considered as possible locations for wind generation installations. Again, the wind farm is assumed to operate by using the voltage regulation mode with a total capacity of 130 MW for all locations. Figure 6-21, Figure 6-22, and Figure 6-23 show the reactive power generation at Bus 8, the market clearing price, and the total generation cost, respectively. As the wind farm installation location gets closer to the transmission system, it is observed that the generation of more reactive power is required to regulate the wind farm bus voltage

to unity, as seen by Figure 6-21, the electricity market-clearing price increases as demonstrated by Figure 6-22, and the total generation cost is only slightly affected (about 1.2% for the time interval with the peak generation cost), as shown in Figure 6-23.

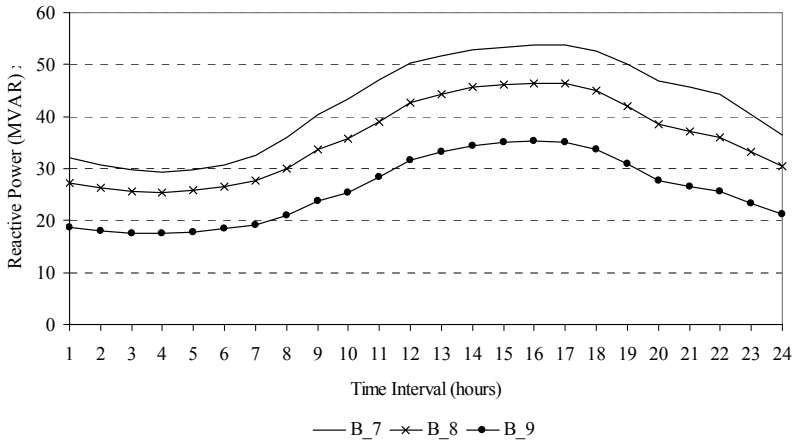

Figure 6-21: Wind farm reactive power generation.

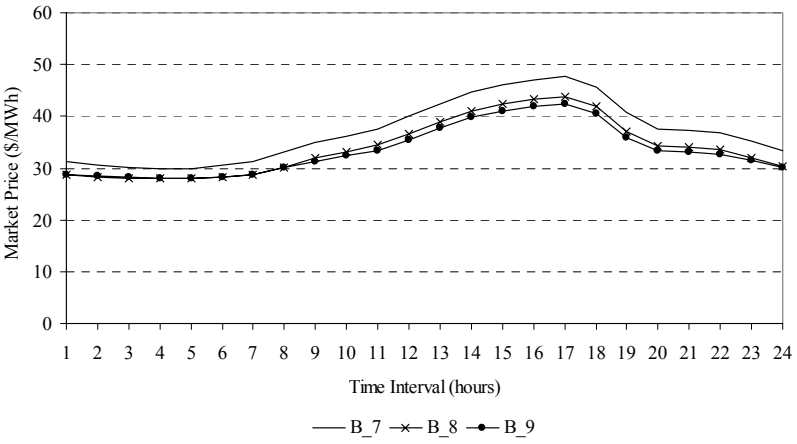

Figure 6-22: Market clearing price.

Figure 6-24 and Figure 6-25 present the difference in the market clearing prices and the savings in the total generation costs, and is referred to the Bus 7 (B_7) location case. These figures reveal that the savings in the electricity prices and the total generation costs increases with the increase in the demand level. Referred to the location case study at Bus 7, the daily average electricity cost

difference is found to be equal to 1405.7 $/hr and 1724.9 $/hr for the Bus 8 (B_8) and Bus 9 (B_9) locations cases, respectively. The corresponding daily average generation cost difference is found to be equal to 94.4 $/hr and 81.4 $/hr, respectively.

Figure 6-26 reflects the impact of changing the installation location on the active power generation at the two central stations. This figure shows that G1 active power generation is slightly affected, especially during the periods with peak load demands, and that the maximum generation costs occurs when the wind farm is installed close to the transmission system (at Bus 7). Also, the figure reveals that the G2 active power generation is hardly affected even during the periods with a peak load demand, where the generation hits the maximum limits.

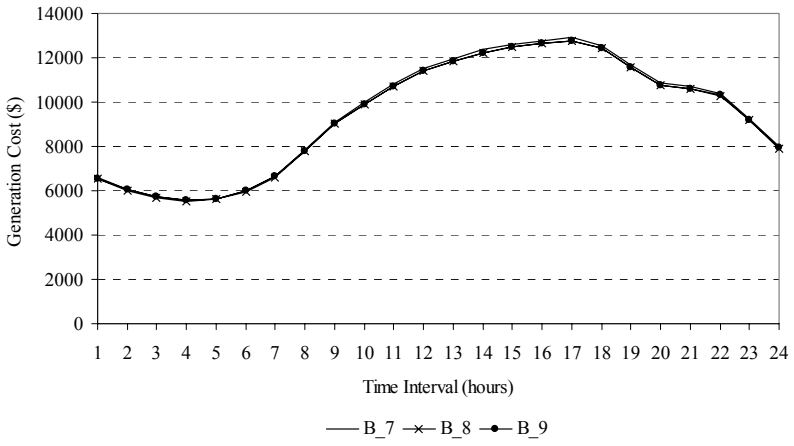

Figure 6-23: Total generation cost.

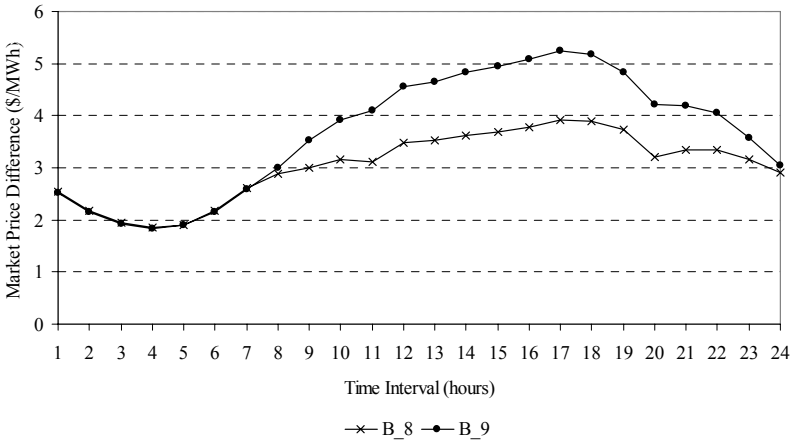

Figure 6-24: Difference in the market clearing price.

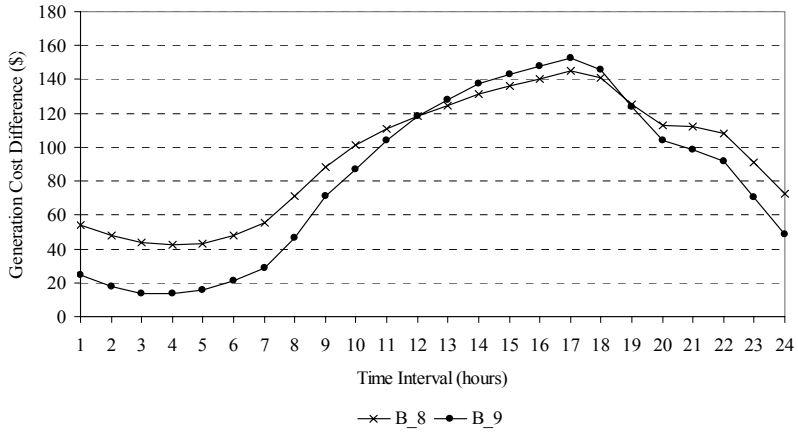

Figure 6-25: Difference in the total generation cost.

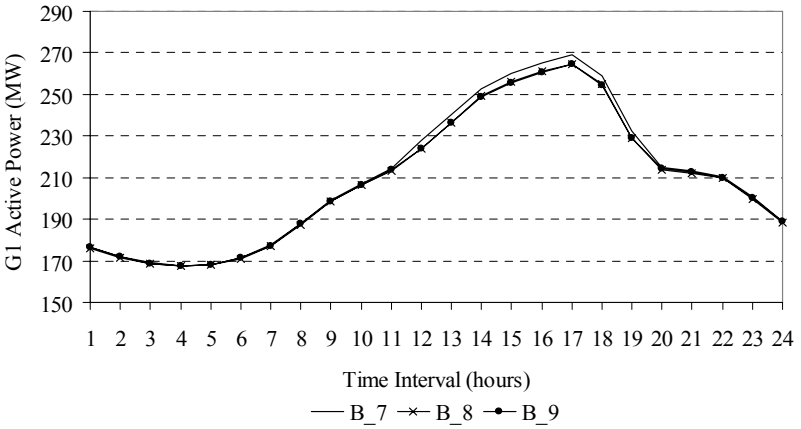

a) Central station G1

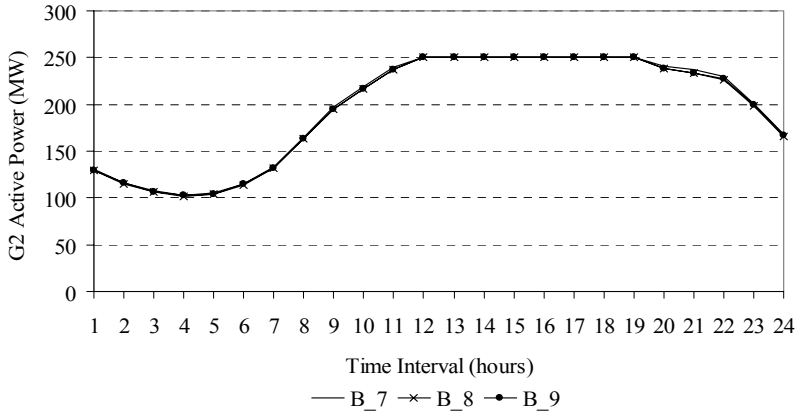

b) Central station G2

Figure 6-26: Central stations' active power generation.

6.4.5 Case Study 5: Wind Power Prediction

This case is dedicated to examine the impact of the accuracy of the wind farm prediction tools, presented in Section 3.2.5, on electricity market-clearing price. Similar to case study 1, two different wind power samples, Wind 1 and Wind 2, are considered. The predication horizon is chosen to be one hour, thus simulating an hour ahead electricity market similar to the Ontario Electricity Market. Figure 6-27 shows the output power that is predicted by using both the averaged GM (1,1) model and the persistent model, and then compared to the actual power. Figure 6-28 shows the one-hour ahead and spot market price. The MAE for the market prices is determined as follows:

$$MAE = \frac{\sum \left| SP_{actual} - SP_{predicted} \right|}{\text{Length of Sampled Data}} \quad , \tag{6-11}$$

where SP_{actual} refers to the expected spot market price, based on actual wind power generation, and $SP_{predicted}$ refers to the spot market price according to the predicted wind power generated (this is the real spot market price).

For sample data 1 “Wind 1”, the MAE of the predicated power for the Grey predictor and the persistent model are 1.27 MW and 1.62 MW, respectively. The error in the predicted values, in turn, affects the electricity market price. Figure 6-29 shows the error in the spot market prices. The MAE of the spot market price for the Grey predictor and persistent model are 0.267 $/MWH and 0.328 $/MWH, respectively. It can be seen that for both predictors, there are time intervals where SP_{actual} is higher than $SP_{predicted}$ and others where SP_{actual} is lower. Thus, in some intervals, customers can benefit from this error by buying electricity at lower rates than actual prices. However, there are intervals where the opposite is true, i.e. customers pay more than the actual electricity price. Figure 6-30 shows the difference in electricity costs due to the market price error for both predictors. This is determined by the following:

$$C_d = (SP_{actual} - SP_{predicted}) \sum_{i=1}^{N_G+N_L} P_i \quad , \tag{6-12}$$

where C_d is the gain in the electricity costs due to market price error. The daily average electricity cost difference is determined and found to be equal to -35.94 $/hr and 0.5 $/hr for the Grey predictor and persistent model, respectively. The positive daily average indicates a gain in the customer savings

for the electricity bills or a loss in generator revenue (the negative value indicates the reverse). If these numbers are considered the average cost difference over the three-month period at which the wind power pattern has been recorded, it is expected that the total savings/loss is $ -77,630.4 and $ 1,080.0, referred to the customer savings. Figure 6-33 denotes the impact of the wind generation prediction on the active power generation at the two central stations.

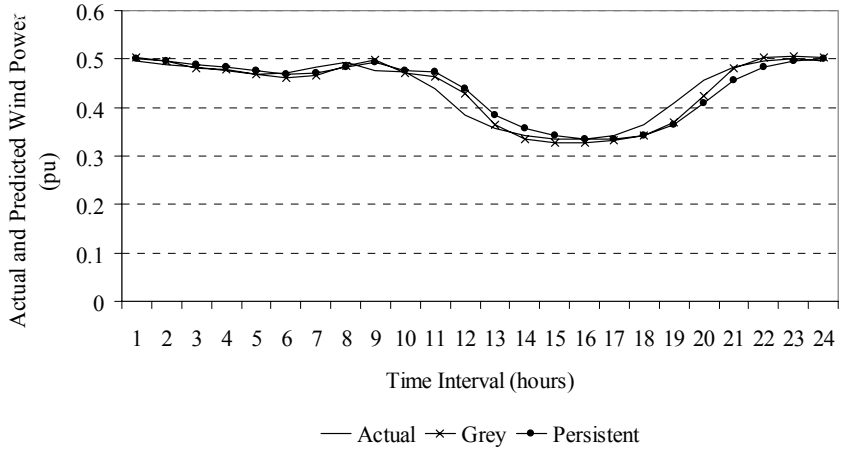

Figure 6-27: Wind farm generated power (Wind 1 pattern).

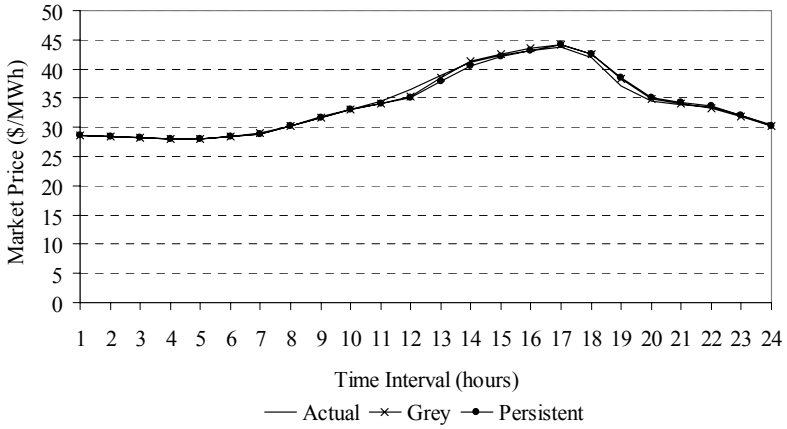

Figure 6-28: One-hour ahead and spot market price (Wind 1 pattern).

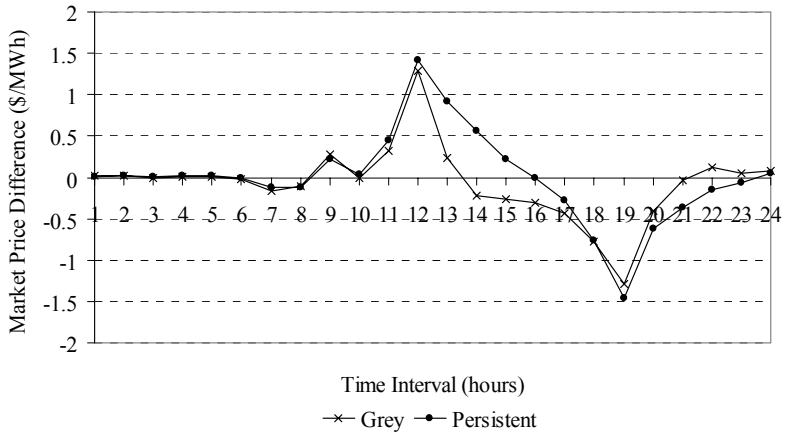

Figure 6-29: Market price error (Wind 1 pattern).

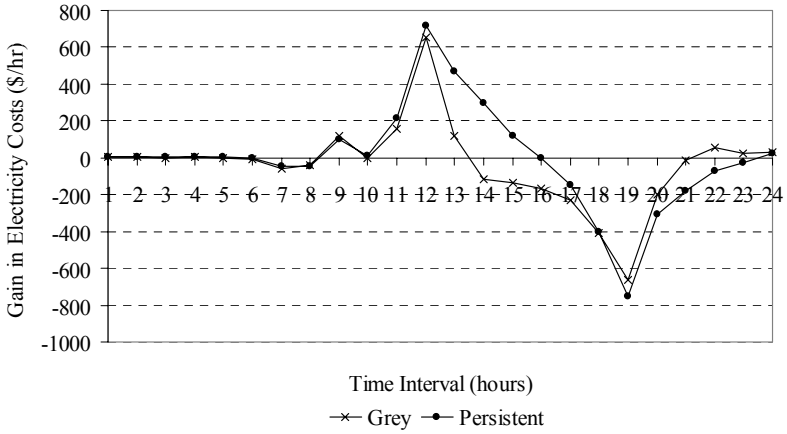

Figure 6-30: Gain in electricity costs due to market price error (Wind 1 pattern).

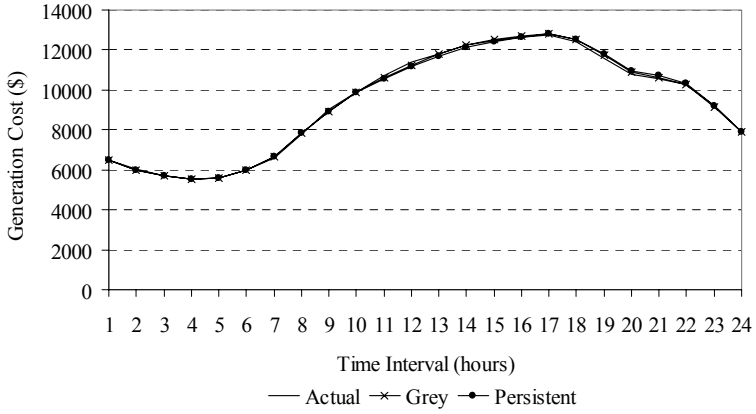

Figure 6-31: Total generation cost.

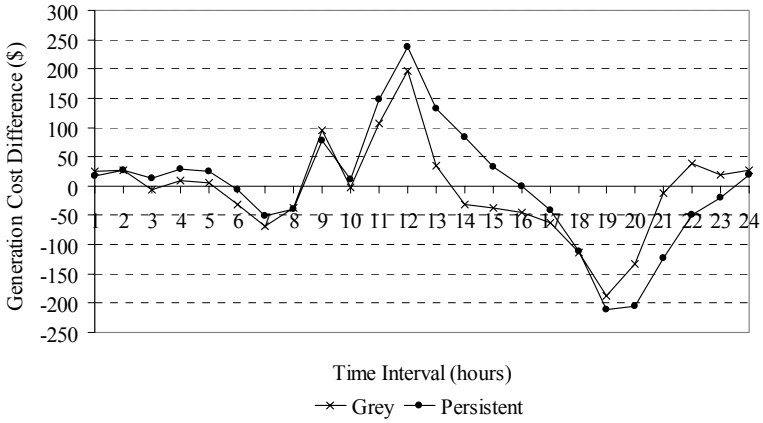

Figure 6-32: Difference in the total generation cost.

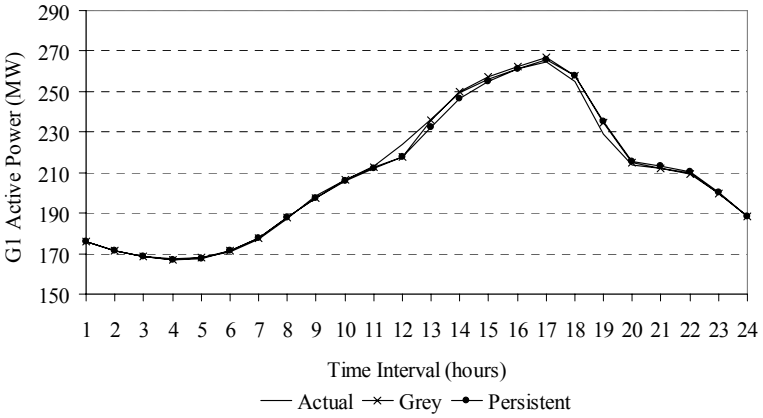

a) Central station G1

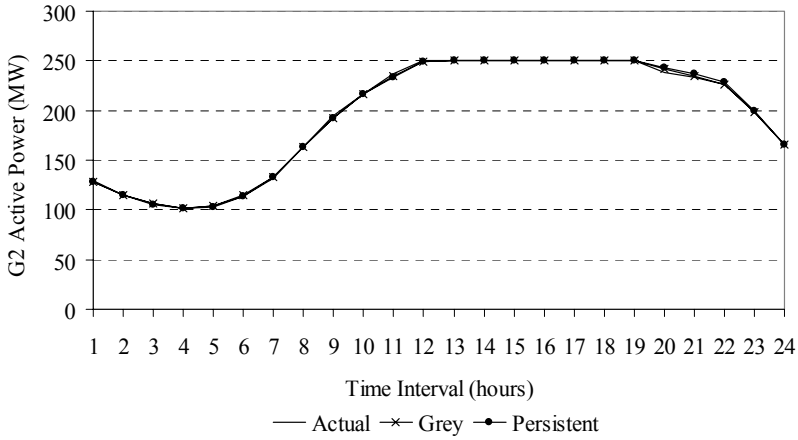

b) Central station G2

Figure 6-33: Central stations' active power generation (Wind 1 pattern).

Figure 6-34 - Figure 6-37 reflect the wind farm generation, electricity market price, errors in the market price, and difference in electricity costs due to the market price errors for both prediction models, for the second sample data "Wind 2", respectively. For this sample data, the MAE of the predicated power for the Grey predictor and the persistent model are 1.73 MW and 2.3 MW, respectively. Accordingly, the corresponding MAEs for the spot market price are 0.41 $/MWH and 0.51 $/MWH, respectively. From Figure 6-35, the daily average electricity cost difference is found to be -98.52 $/hr and -109.27 $/hr for the Grey predictor and persistent model, respectively. Similarly, the total savings/loss expected, over the three-month period at which this wind power pattern has been recorded, is $ -217,532.16 and $ -241,268.16, referred to the customer savings.

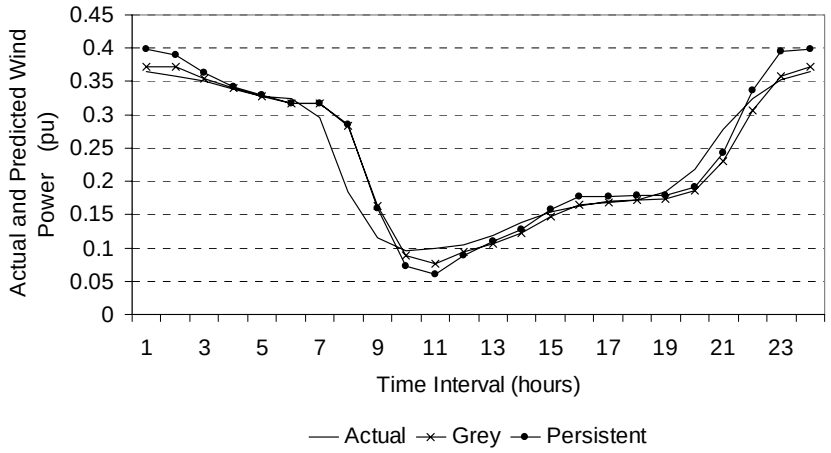

Figure 6-34: Wind farm generated power (Wind 2 pattern).

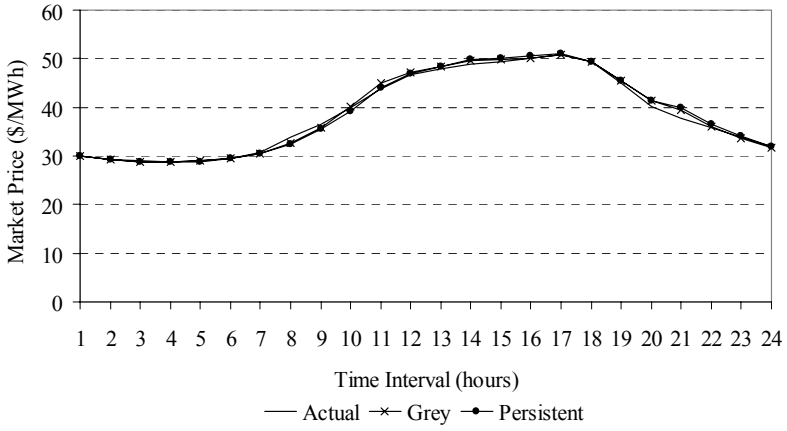

Figure 6-35: One hour ahead and spot market price (Wind 2 pattern).

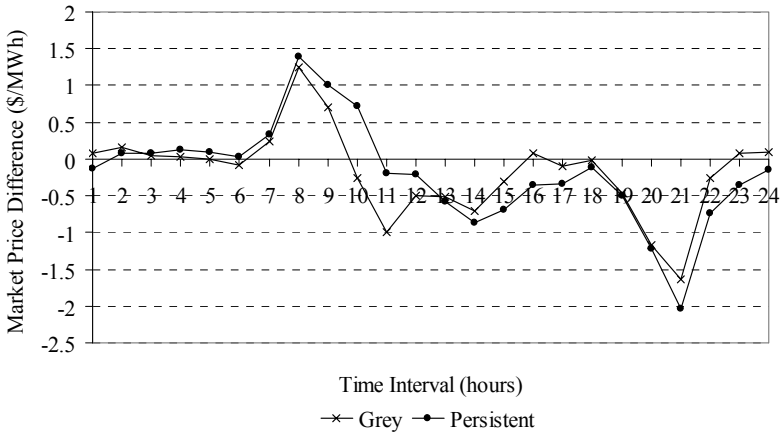

Figure 6-36: Market price error (Wind 2 pattern).

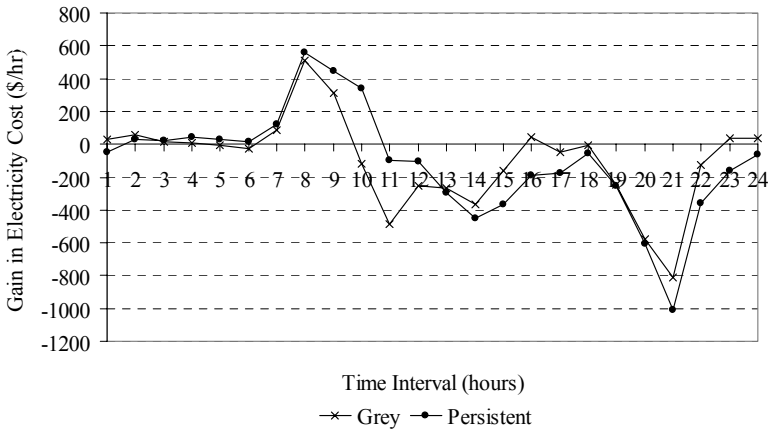

Figure 6-37: Gain in electricity costs due to market price error (Wind 2 pattern).

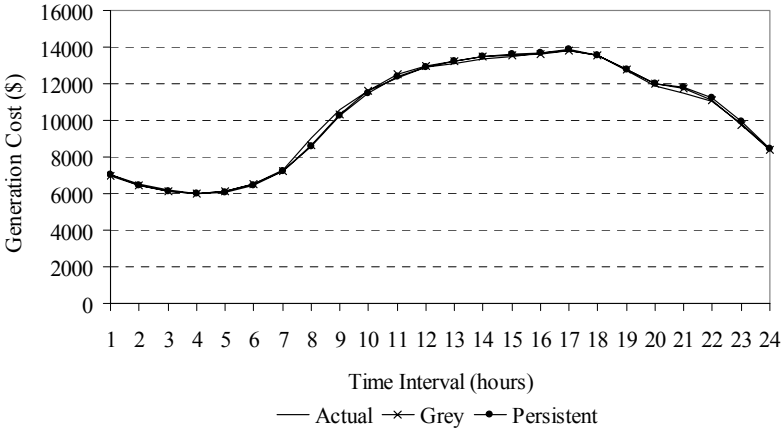

Figure 6-38: Total generation cost.

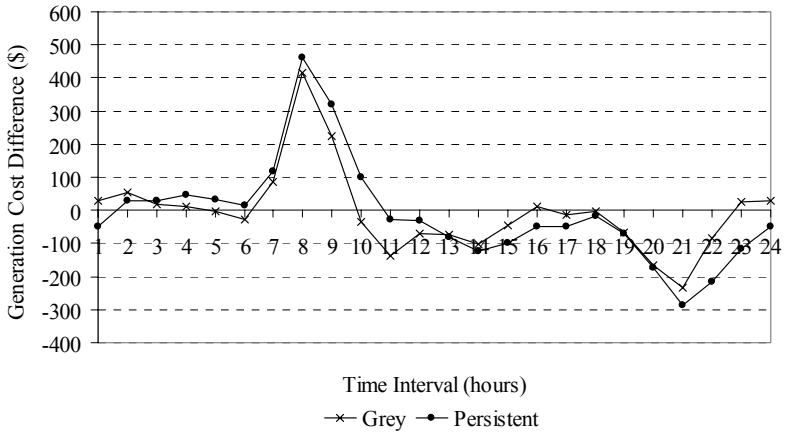

Figure 6-39: Difference in the total generation cost.

Figure 6-40 presents the impact of wind generation prediction on the active power generation at the two central stations. From these prediction results for the specific samples under consideration, it is evident that in both cases there is a daily customer savings/generator loss in electricity costs. This is due to the errors in the predicted wind power generation. The results prove that it is essential to take into account the prediction errors when settling electricity market prices.

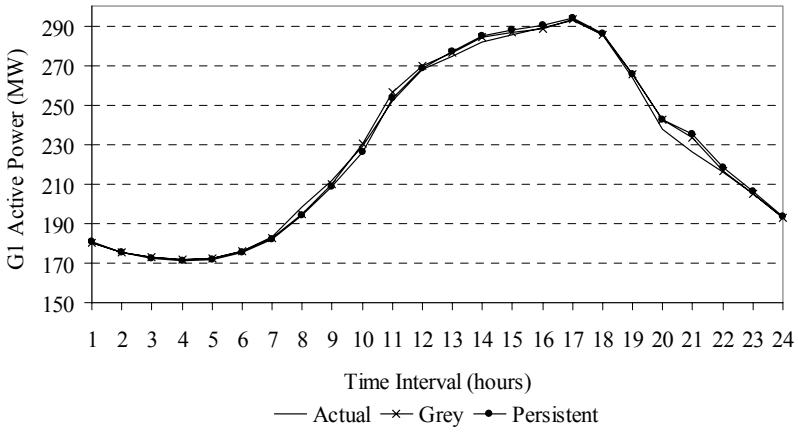

a) Central station G1

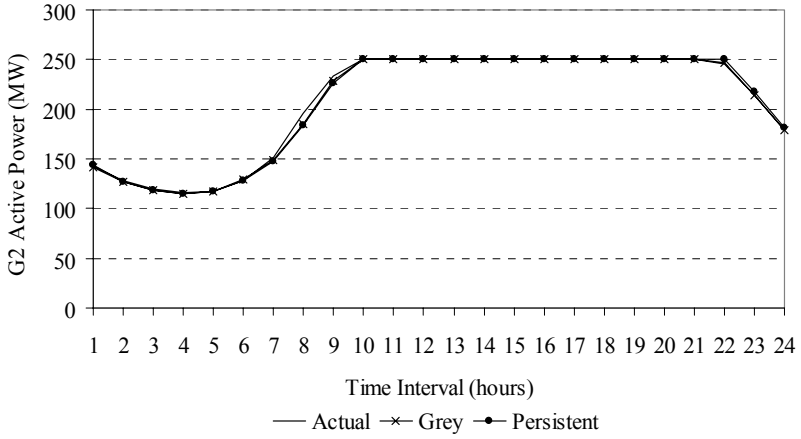

b) Central station G2

Figure 6-40: Central stations active power generation (Wind 2 pattern).

6.5 Chapter Assessment

This chapter investigates the possible impacts of wind farms' production variability, control strategies, location, penetration levels, and prediction accuracy, on the close to real-time electricity market prices and the total generation costs. A 9-bus network configuration, consisting of a 6-bus transmission system and a 3-bus distribution system, is studied. The addition of a wind farm in the network can significantly reduce market prices. However, when compared to a constant power DG, an increase in the market price occurs due to the variable nature of the wind and the shift between the wind power generation and load demand peak times.

During periods with low demand, the uniform market prices are slightly affected by changing the control strategy, but a significant impact is observed for intervals under high demand conditions. Moreover, the lowest market prices are achieved, when the wind farm is operated in the voltage regulation mode. Consequently, the use of such mode increases the customers' savings in electricity bills. It is also noticed that a slight reduction in the total generation costs (≈ 0.8 % of the highest generation costs) is attained, when the control mode of operation of the wind farm is changed.

Regarding the impact of changing the wind energy penetration level (wind farm capacity), a reduction in the market prices, with an increase in the penetration level, are detected. However, this reduction is very small for the periods with low demands. Moreover, the study highlights that a decrease in the generation costs is observed with the increase in the penetration level.

Studying the impact of changing the candidate wind farm location reveals that as the installation location approaches that of the transmission system, more reactive power generation is required to regulate the wind farm bus voltage to unity; and an increase in the electricity market-clearing prices is observed. As for the total generation costs, it is noticed that changing the wind farm location slightly affects such costs (≈ 1.2% of the highest generation costs).

Finally, it can be concluded, based on the results for the impact of wind power prediction case study, that there are instants where customers buy electricity at lower rates than the actual prices. On the other hand, there are instants where the opposite is true, i.e. customers pay more than the actual electricity price. For the specific wind power samples, presented in this chapter, a gain in the daily customer savings in electricity bills is observed. However, it should be pointed out that for other samples, the opposite is possible. Thus, wind power prediction accuracy can significantly impact the close to real-time market prices and the generation revenue. In addition, wind farm control strategy, penetration level, and installation location can significantly impact the close to real-time electricity market prices and the generation revenue.

Chapter 7
Conclusions and Future Research Direction

7.1 Summary, Contributions, and Conclusions

Wind power generation is characterized by its variability and uncertainty. Therefore, the integration of wind facilities to utility grids have several impacts on the optimum power flow, transmission congestion, power quality issues, system stability, load dispatch, protection system, economic analysis, and electricity market clearing prices. These impacts present major challenges to power system operators. This thesis tackles some of these challenges. The main contributions and conclusions of this research are as follows:

1. Due to the irregular nature of wind power, production prediction represents one of the major challenges to power system operators. Therefore, in this thesis, a new prediction tool is proposed for one hour ahead (short term prediction) average hourly wind speed and wind power using the Grey prediction technique {GM(1,1)}. The generated results from the traditional GM(1,1) model reveal an improvement over the persistent model (traditional reference model) in tracking the actual wind speed time series. However, this model is characterized by the occurrence of some overshoots in the predicted time series. Such overshoots can result in predicting wind speed time series worse than that of the persistent model. To overcome the problem of overshoots occurrence, this thesis investigated the application of the adaptive alpha based grey model that achieved higher levels of improvement over the persistent model than the traditional GM(1,1) model. However, results of this model demonstrated that the adaptive alpha based grey model lacks the good tracking characteristic for the actual wind speed time series of the traditional model. For a further reduction of the overshoots and the prediction error, the improved Grey model and the averaged Grey model have been proposed and investigated. Studied samples revealed that the proposed averaged Grey model attained the highest level of wind speed forecasting and wind power prediction accuracy, compared with the persistent model and the other presented Grey models. Moreover, the averaged Grey model also demonstrates a very good tracking feature and a reduction in the overshoot occurrence. However, it is expected that, for samples where

the errors generated from the overshoots dominates those generated from inaccurate tracking, the proposed improved model would generate better results than the proposed averaged model. This is because the reductions in the overshoot errors by the averaged model are less than their corresponding reductions by the improved model.

2. Prediction horizons differ with the required application. One hour ahead prediction is suitable for small power systems operations and one hour electricity markets. However, longer horizons such as one day or more (24 ahead prediction and more) are appropriate for interconnected power system operations such as unit commitments, conventional generators scheduling, as well as one day electricity markets. Therefore, new one day (medium term prediction) forecasting models are developed for wind speed and direction. These models are based on relating the forecasted value to their corresponding historical value in previous years within the same time period. Linear prediction models are developed using current data and data from the same time period but one (or two) years in the past. These models are assumed to be extended to the near future. The generated results revealed the accuracy of the proposed models. The proposed technique is characterized by its simplicity, its independence from data recorded from neighbouring sites, and its independence from NWP models.

3. Accurate modelling of wind farms plays an important role in studying the impact of wind facilities integration to utility grids, as well as in predicting the total production of a given wind farm. For this reason, the thesis investigated new technique to model the wind field distribution within a wind farm. Developed results highlight the importance of including the dynamic wake model and the time delay models to appropriate simulate the dynamic performance of the wind farms and the close to reality modelling of their production fluctuations. Moreover, the results also revealed that the improper modelling of the wind profiles affects the dynamic simulation of the entire system especially in the presence of protective devices.

4. Wind production variability and the technique by which it is controlled have a direct impact on utility grid operation. A control technique is proposed for wind turbines, driven by doubly-fed induction generators (DFIGs), to regulate the terminal voltage by equally sharing the generated/absorbed reactive power between the rotor-side and the grid-side converters. Presented results demonstrate the effectiveness and the accuracy of the proposed technique. Moreover, an economic evaluation for the impact of the developed technique in reducing the

power loss in the generator set has been highlighted.

5. Electricity market clearing prices depend on the generated power, the system demands, and the generation costs. Therefore, integrating free sources of energy such as wind facilities to the utility grid does have an impact on electricity prices. The thesis investigated several scenarios regarding this issue and it was concluded that;

    a. The addition of a wind farm in the network can significantly reduce market prices. However, when compared to a constant power DG, an increase in market price occurs due to the variable nature of the wind and the shift between the wind power generation and load demand peak times.

    b. The lowest market prices can be achieved when the wind farm is operating in the voltage regulation mode.

    c. A reduction in the market prices with the increase in the penetration level was detected.

    d. As the wind farm is installed closer to the transmission system, an increase in the electricity market-clearing prices was observed.

    e. Based on the results for the prediction case study, it was detected that there are instants where the customer buys electricity at lower rates than the actual prices. On the other hand, there are instants where the opposite is true i.e. customers will pay more than the actual electricity price. Thus, wind power prediction accuracy can significantly impact the close to real time market prices and the generation revenue.

It is also worth mentioning that each of the proposed techniques for wind power prediction (one-hour and / or one-day ahead) are applicable for both single unit and large scale wind farms.

7.2 Recommendations for Future Research Directions

With the increased penetration levels of wind farm capacities in power systems, more research is required. This section recommends some future research directions as follows:

1. With the availability of sufficient data for actual wind farm production, the developed wind power prediction tools and the wind farm model can be further examined and analyzed for the prediction of large scale wind farm production.

2. Linear relationship was assumed for the one-day ahead prediction technique. Other relationships can be examined. Moreover, Artificial Intelligent based model can also be developed and investigated.
3. The thesis used wind speed data series recorded at Madison Weather Station. Further evaluation and accuracy investigation of the proposed prediction models can be conducted on wind data collected from other wind facilities sites.
4. Further investigation of the impact of the integration of wind power facilities on electricity market structures can be tackled by considering double auction markets. In addition, day-ahead electricity market structures can also be investigated, where the problem formulation will be modified by adding the costs of shutting down and starting up the conventional generators.

Appendix A
Wind Turbines

A.1 Wind Turbine Classifications

Wind turbines are classified according to their axis of rotation as *horizontal axis* and *vertical axis* wind turbines, as shown in Figure A.1. Horizontal axis wind turbines can capture more wind power than vertical axis wind turbines; however, they are more expansive. Wind turbines can be also categorized according to the direction of the incident wind into *upwind* and *downwind* turbines, as shown in Figure A.2. Upwind turbines operate facing the wind and require a Yaw drive mechanism to keep the rotor aligned with the wind direction; downwind turbines operate facing away from the wind. They are self-oriented turbines, because they use the turbulence created by the towers in the blades' path. Thus, according to the site's wind condition operators can decide which turbine to use.

According to their operation mode, wind turbines are classified as c*onstant speed* and v*ariable speed* turbines. Variable speed wind turbines can capture more wind power and produce less fluctuation in their generated power than constant speed turbines. However, variable speed wind turbines require power electronic devices to control the generated power and contributing to the injection of harmonics into the grid. Furthermore, wind turbines are classified according to the number of blades as *two-blade* and *three-blade* turbines as illustrated in Figure A.3. Downwind turbines have two blades, whereas upwind turbines are designed with three blades.

a) Vertical axis b) Horizontal axis

Figure A.1: vertical axis and horizontal axis wind turbines.

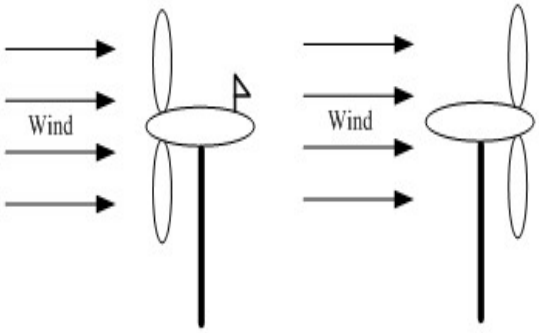

a) Upwind b) Downwind

Figure A.2: Upwind and downwind turbines.

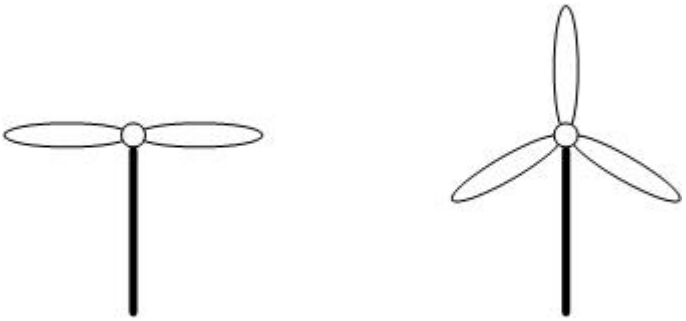

a) Two-Blades b) Three-Blades

Figure A.3: Two-blades and three-blades turbines.

A.2 Wind Turbines Main Components

Fig. A.4 illustrates the main components for a wind turbine [86]. These components are:

Rotor: It consists of the blade and the hub.

Hub: It connects the blades to the low speed shaft. Hubs are rigid, hinged or teetering. The most common one is the rigid type.

Blades: They are the main components of the rotor. Most turbines used in electricity generation have either two or three blades. They are used to catch the wind energy and convert it into mechanical energy to force the rotor to rotate.

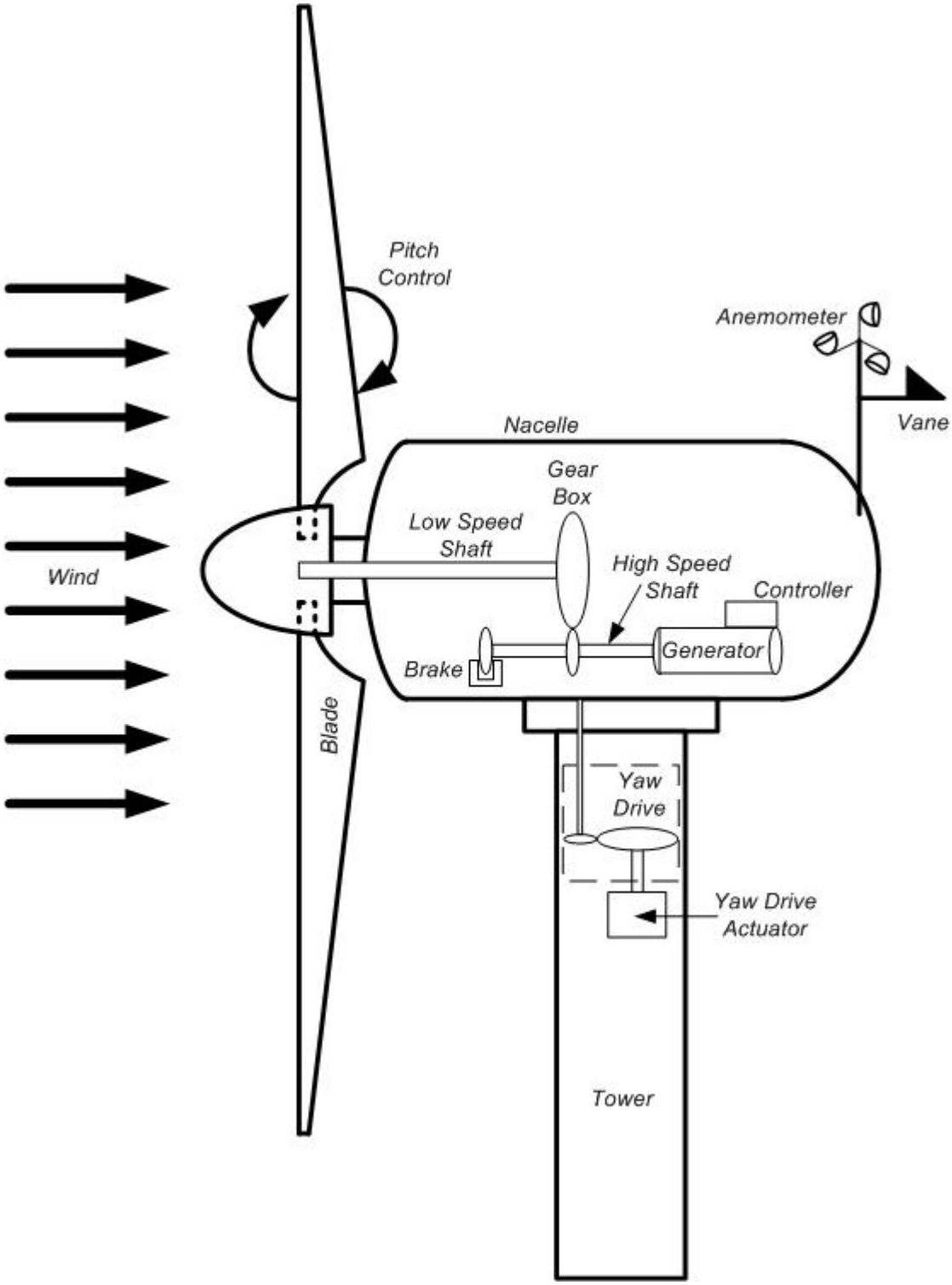

Fig. A.4: Main components of a wind turbine.

Pitch: The blades are turned in / out of the wind to keep the rotor from rotating in winds that are too high or too low. Also, pitch control is important to maintain a nearly constant speed of rotation for the low speed shaft, or to limit the power generation at the rated value for variable speed mode of operation.

Nacelle: The nacelle contains the gearbox, low- and high-speed shafts, generator, controller, and brake. The nacelle is installed at the top of the tower and its cover protects the components inside the nacelle from different weather conditions.

Brake: It is used to stop the rotor in emergencies, and can be achieved mechanically, electrically, or hydraulically.

Yaw Drive: The upwind turbine requires a Yaw drive to keep the rotor facing into the wind as the wind direction changes. The downwind depends on aerodynamics to align the rotor of the turbine.

Yaw Motor: It is used to activate the yaw drive.

Tower: Towers are used to raise the turbine to the upper air levels (with higher wind speeds) to catch as much wind energy as possible. They are made from steel or concrete in the case of large turbines. The tower height ranges from 1 to 1.5 times the rotor diameter and usually it is not less than 20 m high.

Low-Speed Shaft: It is considered the main shaft of the turbine. The rotor turns the low-speed shaft at 30 to 60 r.p.m.

Gear Box: Gears connect the low-speed shaft to the high-speed shaft of the generator. They increase the rotational speeds from about a few hundred rpm (or even less) to about 1000 or 1800 rpm. The gearbox is the most expensive and heaviest component of a wind turbine.

High-Speed Shaft: It is connected between the gear box and the generator and used to drive the generator.

Generator: The generator is used to convert the mechanical power into electrical power. The most commonly used generators with wind turbines are the induction or a synchronous AC generators that produce 50 or 60 Hz electricity. The induction generator has been more widely adopted because they offer several advantages over conventional synchronous generators for operation in large power grids. These advantages are the reduced unit cost, brushless rotor construction, absence of separate source for excitation, ruggedness, and ease of maintenance. Induction generators used in wind turbines are

either squirrel cage or doubly fed machines. In addition, permanent magnet generators and switched reluctance generators are sometimes used.

Controller: The controller starts up the machine at its cut in speed and shuts off the machine at its cut out speed. Turbines cannot operate at wind speeds above the cut out speed to avoid overheating in their generators and/or mechanical damage of the rotor shaft.

Anemometer: It is a sensor to measure the wind speed and sends this information to the controller. The most commonly used anemometers are the cup anemometer and the propeller anemometer.

Wind Vane: It is a sensor for the direction of the wind. Typical wind vanes creates a signal by using contacts or potentiometers. They communicate with the yaw drive to align the turbine properly in the direction of the wind. They are not present in downwind turbines.

Appendix B
DFIG Model

B.1 Induction Generator Model

The dynamic voltage equations used to model the wound rotor induction generator are expressed in the d-q axis quantities as follows [17, 18];

$$V_{qs} = R_s \cdot i_{qs} + p\psi_{qs} + \omega\psi_{ds} \,, \tag{B.1}$$

$$V_{ds} = R_s \cdot i_{ds} + p\psi_{ds} - \omega\psi_{qs} \,, \tag{B.2}$$

$$V'_{qr} = R'_r \cdot i'_{qr} + p\psi'_{qr} + (\omega - \omega_r)\psi'_{dr} \,, \tag{B.3}$$

and

$$V'_{dr} = R'_r \cdot i'_{dr} + p\psi'_{dr} - (\omega - \omega_r)\psi'_{qr} \,. \tag{B.4}$$

where V_{qs} and V_{ds} are the stator's q- and d- axis voltages, respectively, V'_{qr} and V'_{dr} are the rotor's q- and d- axis voltages referred to the stator, respectively, i_{qs} and i_{ds} are the stator's q- and d- axis currents, respectively, i'_{qr} and i'_{dr} are the rotor's q- and d- axis currents referred to the stator, respectively, Ψ_{qs} and Ψ_{ds} are the stator's q- and d- axis fluxes, respectively, Ψ'_{qr} and Ψ'_{dr} are the rotor's q- and d- axis fluxes referred to the stator, respectively, R_s is the stator resistance, R'_r is the rotor resistance referred to the stator, p is d/dt, ω is the electrical angular frequency, and ω_r is the rotor angular velocity.

The d- and q- axis fluxes of the induction generator are expressed in terms of the generator d- and q- axis currents as follows [5]:

$$\psi_{qs} = L_s \cdot i_{qs} + L_m \cdot i'_{qr} \,, \tag{B.5}$$

$$\psi_{ds} = L_s \cdot i_{ds} + L_m \cdot i'_{dr} \,, \tag{B.6}$$

$$\psi'_{qr} = L'_r \cdot i'_{qr} + L_m \cdot i_{qs} \,, \tag{B.7}$$

$$\psi'_{dr} = L'_r \cdot i'_{dr} + L_m \cdot i_{ds} \,, \tag{B.8}$$

$$L_s = L_{ls} + L_m \,, \tag{B.9}$$

and

$$L'_r = L'_{lr} + L_m \quad . \tag{B.10}$$

where L_s is the stator inductance, L'_r is the rotor inductance referred to the stator, L_{ls} is the stator leakage inductance, L'_{lr} is the rotor leakage inductance referred to the stator, and L_m is the magnetizing inductance.

The mechanical system equations for the wound rotor are expressed as follows;

$$p\omega_m = \frac{1}{2H}\left(T_e - F\omega_m - T_m\right) \tag{B.11}$$

and

$$T_e = 1.5\ P\left(\psi_{ds} \cdot i_{qs} - \psi_{qs} \cdot i_{ds}\right). \tag{B.12}$$

where T_e and T_m are the electromechanical and the mechanical torques, respectively, F is the combined friction constant for the rotor and the stator, H is the combined inertia constant for the rotor and the stator, and P is the number of pole pairs.

B.2 Wind Turbine Aerodynamic Model

The per unit aerodynamic equation for modelling the wind turbine [19] is given as follows:

$$P_{m,\,pu} = K \cdot C_{P,\,pu} \cdot v_{pu}{}^3 \tag{B.13}$$

where $P_{m,\,pu}$ is the turbine output mechanical power in pu, $c_{p,\,pu}$ is the turbine performance coefficient $C_P(\lambda, \beta)$ in pu, v_{pu} is the per-unit value of the incident wind speed, K is the power gain factor for $C_{p,\,pu} = 1$ pu and $v_{pu} = 1$ pu, β is the blades pitch angle, and λ is the blades tip speed ratio and is equal to $\omega R / v$, where ω is the turbine rotational speed and R is the turbine rotor radius.

The turbine performance coefficient is determined by the following equation:

$$C_P(\lambda, \beta) = a_1\left(\frac{a_2}{\lambda_i} - a_3\beta - a_4\right)e^{\frac{-a_5}{\lambda_i}} + a_6\lambda \tag{B.14}$$

where the c coefficients are given in the Appendix and $\lambda_{i,}$ is given by

$$\frac{1}{\lambda_i} = \frac{1}{0.08\ \beta + \lambda} - \frac{0.035}{1 + \beta^3}\ . \tag{B.15}$$

Appendix C

System Parameters

C.1 Distribution Grid Parameters

120 kV, three-phase, 60 Hz, AC source

50 MVA, 120/25 kV three-phase, star/delta transformer

25 kV feeders

C.2 Induction Generator Parameters

1.66 MVA, 575 V, 6 pole, 60 Hz three-phase induction generator

Stator resistance (R_s) = 0.00706 pu

Rotor resistance (R'_r) = 0.005 pu

Stator leakage inductance (L_{ls}) = 0.171 pu

Rotor leakage inductance (L'_{lr}) = 0.156 pu

Magnetizing inductance (L_m) = 2.9 pu

Inertia constant (H) = 5.04 s

Friction constant (F) = 0.01 pu

Number of pair poles (P) = 3

C.3 Turbine Parameters

Rotor diameter = 66 m

Turbine separation = 330 m

Thurst coefficient (C_T) = 0.88

Hub height (z) = 67 m

Ground roughness (z_o) = 0.3 m

Base wind speed = 12 m/s

Cut in wind speed = 3.5 m/s

Under voltage limits = 0.8 pu for 0.1s

Over voltage limits = 1.1 pu for 0.1s

Over current limits = 1.1 pu for 5s

Under speed limits = 0.3 pu for 5s

Over speed limits = 1.5 pu for 5s

$C_P(\lambda, \beta)$ coefficients: $a_1 = 0.5176$, $a_2 = 116$, $a_3 = 0.4$, $a_4 = 5$, $a_5 = 21$, and $a_6 = 0.0068$.

$C_{P,\,max} = 0.48$

$\lambda_{nom} = 8.1$

$K = 0.73$

$\omega_{base} = 1.2$

C.4 Converters Parameters

Grid-side coupling inductor = 0.15 pu

Grid-side coupling inductor internal resistance = 0.0015 pu

DC bus capacitor = 10 mF

DC bus reference voltage 1200 V

C.5 Turbine Transformer Parameters

2 MVA, 575/25000 V, three-phase, delta/star transformer

C.6 Motor Plant Parameters

2 MVA, 25/2.3 kV, three-phase, delta/star transformer

1.68 MW, 2.3 kV, 0.93 PF lagging, three-phase induction motor

200 kW three-phase local load

800 kVAR power factor correction three-phase capacitor bank

Under voltage limits = 0.8 pu for 0.2s

Over voltage limits = 1.1 pu for 0.2s

Over current limits = 1.1 pu for 5s

Under speed limits = 0.9 pu for 1s

Over speed limits = 1.1 pu for 1s

C.7 Local Load Parameters

2 MW static load. (for section 3.4)

3 MW static load. (for section 4.3)

C.8 Static Loads Parameters

5 MVA static load at 0.9 PF lagging. (for section 3.4)

15 MVA static load at 0.9 PF lagging. (for section 4.3)

C.9 Switched Static Load Parameters

2.5 MVA static load at 0.9 PF lagging. (for section 3.4)

7.5 MVA static load at 0.9 PF lagging. (for section 4.3)

Publications

➢ Journal Papers

1. T.H.M. El-Fouly, E.F. El-Saadany, and M.M.A. Salama, "Grey Predictor for Wind Energy Conversion Systems Output Power Prediction," *IEEE Transactions on Power Systems* (Letter). vol. 21, no. 3, August 2006, pp. 1450 - 1452.
2. T.H.M. El-Fouly, E.F. El-Saadany, and M.M.A. Salama**,** "One Day Ahead Prediction of Wind Speed and Direction," Accepted paper at the *IEEE Transactions on Energy Conversions* (In press).
3. T.H.M. El-Fouly, E.F. El-Saadany, and M.M.A. Salama, "Improved Grey Predictor Rolling Models for Wind Power Prediction," Accepted paper at the *IET Proceedings on Generation, Transmission, and Distribution* (In press).
4. T.H.M. El-Fouly, E.F. El-Saadany, and M.M.A. Salama, "Hourly Wind Power Prediction using Grey Predictor Rolling Model," Submitted journal paper to the *International Journal of Electric Power System Research*.
5. T.H.M. El-Fouly, H.H. Zeineldin, E.F. El-Saadany, and M.M.A. Salama, "Impact of Wind Generation Control Strategies, Penetration Level, and Installation Location on Electricity Market Prices**,**" Submitted journal paper to the *IET Renewable Power Generation*.
6. T.H.M. El-Fouly, E.F. El-Saadany, and M.M.A. Salama, **"**Reactive Power Shared Voltage Regulation based Technique for Doubly-Fed Induction Generators Wind Turbines," Submitted journal paper to the *IEEE Transactions on Power Systems*.
7. T.H.M. El-Fouly, E.F. El-Saadany, and M.M.A. Salama, **"**Impacts of Wake Effect and Time Delay on the Dynamic Analysis of Wind Farms Models," Submitted journal paper to the *Special Bulletin of Science, technology and Society on Renewable Energy and Sustainability*.

➢ Conference Papers

1. T.H.M. El-Fouly, E.F. El-Saadany, and M.M.A. Salama, "Voltage Regulation of Wind Farms Equipped with Variable-Speed Doubly-Fed Induction Generators Wind Turbines," in *Proceedings of the IEEE Power Engineering Society General Meeting*, Tampa, USA, June, 24-28, 2007.
2. T.H.M. El-Fouly, E.F. El-Saadany, and M.M.A. Salama, "One Day Ahead Prediction of Wind Speed Using Annual Trends," in *Proceedings of the IEEE Power Engineering Society General Meeting*, Montreal, Canada, June, 18 - 22, 2006.

3. T.H.M. El-Fouly, E.F. El-Saadany, and M.M.A. Salama, "A Novel Technique for Wind Speed Forecasting Using Grey Predictor," in *Proceedings of the Tenth Americas Conference on Wind Engineering (10ACWE)*. Louisiana, USA. Publishing Date: May, 31 – June, 4, 2005.

4. T.H.M. El-Fouly, E.F. El-Saadany, and M.M.A. Salama, "A Study of Wind Farms Output Power Prediction Techniques," in *Proceedings of the 36th North American Power Symposium "NAPS 2004"*. Idaho, USA. pp. 249 - 254.

Bibliography

[1] "Wind Vision for Canada", Recommendations for Achieving Canada's Wind Energy Potential, Report by the Canadian Wind Energy Association (CanWEA), June 2001, http://www.canwea.ca/pdfs/CanWEA-WindVision.pdf.

[2] Wind Power Monthly, January 2001.

[3] World Wind Energy Association. http://www.wwindea.org/home/index.php?option=com_frontpage&Itemid=1

[4] "Wind Force 12", Report by the European Wind Energy Association (EWEA), October 2002, http://www.ewea.org/doc/WindForce12.pdf.

[5] Quick Facts about Wind Energy, Canadian Wind Energy Association (CanWEA), http://www.canwea.ca.

[6] Wind Power Monthly, January 2002.

[7] "Ontario Wind Power Task Force" Industry Report and Recommendations by the CanWEA, July 2002, http://www.canwea.ca/pdfs/OntarioWindPowerTaskForceReport.pdf.

[8] Sorensen, P., Bak-Jensen, B., Kristiansen, J., Hansen, A.D., Janosi, L., and Bech, J., "Power Plant Characteristics of Wind Farms 2000" in *Proceedings Kassel*.

[9] Twidell, J. W. and Weir, A. D., "*Renewable Energy Resources*" London, 1986.

[10] "Permitting of Wind Energy Facilities", A handbook prepared by National Wind Coordinating Committee (NWCC) Siting Subcommittee, August 2002.

[11] Hansen, L.H., Madsen, P.H., Blaabjerg, F., Christensen, H.C., Lindhard, U., and Eskildsen, K., "Generators and power electronics technology for wind turbines", *IECON '01. The 27th Annual Conference of the IEEE Industrial Electronics Society*, 2001, vol. 3, 29 Nov.-2 Dec. 2001. pp. 2000 -2005.

[12] Rodrigo, F.M., Ruiz Gonzalez, J.M., Dominguez Vazquez, J.A., and Herrero de Lucas, L.C., "Sensorless control of a squirrel cage induction generator to track the peak power in a wind turbine", *IECON 02 The 28th Annual Conference of the IEEE Industrial Electronics Society*, 2002, vol. 1 , November 5 - 8, 2002. pp. 169 -174.

[13] Itoh, Y. and Nozawa, N., "The design of control configuration of variable speed generator system", *in Proceedings of the Power Conversion Conference* - Nagaoka 1997, vol. 2, 3-6 Aug. 1997. pp. 751 -754.

[14] Dambrosio, L. and Fortunato, B., "One step ahead adaptive control technique for a wind turbine-synchronous generator system", *IECEC-97. Proceedings of the 32nd Intersociety Energy Conversion Engineering Conference*, 1997, vol. 3, 27 July-1 Aug. 1997. pp. 1970 -1975.

[15] Slootweg, J.G., Polinder, H., and Kling, W.L., "Dynamic Modelling of a Wind Turbine with Doubly Fed Induction Generators", *IEEE Power Engineering Society Summer Meeting, 2001*, vol. 1, 15-19 July 2001. pp. 644 -649.

[16] Ekanayake, J.B., Holdsworth, L., XueGuang Wu, and Jenkins, N., *"*Dynamic modeling of doubly fed induction generator wind turbines", *IEEE Transactions on Power Systems*, vol. 18, no. 2, May 2003. pp. 803 -809

[17] Chen, H., Zhang, C., and Zhao, X., "Research on the Switched Reluctance Wind Generator System", *IEEE International Conference on Systems, Man, and Cybernetics*, 2001, vol. 3 , 7-10 Oct. 2001, pp. 1936 -1941.

[18] Qixue, Z., Xiangheng, W., Xuezhong, Z., and Diji, L., "small single-phase switched reluctance generator for wind power generation", *ICEMS 2001. Proceedings of the Fifth International Conference on Electrical Machines and Systems*, 2001, vol. 2, 18-20 Aug. 2001. pp. 1003 -1006.

[19] EL-Fouly, T.H.M., EL-Saadany, E.F., and Salama, M.M.A., "A Combined Electro-Mechanical Control Technique for Dynamic Voltage Regulation of a Stand-Alone Wind Turbine Generator," *International Journal of Global Energy Issues (IJGEI), Special Issue on: "Renewable Energy and Distributed Generation Systems"*. vol. 26, Nos. 3/4, October 2006, pp. 361 - 381.

[20] Marei, M.I., EL-Fouly, T.H.M., EL-Saadany, E.F., and Salama, M.M.A., "A Flexible Wind Energy Scheme for Voltage Compensation and flicker Mitigation," *in Proceedings of the IEEE Power Engineering Society General Meeting*, 2003, pp. 2491 – 2497.

[21] Manwell, J.F., McGowan, J.G., and Rogers, A.L., "*Wind Energy Explained, Theory, Design And Applicatio*n", Amherst, USA: John Wiley & Sons, LTD, 2002.

[22] Eggleston, D.M. and Stoddard, F.S., "*Wind Turbine Engineering Design*", New York, USA: Van Nostrand Reinhold Company, 1987.

[23] *IEEE Recommended Practice for the Electrical Design and Operation of Windfarm Generating Stations*, IEEE Standard 1094-1991, April. 1991.

[24] Smith, G.J., **"**SCADA in wind farms", *IEE Colloquium on Instrumentation in the Electrical Supply Industry*, 29, Jun 1993, pp. 11/1 -11/2

[25] Brobak, B. and Jones, L., "SCADA systems for large wind farms: Grid integration and market requirements", *IEEE Power Engineering Society Summer Meeting*, 2001, vol. 1, 15-19 July 2001, pp. 20 -21.

[26] Slootweg, J.G. and Kling, W.L., "Modeling of large wind farms in power system simulations", *IEEE Power Engineering Society Summer Meeting*, 2002, vol. 1, 21-25, July 2002, pp. 503 -508.

[27] Ackermann, T. "*Wind Power in Power Systems*". John Wiley & Sons, Ltd, England, 2005.

[28] EL-Fouly, T.H.M., EL-Saadany, E.F., and Salama, M.M.A., "A Study of Wind Farms Output Power Prediction Techniques," *in Proceedings of the 36th North American Power Symposium "NAPS 2004"*. Idaho, USA. pp. 249 - 254.

[29] Damousis, I.G. and Dokopoulos, P., "A fuzzy expert system for the forecasting of wind speed and power generation in wind farms", *PICA 2001. 22nd IEEE Power Engineering Society International Conference on Power Industry Computer Applications*, 2001. Innovative Computing for Power - Electric Energy Meets the Market, 20-24 May 2001, pp. 63 -69.

[30] Alexiadis, M.C., Dokopoulos, P.S., and Sahsamanoglou, H.S., "Wind Speed and Power Forecasting Based on Spatial Correlation Models", *IEEE Transactions on Energy Conversion,* vol. 14 no. 3, Sep. 1999, pp. 836 - 842.

[31] Damoisis, I.G., Alexiadis, M.C., Theocharis, J.B., and Dokopoulos, P.S., "A Fuzzy Model for Wind Speed Prediction and Power Generation in Wind Parks Using Spatial Correlation", *IEEE Transactions on Energy Conversion,* vol. 19, no. 2, June. 2004, pp. 352 - 361.

[32] Barbounis, T.G., Theocharis, J.B., Alexiadis, M.C., and Dokopoulos, P.S., "Long Term Wind Speed and Power Forecasting Using Local Recurrent Neural Network Models", *IEEE Transactions on Energy Conversion,* vol. 21, no. 1, March. 2006, pp. 273 - 284.

[33] Barbounis, T.G., and Theocharis, J.B., "A Locally Recurrent Fuzzy Neural Network with Application to the Wind Speed Prediction using Spatial Correlation", *Neurocomputing,* vol. 70, 2007, pp. 1525 - 1542.

[34] Huang, Z. and Chalabi, Z.S., "Use of time-series analysis to model and forecast wind speed", *Journal of Wind Engineering and Industrial Aerodynamics*, vol. 56, no. 2-3, May, 1995, pp. 311-322.

[35] Kamal, L. and Jafri, Y. Z. , "Time series models to simulate and forecast hourly averaged wind speed in Quetta, Pakistan", *Solar Energy*, vol. 61, no. 1, July, 1997, pp. 23-32

[36] More, Anurag and Deo, M.C., "Forecasting wind with neural networks", *Marine Structures*, vol. 16, no. 1, January - February, 2003, pp. 35-49.

[37] Sfetsos, A., "A comparison of various forecasting techniques applied to mean hourly wind speed time series", *Renewable Energy*, vol. 21, no. 1, September 1, 2000, pp. 23-35

[38] Costa, M. and Pasero, E., "Artificial neural systems for verglass forecast", *in Proceedings of the IJCNN '01. International Joint Conference on Neural Networks*, 2001, vol. 1, 15-19 July 2001, pp. 258 -262.

[39] Miranda, M.S. and Dunn, R.W., "One-Hour-ahead Wind Speed Prediction Using Bayesian Methodology", *in Proceedings of the IEEE Power Engineering Society General Meeting*, 2006.

[40] Pashardes, S. and Christofides, C., "Statistical Analysis of Wind Speed and Direction in Cyprus", *Solar Energy,* vol. 55, no. 5, Nov., 1995, pp. 405 - 414.

[41] Jangamshetti, S. H. and Rau, V.G., "Optimum Siting of Wind Turbine Generators", *IEEE Transactions on Energy Conversion,* vol. 16, no. 1, March 2001, pp. 8 - 13.

[42] Gavanidou, E.S., Bakirtzis, A.G., and Dokopoulos, P.S., "A Probabilistic Method for the Evaluation of the Performance of Wind-Diesel Energy Systems", *IEEE Transactions on Energy Conversion,* vol. 7 no. 3, Sept. 1992, pp. 418 - 425.

[43] Sideratos, G. and Hatziargyriou, N.D., "An Advanced Statistical Method for Wind Power Forecasting", *IEEE Transactions on Power Systems*, vol. 22 no. 1, Feb. 2007, pp. 258 - 265.

[44] Larson, K.A. and Westrick, K., "Short-term Wind Forecasting using Off-site Observations", *Wind Energy,* vol. 9, 2006, pp. 55 – 62.

[45] Feijoo, A.E., Cidras, J., and Dornelas, J.L.G., "Wind speed simulation in wind farms for steady-state security assessment of electrical power systems", *IEEE Transactions on Energy Conversion*, vol. 14 no. 4, Dec. 1999, pp. 1582 -1588.

[46] Landberg, L., "A mathematical look at a physical power prediction mode", *Wind Energy*, vol. 1, no. 1, September 1998, pp. 23 – 28.

[47] Landberg, L., "Short-term prediction of the power production from wind farms", *Journal of Wind Engineering and Industrial Aerodynamics*, vol. 80, no. 1-2, March 1, 1999, pp. 207-220.

[48] Focken, U., Lange, M., Mönnich, K., Waldl, H., Beyer, H., and Luig, A., "Short-term prediction of the aggregated power output of wind farms—a statistical analysis of the reduction of the prediction error by spatial smoothing effects", *Journal of Wind Engineering and Industrial Aerodynamics*, vol. 90, no. 3, March, 2002, pp. 231-246.

[49] Saad-Saoud, Z. and Jenkins, N., "Simple wind farm dynamic model", *IEE Proceedings-Generation, Transmission and Distribution*, vol. 142 no. 5, Sept. 1995, pp. 545 -548.

[50] Krause, P.C., **"***Analysis of Electric Machinery"*, McGraw-Hill Inc., USA, 1986.

[51] Tapia, A., Tapia, G., Ostolaza, X., Fernandez, E., and Saenz, J.R., "Modeling and dynamic regulation of a wind farm", *CIEP 2000. VII IEEE International Power Electronics Congress*, 2000, 15-19 Oct. 2000, pp. 293 -297.

[52] Feijoo, A.E. and Cidras, J., "Modeling of wind farms in the load flow analysis", *IEEE Transactions on Power Systems*, vol. 15, no. 1, Feb. 2000, pp. 110 -115.

[53] Fuerte-Esquivel, C.R., Tovar-Hernandez, J.H., Gutierrez-Alcaraz, G., Cisneros-Torres, F., Feijoo, A.E., and Cidras, J., "Discussion of "Modeling of wind farms in the load flow analysis"", *IEEE Transactions on Power Systems*, vol. 16, no. 4, Nov. 2001, pp. 951 -952.

[54] Feijoo, A.E. and Cidras, J., "Closure to discussion of "modeling of wind farms in the load flow analysis"", *IEEE Transactions on Power Systems*, vol. 16, no. 4, Nov. 2001, pp. 951 -952.

[55] Feijoo, A. and Cidras, J., "Corrections to "modeling of wind farms in the load flow analysis", *IEEE Transactions on Power Systems*, vol. 16, no. 4 , Nov. 2001, pp. 955 -955.

[56] Papantoniou, A., "Modelling and simulation of the effects of grid connected wind farms on the cyprus electricity grid", *MELECON 2000. 10th Mediterranean Electrotechnical Conference*, 2000, vol. 3, May 29-31, 2000, pp. 1145 -1148.

[57] Tande, J.O.G., "Grid Integration of Wind Farms", *Review Article in Wind Energy*, vol. 6, no. 3, July/September 2003, pp. 281 -295.

[58] Ledesma, P., Usaola, J., and Rodriguez, J.L., " Transient Satbility of a fixed speed Wind Farm", *Renewable Energy*, vol. 28, no. 9, July, 2003, pp. 1341 - 1355.

[59] Chompoo-inwai, C., Lee, W.J., Fuangfoo, P., Williams, M., and Liao, J.R., "System Impact Study for the Interconnection of Wind Generation and Utility System", *IEEE Transactions on Industry Applications*, vol. 41 no. 1, Jan./Feb. 2005, pp. 163 -168.

[60] Hansen, A.D., Sorensen, P., Janosi, L., and Bech, J., "Wind farm modelling for power quality", *IECON '01. The 27th Annual Conference of the IEEE Industrial Electronics Society*, 2001, vol. 3, 29 Nov.-2 Dec. 2001, pp. 1959 -1964.

[61] Akhmatov, V. and Knudsen, H., "An aggregate model of a grid-connected, large-scale, offshore wind farm for power stability investigations—importance of windmill mechanical system", *International Journal of Electrical Power and Energy Systems*, vol. 24, no. 9, November, 2002, pp. 709-717.

[62] Akhmatov, V., Knudsen, H., Nielsen, A.H., Pedersen, J.K., and Poulsen, N.K., "Modelling and transient stability of large wind farms", *International Journal of Electrical Power and Energy Systems*, vol. 25, no. 2, February, 2003, pp. 123-144.

[63] Funabashi, T., Koyanagi, K., and Yokoyama, R., "Digital simulation examples of custom power controllers", *IEEE Power Engineering Society Winter Meeting*, 2002, vol. 1, 27-31 Jan. 2002, pp. 499 -501.

[64] Komatsu, T., Fujimitsu, M., Koyanagi, K., Funabashi, T., Fujita, G., Furukawa, R., and Yokoyama, R., "A Study on a New Rotary Frequency Converter for Wind Farm Power System", *ICEE 2001*, China.

[65] Bonhomme, A., Cortinas, D., Boulanger, F., and Fraisse, J.-L., "A new voltage control system to facilitate the connection of dispersed generation to distribution networks", *CIRED 16th International Conference and Exhibition on Electricity Distribution*, 2001. Part 1: Contributions. (IEE Conf. Publ No. 482), vol. 4, 18-21 June 2001, pp. 4.8.

[66] Tapia, A., Tapia, G., Ostolaza, X., Fernandez, E., and Saenz, J.R., "Modeling and dynamic regulation of a wind farm", *CIEP 2000. VII IEEE International Power Electronics Congress*, 2000, 15-19 Oct. 2000, pp. 293 -297.

[67] Saenz, J.R., Tapia, A., Tapia, G., Jurado, F., Ostolaza, X., and Zubia, I., "Reactive power control of a wind farm through different control algorithms", *in Proceedings of the 2001 4th IEEE International Conference on Power Electronics and Drive Systems*, 2001, vol. 1 , 22-25 Oct. 2001, pp. 203 -207.

[68] Tapia, A., Tapia, G., Ostolaza, J.X., Saenz, J.R., Criado, R., and Berasategui, J.L., "Reactive power control of a wind farm made up with doubly fed induction generators. I", *IEEE Power Tech Proceedings*, 2001, Porto , vol. 4 , 10-13 Sept. 2001, pp. 6 pp.

[69] Tapia, A., Tapia, G., Ostolaza, J.X., Saenz, J.R., Criado, R., and Berasategui, J.L., "Reactive power control of a wind farm made up with doubly fed induction generators. II", *IEEE Power Tech Proceedings*, 2001, Porto, Vol. 4, 10-13 Sept. 2001, pp. 5 pp.

[70] Tapia, G., Tapia, A., and Saenz, J.R., "A new simple and robust control strategy for wind farm reactive power regulation", *in Proceedings of the 2002 International Conference on Control Applications*, 2002, vol. 2, 18-20 Sept. 2002, pp. 880 -885.

[71] Tapia, A., Tapia, G., Ostolaza, X., Molina, J., and Saenz, J., "Digital simulation performance of a wind farm", *MELECON 2000. 10th Mediterranean Electrotechnical Conference*, 2000, vol. 3. May, 29-31, 2000, pp. 1153 -1156.

[72] Saenz, J.R., Tapia, G., Ostolaza, X., Tapia, A., Criado, R., and Berastegui, J.L., "Simulation of a wind farm performance under wind speed changes", *CIRED 16th International Conference and Exhibition on Electricity Distribution*, 2001. Part 1: Contributions. (IEE Conf. Publ No. 482), vol. Summaries, 2001, pp. 243 -243.

[73] Saenz, J.R., Tapia, G., Ostolaza, X., Tapia, A., Criado, R., and Berasategui, J.L., "Simulation of a wind farm performance under wind speed changes", *CIRED 16th International Conference and Exhibition on Electricity Distribution*, 2001. Part 1: Contributions. (IEE Conf. Publ No. 482), Vol. 4, 18-21 June 2001, pp. 5

[74] Rodriguez-Amenedo, J.L., Arnalte, S., and Burgos, J.C., "Automatic generation control of a wind farm with variable speed wind turbines", *IEEE Transactions on Energy Conversion*, vol. 17, no. 2 , June 2002, pp. 279 -284.

[75] Saad-Saoud, Z. and Jenkins, N., "The application of advanced static VAR compensators to wind farms", *IEE Colloquium on Power Electronics for Renewable Energy* (Digest No: 1997/170), 16, June 1997, pp. 6/1 -6/5.

[76] Saad-Saoud, Z., Lisboa, M.L., Ekanayake, J.B., Jenkins, N., and Strbac, G., "Application of STATCOMs to wind farms", *IEE Proceedings- Generation, Transmission and Distribution*, vol. 145, no. 5, Sept. 1998, pp. 511 -516.

[77] Sobtink, K.H., Renz, K.W., and Tyll, H., "Operational experience and field tests of the SVG at Rejsby Hede", *in Proceedings POWERCON '98. 1998 International Conference on Power System Technology*, 1998, vol. 1, 18-21 Aug. 1998, pp. 318 -322.

[78] Weixing Lu and Boon Teck Ooi, "Multi-terminal DC transmission system for wind-farms", *IEEE Power Engineering Society Winter Meeting*, 2001. vol. 3, 28 Jan.-1 Feb. 2001, pp. 1091 -1096.

[79] Weixing Lu and Boon-Teck Ooi, "Optimal acquisition and aggregation of offshore wind power by multiterminal voltage-source HVDC", *IEEE Transactions on Power Delivery*, vol. 18, no. 1, Jan. 2003, pp. 201 -206.

[80] Weixing Lu and Boon Teck Ooi, "Multi-terminal LVDC system for optimal acquisition of power in wind-farm using induction generators", *PESC. 2001 IEEE 32nd Annual Power Electronics Specialists Conference*, 2001., vol. 1, 17-21 June 2001, pp. 210 -215.

[81] Weixing Lu and Boon Teck Ooi, "Multiterminal LVDC system for optimal acquisition of power in wind-farm using induction generators", *IEEE Transactions on Power Electronics*, vol. 17, no. 4, July 2002, pp. 558 -563.

[82] Bayod, A.A., Dominguez, J.A., Mur, J., and Melero, J.J., "Combined system for reactive power control in wind farms", *IECON 02, 28th Annual Conference of the IEEE Industrial Electronics Society*, 2002, vol. 4 , Nov. 5-8, 2002, pp. 3291 -3296

[83] Papantoniou, A. and Coonick, A., "Simulation of FACTS for wind farm applications", *IEE Colloquium on Power Electronics for Renewable Energy* (Digest No: 1997/170), 16, June 1997, pp. 8/1 -8/5

[84] Papantoniou, A. and Coonick, A., "Fuzzy logic control of a unified power flow controller for wind farm applications", *IEE Colloquium on Power Electronics for Renewable Energy* (Digest No: 1997/170), 16, June 1997, pp. 9/1 -9/6.

[85] J.C. Smith, E.A. DeMeo, B. Parsons, and M. Milligan, "Wind Power Impacts on Electric Power System Operating Costs: Summary and Perspective on Work to Date", *in Proceedings of the 2004 Global WINDPOWER Conference*, Chicago, Illinois, March 29-31, 2004.

[86] G. N. Bathurst, J. Weatherill, and G. Strbac, "*Trading* Wind Generation in Short Term Energy Markets", *IEEE Transactions on Power Systems*, vol. 17, no. 3, August 2002, pp. 782 - 789.

[87] A. Fabbri, T. G. S. Román, J. R. Abbad, and V. H. M. Quezada, "Assessment of the Cost Associated With Wind Generation Prediction Errors in a Liberalized Electricity Market", *IEEE Transactions on Power Systems*, vol. 20, no. 3, August 200, pp. 1440 - 1446.

[88] Korpas, M., Hildrum, R., and Holen, A.T., "Operation and sizing of Energy Storage for Wind Power Plants in a Market System", *International Journal of Electrical Power and Energy Systems*, vol. 25, Oct., 2003, pp. 599 - 606.

[89] Korpas, M., and Holen, A.T., "Operation Planning of Hydrogen Storage Connected to Wind Power Operating in a Power Market", *IEEE Transactions on Energy Conversion*, vol. 21, no. 3, Sept. 2006, pp. 742 - 749.

[90] Madison weather station, http://www.oardc.ohio-state.edu/centernet/stations/mahome.asp

[91] Piwko, R., Osborn, D., Gramlich, R., Jordan, G., Hawkins, D., and Porter, K., "Wind Energy Delivery Issues", *IEEE Power and Energy Magazine,* vol. 3, no. 6, pp.47-56, November / December 2005.

[92] Deng, J.L., "Control Problems of Grey Systems", *Systems and Control Letter*, vol. 1, no. 5, 1982, pp. 288 - 294.

[93] Wen, K., "*Grey Systems: Modeling and Prediction*", Yang's Scientific Press, Arizona, USA, October 2004.

[94] Liu, S., and Lin, Y., "*Grey Information: Theory and Practical Applications*", Springer, December 2005.

[95] Yang, H.T., Liang, T.C., Shih, K.R., and Huang, C.L., "Power System Yearly Peak Load Forecasting: A Grey System Modeling Approach", *in Proceedings of EMPD '95., 1995 International Conference on Energy Management and Power Delivery*, vol. 1, 1995. pp. 261 - 266.

[96] Chang, B.R., and Tsai, S.F., "A grey-cumulative LMS hybrid predictor with neural network based weighting for forecasting non-periodic short-term time series", *IEEE International Conference on Systems, Man and Cybernetics*, vol. 6, 2002, pp. 5.

[97] Luo, R.C., and Chen, T.M., "Target tracking by grey prediction theory and look-ahead fuzzy logic control", *in Proceedings of the 1999 IEEE International Conference on Robotics and Automation*, vol. 2, 1999, pp. 1176 -1181.

[98] Wai, R.J., Duan, R.Y., and chang, L.J., "Grey feedback linearization speed control for induction servo motor drive", *IECON '01. The 27th Annual Conference of the IEEE Industrial Electronics Society*, vol. 1, 2001, pp. 580 -585.

[99] EL-Fouly, T.H.M., EL-Saadany, E.F., and Salama, M.M.A., "Grey Predictor for Wind Energy Conversion Systems Output Power Prediction", *IEEE Transactions on Power Systems (Letter)*, vol. 21, no. 3, August 2006, pp. 1450 – 1452.

[100] EL-Fouly, T.H.M., EL-Saadany, E.F., and Salama, M.M.A., "A Novel Technique for Wind Speed Forecasting Using Grey Predictor", *in Proceedings of the Tenth Americas Conference on Wind Engineering (10ACWE)*. Louisiana, USA. Publishing Date: May, 31 – June, 4, 2005.

[101] Yao, A.W.L., Chi, S.C., and Chen, J.H., "An Improved Grey-Based Approach for Electricity Demand Forecasting", *Electric Power Systems Research,* vol. 67, 2003, pp. 217 -224.

[102] EL-Fouly, T.H.M., EL-Saadany, E.F., and Salama, M.M.A., "Improved Grey Predictor Rolling Models for Wind Power Prediction", Accepted paper (In press) at the *IET Proceedings on Generation, Transmission, and Distribution*

[103] S.C. Chang, J. Wu, and C.T. Lee, "A study on the characteristics of $\alpha(k)$ of Grey prediction", *in Proceedings of the 4th Conference on Grey Theory and Applications*, 1999, pp. 291-296.

[104] Marei, M.I., EL-Saadany, E.F., and Salama, M.M.A., "Envelope Tracking Techniques for Flicker Mitigation and Voltage Regulation", *IEEE Transactions on Power Delivery,* vol. 19, no. 4, October 2004, pp. 1854 – 1861.

[105] Dash, P.K., Swain, D.P., Routary, A., and Liew, A.C., "Harmonic Estimation In A Power System Using Adaptive Perceptrons", *IEE Proc -Gener Transm. Distrib*., vol. 143, no. 6, November 1996, pp. 565 – 574.

[106] Grabic, S. and Katic, V., "A comparison and trade-offs between induction generators control options for variable speed wind turbine applications", *in Proceedings 2004 IEEE International Conference on Industrial Technology (ICT)*, vol. 1, pp. 564 – 568.

[107] Tapia, G. and Tapia, A., "Wind generation optimization algorithm for a doubly fed induction generator", *IEE Proceedings- Generation, Transmission and Distribution*, vol. 152, no. 2 pp. 253-263, Mar. 2005.

[108] Xin-fang, Z., Da-ping, X., and Yi-bing, L., "Predictive functional control of a doubly fed induction generator for variable speed wind turbines", *in Proceedings 2004 Fifth World Congress on Intelligent Control and Automation*, WCICA 2004, vol. 4, pp. 3315-3319.

[109] Panda, D., Benedict, E.L., Venkataramanan, G., and Lipo, T.A., "A novel control strategy for the rotor side control of a doubly-fed induction machine", *in Proceedings 2001 IEEE Thirty-Sixth IAS Annual Meeting Industry Applications Conf*., vol. 3, pp. 1695 - 1702.

[110] Zhang, L., Watthanasarn, C., and Shepherd, W., "Application of a matrix converter for the power control of a variable-speed wind-turbine driving a doubly-fed induction generator", *in Proceedings 1997 23rd International Conference on Industrial Electronics, Control and Instrumentation*, IECON 97, vol. 2, pp. 906-911.

[111] Pena, R., Clare, J.C., and Asher, G.M., "Doubly fed induction generator using back-to-back PWM converters and its application to variable-speed wind-energy generation", *IEE* Proc-Electr. Power Appl.., vol. 143, no. 3 pp. 231-241, May 1996.

[112] Sun, T., Chen, Z., and Blaabjerg, F., "Transient analysis of grid-connected wind turbines with DFIG after an external short-circuit fault", *in Proceedings 2004 NORDIC Wind Power Conference*, pp. 1-6.

[113] Tapia, A., Tapia, G., and Ostolaza, J.X., "Reactive power control of wind farms for voltage control applications", *Renewable Energy*, vol. 29, pp. 377-392, 2004.

[114] Holdsworth, L., Wu, X.G., Ekanayake, J.B., and Jenkins, N., "Comparison of fixed speed and doubly fed induction wind turbines during power system disturbances", *IEE Proceedings-Generation, Transmission and Distribution*, vol. 150, no. 3 pp. 343-352, May. 2003.

[115] Ekanayake, J.B., Holdsworth, L., and Jenkins, N., "Comparison of 5th order and 3rd order machine models for doubly fed induction generator (DFIG) wind turbines", *Electric Power Systems Research*, vol. 67, pp. 207-215, 2003.

[116] deAlmeida, R.G., Pecas Lopes, J.A., and Barreiros, J.A.L., "Improving power system dynamic behavior through doubly fed induction machines controlled by static converter using fuzzy control", *IEEE Trans. Power Systems*, vol. 19, no. 4, pp. 1942-1950, Nov. 2004.

[117] EL-Fouly, T.H.M., EL-Saadany, E.F., and Salama, M.M.A., "Voltage Regulation of Wind Farms Equipped with Variable-Speed Doubly-Fed Induction Generators Wind Turbines", *in Proceedings of the IEEE Power Engineering Society General Meeting*, Tampa, USA, June, 24-28, 2007.

[118] Rabelo, B., Hofmann, W., and Pinheiro, L., "Loss Reduction Methods for Doubly-Fed Induction Generator Drives for Wind Turbines", *International Symposium on Power Electronics, Electrical Drives, Automation*, and Motion, SPEEDAM 2006, pp. S3-16 – S3-21.

[119] Gagnon, R., Sybille, G., Bernard, S., Pare, D., Casoria, S., and Larose, C., "Modeling and Real-Time Simulation of a Doubly-Fed Indution Generator Driven by a Wind Turbine", *in Proceedings of the International Conference on Power systems Transients (IPST'05)*, Montreal, Canada, June 19-23, 2005.

[120] G.M. Masters, "*Renewable and Efficient Electric Power Systems*", John Wiley & Sons Ltd, 2004.

[121] Ontario Independent Electricity System Operator (The IESO) http://www.ieso.ca/imoweb/market/mi_index.asp

[122] Grady, S.A., Hussaini, M.Y., and Abdullah, M.M., "Placement of Wind Turbines using Genetic Algorithms", *Renewable Energy*, vol. 30, 2005, pp. 259 – 270.

[123] Katic, I., Hojstrup, J., and Jensen, N.O., "A Simple Model for Cluster Efficiency", *in Proceedings of the European Wind Energy Conference*, October 7-9, 1986, Rome, Italy.

[124] EL-Fouly, T.H.M., EL-Saadany, E.F., and Salama, M.M.A., "One Day Ahead Prediction of Wind Speed and Direction", Accepted paper (In press) at the *IEEE Transactions on Energy Conversions*.

[125] EL-Fouly, T.H.M., EL-Saadany, E.F., and Salama, M.M.A., "One Day Ahead Prediction of Wind Speed Using Annual Trends", *in Proceedings of the IEEE Power Engineering Society General Meeting*, Montreal, Canada, June, 18 - 22, 2006.

[126] Zeineldin, H.H., Bhattacharya, K., EL-Saadany, E.F., and Salama, M.M.A., "Impact of Intentional Islanding of Distributed Generation on Electricity Market Prices", *IEE Proceedings-Generation, Transmission and Distribution*, vol. 153, Issue 2, 16 March 2006, pp. 147 - 154.

[127] http://www.nyiso.com/public/company/about_us/index.jsp

[128] Bhattacharya, K., Bollen, M.H.J., and Daalde, J.E., "*Operation of Restructured Power Systems*", Kluwer, USA, 2001.

[129] M.L. Baughman, and S.N. Siddiqi, "Real-Time Pricing Of Reactive Power Theory and Case Study Results", *IEEE Transactions on Power Systems*, vol. 6, no. 1, February 1991, pp. 23 - 29.

[130] R. Piwko, D. Osborn, R. Gramlich, G. Jordan, D. Hawkins, and K. Porter, "Wind Energy Delivery Issues", *IEEE Power and Energy Magazine,* vol. 3, no. 6, pp.47-56, November / December 2005.

[131] www.gams.com

[132] Zareipour, H., Canizares, C.A., and Bhattacharya, K., "An Overview of the Operation of Ontario's Electricity Market", *in Proceedings of the IEEE Power Engineering Society General Meeting*, Montreal, Canada, June, 18 - 22, 2006.